



HAL
open science

Topological order at finite temperature in string-net and quantum double models

Anna Ritz-Zwilling

► **To cite this version:**

Anna Ritz-Zwilling. Topological order at finite temperature in string-net and quantum double models. Physics [physics]. Sorbonne Université, 2024. English. NNT : 2024SORUS268 . tel-04824229

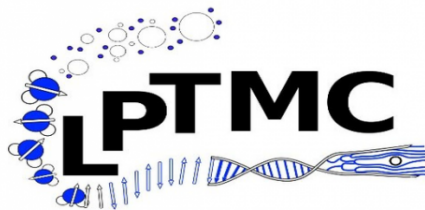
HAL Id: tel-04824229

<https://theses.hal.science/tel-04824229v1>

Submitted on 6 Dec 2024

HAL is a multi-disciplinary open access archive for the deposit and dissemination of scientific research documents, whether they are published or not. The documents may come from teaching and research institutions in France or abroad, or from public or private research centers.

L'archive ouverte pluridisciplinaire **HAL**, est destinée au dépôt et à la diffusion de documents scientifiques de niveau recherche, publiés ou non, émanant des établissements d'enseignement et de recherche français ou étrangers, des laboratoires publics ou privés.



Thèse de doctorat de Sorbonne Université

École Doctorale de Physique en Île-de-France - ED 564

réalisée au

Laboratoire de Physique Théorique de la Matière Condensée

sous la direction de

Jean-Noël FUCHS et Julien VIDAL

présentée par

Anna RITZ-ZWILLING

Sujet de la thèse:

Topological order at finite temperature in string-net and quantum double models

Soutenue à Paris le 27 septembre 2024 devant le jury composé de:

Gwendal FÈVE	Sorbonne Université	Président du jury
Cécile REPELLIN	CNRS, Université Grenoble Alpes	Examinatrice
Benoît DOUÇOT	CNRS, Sorbonne Université	Examinateur
Sofyan IBLISDIR	Universitat de Barcelona	Rapporteur
Joost SLINGERLAND	Maynooth University	Rapporteur
Jean-Noël FUCHS	CNRS, Sorbonne Université	Directeur de thèse
Julien VIDAL	CNRS, Sorbonne Université	Invité, Directeur de thèse
Benoît ESTIENNE	Sorbonne Université	Invité

" ..quelquefois, au bout de très longues marches, non pas au but, mais en vue du but, lorsque vous savez que vous l'atteindrez, se produit une sorte d'irruption du monde dans votre mince carcasse, fantastique, dont on ne parvient pas à rendre compte avec des mots."

Nicolas Bouvier

"Die Wissenschaft hilft uns vor Allem, dass sie das Staunen, wozu wir von Natur berufen sind, einigermaßen erleichtere."

Johann Wolfgang von Goethe

Remerciements

Je souhaite tout d'abord remercier mes directeurs de thèse, Jean-Noël Fuchs et Julien Vidal, pour m'avoir fait découvrir et apprécier l'ordre topologique, et pour m'avoir conseillée et guidée scientifiquement, depuis le stage de M2 jusqu'à l'issue de cette thèse. Merci également pour les conseils et la disponibilité lors de la rédaction du manuscrit et la préparation de la soutenance.

Durant les trois années de cette thèse, nous avons étroitement collaboré avec Steve Simons, et je l'en remercie. J'aimerais par ailleurs remercier Benoît Douçot pour les nombreuses explications sur la théorie des catégories. Les travaux présentés dans cette thèse ont aussi bénéficié de discussions éclairantes avec André Soares, Laurens Lootens, Julio Magdalena de la Fuente, Nick Bultinck et Sofyan Iblisdir. Merci également aux membres de mon jury de thèse pour leurs retours et commentaires sur ce manuscrit.

Merci au LPTMC de m'avoir offert un cadre de travail durant ces trois années, avec des journées rythmées par des repas de midi très ponctuels à 11h30. En particulier, merci à Olivier Bénichou pour son écoute et ses encouragements, ainsi que pour de nombreuses discussions intéressantes. Merci également à Maxim Dolgushev (ou plutôt danke), Aurélien Grabsch, Maria Barbi, Laura Messio et Rémy Mosseri pour les nombreux échanges. Merci à Liliane Cruzel de s'être occupée des questions administratives avec gentillesse et efficacité. Merci à tous ceux qui ont assisté à une répétition de ma soutenance, vous avez grandement contribué à me faire gagner en confiance. Aux "non-permanents" passés et présents du laboratoire, Louise, Léo, Julien, Thibault, Vincent, Nicolas, Théotim, Sankarshan, Sumeja, Davide, Marc, Jérémy, Tim, Paul, Arthur, Pierre-Louis, Louis-Martin et Nathan, merci pour votre compagnie durant les repas de midi, les pauses cafés, ainsi que pour les "cinémaïres" et les bars à la sortie de Jussieu. Merci tout particulièrement à Louise pour tous les moments partagés, ton soutien et tes conseils, ou plus généralement pour avoir été la meilleure co-bureau que j'aurais pu avoir.

J'aimerais également remercier les personnes qui, au-delà du LPTMC, ont contribué à faire de Jussieu un lieu accueillant: les doctorants du bureau 414 du LJP pour m'avoir accueillie tant de fois chez eux pour le burger ou libanais du vendredi midi, ainsi que les doctorants du LPTHE (en particulier Francesco et Andriani) et ceux de l'IMPMC pour les pauses café et les soirées.

Durant ces trois années, j'ai toujours pu compter sur mes ami.e.s, qu'ils soient physicien.ne.s ou non, parisien.ne.s ou non, pour m'écouter parler de ma thèse, me soutenir et me conseiller (et

aussi, pour me changer les idées!): merci pour cela à Erik, Andriani, Zosia, Anna, Lea, Kim, Ester, Théophile, Isabelle, Sarah et Marie. Merci particulièrement à Erik pour la relecture d'une grande partie de ce manuscrit de thèse. A Yuval, merci pour le temps passé ensemble aux Houches (je suis ravie qu'on se soit rencontrées) ainsi que pour avoir répété avec moi ma soutenance.

Finalement, je souhaite remercier ma famille, mes parents, mon soeur, mon frère, ainsi que mes grands-parents, pour leur soutien inconditionnel, leurs encouragements et de l'intérêt qu'ils ont porté à mon travail tout au long du parcours. Enfin, merci à Matteo, pour m'avoir soutenue, écoutée, et particulièrement épaulée durant la phase finale de rédaction, pour les nombreux cafés, les journées et nuits passées à rédiger ensemble, et pour tout le reste.

Abstract

Topological order is a special sort of quantum order which usually appears in strongly interacting gapped quantum systems and does not admit a local order parameter. In two dimensions and at zero temperature, it is instead characterized by a ground-state degeneracy dependent on the topology, long-range entanglement, and the presence of quasiparticles with fractional quantum numbers and fractional exchange statistics. This thesis investigates topological order at finite temperature by means of two exactly solvable toy-models: the string-net model and the Kitaev quantum double model. The main focus is on the string-net model, which realizes all achiral topological orders, i.e., all topological orders described by Drinfeld centers. This model takes a unitary fusion category as an input, and produces the corresponding Drinfeld center as an output. Initially, we derive a formula for the spectral degeneracies of the model. These depend on both the topology, and the topological order considered. In particular, we show that in order to describe the degeneracies, one needs to know the Drinfeld center as well as the unitary fusion category which realizes it. Next, we derive the partition function of the string-net models, from which we obtain the entropy, specific heat, and show that there is no phase transition at finite temperature in this model. We identify a particular set of objects of the Drinfeld center, pure fluxons, which drive the thermodynamic behaviour of the partition function, and study their properties. We also obtain the thermal averages of closed string operators, and study the mutual information of string net models. Finally, we carry over our approach to the Kitaev quantum double model, where we also derive a general formula for the spectral degeneracies, partition function and entanglement entropy, allowing for a more general and detailed study of finite temperature properties compared to previous studies.

Résumé

L'ordre topologique est un ordre quantique particulier qui apparaît dans des systèmes quantiques gappés et généralement fortement corrélés, qui n'admettent pas de paramètre d'ordre local. En deux dimensions et à température nulle, l'ordre topologique est caractérisé par une dégénérescence de l'état fondamental dépendante de la topologie, de l'intrication à longue portée, et la présence de quasi-particules avec des nombres quantiques et des statistiques d'échange fractionnaires. Le but de cette thèse est d'explorer certaines propriétés de l'ordre topologique à température finie au moyen de deux modèles jouets exactement solubles : le modèle des string-nets ("réseaux de corde") et le modèle du double quantique de Kitaev.

L'accent principal est mis sur le modèle des réseaux de cordes, qui réalise tous les ordres topologiques achiraux, c'est-à-dire tous les ordres topologiques décrits par les centres de Drinfeld. Ce modèle utilise une catégorie de fusion unitaire comme entrée et produit le centre de Drinfeld correspondant en sortie. Tout d'abord, nous dérivons une formule pour les dégénérescences spectrales du modèle. Celles-ci dépendent à la fois de la topologie et de l'ordre topologique considéré. En particulier, nous montrons que pour décrire les dégénérescences, il est nécessaire de connaître le centre de Drinfeld ainsi que la catégorie de fusion unitaire qui le réalise.

Ensuite, nous dérivons la fonction de partition des modèles de réseaux de cordes, à partir de laquelle nous obtenons l'entropie et la chaleur spécifique, et montrons qu'il n'y a pas de transition de phase à température finie dans ce modèle. Nous identifions un ensemble particulier d'objets du centre de Drinfeld, les flux purs, qui déterminent le comportement thermodynamique de la fonction de partition, et étudions leurs propriétés. Nous obtenons également les moyennes thermiques des opérateurs de corde fermée et étudions l'information mutuelle des modèles de réseaux de cordes.

Enfin, nous appliquons notre approche au modèle du double quantique de Kitaev, où nous dérivons également une formule générale pour les dégénérescences spectrales, la fonction de partition et l'entropie d'enchevêtrement, permettant une étude plus générale et détaillée des propriétés à température finie par rapport aux études précédentes.

Contents

Introduction	2
1 Introduction	2
1.1 Anyons	2
1.2 Topological order	4
1.3 Models of topological order	6
1.4 Application to topological quantum computation	7
1.5 Topological order at finite temperature	8
1.6 Goal and structure of the thesis	8
I Theoretical Background	11
2 Algebraic theory of anyons	12
2.1 Unitary fusion categories	12
2.1.1 Fusion matrices	12
2.1.2 Fusion trees and Hilbert space dimensions	13
2.1.3 F -symbols	15
2.1.4 Evaluating planar diagrams	15
2.2 Unitary modular tensor categories	17
2.2.1 Braiding	17
2.2.2 T - and S -matrices	18
2.2.3 Chirality	21
2.3 Examples	21
2.4 Overview on categories	24
2.5 Drinfeld centers	24
2.5.1 Properties of Drinfeld centers	25
2.5.2 Drinfeld centers from UMTCs	26
2.5.3 Tube algebra	27
2.5.4 Morita equivalence	31

2.6	Summary	31
II	String-net models	33
3	Introduction to string-net models	34
3.1	Hilbert space and Hamiltonian	34
3.2	Ground-state wave function	36
3.3	Explicit form of the plaquette operator	38
3.4	Topological excitations	39
4	Spectral degeneracies	41
4.1	Introduction	41
4.2	Ground-state degeneracy	43
4.3	Moore-Seiberg-Banks formula	46
4.4	Spectral degeneracies for string-net models	47
4.4.1	Fluxons	47
4.4.2	Adapting the Moore-Seiberg-Banks formula	50
4.4.3	Total Hilbert-space dimension	52
4.5	Special cases	53
4.5.1	Modular categories	54
4.5.2	Commutative categories	54
4.6	Examples	55
4.6.1	$\text{Rep}(S_3)$ and $\text{Vec}(S_3)$ categories	56
4.6.2	Tambara-Yamagami category TY_3	59
4.6.3	Haagerup category \mathcal{H}_3	61
4.6.4	Hagge-Hong category \mathcal{E}	62
4.7	Refined string-net model	63
4.8	Conclusion	64
5	Finite-temperature properties	67
5.1	Introduction	67
5.2	Partition function for the RSN model	68
5.2.1	Thermodynamic limit	69
5.2.2	Infinite-temperature limit and Hilbert-space dimension	70
5.3	Partition function for the SN model	71
5.3.1	Energy, specific heat, and entropy	72
5.3.2	Comparison with classical models	73
5.4	Fluxons, pure fluxons and fusion product of fluxons	74
5.5	Projectors on topological quasiparticles	77
5.5.1	Degeneracies from gluing surfaces	77
5.5.2	General definition of projectors	78
5.5.3	Loops around handles	80

5.5.4	Loops around throats	83
5.5.5	Contractible loops	84
5.6	Wegner-Wilson loops	86
5.6.1	Wegner-Wilson loops at zero temperature	86
5.6.2	From projectors to WWL	88
5.6.3	WWL at finite temperature	89
5.6.4	Numerical implementation of WWL	90
5.7	Topological mutual information	92
5.7.1	Entanglement entropy and topological order at $T = 0$	93
5.7.2	Area law for string-net models	94
5.7.3	Entanglement entropy at infinite temperature	96
5.7.4	Topological mutual information at finite temperature	97
5.7.5	Numerical results on entanglement entropy	101
5.8	Conclusion	104
 III Kitaev quantum double models		107
 6 Introduction to Kitaev quantum double models		108
6.1	Hamiltonian	108
6.2	Topological phase	112
6.3	Relation to string-net models	115
6.4	Examples	116
6.4.1	Toric code	116
6.4.2	S_3 quantum double	116
 7 Degeneracies and finite temperature properties		119
7.1	Introduction	119
7.2	Spectral degeneracies	120
7.2.1	Plaquette and vertex excitations	120
7.2.2	Formula for degeneracies	123
7.2.3	Hilbert space dimension	124
7.3	Partition Function	125
7.4	Projectors and mutual information	126
7.5	Outlook and conclusion	130
 Conclusion		133
 8 General conclusion		133

Appendix	137
A Structure coefficients for the tube algebra	137
B Fluxon identities	139
B.1 S and T identities from the tube algebra	139
B.2 Stability inequality from anyon condensation	141
C Fusion of tubes	143
C.1 Fusion rules from the tube algebra	143
C.2 Fusion of a pure fluxon with a fluxon	146
C.3 Example: Fibonacci	147
D Elements of a proof for I_{topo}	148
D.1 Density matrix at finite temperature	148
D.2 Entanglement entropy	149
D.3 Topological entanglement entropy and I_{topo}	151
Bibliography	157

Introduction

Introduction

1.1 Anyons

In three dimensions, elementary quantum mechanical particles can be classified into two categories: *bosons* and *fermions*. This classification is based on the particle's exchange statistics, which describe how a many-particle wavefunction behaves when two or more identical particles exchange their positions. If two identical bosons (e.g., photons) are exchanged, the wavefunction describing the system remains unchanged. If two identical fermions (e.g., electrons or protons) are exchanged, the wavefunction acquires a global minus sign. However, it was realized [1] about fifty years ago that two-dimensional space allows for the possibility of exchange statistics that differ from those of bosons or fermions.

More formally, if two identical particles in positions x_1 and x_2 are exchanged, the physical state of the system should not change in a measurable way, but the wavefunction $\psi(x_1, x_2)$ describing the quantum state of the system may change by a phase factor:

$$\psi(x_1, x_2) \rightarrow e^{i\alpha}\psi(x_2, x_1), \quad (1.1)$$

where α is real. It is reasonable to expect that if one exchanges two particles twice, the resulting final state will be the same as the initial one. Then, the overall accumulated phase factor $e^{2i\alpha} = 1$, and the two only possibilities for α are 0 (bosons) or π (fermions). However, in two dimensions, a double exchange of identical particles does not necessarily bring the system back to its initial state.

A simple argument for this comes from considering the path of two identical particles in space-time (their worldlines) when a particle is moved around another one. This process is equivalent to exchanging twice the positions of the particles [see Fig. 1.1a)]. In fact, the two configurations of paths can be continuously deformed into each other, and the phase factor accumulated during an exchange depends only on the homotopy class of the exchange path, not the specific path taken during the exchange. In three space dimensions, the path of a particle turning around the other can be contracted into a point [see Fig. 1.1b)], so that the double exchange must act as the identity. In two dimensions, however, the path is not contractible. The phase acquired by the wavefunction when one particle is moved around the other, or when two identical particles exchange their

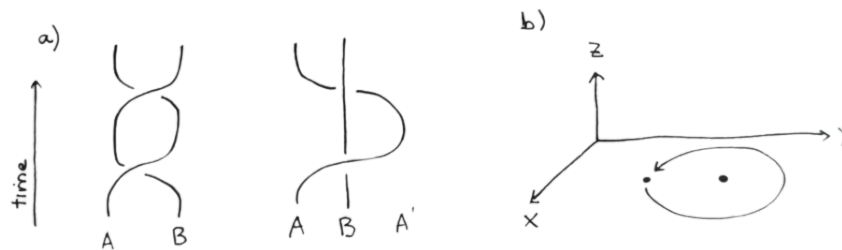


Figure 1.1: a) A double exchange is equivalent to a full circle of one particle around another. Time direction upwards. b) Path of a particle circling around another in a 2D x - y plane. In 3D, the z dimension can be used to deform this path continuously into a point. In 2D, this is not possible.

positions, can thus in principle take *any* value, which motivated calling particles with these exchange statistics *anyons* [2]. The concept of anyons can be generalized to the case where the configuration of many identical particles is not fully specified by their positions. Then, exchanging the particles could result in a unitary transformation inside the degenerate configuration subspace [3, 4, 5]. Because phases commute with each other, the first type of anyons is also called *Abelian anyons*. The second type of anyons is also called *non-Abelian*, because unitary transformations do not commute with each other in general [6].

Since the world we live in is three-dimensional, it is assumed that all elementary particles are either fermions or bosons. However, anyons may emerge as quasiparticles (i.e., point-like excitations that can be described as particles) in two-dimensional materials.

An illustrative example for Abelian anyons is due to Wilczek [2], and is based on the Aharonov-Bohm effect [7]. The latter describes the fact that the wavefunction of a charged particle moving around a region containing a magnetic field experiences a phase shift, even if the magnetic field B is zero in the region where the particle moves. This phase shift $\Delta\phi$ is proportional to the charge of the particle q and to the magnetic flux Φ_B through the encircled region¹: $\Delta\phi = q\Phi_B/\hbar$. A toy model for anyons can be realized by considering a particle with charge q attached to a thin magnetic flux tube Φ_B , moving in a two-dimensional plane. This *charge-flux composite* is then labeled by (q, Φ_B) . Imagine exchanging the positions of two such charge-flux composites (see Fig. 1.2). Due to the Aharonov-Bohm effect, the wavefunction of each charge-flux composite will

¹Here, \hbar denotes the reduced Planck constant.

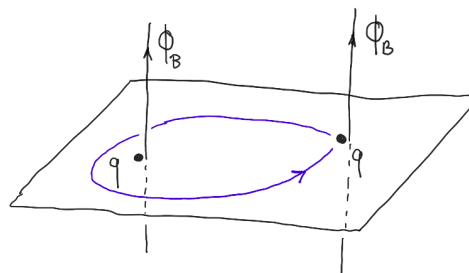


Figure 1.2: Two charge-flux composites (q, Φ_B) in a two-dimensional plane. The blue line indicates the path on one charge-flux composite as it moves around the other (which is equivalent to two exchanging their positions twice).

experience a phase shift of $q\Phi_B/2\hbar$ (the one half factor arises because one considers only one exchange), resulting in an overall phase shift $q\Phi_B/\hbar$. This phase shift clearly allows for values different from 0 or π .

If two charge-flux composites are brought close together, from far away they can be seen as a single charge-flux composite with overall charge $2q$ and overall magnetic flux $2\Phi_B$, i.e., $(2q, 2\Phi_B)$. This provides a simple example for another property of anyons, which is known as fusion.

The discovery of the fractional quantum Hall effect (FQHE) [8] in 1982 provided the first experimental example of a condensed matter system hosting anyons. In the FQHE, a two-dimensional electron gas subjected to a strong perpendicular magnetic field shows special values of Hall conductance, which are rational fractional multiples of the electrical conductance [9]. Recent experiments have confirmed the presence of Abelian anyons in the fractional quantum Hall state of filling fraction $\nu = 1/3$ [10, 11]. Other fractional quantum Hall states (e.g. $\nu = 5/2$) are expected to host non-Abelian anyons [12]. Shortly after the discovery of the FQHE, it was shown that anyons are intimately related to a special type of structure in the ground state, called *topological order* [13, 14].

1.2 Topological order

According to the Landau theory of phase transitions [15], different phases of matter can be classified based on their symmetries (or their "order"). The change of a system from a phase into another - i.e., a phase transition - is associated to a change in symmetry, also called spontaneous symmetry breaking. A well-known example of a phase transition with spontaneous symmetry breaking is the ferromagnetic-paramagnetic phase transition. In the paramagnetic phase, spins are randomly oriented, making the system rotationally invariant. Below a critical temperature, the spins align in a preferred direction, leading to a net magnetization and breaking the rotational invariance. The idea of symmetry as an indicator of a specific phase, and its breaking as an indicator of a phase transition, allows to identify phase transitions by introducing a local order parameter (such as the magnetization in the above example), taking a zero value in the symmetric (or disordered) phase, and a non-zero value in the symmetry-broken (or ordered) phase.

The Landau paradigm is very powerful. In fact, for some time, it was believed that it allowed for the description and classification of all known phases of matter. However, it was discovered at the end of the 1970's that some phases elude this classification in terms of symmetries. In the FQHE [8, 16], different phases correspond to the same symmetries. The same is true for chiral spin liquids [17, 18], a theoretical construction which was originally introduced in order to explain high-temperature superconductivity [19]. Connections between these two cases were soon established [20]. It was understood that an effective low-energy description of these phases was provided by topological quantum field theory [5], which motivated the introduction of the

name of *topological order*² [22, 13]. Since then, it has been argued that topological order is also present in ordinary superconductivity [23]. In general, topological order can exist in quantum systems which have a finite energy gap between the ground state and the first excited state, and are strongly interacting. While we focus on two-dimensional systems in this thesis, topological order can also occur in higher dimensions [24].

Topologically ordered phases cannot be distinguished by their symmetries or through a local order parameter. But then, what characterizes topological order? The ground state of a topologically ordered phase shows two remarkable features. The first one is the topological ground-state degeneracy [13, 20, 25]. This degeneracy is robust to any weak enough local perturbation [26, 13], and depends on the topology of the surface on which the system is placed. For example, the ground-state degeneracy of a given topologically ordered phase may be different on a sphere (genus 0) than on a torus (genus 1). The ground-state degeneracy is a topological invariant (i.e., it does not depend on small continuous deformations of space) that can also be computed directly from the topological quantum field theory describing the topological order at low energy and long wavelength [27, 28].

The second feature of a topologically ordered ground state is the presence of long-range entanglement in the ground-state wave function [29, 30]. Entanglement is a purely quantum mechanical property, which describes the fact that two or more quantum objects might "know" of each other's state even if they are far apart, so that their states are not independent of each other. In most condensed matter systems, entanglement is short-ranged, and typically happens on the lengthscale of correlations between the microscopic degrees of freedom. In contrast, topological order shows long-range entanglement even if correlations are short-ranged. The entanglement between a simply-connected region and the rest of the system can be measured by means of the Von Neumann entropy [31]. For locally interacting gapped Hamiltonians, this entropy typically grows with the length of the boundary between the region and the rest of the system, (which is also known as an "area law"). If the system has topological order and thus long-range entanglement, then the entanglement entropy is supplemented by a constant term, known as the topological entanglement entropy, which does not depend on the size of the system but only on the type of topological order [29, 30].

Finally, topological order is characterized by the presence of special excitations, which may carry fractional quantum numbers, such as spin, or charge, and have fractional exchange statistics. These excitations are anyons, which were discussed in the beginning of this introduction.

In order to describe anyons formally, one needs precisely the two pieces of information which we discussed in the example of a charge-flux composite: their exchange statistics (also called *braiding*), and their fusion. In particular, while in the (Abelian) case of a charge-flux composite there is only one fusion outcome when two anyons are fused together, for non-Abelian anyons

²In condensed matter physics, another type of phases also goes under the name of "topological phases", or symmetry protected topological phases. These phases include topological insulators and topological superconductors. Despite similar names, these phases are actually quite different from phases with topological order, and should not be confused with it. Although they also go beyond the Landau scheme of spontaneous symmetry breaking (i.e., they cannot be classified through a local order parameter), they have in general no long-range entanglement, no topological ground-state degeneracy, and no fractionalized excitations in the bulk. Also, they need no interactions between microscopic constituents, while topological order is necessarily strongly interacting [21].

the fusion outcome may not be unique. This information is encoded in the *fusion rules*. In order to correctly describe fusion and braiding of anyons mathematically, the structure of unitary modular tensor categories (UMTC) is needed [32, 33]. In a UMTC, the information about braiding and fusion can be derived from two matrices, known as the modular matrices, or S and T .

Two different topological orders may have the same ground-state degeneracy on different genus surfaces, and also the same entanglement entropy [13]. However, topological order on a closed surface can often be characterized in a non-ambiguous way through the two modular matrices S and T . In order to describe topological order on a surface with boundaries, supplementary information is needed to specify the edge. This information is given by the chiral central charge c , which is related to the thermal Hall conductance [32]. The knowledge of S and T allows one to predict $c \bmod 8$ (sometimes known as the topological central charge), but not the exact value of c which depends on the nature of the edges. Thus, the triplet (S, T, c) constitutes a complete description of (2+1)D topological order³. [37, 36].

It is worth noting that in recent years, some works have attempted to generalize the concept of spontaneous symmetry breaking in order to include phases without global symmetries and local order parameters like topologically ordered phases. This framework is called generalized or higher-form symmetries, and it allows introducing d -dimensional symmetries, where d reaches from 0 to D , the dimension of space. For (2+1)D topological order, the relevant symmetries are 1-dimensional: they correspond to the existence of string-like operators which wind around non-trivial cycles of the surface (for example, around the handle of the torus). A non-zero expectation value of such a topological symmetry operator might then indicate the presence of topological order [38, 39, 40]. In the end, topological order may be a special kind of symmetry-breaking phase in which the broken symmetry is intermediate between global and local.

1.3 Models of topological order

One of the earliest theories of a phase transition without local order parameter and spontaneous symmetry breaking is the \mathbb{Z}_2 lattice gauge theory of Wegner [41]. In order to distinguish the two phases of this theory, the confining and the deconfining phase, Wegner computed the expectation values of non-local observables, known today as the Wegner-Wilson loop [42]. The same observables were also introduced by Wilson [43] in the context of quantum chromodynamics, in order to measure the confinement or deconfinement of quarks. Today, it is known that the deconfined phase of a lattice gauge theory corresponds to the presence of topological order [42]. The study of anyons in the context of discrete gauge theories was further carried on in [44, 45, 46].

An important class of models for topological order takes inspiration from lattice gauge theories. These models all have a Hamiltonian made of a sum of local commuting projectors, and are exactly solvable. The probably simplest model among those is the *toric code model* of Kitaev [47], which

³In some cases, even the data of S , T and c does not specify completely the topological order, see [34]. Note, also, that the classification in terms of modular data is valid for bosonic topological order (i.e. topological order emerging from quantum spin systems or local boson systems). For fermionic topological order, the correct mathematical framework are unitary braided fusion categories [35, 36]. However, in this thesis we will focus on bosonic topological order.

is a Hamiltonian realization of a \mathbb{Z}_2 lattice gauge theory. In this model, the degrees of freedom (which can be seen as spin $1/2$, or as elements of the group \mathbb{Z}_2) are located on the links of a lattice. Local operators act on the plaquettes and vertices of the lattice and enforce interactions between the degrees of freedom. This gives rise to a topologically ordered phase, mathematically described by the quantum double $D(\mathbb{Z}_2)$. The toric code model is a special case of the more general *Kitaev quantum double model*, which is defined for any finite discrete group G , and realizes a topological phase described by the quantum double of that group, $D(G)$. The *string-net model* introduced by Levin and Wen [48] can in many aspects be seen as a generalization of the Kitaev quantum double model [49, 50]. Instead of elements of a group, the microscopic degrees of freedom and their interactions are described by a more general mathematical structure known as unitary fusion category. The resulting phase is described by a UMTC which is the Drinfeld center of the input category. All of these models generate a particular class of topological phases known as achiral (which means they have a chiral central charge $c = 0 \pmod{8}$) [51, 52, 53]. Therefore, they cannot describe systems with chiral topological order⁴, as for example the FQHE. Nevertheless, both the Kitaev quantum double model and the string-net model are powerful tools to study the properties of topological order and anyons.

1.4 Application to topological quantum computation

Along with the introduction of the quantum double model [47], Kitaev suggested that this model could be used as a platform to perform fault-tolerant quantum computation [47, 54, 55]. In fact, as topological order is robust to small local perturbations [56], these perturbations cannot cause decoherence in topologically ordered systems. The application of topological order is twofold. First, the degenerate ground-state space of a topologically ordered system can be used to store information in a decoherence protected way. For example, the toric code model based on a torus has a four-fold degenerate ground-state. A local perturbation may change the state of the spins on the lattice locally, but cannot make the system change from one ground-state into the other. Thus, the toric code has two topologically-protected qubits, and can serve as a quantum memory. Second, if one wants to realize actual quantum computation, more structure is needed. The global state of several non-Abelian anyons can have multiple outcomes, and each of these orthogonal states can serve as topologically protected qubits. By braiding these anyons with each other, it is then possible to process the encoded information [57, 55].

Motivated by these ideas, there has been in recent years an increased effort towards realizing toy models of topological order in experiments. In particular, several setups have realized the toric code model [58, 59, 60, 61, 62, 63]. Even the more complex string-net model has very recently been designed in experiments [64, 65, 66].

Both the possibility of using these models for topological quantum computation, and realizing them in experiments, raise the questions of how resistant topological order is to temperature, and how topological order can be characterized at finite temperature.

⁴An example of a model which realizes chiral topological order is the Kitaev honeycomb model [32], when supplemented by a three-spin term that breaks time-reversal symmetry.

1.5 Topological order at finite temperature

Since the middle of the 2000's, several works have studied the effects of finite temperature on topologically ordered systems. It has been shown that two-dimensional topological systems may be very fragile with respect to thermal fluctuations [38]. In particular, a general result concerning the thermodynamic limit has been obtained by Ref. [67] and states that, for two-dimensional Hamiltonians made of a sum of local commuting projectors such as the quantum double models or the string-net models, topological order does not survive at finite temperature. Nevertheless, results on the toric code and Kitaev quantum double model have revealed that topological order can persist below a size-dependent temperature [68, 69, 70].

An important question is how to characterize topological order at finite temperature. For example, the ground-state degeneracy can no longer be used to qualify topological order, as the thermal state is unique. Different proposals have been advanced in the literature: the coherence time for quantum memory [71, 72, 57, 73], non-zero expectation values of topological symmetry operators [38], or the persistence of long-range entanglement, which can be probed via the von Neumann entanglement entropy or the mutual information [74, 68, 69, 70]. Most of these studies have concentrated on the toric code model or on the quantum double model. Refs. [38, 39] found that the expectation value of topological symmetry operators for the toric code is zero at finite temperature. Additionally, Ref. [71] established that the coherence time of quantum memory in the toric code scales as $e^{\beta\Delta}$, where β is the inverse temperature and Δ the size of the spectral gap, which means that the coherence time is bounded from above in a way which does not depend on the system size. This means that, at finite temperature and in the thermodynamic limit, the information is lost after a finite time. Moreover, it has been shown that the toric code model is in the same universality class as the 1D Ising model, and therefore does not exhibit a finite temperature phase transition [39, 75].

Finally, Refs. [68, 69, 70] have analyzed the behavior of the topological mutual information for the toric code and the quantum double model and shown that it decreases to zero following a scaling law between temperature and system size. Topological entanglement entropy has also been studied in classical versions (i.e., in the infinite temperature limit) of string-nets and loop gases [74, 76].

1.6 Goal and structure of the thesis

The main focus of this thesis is to extend the study of finite temperature properties to the string-net models, that is, to all topological orders described by Drinfeld centers. We first approach the problem from a statistical mechanics point of view: from the study of the energy spectrum and its degeneracies, we derive the partition function of the string-net models. While it is simple to obtain the energy levels of these models, deriving their degeneracies is rather intricate. From the partition function, key object of statistical mechanics, most thermodynamical properties, such as energy, entropy, specific heat and the existence or absence of finite temperature phase transitions, can be derived easily.

In a second step, we also obtain the thermal averages of closed string operators, and study the mutual information of string net models. Finally, we show that many of the approaches can be carried over to the Kitaev quantum double model, where it also allows for a more general and detailed study of finite temperature properties as what was done previously.

The thesis is structured as follows. In part one (*chapter 2*), the necessary tools for studying anyons and topological order are introduced. This means in particular an introduction to unitary fusion categories (which are used to build the string-net models), to unitary modular tensor categories (which are used to describe anyons), and to the tube algebra, which is a tool to derive the Drinfeld center of a given unitary fusion category.

Part two contains the core work of the thesis, on the string-net models. In *chapter 3*, the string-net model is introduced. In *chapter 4*, using results from the tube algebra and the language of UMTCs, a general formula for the spectral degeneracies of string-net models is derived, which holds for any closed surface, any genus and any number of boundaries. We also discuss which degeneracies are topological in nature and which not, and introduce a refined Hamiltonian which splits all non-topological degeneracies. Additionally, several examples of categories and numerical results on their degeneracies are provided, and special cases are discussed. In *chapter 5*, the result on degeneracies is used to obtain the partition function for string-net models. From the partition function, we derive the entropy, average energy, and specific heat of the models, and show that there is no phase transition at finite temperature. This study also allows us to identify a special type of excitations in the Drinfeld center, pure fluxons, whose properties we discuss in greater detail. We then turn to compute thermal averages of quasiparticle operators. Using effective degeneracies for surfaces with punctures, we obtain an exact expression for the thermal average of projectors on quasiparticles. This allows us to derive closed loop operators, both non-contractible (around handles of the surface) and contractible. The latter are Wegner-Wilson loops, and can probe the presence of deconfined quasiparticles. We also present how to compute Wegner Wilson loops numerically. Finally, we study entanglement entropy and mutual information, and derive a scaling law between system size and temperature using a conjecture [69, 70] on the topological mutual information.

Part three focuses on the Kitaev quantum double model. In *chapter 6*, we present the model, and discuss similarities and differences with the string-net model. Finally, in *chapter 7*, following a similar reasoning as for the string-net model, we derive the spectral degeneracies of the quantum double model, as well as its partition function and the thermal average of projectors on quasiparticle sectors, from where we obtain the topological mutual information. *Chapter 8* contains a general conclusion. In the *Appendices A, B, and C*, we provide additional details on the connections between the tube algebra and the excitations of the string-net model. *Appendix D*, finally, present elements of a proof for a conjecture [69, 70] for topological mutual information both for the Kitaev quantum double model and the string net model.

This manuscript is based on the following publications:

- Chapter 4 is based on: A. Ritz-Zwilling, J.-N. Fuchs, S. H. Simon, and J. Vidal, *Topological and*

nontopological degeneracies in generalized string-net models, Phys. Rev. B 109, 045130 (2024),

- Chapter 5 is based on: A. Ritz-Zwilling, J.-N. Fuchs, S. H. Simon, and J. Vidal, *Finite-temperature properties of string-net models*, (2024), arXiv:2406.19713 (submitted to Phys. Rev. B).

During my thesis, I was also involved in a separate project related to the Kitaev honeycomb model [32], which is not included in this manuscript. The results of this project are published in:

- D. J. Alspaugh, J.-N. Fuchs, A. Ritz-Zwilling, J. Vidal, *Effective models for dense vortex lattices in the Kitaev honeycomb model*, Phys Rev. B 109, 115107 (2024).

Part I

Theoretical Background

Algebraic theory of anyons

This chapter contains an introduction to the main mathematical concepts on which the work of this thesis is based. Unitary fusion categories (UFC), on which the string-net model construction relies, are introduced. Then, more structure is added to the UFC in order to obtain a unitary modular tensor category (UMTC), which is the correct description of an anyon theory. The main ideas are summarized in Sec. 2.6.

2.1 Unitary fusion categories

The string-net models which will be discussed in this thesis are based on the data of unitary fusion categories (UFC). The data we need consists essentially of three pieces: a finite set of objects (the simple objects of a UFC \mathcal{C}), the fusion rules of these objects, and basis transformations between the fusion spaces of several objects. The structure of UFCs is discussed in the context of string-net models in, e.g., [48, 77, 78], and [28]. Further information on UFCs can be found e.g. in [79, 33, 80].

2.1.1 Fusion matrices

Let us consider a UFC \mathcal{C} with $N_{\mathcal{C}}$ simple objects $^1a, b, c, \dots$ (where simple means that it cannot be further decomposed into a direct sum of simple objects of \mathcal{C}). These objects obey fusion rules of the form

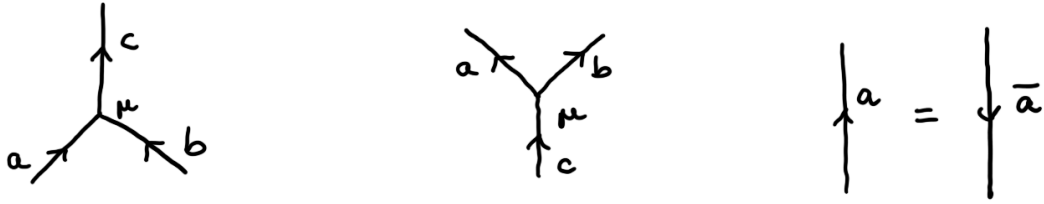
$$a \times b = \sum_c N_{ab}^c c, \quad (2.1)$$

where the fusion coefficients N_{ab}^c are nonnegative integers. When $N_{ab}^c = 0$, it means that c is not contained in the fusion outcome of $a \times b$. For a given a and b , there might be several non-zero N_{ab}^c . That is, there might be several fusion outcomes to the fusion of a with b . Objects with only one fusion outcome to the fusion with themselves (i.e., there is only one c for which N_{aa}^c is non-zero), are called *Abelian*. If there are several fusion outcomes, they are called *non-Abelian*. Note that the use of Abelian/non-Abelian is not the same here as for groups. Independently of the objects being Abelian or not, their fusion rules can in general be non-commutative, i.e., $a \times b \neq b \times a$.

¹Throughout the literature, and depending on the context, these objects are given different names: labels, anyons, particles, strings, topological sectors...

A fusion coefficient N_{ab}^c may be larger than 1. In this case, we say that there is a *fusion multiplicity*. It means that there are N_{ab}^c different, orthogonal, ways to obtain c from the fusion of a and b .

The fusion of a and b to c can be represented graphically as a fusion vertex, see Fig. 2.1a. To every directed edge, we associate a label $\in \mathcal{C}$. Here and for the rest of the thesis, we choose the convention that a fusion vertex is read counterclockwise, and $a \times b = c$ means that a and b are oriented towards the center of the vertex, and c is outwardly oriented, as shown in Fig. 2.1a. Such a vertex is further indexed by a quantum number μ that ranges from 1 to N_{ab}^c . The same fusion rules also apply to the upward vertex represented in Fig. 2.1b. If time is taken to run upwards, this vertex represents the splitting of c to a and b .



(a) A fusion vertex representing a particular vector in the N_{ab}^c -dimensional fusion space corresponding to $a \times b \rightarrow c$. The fusion vertex is read counterclockwise.

(b) Splitting of c to a and b . This vertex represents a particular vector in the N_{ab}^c -dimensional splitting space corresponding to $c \rightarrow a \times b$. This vertex can also be read as $\bar{b} \times \bar{a} = \bar{c}$. This is in fact the same as $a \times b = c$.

(c) Reversing the orientation of an edge changes a label to its dual.

Figure 2.1: Graphical rules for fusion

In a UFC, there always exists one object (we will denote it 1 in the following, and call it the *vacuum* or *trivial object* or *identity*) which fuses trivially with all the others: $a \times 1 = 1 \times a = a$, $\forall a$. For each object a there is also a unique dual object \bar{a} such that $N_{a\bar{a}}^1 = N_{\bar{a}a}^1 = 1$. It is possible that $a = \bar{a}$, this object is then called *self-dual*. Graphically, one can go from an object to its dual by reversing the corresponding arrow, see Fig. 2.1c. With this property, it is easy to see from Fig. 2.1a that $N_{ab}^c = N_{ca}^{\bar{b}} = N_{bc}^{\bar{a}}$. If a UFC possesses only self-dual objects, it is said to be self-dual and arrows are not needed.

A fusion coefficient N_{ab}^c can be thought of as an element $[N_a]_{b,c}$ of a $N_{\mathcal{C}}$ -dimensional square matrix N_a . The $N_{\mathcal{C}}$ matrices N_a , with $a \in \mathcal{C}$, are called fusion matrices.

2.1.2 Fusion trees and Hilbert space dimensions

Fusion vertices as shown in Fig. 2.1a, with $\mu = 1 \dots N_{ab}^c$, span a Hilbert space of dimension N_{ab}^c , i.e.,

$$\dim \mathcal{H}_{a \times b \rightarrow c} = N_{ab}^c. \quad (2.2)$$

We can also compute the Hilbert space dimension for n consecutive fusion processes of objects $a_1, a_2, a_3, \dots, a_n \in \mathcal{C}$, with overall fusion outcome $c \in \mathcal{C}$. This space is spanned by fusion trees as shown on the right-hand side of Fig. 2.2. Computing the Hilbert space dimension for this fusion

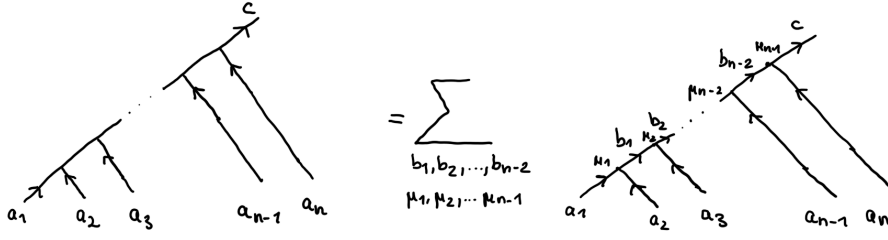


Figure 2.2: The fusion tree on the left-hand side represents the Hilbert space for the fusion of objects a_1, a_2, \dots, a_n into c . In order to compute the dimension of this Hilbert space, one has to sum over all possible labels of the intermediate fusion channels (unlabeled edges on the left-hand-side). This dimension is given by Eq. (2.3).

process means counting the number of all possible trees of the form of Fig. 2.2. This can be done by taking the product of the fusion coefficients associated to each vertex and summing over all possible internal edge labels:

$$\dim \mathcal{H}_{a_1 \times a_2 \times \dots \times a_n \rightarrow c} = \sum_{b_1, b_2, \dots, b_{n-2} \in \mathcal{C}} N_{a_1, a_2}^{b_1} N_{b_1, a_3}^{b_2} \dots N_{b_{n-2}, a_n}^c = [N_{a_2} N_{a_3} \dots N_{a_n}]_{a_1, b}, \quad (2.3)$$

where the second equality is given in terms of matrix products. In the following, we will adopt the convention that unlabeled edges and vertices mean that we sum over all possible values they can assume, see Fig. 2.2. Note that if one of the outer edges is labeled with the trivial object, one can erase this edge without changing the dimension of the Hilbert space. In the same way, one can also add edges labeled with the trivial object without changing the Hilbert space dimension.

If one fuses together n objects a , the corresponding Hilbert space dimension scales asymptotically (for large n) as $N_a^n \sim d_a^n$, where d_a is the largest eigenvalue of the fusion matrix N_a . The quantity d_a is called the *quantum dimension* of the object a . That is, the quantum dimension of an object is associated to the way how the Hilbert space grows with the number of objects. The quantum dimension is equal to one for an Abelian object (it is always one for the trivial object, $d_1 = 1$), and is larger than one for non-Abelian objects. However, it is not necessarily an integer. The quantum dimensions are conserved under fusion:

$$d_a \times d_b = \sum_{c \in \mathcal{C}} N_{ab}^c d_c. \quad (2.4)$$

From the quantum dimensions, one can define the *total quantum dimension* of the UFC:

$$\mathcal{D}_{\mathcal{C}} = \sqrt{\sum_{a \in \mathcal{C}} d_a^2}. \quad (2.5)$$

In the following, for notational convenience, we restrict the discussion to multiplicity-free cases, i.e., we set $N_{ab}^c = 1$ or $0 \forall a, b, c \in \mathcal{C}$. Therefore, we can omit in the following indices at the vertices. However, fusion multiplicities can be easily introduced if needed (see e.g. Appendix A of [48]).

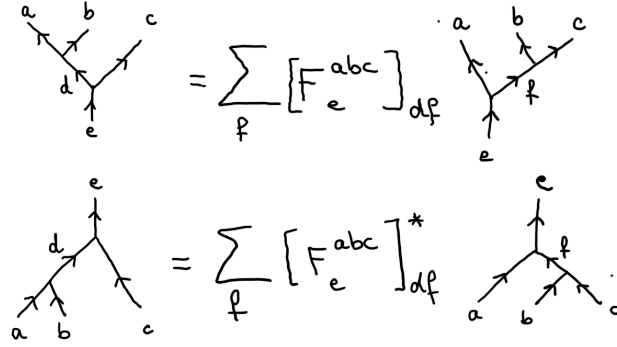


Figure 2.3: The F -matrix describes the unitary basis transformation between the two descriptions of the same fusion (or splitting) space. The star denotes complex conjugation.

2.1.3 F -symbols

The fusion rules are always associative:

$$a \times (b \times c) = (a \times b) \times c, \text{ for all } (a, b, c) \in \mathcal{C}. \quad (2.6)$$

This means, in particular, that the Hilbert space of the process of fusing first a and b and then c to e (spanned by fusion diagrams as represented on the left-hand side of Fig. 2.3), should have the same dimension as the Hilbert space for the process of first fusing b and c and then a to e (spanned by fusion diagrams as represented on the right-hand side of Fig. 2.3). That means, one should have

$$\sum_d N_{ab}^d N_{dc}^e = \sum_f N_{bc}^f N_{af}^e. \quad (2.7)$$

The unitary basis transformation between these two descriptions is given by the F -symbols (see Fig. 2.3). The convention adopted here to write the F -symbols follows Refs. [81, 28, 77]. A condition for an F -symbol not to be zero is that it relates two allowed fusion configurations, i.e., $N_{ab}^d, N_{dc}^e, N_{bc}^f, N_{af}^e$ are all non-zero.

Given a set of fusion rules, there is a set of consistency conditions on the F -symbols, known as the pentagon equations [32, 82, 83, 28] (see Fig.2.4), that assure that multiple changes of basis in complicated diagrams will give a consistent result (see Fig. 2.4). This condition reads

$$[F_e^{fcd}]_{gl} [F_e^{abl}]_{fk} = \sum_h [F_g^{abc}]_{fh} [F_e^{ahd}]_{gk} [F_k^{bcd}]_{hl}, \quad (2.8)$$

where the left-hand side corresponds to the upper route of Fig. 2.4 and the right-hand side to the lower route. For a given set of fusion rules, there may be several valid solutions to the pentagon equations, corresponding to different categories. These solutions are determined up to multiplicative constants (for multiplicity-free categories), which can be fixed by choosing an appropriate gauge [28, 78, 84].

2.1.4 Evaluating planar diagrams

So far, we have introduced fusion diagrams as a way to count the Hilbert space dimension associated with fusion or splitting of several objects. However, fusion diagrams which consist

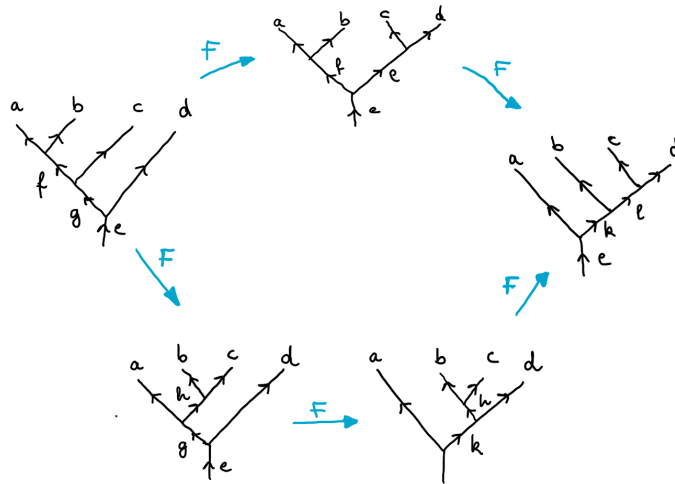


Figure 2.4: The pentagon equations ensure that different fusion processes yield consistent results.

both of fusion and splitting processes can also be evaluated to a complex number. For example, this complex number determines the quantum amplitude of a fusion or splitting process of anyons. The assembling of a fusion and a splitting vertex is evaluated as shown on Fig. 2.5 (here, time is taken to run upwards). The coefficient on the right-hand side, in terms of quantum dimensions, relies on a specific choice of normalization of the fusion vertices (see e.g. Appendix A in [77] for details). With the same normalization, the amplitude for a closed loop of an object a (which corresponds to the trivial object 1 splitting into a pair of a and \bar{a} , which then fuse back to 1) is simply the quantum dimension of a , d_a (see Fig. 2.6).

In addition, we introduce the completeness relation Fig. 2.7.

$$\begin{array}{c} \uparrow b \\ \circlearrowleft \\ \uparrow a \end{array} = \sqrt{\frac{d_c d_d}{d_a}} \delta_{a,b} \begin{array}{c} | \\ \uparrow \\ | \\ a \end{array}$$

$$\begin{array}{c} \circlearrowleft \\ a \end{array} = d_a$$

Figure 2.5: Evaluation of a splitting process followed by a fusion process.

Figure 2.6: A particular case of Fig.2.5 is when the splitting comes from the vacuum and objects fuse back to the vacuum.

$$\begin{array}{c} | \\ \uparrow \\ | \\ a \end{array} \begin{array}{c} | \\ \uparrow \\ | \\ b \end{array} = \sum_c \sqrt{\frac{d_c}{d_a d_b}} \begin{array}{c} \begin{array}{c} \uparrow a \\ \circlearrowleft \\ \uparrow b \end{array} \\ \uparrow c \\ \begin{array}{c} \downarrow a \\ \downarrow b \end{array} \end{array}$$

Figure 2.7: Completeness relation

The three rules represented on Fig. 2.6, 2.5 and 2.7 along with the F -symbols defined above (Fig. 2.3) provide a consistent description of a planar diagram algebra. In particular, any planar

diagram without open ends (i.e., coming from the vacuum and going back to the vacuum, see e.g. Fig. 2.8) can be evaluated to a complex amplitude.

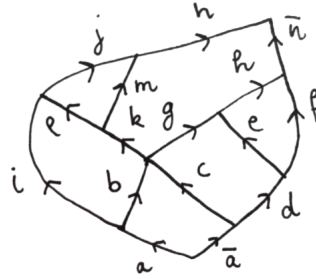


Figure 2.8: A planar diagram that can be reduced to a complex number by applying F -moves and the relations of Fig. 2.6, 2.5 and 2.7.

2.2 Unitary modular tensor categories

With the content of UFCs, we can describe fusion and splitting processes in the two-dimensional plane. In fact, in the context of anyons, we may read the previously introduced fusion diagrams as representing worldlines of a particle in 1+1D. However, if we want to describe anyons in 2+1D, we also need to describe braiding, and hence to allow for under- and over-crossings of worldlines. To do so, we need to add some additional structure to UFCs. As we have seen, UFCs can have commutative or non-commutative fusion rules. When fusion rules are commutative, one may add a braiding structure, in order to get a unitary braided fusion category (UBFC). For UBFCs, two matrices, called T and S , are of particular importance. If these matrices are unitary, the category becomes a unitary modular tensor category (UMTC). UMTCs provide the appropriate framework for describing anyons and topological order. In fact, a UMTC determines uniquely a 2+1D topological quantum field theory [85, 86]. In the following sections, we will discuss the additional structure required for UMTCs. The following discussion is mainly based on Refs. [32, 82] and [28].

2.2.1 Braiding

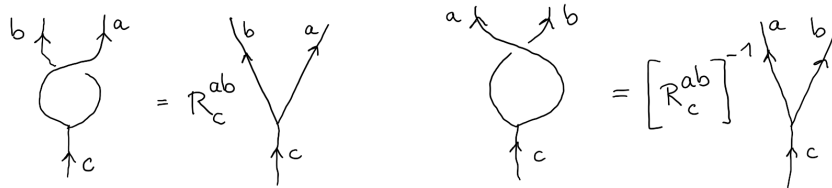


Figure 2.9: R -move and its inverse.

As discussed in the introduction, an essential property of anyons are their (non-trivial) braiding properties. The crossing of the worldlines of two anyons a and b is encoded in the R -moves, as

shown in Fig. 2.9. The R -move relates a process in which an object c splits into a and b , and the lines of a and b cross, to a process where lines do not cross, see Fig. 2.9. More precisely, R_c^{ab} defines the process in which a crosses over b , and $[R_c^{ba}]^{-1}$ the process in which a crosses under b . By definition, R_c^{ab} is zero if $N_{ab}^c=0$. The crossing of the vacuum with any other object is trivial: $R_a^{1a} = R_a^{a1} = 1$.

An overcrossing followed by an undercrossing (or vice versa) generates a braid, see Fig. 2.10. The amplitude of a full braid can be related to the case of no braiding by applying an F -move followed by two R -moves.

An object which braids trivially with all other objects in the category, i.e.,

$$R_c^{ab} R_c^{ba} = 1 \forall b, c \text{ if } N_{ab}^c > 0, \tag{2.9}$$

is said to be *transparent*. The vacuum is always transparent.

In the same way as F -moves have to satisfy the pentagon equations in order to be consistent with the fusion rules, the R -moves have to satisfy a set of consistency equations (which actually involves combinations of F -moves and R -moves) called the hexagon equations [32, 82, 83, 28, 85] (see Fig. 2.11):

$$R_e^{ca} [F_d^{acb}]_{eg} R_g^{cb} = \sum_f [F_d^{cab}]_{ef} R_d^{cf} [F_d^{abc}]_{fg}, \tag{2.10}$$

$$[R_e^{ac}]^{-1} [F_d^{acd}]_{eg} [R_g^{bc}]^{-1} = \sum_f [F_d^{cab}]_{ef} [R_d^{fc}]^{-1} [F_d^{abc}]_{fg}. \tag{2.11}$$

Unitary fusion categories which have a braiding defined are called unitary braided fusion categories, or UBFC. With the R -moves, the F -symbols and the rules from Sec. 2.1.4, one can evaluate any process in $2 + 1D$.

2.2.2 T - and S -matrices

For UBFCs, one can consider two additional quantities which derive from the braiding properties: the T -matrix (linked to self-statistics, or twist, of the anyons) and the S -matrix (linked to mutual exchange statistics of two different anyon types). If the S -matrix is unitary, the UBFC is known as unitary modular tensor category (UMTC). In this case, T and S are collectively known as the *modular matrices* [85]. However, T and S can also be defined if S is not unitary.

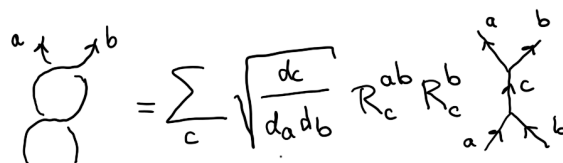


Figure 2.10: A full braid can be resolved by using the completeness relation of Fig. 2.7, the relation of Fig. 2.5, and two R -moves as defined in Fig. 2.9.

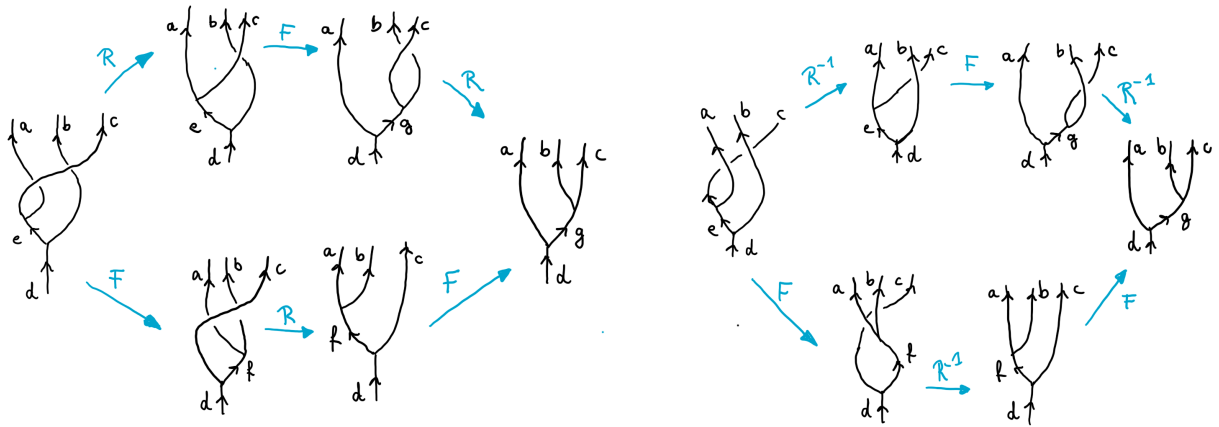


Figure 2.11: Diagrammatic representation of the hexagon equations.



Figure 2.12: On the left, definition of a T -matrix element T_{aa} , which corresponds to an exchange between two identical anyons a . The picture on the right shows how this exchange is equivalent to a twist in the worldline of an anyon a . On the right-hand-side of this picture, we enlarge the worldline into a ribbon in order to clearly show the rotation by 2π .

T -matrix

The T -matrix is a diagonal and unitary matrix with elements $T_{ab} = \theta_a \delta_{a,b}$, where θ_a describes the twist in a worldline of an anyon a . This is represented on the left side of Fig. 2.12. Importantly, an anyon and its dual have the same twist:

$$\theta_a = \theta_{\bar{a}}. \tag{2.12}$$

Imagining the worldline to have some thickness (like a ribbon) and pulling straight the diagram on the left side of Fig. 2.12 leads to the representation on the right side, which shows a twisted worldline. This twist corresponds to a 2π rotation of the anyon around itself. The phase accumulated during this rotation can be related to the topological spin s_a of the anyon

$$\theta_a = e^{2i\pi s_a}. \tag{2.13}$$

In fact, for integer spins (bosons), via Eq. (2.13), one obtains a twist of $\theta_b = 1$ in agreement with their mutual exchange statistics, and for half-integer spins (fermions) one obtains $\theta_f = -1$. The vacuum has $\theta_1 = 1$.

S -matrix

Just as one can write a special matrix T for self-statistics of anyons, one can write a matrix, called the S -matrix, which describes the mutual exchange statistics for two different anyons. As

represented in Fig. 2.13, a matrix element $S_{a,b}$ gives the amplitude of a process in which two pairs of anyons (a, \bar{a}) and (b, \bar{b}) are created, a is brought around b , and then the pairs reannihilate again, normalized by the total quantum dimension \mathcal{D} .

In the particular case where anyon b is transparent, the S -matrix takes a simple value in terms of the quantum dimensions:

$$S_{a,b} = \frac{d_a d_b}{\mathcal{D}}. \quad (2.14)$$

In particular, in the case where one of the anyons is the vacuum, the S -matrix is

$$S_{a,1} = S_{1,a} = \frac{d_a}{\mathcal{D}}. \quad (2.15)$$

Note that this is in agreement with the normalization of Fig. 2.6.

The S -matrix is unitary (as a consequence, the determinant of S is non-zero, $\det S \neq 0$) if and only if the only transparent particle in the theory is the vacuum particle [32, 28] (if there were another transparent particle a besides the identity, the rows S_{ab} and S_{1b} would be proportional to each other, and the matrix could not be unitary). The unitary S -matrix is also called the *modular S -matrix*. We will make extensive use of the modular S -matrix throughout this thesis, and therefore detail its properties below.

The modular S -matrix is symmetric:

$$S_{a,b} = S_{b,a} \quad \forall a, b \quad (2.16)$$

Additionally,

$$S_{\bar{a},b} = S_{a,b}^*. \quad (2.17)$$

As a consequence of unitarity,

$$S^\dagger S = S S^\dagger = 1 \quad \rightarrow \quad \sum_c S_{a,c} S_{b,c}^* = \delta_{a,b}. \quad (2.18)$$

In general, if the fusion rules of a UFC are commutative, one can find a unitary matrix that diagonalizes simultaneously all the fusion matrices. If the category is modular (i.e., is a UMTC), this unitary matrix is precisely the S -matrix, so that

$$N_a = S \lambda_a S^\dagger, \quad [\lambda_a]_{b,c} = \delta_{b,c} \frac{S_{a,b}}{S_{1,b}}, \quad (2.19)$$

or in other terms,

$$N_{ab}^c = \sum_k \frac{S_{ak} S_{bk} S_{ck}^*}{S_{1k}}. \quad (2.20)$$

This is the famed Verlinde formula [87, 27]. In cases where the category is not modular but commutative, one can still find a unitary matrix (which is not the S -matrix) diagonalizing the

$$S_{a,b} = \frac{1}{\mathcal{D}} \times \text{Diagram}$$

Figure 2.13: Graphical representation of an S -matrix element.

fusion matrices. This matrix then also verifies the Verlinde formula, and is sometimes called the *mock S-matrix*. To distinguish it from the modular S -matrix, we will denote it with a tilde, \tilde{S} , throughout the thesis.

The origin of the name *modular matrices* for T and S comes from the fact that together they generate a set of operations forming a group known as the *modular group* [28]:

$$S^2 = C, \quad C^2 = 1, \quad (ST)^3 = C. \quad (2.21)$$

Here, C is the charge-conjugation matrix defined as $C_{a,b} = \delta_{a,\bar{b}}$, i.e., a matrix element $C_{a,b}$ is non-zero if a is the dual of b . Finally, the S -matrix elements can be expressed in terms of the twists (see e.g. Eq. 223 in [32]):

$$S_{a,b} = \frac{1}{\mathcal{D}} \sum_c N_{a\bar{b}}^c \frac{\theta_c}{\theta_a \theta_b} d_c. \quad (2.22)$$

2.2.3 Chirality

A quantity known as the topological central charge c may be defined via [3]

$$e^{2i\pi c/8} = \frac{1}{\mathcal{D}} \sum_a d_a^2 \theta_a. \quad (2.23)$$

A theory is said to be achiral if $c = 0$. The topological central charge is equal to the chiral central charge modulo 8. The latter depends on the edges and quantifies the heat transport by the edge states [88, 32].

2.3 Examples

As an illustration of the concepts discussed in this chapter, we present here three cases of UFC/UMTC which are well-known in the literature: $\text{Vec}(\mathbb{Z}_2)$, $\text{Rep}(S_3)$, and Fibonacci (see e.g. [82, 6, 28]). The first one is an example of a UFC built from the elements of a group (\mathbb{Z}_2), and is braided but not modular. The second one is an example of a UFC built from the irreducible representations of a non-commutative group (irreducible representations of S_3). It is also braided but not modular. The last one is an example of a UMTC containing one non-Abelian anyon.

$\text{Vec}(\mathbb{Z}_2)$

$\text{Vec}(\mathbb{Z}_2)$ has two objects, which are the elements of the group \mathbb{Z}_2 : 1 and s , 1 being the trivial object. Both objects are self-dual. The fusion rules correspond to the multiplication rules of the group. They are shown on Fig. 2.14, next to a graphical representation in terms of fusion vertices (we adopt the convention that 1 is represented by a black line and s by a red line, and do not draw arrows as the objects are self-dual). These fusion rules can also be written in the form of two 2×2 -dimensional fusion matrices (where the first line/column corresponds to object 1 and the second line/column to s):

$$N_1 = \begin{pmatrix} 1 & 0 \\ 0 & 1 \end{pmatrix}, \quad N_s = \begin{pmatrix} 0 & 1 \\ 1 & 0 \end{pmatrix}. \quad (2.24)$$

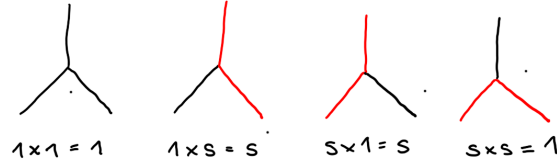


Figure 2.14: Fusion rules and fusion vertices for $\text{Vec}(\mathbb{Z}_2)$. We adopt the convention that 1 is represented by a black line and s by a red line, and do not draw arrows as the objects are self-dual.

As all objects are Abelian, the quantum dimensions are $d_1 = d_s = 1$ and the total quantum dimension is $\mathcal{D} = \sqrt{2}$. The F -symbols are all given by the fusion rules (i.e., they are all 0 or 1):

$$[F_d^{abc}]_{ef} = N_{ab}^d N_{dc}^e N_{bc}^f N_{af}^e, \quad \forall a, b, c, d, e, f \in \{1, s\}. \quad (2.25)$$

In general, for any UFC built from a group G , one valid set of solution is given by choosing all quantum dimensions to be 1 and all F -symbols to be 1 or 0. The only potentially non-trivial R -move is the one where s crosses with s , that is R_1^{ss} . From the hexagon equations, one finds the constraint $[R_1^{ss}]^2 = 1$ so that $R_1^{ss} = \pm 1$. The choice $R_1^{ss} = +1$ leads to $\theta_s = 1$. Then, s is a boson. The choice $R_1^{ss} = -1$ leads to $\theta_s = -1$, then s is a fermion. In both cases, the S -matrix is

$$S_{\mathbb{Z}_2} = \frac{1}{\sqrt{2}} \begin{pmatrix} 1 & 1 \\ 1 & 1 \end{pmatrix}, \quad (2.26)$$

which is not unitary. As the fusion rules are commutative, one can however find a unitary mock- S matrix which diagonalizes the fusion rules:

$$\tilde{S}_{\mathbb{Z}_2} = \frac{1}{\sqrt{2}} \begin{pmatrix} 1 & 1 \\ 1 & -1 \end{pmatrix}. \quad (2.27)$$

This matrix is also the modular S -matrix of the semion UMTC, which has the same objects and fusion rules as $\text{Vec}(\mathbb{Z}_2)$, but a different set of F -matrices.

$\text{Rep}(S_3)$

Besides elements of a group, another possible set of simple objects for a UFC are the irreducible representations of a group. Here, we consider the irreducible representations of S_3 , which is the group of symmetries of the equilateral triangle, comprising the identity e , two rotations of angle $2\pi/3$ y and y^2 and three reflections along the symmetry axes x , xy and xy^2 . The fusion rules of the group are non-commutative, in fact one has $xy^2 = yx$. The group has three irreducible representations (irreps), two of which are one dimensional, Γ_1 the trivial representation, and Γ_{-1} the alternating representation, and one is two-dimensional (Γ_2). The UFC $\text{Rep}(S_3)$ has three elements which we will denote 1, 2, 3 and which correspond respectively to Γ_1 , Γ_{-1} and Γ_2 . The quantum dimensions of these objects correspond to the dimensions of the irreps: $d_1 = d_2 = 1$, $d_3 = 2$. The fusion rules (see Fig. 2.15) correspond to the composition rules of the irreducible representations. Object 3 is non-Abelian, and its fusion rule $3 \times 3 = 1 + 2 + 3$ takes the same form as $\Gamma_2 \otimes \Gamma_2 = \Gamma_1 \oplus \Gamma_{-1} \oplus \Gamma_2$. The S -matrix is non-modular, but one can define a mock- S -matrix

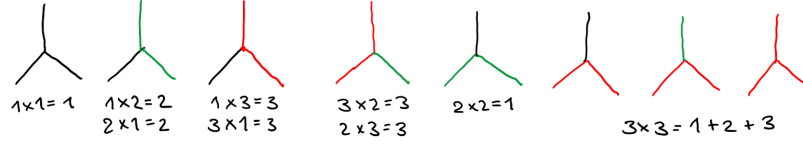


Figure 2.15: Fusion rules and allowed fusion vertices of $\text{Rep}(S_3)$. As fusion rules are commutative, we represent only one fusion vertex for $a \times b = b \times a$. Objects are represented by the following colors: 1 black, 2 green, 3 red.

which diagonalizes the fusion rules:

$$S_{\text{Rep}(S_3)} = \frac{1}{\sqrt{6}} \begin{pmatrix} 1 & 1 & 2 \\ 1 & 1 & 2 \\ 2 & 2 & 4 \end{pmatrix}, \quad \tilde{S}_{\text{Rep}(S_3)} = \frac{1}{\sqrt{6}} \begin{pmatrix} 1 & \sqrt{2} & \sqrt{3} \\ 1 & \sqrt{2} & -\sqrt{3} \\ 1 & -\sqrt{2} & 0 \end{pmatrix}. \quad (2.28)$$

Fibonacci

The Fibonacci category will be our preferred example throughout the rest of this chapter. It is a UMTC which contains two objects (anyons): the trivial object 1 and a non-Abelian object τ . Both objects are self-dual. We depict their fusion rules on Fig. 2.16.

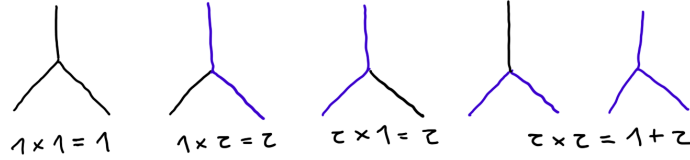


Figure 2.16: Fusion rules for the Fibonacci category. 1 is represented in black and τ in blue.

These fusion rules can also be written in the form of two 2×2 -dimensional fusion matrices (where the first line/column corresponds to object 1 and the second line/column to τ):

$$N_1 = \begin{pmatrix} 1 & 0 \\ 0 & 1 \end{pmatrix}, \quad N_\tau = \begin{pmatrix} 0 & 1 \\ 1 & 1 \end{pmatrix}. \quad (2.29)$$

Quantum dimensions are $d_1 = 1$ and $d_\tau = \phi$, where ϕ is the golden ratio $\phi = \frac{1+\sqrt{5}}{2}$. The total quantum dimension is $\mathcal{D} = \sqrt{1 + \phi^2}$. Most F -symbols are simply given by the fusion rules (i.e. are 0 or 1):

$$[F_d^{abc}]_{ef} = N_{ab}^d N_{dc}^e N_{bc}^f N_{af}^e, \quad \text{with } a, b, c, d, e, f \in \{1, \tau\}. \quad (2.30)$$

The only non-trivial F -symbols are:

$$\begin{aligned} [F_\tau^{\tau\tau\tau}]_{11} &= \phi^{-1}, & [F_\tau^{\tau\tau\tau}]_{1\tau} &= \phi^{-1/2}, \\ [F_\tau^{\tau\tau\tau}]_{\tau 1} &= \phi^{-1/2}, & [F_\tau^{\tau\tau\tau}]_{\tau\tau} &= -\phi^{-1}. \end{aligned} \quad (2.31)$$

The only non-trivial braiding is τ with τ . The corresponding R -symbols are: $R_1^{\tau\tau} = e^{-4\pi i/5}$ and $R_\tau^{\tau\tau} = e^{3\pi i/5}$. The twist of τ is $\theta_\tau = e^{4\pi i/5}$. The S -matrix is unitary:

$$S_{\text{Fib}} = \frac{1}{\sqrt{1+\phi^2}} \begin{pmatrix} 1 & \phi \\ \phi & -1 \end{pmatrix}. \quad (2.32)$$

2.4 Overview on categories

As an intermediate summary, we present below on Fig. 2.17 a possible classification of UFCs, according to the additional structure discussed in this chapter. In blue, examples of categories, which have been discussed in Sec. 2.3 or will be discussed in later chapters. Many examples of categories can be found in [82], [85] and on [89].

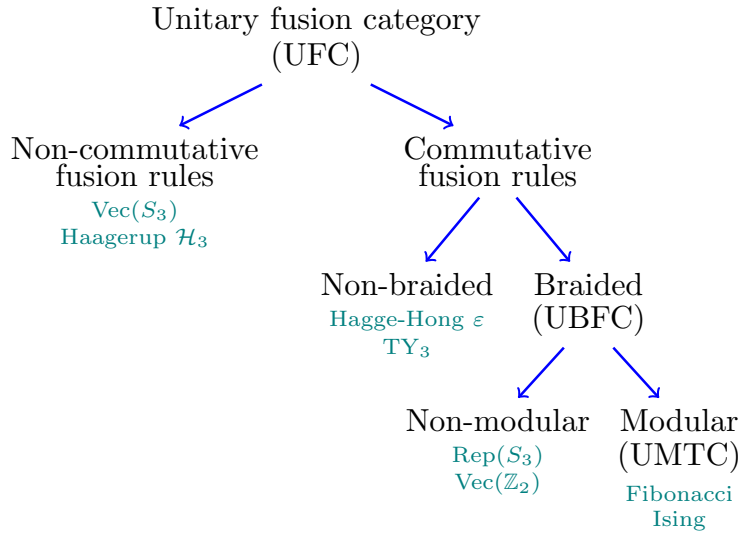


Figure 2.17: A possible classification of unitary fusion categories. In teal, examples that are presented in this thesis. Other characteristics mentioned in this chapter but left out of this classification are Abelian (only \mathbb{Z}_2 in the presented examples) or non-Abelian and with or without fusion multiplicities (only Hagge-Hong in the presented examples has fusion multiplicities).

2.5 Drinfeld centers

Both models discussed in this thesis (string-net models and Kitaev quantum double, see Chap. 3 and Chap. 6) realize topological orders corresponding to the Drinfeld center $\mathcal{Z}(\mathcal{C})$ of a unitary fusion category \mathcal{C} . A Drinfeld center is a special type of UMTC. Here, we present how to describe specifically a Drinfeld center, and how to construct a Drinfeld center $\mathcal{Z}(\mathcal{C})$ from the corresponding UFC \mathcal{C} . We first discuss the simpler case when \mathcal{C} is a unitary modular tensor category, and then address the more general case, which requires the use of the *tube algebra* construction [90, 84]. In the following, we adopt the convention that lowercase roman letters denote objects of \mathcal{C} while capital roman letters denote objects of $\mathcal{Z}(\mathcal{C})$. The vacua of both theories are respectively denoted 1 and $\mathbf{1}$.

$$\text{Loop } A = \sum_{s \in \mathcal{C}} n_{A,s} \text{Loop } s$$

Figure 2.18: Relation between a single loop of $A \in \mathcal{Z}(\mathcal{C})$ and single loops of simple objects of \mathcal{C} .

2.5.1 Properties of Drinfeld centers

A simple object A of the Drinfeld center is formally given by [83]

$$A = \left(\bigoplus_s n_{A,s} s, \Omega_A \right), \quad (2.33)$$

where $n_{A,s}$ is a nonnegative integer, also called *multiplicity*, counting the number of times the simple object $s \in \mathcal{C}$ appears in the simple object $A \in \mathcal{Z}(\mathcal{C})$, and where the halfbraiding tensor Ω_A contains all braiding properties of A . Let us stress that these multiplicities are unrelated to the fusion multiplicities introduced in the previous sections. Thinking about our graphical representation for objects/anyons, one may see A as a rope made of different types of strands (with a weight $n_{A,s}$ for the strand s) endowed with braiding properties defined by Ω_A . If the input category \mathcal{C} is commutative, one has $n_{A,s} \in \{0, 1\}$. By contrast, for noncommutative \mathcal{C} , $n_{A,s}$ can take integer values larger than 1 (see Sec. 2.5.3 below). The multiplicities also relate the quantum dimensions of the objects in $\mathcal{Z}(\mathcal{C})$ to those of \mathcal{C} (see Fig. 2.18):

$$d_A = \sum_{s \in \mathcal{C}} n_{A,s} d_s. \quad (2.34)$$

The total quantum dimension of the Drinfeld center, $D_{\mathcal{Z}}$ is the square of the total quantum dimension of \mathcal{C} , $D_{\mathcal{C}}$:

$$D_{\mathcal{Z}} = D_{\mathcal{C}}^2. \quad (2.35)$$

The halfbraidings Ω_A for $A \in \mathcal{Z}(\mathcal{C})$ are complex matrices $[\Omega_{A,tsj}^i]_{a,b}$ (here we follow the notations of [48]). i, t, s, j take values in \mathcal{C} and a, b are two additional indices that range respectively from 1 to $n_{A,t}$ and from 1 to $n_{A,s}$. Graphically, the Ω_A define the crossing of a simple object of $\mathcal{Z}(\mathcal{C})$ with a simple object of \mathcal{C} :

$$\text{Crossing } A \text{ and } i = \sum_{t,s,j \in \mathcal{C}} n_{A,t} n_{A,s} \sum_{a=1}^{n_{A,t}} \sum_{b=1}^{n_{A,s}} [\Omega_{A,tsj}^i]_{a,b} \text{Crossing } t \text{ and } s$$

Here, the indices a, b are associated to the open ends of the strings t and s . These indices get contracted when strings are fused together [78]. Halfbraidings which describe a crossing of $A \in \mathcal{Z}(\mathcal{C})$ with the vacuum $1 \in \mathcal{C}$ have a particularly simple expression,

$$[\Omega_{A,tsj}^1]_{a,b} = \delta_{t,s} \delta_{j,s} \delta_{a,b}, \quad (2.37)$$

where we recover the fact that an object A is a superposition of strings $s \in \mathcal{C}$, in agreement with Eq. (2.33). Similarly to the F -symbols, the halfbraidings are non-zero only if fusion rules are respected

(and additionally, if $n_{A,s}$ and $n_{A,t}$ are non-zero). That is,

$$[\Omega_{A,t;sj}^i]_{a,b} \propto N_{is}^j N_{ti}^j n_{A,t} n_{A,s}. \quad (2.38)$$

Moreover, the halfbraidings verify a consistency condition with the F -symbols of \mathcal{C} , which is similar to the hexagon equations (see [78, 48]). The T -matrix and the S -matrix of the Drinfeld center can both be expressed in terms of the halfbraidings (for the exact expressions, see [78, 48]). By construction, the topological central charge [see Eq. (2.23)] of a Drinfeld center is always $c = 0$ [51].

2.5.2 Drinfeld centers from UMTCs

Only in this section, we denote by a bar over an object \bar{a} the mirror object of a of inverse chirality, and not its dual object. A special case of a Drinfeld center is when the input theory \mathcal{C} itself is a UMTC. Then, the Drinfeld center is the product of two copies of \mathcal{C} of opposite chiralities [51]:

$$\mathcal{Z}(\mathcal{C}) = \mathcal{C} \times \bar{\mathcal{C}}. \quad (2.39)$$

In this case, any simple object A of the center can be represented by a couple (i, \bar{j}) of simple objects $i \in \mathcal{C}$ and $\bar{j} \in \bar{\mathcal{C}}$, and if \mathcal{C} has $\mathcal{N}_{\mathcal{C}}$ simple objects, its Drinfeld center has $\mathcal{N}_{\mathcal{C}}^2$ simple objects. The vacuum $\mathbf{1}$ is given by the pair $(1, \bar{1})$. Any property of $\mathcal{Z}(\mathcal{C})$ can simply be derived from the properties of the input objects. For example for $A = (i, \bar{j})$, the quantum dimension will be $d_A = d_i d_{\bar{j}}$. Fusion rules can be derived in a similar way:

$$A \times B = (i, \bar{j}) \times (i', \bar{j}') = \sum_{k, \bar{q}} N_{ii'}^k N_{\bar{j}\bar{j}'}^{\bar{q}}(k, \bar{q}) = \sum_{\mathcal{C}} N_{AB}^{\mathcal{C}}. \quad (2.40)$$

In the same way, the twist is given by:

$$\theta_{(i, \bar{j})} = \theta_i \theta_{\bar{j}} = \theta_i \theta_{\bar{j}}^{-1}, \quad (2.41)$$

because inverting the chirality inverts the twist of the objects. Finally, an important property which we will use later on is that the S -matrix of the Drinfeld center $\mathcal{Z}(\mathcal{C})$ has a simple expression in terms of the S -matrix of the input category \mathcal{C} (for clarity, we will denote them respectively S and s):

$$S_{A,B} = S_{(i, \bar{j}), (p, \bar{q})} = s_{i,p} s_{\bar{j}, \bar{q}}^*. \quad (2.42)$$

Example: Fibonacci

Let us construct, as an example, the Drinfeld center of the Fibonacci category which we introduced in Sec. 2.3. Starting from the two objects 1 and τ and taking $\mathcal{Z}(\text{Fib}) = \text{Fib} \times \overline{\text{Fib}}$, we find that the Drinfeld center has four objects labeled by $(1, \bar{1})$, $(1, \bar{\tau})$, $(\tau, \bar{1})$, $(\tau, \bar{\tau})$, with respective dimensions $(1, \phi, \phi, \phi^2)$ and twists $1, e^{i4\pi/5}, e^{-i4\pi/5}, 1$. From Eq. (2.23), we can verify that the topological central charge is in fact $c = 0 \pmod{8}$. Since the input category Fib has commutative fusion rules,

we know that $n_{A,s} = 0$ or 1 . Using Eq. (2.34), we can deduce the multiplicities (which we represent in the form of a rectangular matrix $\mathbf{n} = \{n_{A,s}\}$ with rows $A \in \mathcal{Z}(Fib)$ and columns $s \in Fib$):

$$\mathbf{n} = \begin{pmatrix} 1 & 0 \\ 0 & 1 \\ 0 & 1 \\ 1 & 1 \end{pmatrix}. \tag{2.43}$$

2.5.3 Tube algebra

In the general case, the construction of the Drinfeld center is less obvious. As a matter of fact, it is not even possible, in the general case, to make a prediction on the number of objects in $\mathcal{Z}(\mathcal{C})$ based solely on the number of objects in \mathcal{C} .

One systematic way to build the Drinfeld center of a UFC consists in deriving and decomposing the *Ocneanu tube algebra* [90, 91] (also called "*Q-algebra*" in [84]). The tube algebra method starts from the simple objects and their fusion rules in \mathcal{C} and derives the simple objects in $\mathcal{Z}(\mathcal{C})$, their halfbraidings and their multiplicities. Note that there exist different types of tube algebra, depending on the number of open ends or legs of the tubes. Here, we present the tube algebra approach adapted to the string-net model [48, 84, 77, 78]. Other versions of tube algebra have been studied e.g. in [92, 93, 94].

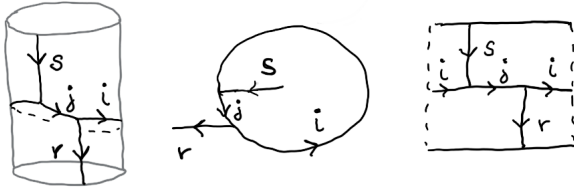


Figure 2.19: Three equivalent representations of a tube. A tube Q_{rsj}^i is labeled by four objects $i, j, r, s \in \mathcal{C}$. The open ends r and s determine the sector of the tube algebra.

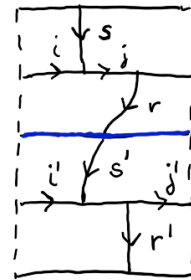


Figure 2.20: Two tubes are stacked vertically (the shared border is shown in blue). This stacking is non-zero only if $r = s'$.

The starting point of this method are the tubes. A tube consists of two open string ends s and r , and two strings without open ends i and j , with $i, j, r, s \in \mathcal{C}$. Fig. 2.19 shows three different, equivalent ways to represent a tube. The left representation underlines the origin of the name: a tube is a small fusion diagram of strings i, r, s, j , placed on a tube so that the strings i and j wind around the tube, while s and r end at the borders of the tube (the rightmost diagram also represents a tube but drawn in the plane, the left and right borders are identified with each other). In fact, tubes are constructed according to the fusion rules of \mathcal{C} , so the number of tubes is given by

$$\mathcal{N}_{\mathcal{T}} = \sum_{i,r,s,j} N_{si}^j N_{j\bar{r}}^i. \tag{2.44}$$

The diagram in the middle of Fig. 2.19 (which is the one chosen in [84]), allows for an intuitive interpretation of the tube algebra. The aim of the tube algebra is to find the simple objects (i.e.,

anyons) of $\mathcal{Z}(\mathcal{C})$, which can be seen as "strands" composed of several objects of \mathcal{C} [see Eq. (2.33)]. A tube inserted around a region containing such an object A will be able to connect to it if the label s on the inner edge of the tube correspond to some string in A . Therefore, tubes can be seen as a pre-stage of projectors onto objects $A \in \mathcal{Z}(\mathcal{C})$. Decomposing the tube algebra will allow us to determine these projectors as linear combinations of the tubes.

In the following, we will denote tubes as Q_a , where a is understood to be an integer ranging from 1 to $\mathcal{N}_{\mathcal{T}}$. The tube algebra (\mathcal{TA}) is defined by the operation of stacking tubes on top of each other (see Fig. 2.20). Formally, we may write

$$Q_a Q_b = \sum_c f_{ab}^c Q_c, \quad (2.45)$$

where the structure factor f_{ab}^c can be derived in terms of the F -symbols of \mathcal{C} (see Appendix A). Importantly, the tube algebra splits into different sectors which behave independently under the stacking operation. These sectors depend on the labels of the open edges r and s of the tubes. The tube algebra is a semi-simple algebra which is, according to the theorem of Artin-Wedderburn, isomorphic to a direct sum of simple matrix algebras (see e.g. [92]). That means one can decompose the tube algebra as

$$\mathcal{TA} \simeq \oplus_A \mathcal{M}_{n_A}, \quad (2.46)$$

where \mathcal{M}_{n_A} are simple matrix algebras (or simple modules over \mathcal{TA}) of dimension n_A . Each of these $\mathcal{N}_{\mathcal{Z}}$ modules corresponds to another simple object of $\mathcal{Z}(\mathcal{C})$. The idea of decomposing the tube algebra is similar to finding irreducible representations of a group. In the latter case, one can use the multiplication rules of the group to derive a canonical representation, and then block-diagonalize this representation to find the irreducible representations. In the present case, we look for a canonical representation of the tube algebra and for its block-decomposition. Each block corresponds to a simple module over the algebra.

The first step is to construct a vector space of dimension $V = \sum_{A=1}^{\mathcal{N}_{\mathcal{Z}}} n_A$ in which to represent \mathcal{TA} . This can be done via idempotent decomposition. It means searching for $\mathcal{N}_{\mathcal{T}}$ operators $p_A^{\alpha\beta}$ as linear combinations of the tubes, so that they verify

$$p_A^{\alpha\beta} p_B^{\gamma\nu} = \delta_{\beta,\gamma} \delta_{A,B} p_A^{\alpha\nu}, \quad \mathbb{1}_{\mathcal{TA}} = \sum_{\alpha,A} p_A^{\alpha\alpha}, \quad \text{Tr}(p_A^{\alpha\beta}) = \delta_{\alpha\beta}, \quad (2.47)$$

and $p_A^{\alpha\beta}$ cannot be written as a sum of other operators verifying the conditions of Eq. (2.47). Among these $\mathcal{N}_{\mathcal{T}}$ operators, V are idempotents $(p_A^{\alpha\alpha})^2 = p_A^{\alpha\alpha}$ and correspond to diagonal elements of the basis. $N_{\mathcal{T}} - V$ are nilpotents $(p_A^{\alpha\beta})^2 = 0$ ($\beta \neq \alpha$) and correspond to off-diagonal elements of the basis.

In particular, the sum of the simple idempotents belonging to a block A is a simple central idempotent of \mathcal{TA} , i.e., they commute with all the tubes:

$$P_A = \sum_{\alpha=1}^{n_{A,1}} p_A^{\alpha\alpha}, \quad P_A P_B = \delta_{A,B} P_A, \quad [Q_a, P_A] = 0 \quad \forall a \in \{1, \dots, \mathcal{N}_{\mathcal{T}}\}. \quad (2.48)$$

There are $\mathcal{N}_{\mathcal{Z}}$ simple central idempotents, and

$$n_A = \sum_{r=1}^{\mathcal{N}_{\mathcal{C}}} n_{A,r} = \text{Tr}(P_A). \quad (2.49)$$

The central idempotents act as projectors on the simple modules of \mathcal{TA} . They are in one-to-one correspondence with the $\mathcal{N}_{\mathcal{Z}}$ simple objects of the Drinfeld center $\mathcal{Z}(\mathcal{C})$. In summary, starting from $\mathcal{N}_{\mathcal{T}}$ tubes, one finds V idempotents, which can be grouped together in $\mathcal{N}_{\mathcal{Z}}$ blocks, with

$$\mathcal{N}_{\mathcal{T}} \geq V \geq \mathcal{N}_{\mathcal{Z}}. \quad (2.50)$$

In practice, the labels of the simple idempotents are $\alpha \equiv r, a$, where r labels a sector of the tube algebra (corresponds to the label of the open edge of a tube), and a is an additional index which ranges from 1 to $n_{A,r}$. If $n_{A,r} = 1$, the label r is enough to uniquely specify a direction in V and the additional index a is not needed.

Expliciting all the indices, the relation between tubes and idempotents can then be written as

$$Q_{rsj}^i = \sum_{A \in \mathcal{Z}(\mathcal{C})} \sum_{a=1}^{n_{A,r}} \sum_{b=1}^{n_{A,s}} [M_{A,rsj}^i]_{a,b} p_A^{rs,ab}, \quad p_A^{rs,ab} = \sum_{i,j \in \mathcal{C}} [M_{A,rsj}^i]_{a,b}^{-1} Q_{rsj}^i, \quad (2.51)$$

where Q_{rsj}^i denotes a tube with open edges rs as represented in Fig. 2.19, and M_A 's are called modules [84]. These modules are closely related to the halfbraidings Ω_A defined in Eq. (2.36):

$$[M_{A,rsj}^i]_{a,b} = d_i \sqrt{\frac{d_s}{d_r}} [\Omega_{A,rsj}^i]_{a,b}. \quad (2.52)$$

The multiplicities $n_{A,s}$ are obtained from

$$n_{A,s} = \text{Tr} (M_{A,sss}^1) = \sum_{a=1}^{n_{A,s}} \text{Tr} (p_A^{ss,aa}), \quad (2.53)$$

which means that they count the number of simple idempotent within a sector ss of the tube algebra.

The 11 sector

As the tube algebra is determined by the open edge labels rs of the tubes, the idempotent decomposition can be performed sector by sector. In this thesis, the 11 sector of the tube algebra will be of particular relevance. Let us therefore comment more specifically on the tube algebra in this sector. Tubes in the 11 sector are simply closed loops of type i , which we will label $Q_i \equiv Q_{11i}^i$. There are as many tubes of this type as objects in \mathcal{C} , so we write

$$\mathcal{N}_{\mathcal{T}}^{11} = \mathcal{N}_{\mathcal{C}}, \quad (2.54)$$

where $\mathcal{N}_{\mathcal{T}}^{11}$ is the number of tubes in the sector 11. The tube algebra in this particular sector simply reproduces the fusion rules of \mathcal{C} , therefore

$$Q_i Q_j = \sum_{k \in \mathcal{C}} N_{ij}^k Q_k. \quad (2.55)$$

We can then distinguish two cases.

- *The fusion rules of \mathcal{C} are commutative.* There are exactly $\mathcal{N}_{\mathcal{C}}$ idempotents in the sector 11 , i.e., no nilpotent in this sector. Therefore, every idempotent corresponds to a different block A , and $n_{A,1} = 1$ or 0 . Moreover, we can find the idempotents simply as the column vectors of the modular S -matrix (if it exists), or of the mock- S -matrix, which diagonalize the fusion matrices.
- *The fusion rules of \mathcal{C} are non-commutative.* There may be some nilpotents in the 11 sector, so that some idempotents may correspond to a same block A , and $n_{A,1} \geq 1$ or 0 .

In both cases, one has

$$\mathcal{N}_{\mathcal{C}} = \sum_{A \in \mathcal{Z}(\mathcal{C})} n_{A,1}^2. \quad (2.56)$$

Finally, let us mention that the projector on the vacuum $\mathbf{1}$ of $\mathcal{Z}(\mathcal{C})$, $P_{\mathbf{1}}$, is always a weighted sum of all tubes in the 11 sector:

$$P_{\mathbf{1}} = p_{\mathbf{1}}^{11} = \sum_{i \in \mathcal{C}} \frac{d_i}{D_{\mathcal{C}}^2} Q_i, \quad (2.57)$$

and $n_{\mathbf{1},1} = 1$. This particular projector is also known as the Kirby strand [28].

Example: Fibonacci

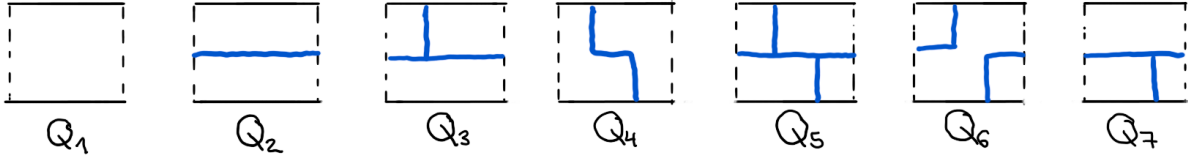


Figure 2.21: Tubes for $\mathcal{C} = Fib$. Edges labeled by τ are drawn in blue. Edges labeled with the vacuum are not drawn.

We illustrate this section with the example of the tube algebra for the Fibonacci category. The idempotent decomposition for Fibonacci can be found, e.g., in [84, 78]. Ref. [78] also provides the halfbraidings. The Fibonacci category has seven tubes, which are shown on Fig. 2.21. To simplify the notations, we denote these tubes Q_i , with i ranging from 1 to 7.

Let us first consider the 11 sector. Here, there are only two tubes, Q_1 and Q_2 , and we know that they verify the fusion rules, which are commutative:

$$Q_1 Q_1 = Q_1, \quad Q_1 Q_2 = Q_2 Q_1 = Q_2, \quad Q_2 Q_2 = Q_1 + Q_2. \quad (2.58)$$

Therefore, we can simply use the modular S -matrix to derive two orthogonal linear combinations of tubes:

$$p_A^{11} = \frac{\mathcal{N}_A}{\sqrt{1 + \phi^2}} (Q_1 + \phi Q_2) \quad (2.59)$$

$$p_B^{11} = \frac{\mathcal{N}_B}{\sqrt{1 + \phi^2}} (\phi Q_1 - Q_2) \quad (2.60)$$

where \mathcal{N}_A and \mathcal{N}_A are normalization constants. Using the identities for idempotents, one can easily derive these constants to be $\mathcal{N}_A = \frac{1}{\sqrt{1+\phi^2}}$ and $\mathcal{N}_B = \frac{2\phi-1}{\sqrt{1+\phi^2}}$. In particular, we see that $n_{A,1} = 1$ and $n_{B,1} = 1$. Besides, we can identify p_A^{11} with the Kirby strand defined above, and conclude that A is the vacuum $\mathbf{1}$.

Using further Eq. 2.47 for the $\tau\tau$ sector, (see e.g. [28] for an explicit calculation), one obtains three other idempotents

$$p_C^{\tau\tau} = \frac{1}{1+\phi^2}(Q_4 + e^{-4\pi i/5}Q_6 + \sqrt{\phi}e^{3\pi i/5}Q_5), \quad (2.61)$$

$$p_D^{\tau\tau} = \frac{1}{1+\phi^2}(Q_4 + e^{4\pi i/5}Q_6 + \sqrt{\phi}e^{-3\pi i/5}Q_5), \quad (2.62)$$

$$p_E^{\tau\tau} = \frac{1}{1+\phi^2}(\phi Q_4 + \phi Q_6 + \frac{1}{\sqrt{\phi}}Q_5). \quad (2.63)$$

The sectors 1τ and $\tau 1$ each contribute a nilpotent:

$$p_F^{\tau 1} = \left(\frac{\phi}{5}\right)^{1/4} Q_3, \quad p_G^{1\tau} = \left(\frac{\phi}{5}\right)^{1/4} Q_7. \quad (2.64)$$

Finally, from Eq. 2.47 one obtains that $p_G^{1\tau}p_F^{\tau 1} = p_B^{11}$ and $p_F^{\tau 1}p_G^{1\tau} = p_E^{\tau\tau}$, which shows that B, E, F and G belong to the same block in the \mathcal{TA} decomposition.

Thus, one finally obtains four central idempotents, that are identified as the four simple objects of the Drinfeld center $\mathcal{Z}(Fib)$. Using the same notations as in Sec. 2.5.2 can be written

$$P_{(1,\bar{1})} = P_{\mathbf{1}} = p_A^{11}, \quad P_{(\tau,\bar{\tau})} = p_B^{11} + p_E^{\tau\tau}, \quad P_{(1,\bar{\tau})} = p_C^{\tau\tau}, \quad P_{(\tau,\bar{1})} = p_D^{\tau\tau}. \quad (2.65)$$

2.5.4 Morita equivalence

Two algebras that have the same modules are said to be *Morita equivalent*. For example, when the tube algebra \mathcal{TA} of a UFC \mathcal{C} and the tube algebra \mathcal{TA}' of a UFC \mathcal{C}' are Morita-equivalent, they lead to equivalent Drinfeld centers $\mathcal{Z}(\mathcal{C}) \simeq \mathcal{Z}(\mathcal{C}')$. To simplify the discussion, we will say that the two categories \mathcal{C} and \mathcal{C}' are Morita equivalent, even if this notion actually applies to their tube algebras. As an important example, the categories $\mathcal{C}_1 = \text{Vec}(G)$ and $\mathcal{C}_2 = \text{Rep}(G)$, i.e. constructed respectively from the elements and the irreducible representations of a same group G , are generally Morita-equivalent [92].

2.6 Summary

In this chapter, we have discussed the mathematical background underlying the work of this thesis. In particular, we have seen that:

- A unitary fusion category (UFC) \mathcal{C} is determined by the following data: a set of objects, fusion rules for these objects, quantum dimensions, and associativity (F -symbols). This data allows for counting Hilbert space dimensions for fusion spaces, and evaluate planar diagrams.

- A unitary modular tensor category (UMTC) \mathcal{U} is a UFC with additional braiding structure. It is the correct description for anyons. From the braiding, one can define the T -matrix, determining the self-statistics or spin of objects, and the S -matrix, which describes exchange statistics between different objects. This S -matrix is unitary (modular) for a UMTC.
- A Drinfeld center $\mathcal{Z}(\mathcal{C})$ is a particular UMTC which is built from a UFC \mathcal{C} . For example, if \mathcal{C} itself is a UMTC, then the Drinfeld center $\mathcal{Z}(\mathcal{C}) = \mathcal{C} \times \bar{\mathcal{C}}$, where $\bar{\mathcal{C}}$ is the copy of \mathcal{C} with opposite chirality. A general way to construct the Drinfeld center is the tube algebra decomposition. Drinfeld centers are always achiral.

Part II

String-net models

Introduction to string-net models

In this chapter, we introduce the generalized string-net model, which will be at the heart of the study of the two next chapters. The string-net model was introduced by Levin and Wen [48]. It takes a unitary fusion category (UFC) as an input and produces the Drinfeld center of this category as an output. Initially limited to UFCs verifying certain additional symmetry requests for the F -symbols, it has been generalized by several later works [95, 84, 78, 77]. The generalized string-net model admits all UFC \mathcal{C} as input, and realizes all topological phases that are described by a Drinfeld center $\mathcal{Z}(\mathcal{C})$. Topological orders associated with Drinfeld centers are believed to be the most general class of bosonic topological order compatible with gapped boundaries [96, 95, 97]. In particular, the string-net model realizes all discrete lattice gauge theories, and doubled theories $\mathcal{Z}(\mathcal{C}) = \mathcal{C} \times \bar{\mathcal{C}}$ if \mathcal{C} is modular [48]. The physical picture underlying the string-net model is that microscopic bosonic degrees of freedom are subjected to local energy constraints that force them to arrange into effective extended objects called *string-nets* [48, 98]. The condensation of these string-nets generates a topologically ordered phase. [48].

3.1 Hilbert space and Hamiltonian

String-net models are defined on any trivalent lattice embedded on an oriented 2D manifold. The input data needed to build a string-net model is the content of a UFC \mathcal{C} , that is, the simple objects, the fusion rules, and the F symbols of \mathcal{C} . Every edge of the lattice is oriented and labeled with a simple object of \mathcal{C} . Inverting the direction of the edge changes the label from a to its dual \bar{a} . In the case where there are fusion multiplicities, a quantum number ranging from 1 to N_{ab}^c is additionally attributed to vertices following the fusion rules of \mathcal{C} . Each geometrically different labeling of the lattice (i.e., lattice configuration) corresponds to a different state, and two different lattice configurations are orthogonal to each other. We will call the orthonormal basis of states spanned by lattice configurations the *link basis* (later, we will also use another basis in terms of the excitations of the system). In particular, if there are no fusion multiplicities (i.e., $N_{ab}^c = 0$ or 1 $\forall a, b, c \in \mathcal{C}$), the full Hilbert space dimension is $\dim \mathcal{H} = \mathcal{N}_{\mathcal{C}}^{N_l}$, with N_l the number of links in the lattice, and $\mathcal{N}_{\mathcal{C}}$ the number of simple objects in \mathcal{C} .

The string-net Hamiltonian is a sum of local, commuting projectors:

$$H = -J_v \sum_{\text{vertices } v} A_v - J_p \sum_{\text{plaquettes } p} B_p, \quad (3.1)$$

where A_v acts on the vertices v and B_p on the plaquettes p of the lattice, and

$$A_v^2 = A_v, \quad B_p^2 = B_p, \quad [B_p, B'_p] = [A_v, A'_v] = [B_p, A_v] = 0, \quad \forall \{b, b', v, v'\}. \quad (3.2)$$

The Hamiltonian is exactly solvable, as operators can be replaced by their eigenvalues $a_v = \pm 1$ and $b_p = \pm 1$. The vertex operators A_v project on states where the labels around the vertex v correspond to an allowed fusion vertex for \mathcal{C} , i.e.,

$$A_v \begin{array}{c} c \uparrow \\ / \quad \backslash \\ a \quad b \end{array} = \delta_{ab}^c \begin{array}{c} c \uparrow \\ / \quad \backslash \\ a \quad b \end{array}. \quad (3.3)$$

where

$$\delta_{ab}^c = \begin{cases} 1 & \text{if } N_{ab}^c \neq 0 \\ 0 & \text{if } N_{ab}^c = 0. \end{cases} \quad (3.4)$$

Of course, when \mathcal{C} is multiplicity-free, $N_{ab}^c = \delta_{ab}^c$. For simplicity, we limit the following discussion to multiplicity-free theories.

The plaquette operators B_p act on the plaquettes p of the lattice by modifying the labels on the edges around a plaquette:

$$B_p = \sum_{s \in \mathcal{C}} \frac{d_s}{D_{\mathcal{C}}^2} B_p^s, \quad (3.5)$$

where $D_{\mathcal{C}}$ is the total quantum dimension of \mathcal{C} and the action of B_p^s on a plaquette p (here, we show the action on a honeycomb plaquette) is to fuse a string s into the plaquette, thus modifying the labels on the links on the contour of the plaquette:

$$B_p^s \begin{array}{c} \text{Diagram of a honeycomb plaquette with labels } a, b, c, d, e, f, g, h, i, j, k, l \end{array} = \sum_{g', h', i', j', k', l'} \text{Coeff}(s, a, \dots, f, g, \dots, h, g', \dots, h') \begin{array}{c} \text{Diagram of a honeycomb plaquette with labels } a, b, c, d, e, f, g', h', i, j, k', l' \end{array} \quad (3.6)$$

A B_p operator acting on a particular state will in general generate a linear combination of states. The coefficients in Eq. (3.6) can be expressed in terms of F -symbols of \mathcal{C} , and we will give their explicit expression in Sec. 3.3. Importantly, $\text{Coeff} = 0$ if any vertex around the plaquette does not verify the fusion rules of \mathcal{C} , i.e.

$$\text{Coeff}(s, a, \dots, f, g, \dots, h, g', \dots, h') \propto N_{ga}^l N_{lf}^k N_{ke}^j N_{jd}^i N_{ic}^h N_{hb}^g N_{g'a}^{l'} N_{l'f}^{k'} N_{k'e}^{j'} N_{j'd}^{i'} N_{i'c}^{h'} N_{h'b}^{g'}. \quad (3.7)$$

The ground-state space of the model is spanned by all states $|\psi_0\rangle$ such that $A_v|\psi_0\rangle = B_p|\psi_0\rangle = |\psi_0\rangle$. Excited states $|\psi\rangle$ correspond to 0 eigenvalues of A_v or B_p , i.e., either $A_v|\psi\rangle = 0$ and/or $B_p|\psi\rangle = 0$ for some vertices v or plaquettes p .

These operators have a nice interpretation when thinking of them in terms of lattice gauge theories. The labels on the edges of the lattice can be seen as labels of electric flux lines, and the vertex operator A_v is in this sense a projector that ensures Gauss law at every vertex. The plaquette operators B_p , on the other hand, can be understood as magnetic flux operators, projecting on the absence of magnetic flux in a plaquette.

Within the subspace where all A_v eigenvalues are 1, all basis states are configurations of labeled edges ("strings") branched together following the fusion rules (forming a "network"). These are precisely the *string-nets*. The string-net model is mostly considered in this subspace, which contains entirely the ground-state. Although we are interested in the excited states of the string-net model, we will also restrict ourselves to the subspace where all A_v have eigenvalue 1. In fact, as can be seen from Eq. 3.7, plaquette and vertex excitations cannot be considered in a completely independent way (as a trivalent vertex is shared between three plaquettes, a vertex excitation always comes together with three plaquette excitations). Therefore, we will work only in the subspace where the vertex constraints are always respected, which corresponds to taking $J_v \rightarrow \infty$ in Eq. (3.1) and considering only low-energy physics. One may also view this constraint as restricting the Hilbert space to include only the states that are +1 eigenstates of A_v for all vertices (i.e. work in the subspace of string-net configurations). Within this restricted Hilbert space and setting $J_p = 1$, the Hamiltonian takes the simpler form

$$H = - \sum_{p=1}^{N_p} B_p. \quad (3.8)$$

which is the form we will consider throughout the rest of this thesis. Note that there exist models such as the "extended string-net models" that attempt to cure this drawback of the original model [93]. However, these models lie beyond the scope of the work presented in this thesis.

For the Hamiltonian of Eq. (3.8), the energy spectrum is very simple. The ground-state energy is $E_0 = -N_p$, as all plaquette operator eigenvalues are $b_p = 1$. For a state with q excited plaquettes with $1 \leq q \leq N_p$ with N_p the total number of plaquettes in the system, the energy is given by:

$$E_q = -N_p + q. \quad (3.9)$$

3.2 Ground-state wave function

The ground-state wavefunction $|\psi\rangle$ of a string-net model can be expressed in the link basis as a superposition of different string-net configurations $X \in \mathcal{H}$ [48, 78]:

$$|\psi\rangle = \sum_X \psi(X) |X\rangle. \quad (3.10)$$

The graphical calculus introduced in Chap. 2 can be used to determine explicitly the form of the ground-state wave function. In fact, the rules 2.3, 2.5, 2.6 and 2.7 allow to relate with each other the amplitudes $\psi(X_1)$ and $\psi(X_2)$ of different string-net configurations X_1 and X_2 which only differ by local moves, as represented below. The configuration of the rest of the lattice, represented

by the gray areas, remains unchanged under such local moves:

$$\psi \left(\begin{array}{c} a \nearrow b \nearrow c \\ d \nwarrow e \end{array} \right) = \sum_f [F_e^{abc}]_{df} \psi \left(\begin{array}{c} a \nearrow b \nearrow c \\ e \nwarrow f \end{array} \right) \quad (3.11)$$

$$\psi \left(\begin{array}{c} e \nearrow \\ d \nwarrow \\ a \nearrow b \nearrow c \end{array} \right) = \sum_f [F_e^{abc}]_{df}^* \psi \left(\begin{array}{c} e \nearrow \\ f \nwarrow \\ a \nearrow b \nearrow c \end{array} \right) \quad (3.12)$$

$$\psi \left(\begin{array}{c} c \uparrow \\ a \nearrow b \nwarrow \\ d \uparrow \end{array} \right) = \delta_{c,d} \sqrt{\frac{d_a d_b}{d_c}} \psi \left(\begin{array}{c} c \uparrow \end{array} \right) \quad (3.13)$$

$$\psi \left(\begin{array}{c} a \uparrow \\ b \uparrow \end{array} \right) = \sum_c \sqrt{\frac{d_a d_b}{d_c}} \psi \left(\begin{array}{c} a \nearrow b \nearrow c \\ a \nwarrow b \nwarrow c \end{array} \right) \quad (3.14)$$

Here, $a, b, c, d, e, f \in \mathcal{C}$. Additionally, F -symbols can be chosen so that $[F_e^{abc}]_{df} = 1$ if a or b or $c = 1$ [78]. With this convention, the amplitude of a wavefunction remains unchanged under vertical bending of strings

$$\psi \left(\begin{array}{c} a \uparrow \end{array} \right) = \psi \left(\begin{array}{c} a \nearrow \end{array} \right) \quad (3.15)$$

All string-net configurations can be related via the local rules defined above to a reference configuration whose amplitude is fixed to 1, typically¹ the vacuum configuration where all edges are labeled with the vacuum 1 of \mathcal{C} . As an example, we show how to evaluate the following configuration (the example is taken from [78]). Edges labeled with the vacuum can be freely erased or added, and are either not displayed or displayed as dotted lines.

$$\begin{aligned} \psi \left(\begin{array}{c} a \nearrow \bar{a} \\ b \nearrow c \\ \bar{c} \nwarrow \end{array} \right) &= [F_1^{abc}]_{\bar{c}\bar{a}} \psi \left(\begin{array}{c} a \nearrow \bar{a} \\ b \nearrow c \\ \bar{c} \nwarrow \end{array} \right) = [F_1^{abc}]_{\bar{c}\bar{a}} \sqrt{\frac{d_b d_c}{d_a}} \psi \left(\begin{array}{c} a \nearrow \bar{a} \\ \bar{c} \nwarrow \end{array} \right) \\ &= [F_1^{abc}]_{\bar{c}\bar{a}} \sqrt{d_b d_c d_a} \psi(\text{vacuum}). \end{aligned} \quad (3.16)$$

For a general UFC, bending edges so as to change their spatial orientation may change the amplitude of the state:

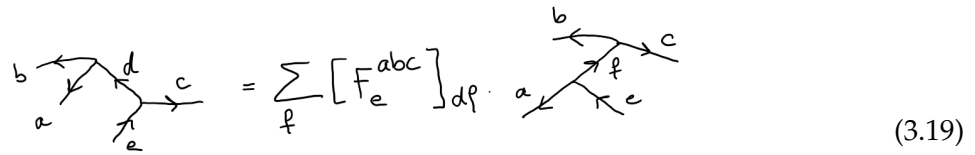
$$\psi \left(\begin{array}{c} a \uparrow \end{array} \right) \neq \psi \left(\begin{array}{c} a \nearrow \bar{a} \end{array} \right) \quad (3.17)$$

¹On a plane or a surface of genus 1, any string-net configuration can be related to the vacuum configuration. On a higher-genus surface, this may not be the case for all configurations.

An exception are certain UFCs for which the F -symbols verify special symmetry conditions, known as the symmetry. In fact, if the amplitude of a tetrahedral configuration (see Fig. 3.1) is the same under all symmetry operations of the tetrahedron, 2-fold rotations, 3-fold rotations and reflections (see e.g. [80, 78] for a detailed discussion of these symmetries), then strings can be bent in arbitrary ways without affecting the amplitude of the wavefunction. In terms of F -symbols, these symmetry requirements result in the following conditions:

$$[F_i^{jkl}]_{nm} = [F_{\bar{l}}^{kj\bar{i}}]_{\bar{n}\bar{m}} = [F_{\bar{j}}^{\bar{i}lk}]_{n\bar{m}} = \sqrt{\frac{d_m d_n}{d_l d_j}} [F_i^{\bar{m}k\bar{n}}]_{\bar{l}\bar{j}}. \quad (3.18)$$

As a consequence, F -symbols (see Fig. 2.3) can also be written, e.g., as

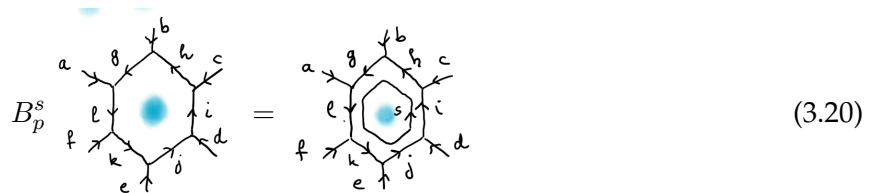


$$\text{Diagram} = \sum_f [F_e^{abc}] \text{Diagram} \quad (3.19)$$

This symmetry condition was imposed on the F -symbols in the original string-net construction of Levin and Wen [48]. However, this condition restricts the possibilities of UFCs one can use to build the model, and consequently of topological phases that can be realized. The generalized string-net models are generalized in the sense that they relax this symmetry constraint.

3.3 Explicit form of the plaquette operator

In order to calculate operators acting on the lattice, it is convenient to introduce the *fat lattice picture* [48]. In this picture, the links of the lattice are pictured as tubes of finite width. Any string configuration inside these tubes can be related to a configuration on the original, unfattened lattice, via the local rules defined above. In this picture, the plaquette operators B_p^s have a simple representation as operators inserting a closed string s around the lattice (we symbolize the boundaries of the fat lattice by blue dots in the core of the plaquette, which signify that the string s cannot be contracted at the center of the plaquette, but can be fused into the links surrounding the plaquette):



$$B_p^s \text{Diagram} = \text{Diagram} \quad (3.20)$$

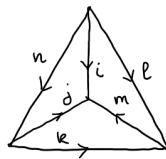


Figure 3.1: The tetrahedral symmetry requests that F -symbols are the same under different symmetry operations of the oriented tetrahedron.

Using the local rules, one can then deduce the exact expression of the matrix elements of the B_p^s operators. For the honeycomb plaquette and generalized string-nets, one obtains:

$$\begin{aligned}
 \text{Diagram} &= \sum_{g',h',i',j',k',l'} d_s \sqrt{\frac{d_{\bar{g}}d_h d_i d_j d_{\bar{k}} d_{\bar{l}}}{d_{g'} d_{h'} d_i d_j d_{k'} d_{l'}}} [F_{\bar{g}}^{\bar{g}\bar{s}s}]_{\bar{g}'1} [F_{\bar{b}}^{g'sh}]_{\bar{g}h'}^* [F_{i'}^{sh\bar{c}}]_{h'i}^* [F_{i'}^{sjd}]_{j'i} \\
 &\times [F_j^{\bar{s}s j}]_{1j'} [F_e^{\bar{k}\bar{s}j'}]_{\bar{k}'j}^* [F_{\bar{l}}^{\bar{a}\bar{g}\bar{s}}]_{\bar{l}g'} [F_{\bar{l}}^{f\bar{k}\bar{s}}]_{\bar{l}k'}^* \\
 &\text{Diagram}
 \end{aligned} \quad (3.21)$$

The steps of derivation of this formula can be found in [77]. A simpler version of the same formula holding only for UFCs with tetrahedral symmetry is derived in [48] and involves only six F -symbols.

3.4 Topological excitations

For a given input UFC \mathcal{C} , the string-net model produces a topological phase corresponding to the Drinfeld center of \mathcal{C} , $\mathcal{Z}(\mathcal{C})$. In particular, the vacuum object of $\mathcal{Z}(\mathcal{C})$ corresponds to the absence of excitations. The projector onto the vacuum P_1 which can be constructed from the tube algebra [compare with Eq. (2.57)], corresponds exactly to the plaquette operator B_p when restricted to a given plaquette p . Other simple objects of $\mathcal{Z}(\mathcal{C})$ correspond to excitations. Among them, excitations of a single plaquette play a special role and are called fluxons.

For each simple object of $\mathcal{Z}(\mathcal{C})$, one can construct quasiparticle operators, see Fig. 3.2, also called string operators. An open string operator is an oriented string labeled by a simple object $A \in \mathcal{Z}(\mathcal{C})$, which is unobservable except at its endpoints, where it creates respectively a quasiparticle A and its dual \bar{A} . Closed string operators have no open ends. These string operators are completely unobservable and commute with the Hamiltonian. Finding all closed string quasiparticle operators commuting with the Hamiltonian equates to finding the halfbraidings discussed in Sec. 2.5 [78,

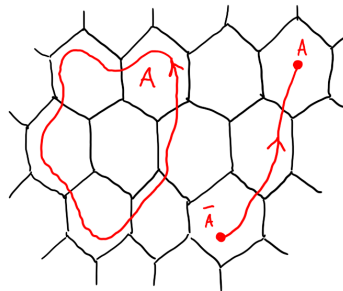


Figure 3.2: Quasiparticle operators on the lattice. Left: A closed operator commutes with the Hamiltonian. Right: An open string operator creates two excitations (which are dual to each other) at the open ends.

48]. In fact, the halfbraidings provide an expression of the matrix elements of the closed string operators in the link basis. We will use this approach later on in Chap. 5.

Spectral degeneracies

4.1 Introduction

A defining feature of topological order is the ground-state degeneracy (GSD) on a closed manifold [13, 20, 18] which depends on the manifold's topology, and is robust against local perturbations. It precisely matches the vector space dimension assigned to the same manifold by the 2+1D topological quantum field theory (TQFT) describing the topological order at low energies [27]. String-net models [48, 95, 84, 77, 78] are lattice realizations of a 2+1D TQFT [99, 100, 101, 28, 102]. This TQFT corresponds to the Drinfeld center $\mathcal{Z}(\mathcal{C})$ of the unitary fusion category (UFC) \mathcal{C} from which the string-net model is built. The ground-state degeneracy of the string-net models can thus be expressed completely in terms of the Drinfeld center $\mathcal{Z}(\mathcal{C})$ (and the genus of the manifold). Another way of computing the ground-state degeneracy of the string-net models is presented in [103] and uses the quantum dimensions and F -symbols of the input UFC \mathcal{C} . Drinfeld centers describe achiral topological orders which have gappable edges [104, 96, 95, 97]. Thus, string-net models may also have a ground-state degeneracy on surfaces with boundaries. This boundary ground-state degeneracy, which can also be used to characterize topological order, has been studied in Ref. [105]. In general, a topological order $\mathcal{Z}(\mathcal{C})$ may admit different types of boundaries, and the ground-state degeneracy depends on the boundary type.

In this chapter, instead of the ground-state degeneracies, we want to consider the degeneracies of the excited states in the string-net models, i.e., when topological quasiparticles are present. Interestingly, while the energy spectrum of these models has the simple form of an equidistant ladder (see Eq. 3.9), the corresponding spectral degeneracies are non-trivial, and topology-dependent. These spectral degeneracies have been the subject of recent studies, which have focused on specific input categories [106, 107, 108, 103, 109], or on the case where the input category is a unitary modular tensor category (UMTC) [110]. Here, we want to extend these results to arbitrary input UFCs, by studying the spectral degeneracies in the generalized string-net models. As in the previous studies, we only consider string-net models in a constrained Hilbert space where fusion rules are strictly imposed at the vertices. As a result, some simple objects of

the Drinfeld center may not appear as excitations on the lattice¹. In particular, the elementary excitations appearing at the level of the plaquettes are a certain subset of the simple objects of $\mathcal{Z}(\mathcal{C})$, called *fluxons*, which are always bosons and can be excited without violating the fusion constraints at every trivalent vertex.

Which objects of the Drinfeld center are fluxons is not a property of the TQFT, but depends on the input theory \mathcal{C} . Therefore, knowledge of \mathcal{C} is necessary in order to derive the degeneracies of excited states. This stands in contrast to the case of the ground-state degeneracy, which is determined solely by $\mathcal{Z}(\mathcal{C})$. In particular, this has an interesting consequence for Morita equivalent categories. We say that two UFCs \mathcal{C} and \mathcal{C}' are Morita-equivalent when the same TQFT may be constructed either as the Drinfeld center $\mathcal{Z}(\mathcal{C})$ of \mathcal{C} or as the Drinfeld center $\mathcal{Z}(\mathcal{C}')$ of \mathcal{C}' (i.e., $\mathcal{Z}(\mathcal{C}') \simeq \mathcal{Z}(\mathcal{C})$). However, the fluxons of the string-net model built from \mathcal{C} are generally different from the fluxons of the string-net model built from \mathcal{C}' . Hence, two Morita-equivalent categories lead to the same ground-state degeneracy of the string-net model, but generally have different excited states degeneracies.

Furthermore, we find that excited states of the string-net model may display both topological and nontopological degeneracies. By *topological degeneracies*, we mean degeneracies that arise from multiple topological fusion channels in the $\mathcal{Z}(\mathcal{C})$ TQFT. The ground-state degeneracy on a surface of nonzero genus, for example, is such a topological degeneracy. This type of degeneracy cannot be split by local perturbations so long as the excitation gap does not close. The notion of locality is here related to operators acting on a typical scale smaller than the systole (shortest noncontractible loops), i.e., at the scale of a single plaquette. In the case where quasiparticle excitations (fluxons) are present in some plaquettes, there may be a degeneracy arising from multiple fusion channels of these fluxons. We also qualify this degeneracy as topological. In fact, such a degeneracy can be split by perturbations only if the perturbing operators connect the positions of the multiple excitations. We find that, upon identifying the fluxons among the simple objects of the Drinfeld center, the topological degeneracy of a 2D orientable manifold, with any number of fluxons on it, can be determined using classic formulas found by Moore, Seiberg and Banks [111] and Verlinde [27]².

Nontopological degeneracies can be lifted completely by local perturbations, and are a result of the fine-tuning of the string-net Hamiltonian. These degeneracies are associated with the fluxons, and appear only if the input category \mathcal{C} has *non-commutative* fusion rules. These nontopological degeneracies are given by the internal multiplicities $n_{A,1}$ originating from the tube algebra.

Hence, we find that studying the spectral degeneracies of string-net models, and in particular those constructed from non-commutative \mathcal{C} , helps to understand how much of the physics of the string-net model is captured by the Drinfeld center of the input category (i.e., topological degeneracies) and how much is left out (non-topological degeneracies). It also shows which physical differences arise from different lattice realizations of the same Drinfeld center. This last

¹Note that in Ref. [93] a particular extension of the string-net model (known as “extended string-net model”) is considered, that contains all topological quasiparticle types but never violates any vertex constraints at the price of some other complications. The study of the spectral degeneracies of this model has been the subject of a recent master thesis [94], following up on the work presented here.

²These formulas were derived at the end of the 1980’s in the context of TQFT and conformal field theory.

point might be particularly interesting in view of recent proposals to simulate simple string-net models on quantum computers [112, 113].

This chapter is structured as follows. In the first two sections, we recall how to compute degeneracies for TQFTs on closed manifolds, in the ground state (Sec. 4.2) and in the presence of quasiparticles (Sec. 4.3). The following Sec. 4.4 contains the main results of this chapter. First, we explain how to determine the set of fluxons among the objects of the Drinfeld center. Then, we adapt the formula of Moore, Seiberg and Banks presented in Sec. 4.3 to the case of a string-net model with fluxon excitations, and possibly smooth boundaries. Finally, we use our formula for degeneracies to compute the full Hilbert-space dimension of the model. Sec. 4.5 discusses some special cases such as modular or commutative input categories. Sec. 4.6 provides some examples. In particular, we study the case of the Morita-equivalent categories $\text{Rep}(S_3)$ and $\text{Vec}(S_3)$ corresponding to the same Drinfeld center $\mathcal{Z}(S_3)$ but having different energy-level degeneracies. We also study more involved cases such as the Haagerup, the Tambara-Yamagami, and the Hagge-Hong categories. Finally, we introduce a refined Hamiltonian featuring only topological degeneracies in Sec. 4.7, and conclude in Sec. 4.8. The results presented in this chapter have been published in [81].

4.2 Ground-state degeneracy

The ground-state degeneracy (GSD) of a string-net model does not depend on the geometric specificities of the lattice, but only on the topology of the manifold in which the lattice is embedded [103, 99, 100, 102]. In fact, the GSD of the string-net model is equivalent to a topological invariant known as the Turaev-Viro invariant [86, 114, 102] in the context of TQFTs. As shown by Refs. [101, 99, 100, 102], the ground-state degeneracy of a string-net model built from a unitary fusion category \mathcal{C} can be obtained from the vector space dimension associated to the same surface by the TQFT defined by the Drinfeld center $\mathcal{Z}(\mathcal{C})$. The TQFT approach is convenient in that it provides a simple formula for the GSD, which can be expressed in terms of the S -matrix of $\mathcal{Z}(\mathcal{C})$. In this section, we introduce this approach of calculating the GSD based on a TQFT description (see e.g. [28] for more details). It will be our starting point for later calculations of spectral degeneracies.

Consider a TQFT defined by a UMTC \mathcal{U} , i.e., the particle content of the TQFT corresponds to the simple objects of \mathcal{U} , with their fusion and braiding properties. The trivial object of \mathcal{U} corresponds to the vacuum, or absence of particles. The dimension of the vector space attributed by the TQFT to an oriented closed 2D surface of genus 0 (a sphere) without any (non-vacuum) particles on it is 1 [28]. Correspondingly, and as was also shown by [103], there is no GSD on the sphere:

$$\dim_{\mathcal{U}}(g = 0) = 1. \quad (4.1)$$

One may create particles on the sphere, at the condition that the overall quantum number is conserved. For instance, a single particle cannot be created from the vacuum. A pair of particles a, b is possible, as long as $b = \bar{a}$. In general, any allowed configuration of particles must have been created by splitting or fusion processes from the vacuum. In a TQFT vision, a particle on a sphere corresponds to a puncture labeled with a simple object $a \in \mathcal{U}$ (see Fig. 4.1). When such a puncture

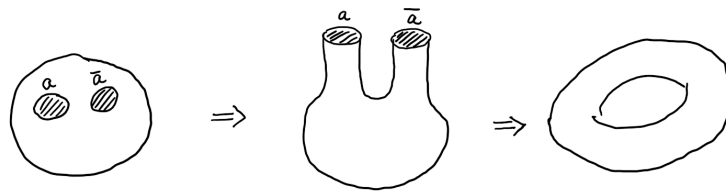


Figure 4.1: Using surgery, a sphere with two labeled punctures can be turned into a torus.

is labeled with the vacuum, it is equivalent to having no puncture. A puncture labeled with $a \in \mathcal{U}$ can be brought ("sewed" or "glued") together with another puncture if this puncture is labeled with its dual \bar{a} , so that the two particles annihilate again (this is known as the *gluing axiom* in TQFT [28]). By doing so for two punctures on a sphere, one obtains a new closed surface without particles in it. This new surface is a torus, see Fig. 4.1. If \mathcal{U} contains $N_{\mathcal{U}}$ simple objects, then there are exactly $N_{\mathcal{U}}$ possibilities of putting a pair of labeled punctures on a sphere and gluing them together to form a torus. Each of these possibilities corresponds to another state in the vector space assigned by the TQFT to this surface. Therefore, the dimension of this vector space, and the GSD on the torus, is [28, 103]:

$$\dim_{\mathcal{U}}(g = 1) = N_{\mathcal{U}}. \quad (4.2)$$

This reasoning (also called *surgery*) can be extended to higher genus surfaces. The fundamental building block for surgery is a sphere with three labeled punctures, a so-called pant diagram, see Fig. 4.2. Any orientable two-dimensional surface of genus $g \geq 2$ (e.g., a two torus as shown on Fig. 4.3) can be generated by gluing together the punctures of pant diagrams.

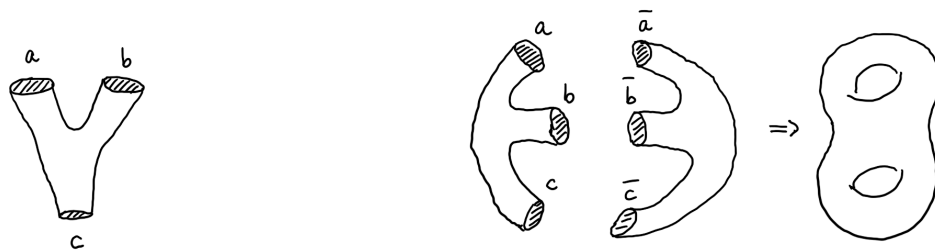


Figure 4.2: A pant diagram is a sphere with three labeled punctures.

Figure 4.3: Gluing together two pant diagrams at their punctures, one obtains a two torus. The condition for gluing together two punctures is that their labels are dual to each other.

A pant diagram with labels a, b, c can exist only if a, b and c can have been created from the vacuum. This is equivalent to saying that there must exist a non-zero fusion coefficient N_{bc}^a . Therefore, a pant diagram can be equivalently represented by a fusion (or splitting) vertex, see Fig. 4.4a. Any surface of arbitrary genus g can then be represented as a fusion tree. A few examples are shown on Fig. 4.4. In particular, the dimension of the vector space attributed to a genus g surface by the TQFT is equivalent to the dimension of the Hilbert space spanned by the corresponding fusion trees. This dimension can be expressed in terms of the fusion matrices of \mathcal{U} (see Chap. 2).

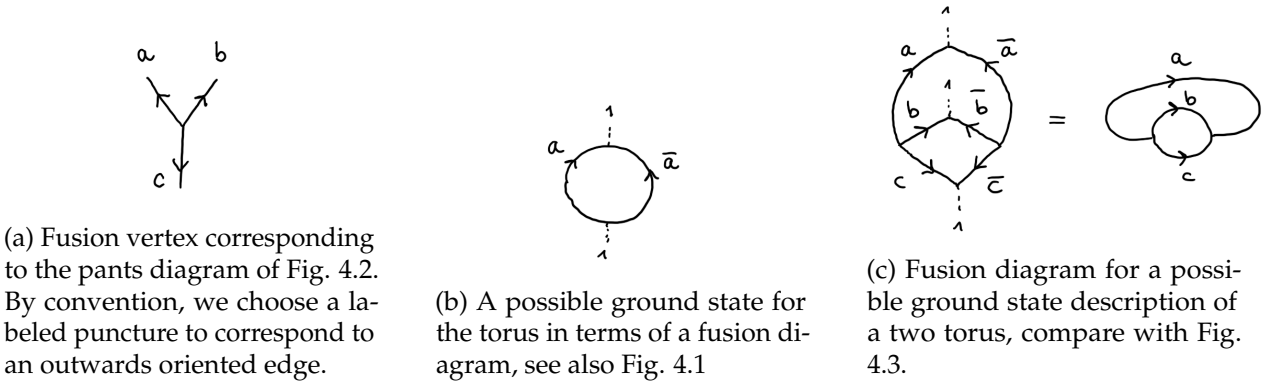


Figure 4.4: Fusion diagrams for different two-dimensional surfaces.

For example, for the torus, we can write

$$\dim_{\mathcal{U}}(g = 1) = \sum_{a \in \mathcal{U}} \text{Diagram} = \sum_{a \in \mathcal{U}} (N_{a\bar{a}}^1)^2 = N_{\mathcal{U}}. \quad (4.3)$$

Similarly, for a two-torus we can write

$$\dim_{\mathcal{U}}(g = 2) = \sum_{a,b,c \in \mathcal{U}} \text{Diagram} = \sum_{a,b,c \in \mathcal{U}} N_{b\bar{a}}^c N_{bc}^{\bar{a}}. \quad (4.4)$$

As discussed in Chap.2, fusion trees can be restructured using the F -symbols of \mathcal{U} (this corresponds to gluing together pant diagrams in a different way). This restructuring does not affect the dimension of the Hilbert space spanned by the fusion trees. For instance, another way to compute the GSD for the two-torus is

$$\dim_{\mathcal{U}}(g = 2) = \sum_{a,d,c \in \mathcal{U}} \text{Diagram} = \sum_{a,d,c \in \mathcal{U}} N_{a\bar{a}}^d N_{c\bar{c}}^d, \quad (4.5)$$

where the fusion diagram is related via an F -move to the one shown in Eq. (4.4). We stress the fact that we are here considering dimensions, and therefore want to conserve the same number of links and vertices even while restructuring a graph. This is a very different procedure then when trying to calculate the amplitude of a quantum process - in which case we can reduce diagrams to a vacuum configuration and the output is a complex number.

Hence, in general, computing the ground-state degeneracy of any surface is equivalent to counting all allowed labelings for the fusion diagram representing that surface. For a surface of genus

$g > 1$, the ground-state degeneracy is then given by a product of $2g - 2$ fusion matrices (one for each vertex), summed over all possible labels:

$$\begin{aligned}
 \dim_{\mathcal{U}}(g) &= \sum_{\substack{a_1, a_2, \dots, a_{2g-2}, \\ b_1, b_2, \dots, b_{g-1} \in \mathcal{U}}} \text{Diagram} \\
 &= \sum_{\substack{a_1, a_2, \dots, a_{2g-2}, \\ b_1, b_2, \dots, b_{g-1} \in \mathcal{U}}} N_{a_1 \bar{a}_1}^{b_1} N_{b_1 \bar{a}_3}^{a_2} N_{a_2 a_3}^{b_2} \dots N_{b_{g-1} a_{2g-2}}^{a_{2g-2}}. \tag{4.6}
 \end{aligned}$$

Equations of this kind can be greatly simplified by making multiple use of the Verlinde formula (2.20) and the properties of the S -matrix (2.18), (2.17). As an example, consider Eq.(4.5). Using the Verlinde formula, we can rewrite this equation as

$$\begin{aligned}
 \dim_{\mathcal{U}}(g = 2) &= \sum_{a, d, c, k, q \in \mathcal{U}} \frac{S_{a, k} S_{\bar{a}, k} S_{\bar{d}, k}^*}{S_{1, k}} \frac{S_{\bar{c}, q} S_{c, q} S_{d, q}^*}{S_{1, q}}, \\
 &= \sum_{a, d, c, k, q \in \mathcal{U}} \frac{S_{a, k} S_{a, k}^* S_{d, k} S_{d, q}^* S_{c, q}^* S_{c, q}}{S_{1, k} S_{1, q}}, \tag{4.7}
 \end{aligned}$$

where in the second line we have rearranged terms and used Eq. (2.17). Now using the unitarity of S [Eq. (2.18)], we obtain

$$\dim_{\mathcal{U}}(g = 2) = \sum_{k \in \mathcal{U}} S_{1, k}^{-2}. \tag{4.8}$$

With a similar reasoning, the general expression of Eq. (4.6) can be restated in the concise form

$$\dim_{\mathcal{U}}(g) = \sum_{a \in \mathcal{U}} S_{1, a}^{2-2g}. \tag{4.9}$$

This equation was first obtained by Verlinde [27].

4.3 Moore-Seiberg-Banks formula

We may also leave some punctures open while sewing. We then obtain a surface of genus g carrying some particles (for example, two pant diagrams sewed together while leaving two punctures open generates a torus with two particles). The most general case we can consider is a genus g surface with m labeled punctures. Again, the Hilbert-space dimension $\dim_{\mathcal{U}}$ associated with this labeled punctured surface just amounts to summing the product of fusion matrices (one for each trivalent vertex) over all possible internal indices of the corresponding fusion diagram:

$$\begin{aligned}
 \dim_{\mathcal{U}}(g; A_1, \dots, A_m) &= \sum_{\substack{a_1, a_2, \dots, a_{2g-1}, \\ b_1, b_2, \dots, b_g \\ c_1, c_2, \dots, c_{m-1} \in \mathcal{U}}} \text{Diagram} \\
 &= \sum_{\substack{a_1, a_2, \dots, a_{2g-1}, \\ b_1, b_2, \dots, b_g \\ c_1, c_2, \dots, c_{m-1} \in \mathcal{U}}} N_{a_1 \bar{a}_1}^{b_1} N_{b_1 \bar{a}_3}^{a_2} N_{a_2 a_3}^{b_2} \dots N_{b_{g-1} \bar{a}_{2g-1}}^{a_{2g-2}} N_{a_{2g-2} a_{2g-1}}^{b_g} N_{b_g c_1}^{A_1} N_{c_1 \bar{c}_2}^{A_2} \dots N_{c_{m-2} \bar{c}_{m-1}}^{A_{m-1}} N_{c_{m-1} 1}^{A_m}.
 \end{aligned} \tag{4.10}$$

Note that the capital letters $A_1, \dots, A_m \in \mathcal{U}$ index the particles or punctures left open, whose values are fixed, so we do not sum over them. Although the sum over so many indices looks quite complicated, it can be simplified by using again the Verlinde formula and unitarity of the S -matrix into

$$\dim_{\mathcal{U}}(g; A_1, \dots, A_m) = \sum_{k \in \mathcal{U}} \left[\prod_{j=1}^m S_{A_j, k} \right] S_{1, k}^{2-2g-m}. \tag{4.11}$$

This formula was first developed by Moore, Seiberg and Banks [111]. We can also observe that when there are no punctures (i.e., $m=0$), we recover the formula for the ground-state degeneracy Eq. (4.9).

4.4 Spectral degeneracies for string-net models

We now build on the results presented in the previous two sections in order to give a general description of the spectral degeneracies of string-net models. In order to do so, we first have to think carefully about which excitations can actually exist on the lattice (in the plaquettes) in the constrained Hilbert space we are considering, i.e., which objects among the simple objects of the Drinfeld center $\mathcal{Z}(\mathcal{C})$ are fluxons. The main ingredient we will introduce is an object $n_{A,1}$ that is equal to 0 for a non-fluxon and equal to a strictly positive integer for a fluxon. If $n_{A,1} = 1$ it means that A is a fluxon with no internal degeneracy. If $n_{A,1} > 1$, it means that A is a fluxon with internal degeneracy given by $n_{A,1}$. Here and in the following, simple objects of \mathcal{C} will be denoted by lowercase roman letters and simple objects of $\mathcal{Z}(\mathcal{C})$ by capital roman letters.

4.4.1 Fluxons

Determining fluxons from the tube algebra

The excitations of the string-net model can be identified with the help of the tube algebra discussed in Sec. 2.5.3. The physical intuition is the following: imagine there is an excitation $A \in \mathcal{Z}(\mathcal{C})$ located in a plaquette p . One can in principle measure this excitation by acting with the corresponding projector P_A at the level of the plaquette [84]. The tube algebra provides a way to construct such a

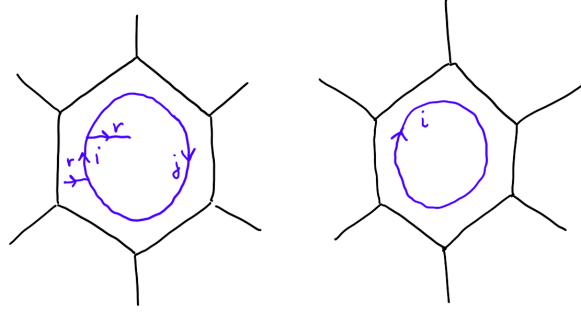


Figure 4.5: Tubes inserted in a plaquette on a honeycomb lattice. A generic tube appearing in a projector as represented on the left has two open edges labeled with $r \in \mathcal{C}$. If both edges are labeled with 1, the tube is simply a loop labeled with a simple object $i \in \mathcal{C}$. Such a loop in a plaquette corresponds to the action of the operator B_p^i , see Sec. 3.3.

projector [see Eqs. (2.48), (2.51)]:

$$P_A = \sum_{r,i,j \in \mathcal{C}} \sum_{a=1}^{n_{A,r}} [M_{A,rrj}^i]_{a,a}^{-1} Q_{rrj}^i. \quad (4.12)$$

That is, acting with a projector P_A on A consists in inserting tubes Q_{rrj}^i with a certain weight given by $[M_{A,rrj}^i]_{a,a}^{-1}$ into the plaquette and around the excitation A , see Fig. 4.5 (a similar approach can be found in the context of extended string-net models [92, 93]).

The object A can be seen as a rope containing several strands $r \in \mathcal{C}$. The number of times a strand r appears in A is given by the multiplicity $n_{A,r}$, which is a non-negative integer [83]. A tube Q_{rrj}^i can "measure" the presence of A if the label r of its open edges matches the label of some strand contained in A , i.e., if $n_{A,r} \neq 0$ (see Sec. 2.5.3 or [84] for more details). However, there is one restriction. A tube with an open edge r violates in general the fusion constraints at its open end, unless $r = 1$. Therefore, in the constrained Hilbert space of the string-net model, one is allowed to act only with tubes that have an open edge label $r = 1$. As a result, the only excitations that are observable are those that respond to these tubes, i.e., the quasiparticles $A \in \mathcal{Z}(\mathcal{C})$ for which $n_{A,1} \neq 0$. The set of these particles is defined as fluxons, $\mathcal{F} \subset \mathcal{Z}(\mathcal{C})$.

In particular, the vacuum $\mathbf{1} \in \mathcal{Z}(\mathcal{C})$ is always a fluxon. In fact, the projector $P_{\mathbf{1}}$ on the vacuum [see Eq. (2.57)] in a plaquette p is exactly the plaquette operator of the string-net Hamiltonian:

$$B_p = \sum_{s \in \mathcal{C}} \frac{d_s}{D_C^2} B_p^s. \quad (4.13)$$

As discussed in Sec. 3.3, the B_p^s operators have a simple graphical representation in terms of closed strings of type s inserted into a plaquette. These correspond precisely to tubes Q_{11s}^s , with the open edges labeled with $1 \in \mathcal{C}$ (see Fig. 4.5). The coefficients for these tubes are $\frac{d_s}{D_C^2} \equiv [M_{\mathbf{1},11s}^s]_{\mathbf{1},\mathbf{1}}^{-1}$, and $n_{\mathbf{1},1} = 1$. In the following, we will denote by \mathcal{F} the set of all fluxons in $\mathcal{Z}(\mathcal{C})$, while that of nontrivial fluxons (i.e., all fluxons except the vacuum) will be denoted \mathcal{F}^* .

A topological quasiparticle $A \in \mathcal{F}^*$ has $n_{A,1} \neq 0$ but may also have $n_{A,r} \neq 0$ for some other $r \neq 1$ in \mathcal{C} . More generally, as explained in Sec. 2.5.3, the projector on $A \in \mathcal{F}^*$ splits into different

simple idempotents

$$P_A = \sum_{r \in \mathcal{C}} \sum_{a=1}^{n_{A,r}} p_A^{rr,aa}, \quad (4.14)$$

which act as projectors on subspaces of A labeled by r and a . In other terms, a simple idempotent $p_A^{rr,aa}$ projects on a subtype of A indexed by (A, r, a) . Although we say that A is a fluxon, strictly speaking only the subtypes labeled by $(A, 1, a)$ are, with a ranging from 1 to $n_{A,1}$ ³. To lighten the notation, we will from now on simply denote a fluxon subtype $A \in \mathcal{F}$ as $(A, a) \equiv (A, 1, a)$. For UFCs \mathcal{C} with commutative fusion rules, $n_{A,1} \leq 1$ for $A \in \mathcal{Z}(\mathcal{C})$, so there is only one fluxon subtype for a given $A \in \mathcal{F}$. Moreover, the number of fluxons $A \in \mathcal{Z}(\mathcal{C})$ is exactly the number of simple objects in \mathcal{C} , $N_{\mathcal{C}}$. If the fusion rules of \mathcal{C} are non-commutative, one may have $n_{A,1} > 1$ for some A , so there may be several fluxon subtypes corresponding to the same topological quasiparticle A . On the other hand, the number of objects $A \in \mathcal{Z}(\mathcal{C})$ having fluxon subtypes is $\leq N_{\mathcal{C}}$.

Using Eq. (2.34), one can also find a relation between the multiplicity $n_{A,1}$ and the quantum dimension d_A of an object A :

$$d_A = \sum_{s \in \mathcal{C}} n_{A,s} d_s = n_{A,1} + \sum_{s \in \mathcal{C}, s \neq 1} n_{A,s} d_s \geq n_{A,1}. \quad (4.15)$$

In particular, for the vacuum $\mathbf{1}$, $d_{\mathbf{1}} = n_{\mathbf{1},1} = 1$. Finally, let us remark that two Morita equivalent categories (i.e., leading to equivalent Drinfeld centers) will in general not have the same fluxon content, since the multiplicities $n_{A,1}$ do not only depend on $\mathcal{Z}(\mathcal{C})$, but also on \mathcal{C} .

Fluxon identities

From the multiplicities, one can define a vector \mathbf{n}_1 with components $n_{A,1}$ where $A = 1, \dots, N_{\mathcal{Z}}$ (and $N_{\mathcal{Z}}$ is the number of simple objects in $\mathcal{Z}(\mathcal{C})$) such that it has non-zero entries only when A is a fluxon. This vector verifies the following identities:

$$T \mathbf{n}_1 = \mathbf{n}_1, \quad (4.16)$$

$$S \mathbf{n}_1 = \mathbf{n}_1, \quad (4.17)$$

where S and T are the modular matrices of $\mathcal{Z}(\mathcal{C})$ see also Sec. 2.2.2. A proof of these identities based on the tube algebra is given in Appendix B. Similar equations first appeared in the context of anyon condensation [116] and gapped boundaries [104, 117]. Here, they are obtained as properties of the fluxons.

Equation (4.16) involving the T -matrix means that fluxons have a trivial twist $\theta_A = 1$. In fact, using Eq. (2.22), one obtains for the left-hand side of Eq. (4.16)

$$\sum_B T_{A,B} n_{B,1} = \sum_B \theta_A \delta_{A,B} n_{B,1} = \theta_A n_{A,1}, \quad (4.18)$$

from which it is straightforward to deduce, comparing with the right-hand side of Eq. (4.16), that $\theta_A = 1$ if $n_{A,1} \neq 0$.

³A similar labeling of quasiparticles in terms of tube algebra sectors s is done e.g. in [115].

Finally, from the theory of anyon condensation we also obtain that the vector \mathbf{n}_1 has to verify the following stability equation [116, 118]:

$$n_{A,1} n_{B,1} \leq \sum_C N_{AB}^C n_{C,1}, \quad (4.19)$$

where N_{AB}^C are the fusion coefficients of the Drinfeld center $\mathcal{Z}(\mathcal{C})$. This relation ensures that the product of two fluxons A and B ($n_{A,1}$ and $n_{B,1} \geq 1$) always contains at least one fluxon (C with $n_{C,1} \geq 1$). Eqs. (4.16), (4.17) and (4.19) are equivalent to the conditions for the existence of a set of condensable bosons [116, 118, 119]. The same conditions also define a Lagrangian algebra [120], and are necessary for the existence of gapped boundaries [104].

4.4.2 Adapting the Moore-Seiberg-Banks formula

We are now ready to compute the degeneracies. We consider a two-dimensional orientable compact manifold of genus g , with N_p plaquettes, and a string-net build from a UFC \mathcal{C} realizing a topological order described by $\mathcal{Z}(\mathcal{C})$. This section contains one of the main results of this thesis: adapting the Moore-Seiberg-Banks formula to the degeneracies of a string-net model.

Closed manifolds

Let us consider first a closed manifold, and a situation in which we have excited q plaquettes by setting $(A_1, a_1) \dots (A_q, a_q)$ fluxon labels with $A \in \mathcal{F}^*$ in these plaquettes. Although the positions and labels of these fluxons are fixed, there still is a degeneracy which comes from the different possibilities how these fluxons can fuse together. The fusion rules are encoded in the fusion matrices of $\mathcal{Z}(\mathcal{C})$ and are not dependent on the subtype of fluxon a which is considered.

We can thus directly apply the Moore-Seiberg-Banks equation (4.11) to this situation, by using $\dim_{\mathcal{Z}(\mathcal{C})}(g; A_1, \dots, A_q)$. This degeneracy, purely described by data from the Drinfeld center, is what we call a *topological* degeneracy.

The standard string-net Hamiltonian makes no energy difference between the different fluxon types and different fluxon subtypes. Therefore, we need to sum over all possibilities in order to get the full degeneracy for q excited plaquettes. Up to a combinatorial prefactor given by the binomial coefficient $\binom{N_p}{q}$ (which accounts for the number of ways to choose q excited plaquettes among N_p plaquettes), the degeneracy on a genus g closed surface is then:

$$\begin{aligned} D_{\mathcal{C}}(g, q) &= \sum_{A_1, \dots, A_q \in \mathcal{F}^*} \prod_{i=1}^q \sum_{\alpha=1}^{n_{A_i,1}} \dim_{\mathcal{Z}(\mathcal{C})}(g; A_1, \dots, A_q) \\ &= \sum_{A_1, \dots, A_q \in \mathcal{F}^*} \dim_{\mathcal{Z}(\mathcal{C})}(g; A_1, \dots, A_q) \prod_{i=1}^q n_{A_i,1}. \end{aligned} \quad (4.20)$$

The factor $\prod_{i=1}^q n_{A_i,1}$ multiplying every term $\dim_{\mathcal{Z}(\mathcal{C})}(g; A_1, \dots, A_q)$ takes into account the number of different fluxon subtypes. This factor is larger than one only if \mathcal{C} is non-commutative. As we have seen in Sec. 4.4.1, one can construct plaquette operators projecting on the different fluxon



Figure 4.6: A sphere (left) with a hole is topologically equivalent to a disk (center). A sphere with two holes is a cylinder (right).

subtypes. Thus, the degeneracy coming from the internal multiplicities is *nontopological*. However, it is interesting to note that, due to this additional degeneracy, the spectral degeneracies of the standard string-net Hamiltonian are not necessarily the same for Morita equivalent categories.

Writing out explicitly Eq. (4.20) and using Eq. (4.11) as well as the fluxon identity of Eq. (4.17), we obtain a simpler form of the q -th level degeneracies:

$$\begin{aligned}
 D_{\mathcal{C}}(g, q) &= \sum_{A_1, \dots, A_q \in \mathcal{F}^*} \sum_{C \in \mathcal{Z}(\mathcal{C})} S_{1, C}^{2-2g-q} \left(\prod_{j=1}^q S_{C, A_j} n_{A_j, 1} \right), \\
 &= \sum_{C \in \mathcal{Z}(\mathcal{C})} S_{1, C}^{2-2g-q} \left(\sum_{A \in \mathcal{F}^*} S_{C, A} n_{A, 1} \right)^q, \\
 &= \sum_{C \in \mathcal{Z}(\mathcal{C})} S_{1, C}^{2-2g-q} \left(\left(\sum_{A \in \mathcal{F}} S_{C, A} n_{A, 1} \right) - S_{1, C} \right)^q, \\
 &= \sum_{C \in \mathcal{Z}(\mathcal{C})} S_{1, C}^{2-2g-q} \left(n_{C, 1} - S_{1, C} \right)^q. \tag{4.21}
 \end{aligned}$$

This equation for the degeneracy of a level with q -fluxons and involving the internal multiplicities $n_{C, 1}$ is one of the main results of this thesis. We have extensively tested this formula numerically (by exact diagonalization on small systems with different Euler-Poincaré characteristics, see Sec. 4.6). One can also check that when setting $q = 0$, one correctly recovers the ground-state degeneracy given by Eq. (4.9). Furthermore, as we show in Sec. 4.4.3, when summed over all possible fluxons on all possible plaquettes, this formula correctly gives the total Hilbert space dimension of the model.

Manifold with boundaries

We now extend the previous results to string-net models on surfaces with boundaries. For a given topological order $\mathcal{Z}(\mathcal{C})$, there are several types of possible gapped boundaries [96, 117]. Here, we only consider smooth boundaries, i.e. described by \mathcal{C} . These boundaries correspond to the condensation of the fluxons to the vacuum.

Consider starting with an orientable manifold without boundary and of genus g . Then we can imagine poking b (potentially large) holes in this manifold to obtain a manifold with boundary. For example, a sphere with one hole is a disk, and a sphere with two holes a cylinder, see Fig. 4.6.

The holes are essentially (potentially large) plaquettes themselves — the only distinction between a boundary hole and a regular plaquette is that in the Hamiltonian we sum only over plaquettes that are not these boundary holes, i.e., the energy cost of a boundary hole is zero.

As a result, even in the ground state we may have some nontrivial fluxons inside these holes. The ground-state degeneracy of the string-net model is then given by summing over all possible fluxons (including the vacuum fluxon) that can be present in each hole. All other plaquettes are assumed to be in the ground state, i.e, contain the vacuum fluxon 1 . The ground-state degeneracy is thus

$$\begin{aligned} D_{\mathcal{C}}(g, b, q = 0) &= \sum_{A_1, \dots, A_b \in \mathcal{F}} \dim_{\mathcal{Z}(\mathcal{C})}(g; A_1, \dots, A_b) \prod_{i=1}^b n_{A_i, 1} \\ &= \sum_{A \in \mathcal{Z}(\mathcal{C})} S_{1, A}^{2-2g-b} n_{A, 1}^b. \end{aligned} \quad (4.22)$$

Apart from the substitution of b with q , the only difference between Eq. (4.22) and Eq. (4.21) comes from the fact that we sum on \mathcal{F} instead than on \mathcal{F}^* . This equation is in agreement with the results given for the GSD with gapped boundaries in Ref. [117]. Equation (4.22) should be considered as a generalization of Eq. (4.9) to the case with boundaries and with internal multiplicities. In the absence of boundary, i.e., for $b = 0$, one recovers Eq. (4.9):

$$D_{\mathcal{C}}(g, 0, 0) = \dim_{\mathcal{Z}(\mathcal{C})}(g) = \sum_{A \in \mathcal{Z}(\mathcal{C})} S_{1, A}^{2-2g}, \quad (4.23)$$

where, by convention, we set $0^0 = 1$.

We are now ready to compute the degeneracies of the excited states in the most general situation, which essentially merges the two previous calculations. We choose q plaquettes that can have any non-vacuum fluxon (punctures labeled from 1 to q), whereas the b boundaries (holes labeled from $q + 1$ to $b + q$) can have any fluxon including the vacuum.

Up to the binomial factor $\binom{N_p}{q}$ discussed before Eq. (4.21), the degeneracy of the q^{th} excitation level, $E_q = -N_p + q$, is then

$$\begin{aligned} D_{\mathcal{C}}(g, b, q) &= \sum_{\substack{A_1, \dots, A_q \in \mathcal{F}^* \\ A_{q+1}, \dots, A_{q+b} \in \mathcal{F}}} \dim_{\mathcal{Z}(\mathcal{C})}(g; A_1, \dots, A_q, A_{q+1}, \dots, A_{q+b}) \prod_{i=1}^{q+b} n_{A_i, 1} \\ &= \sum_{A \in \mathcal{Z}(\mathcal{C})} S_{1, A}^{2-2g-q-b} (n_{A, 1} - S_{1, A})^q n_{A, 1}^b, \end{aligned} \quad (4.24)$$

which coincides with Eq. (4.21) in the compact case ($b = 0$), as expected.

4.4.3 Total Hilbert-space dimension

To conclude this section, we use our results on the degeneracies to compute the total Hilbert space dimension of a string-net model built from a category \mathcal{C} on an orientable surface of genus g with N_p plaquettes, b boundaries, and without vertex defects. To do so, we sum over the degeneracy of the string-net model for all possible fluxon types (including the vacuum 1) being present in all

$(N_p + b)$ “punctures”. We get:

$$\begin{aligned}
 \dim \mathcal{H} &= \sum_{A_1, \dots, A_{N_p+b} \in \mathcal{F}} \dim_{\mathcal{Z}(\mathcal{C})}(g; A_1, \dots, A_{N_p+b}) \prod_{i=1}^{N_p+b} n_{A_i,1}, \\
 &= \sum_{C \in \mathcal{Z}(\mathcal{C})} S_{1,C}^{2-2g-(N_p+b)} \left(\sum_{A \in \mathcal{F}} S_{A,C} n_{A,1} \right)^{N_p+b}, \\
 &= \sum_{C \in \mathcal{Z}(\mathcal{C})} S_{1,C}^{2-2g-(N_p+b)} n_{C,1}^{N_p+b}, \\
 &= D_C(g, N_p + b, 0),
 \end{aligned} \tag{4.25}$$

where we have again used Eq. (4.11) and the fluxon identity Eq. (4.17).

For a trivalent graph, one further has $N_l = \frac{3}{2}N_v$, where N_l and N_v denote the number of links and the number of vertices, respectively. The Euler-Poincaré characteristic on a genus- g surface with b boundaries is then given by

$$\chi = 2 - 2g - b = N_p - N_l + N_v = N_p - \frac{1}{2}N_v. \tag{4.26}$$

Thus, we can also write the Hilbert-space dimension as

$$\dim \mathcal{H} = \sum_{C \in \mathcal{Z}(\mathcal{C})} S_{1,C}^{-N_v/2} n_{C,1}^{N_p+b}. \tag{4.27}$$

One straightforwardly sees that for commutative UFCs ($n_{C,1} = 0$ or 1), this dimension only depends on the number of vertices whereas, in the noncommutative case for which $n_{C,1}$ can be larger than 1, $\dim \mathcal{H}$ also depends on N_p (and b). Hence, in this latter case, the Hilbert-space dimension is sensitive to the surface topology. Replacing $N_p + b$ by $2 - 2g + N_v/2$ and keeping in mind that $S_{1,C} = d_C/D$ [where D is the total quantum dimension of $\mathcal{Z}(\mathcal{C})$] one gets

$$\dim \mathcal{H} = \mathcal{D}^{N_v/2} \sum_{C \in \mathcal{Z}(\mathcal{C})} n_{C,1}^{2-2g} \left(\frac{n_{C,1}}{d_C} \right)^{N_v/2}. \tag{4.28}$$

As $n_{C,1} \leq d_C$, one gets, in the thermodynamic limit:

$$\dim \mathcal{H} \simeq \mathcal{D}^{N_v/2} \sum_{C \in \mathcal{P}} n_{C,1}^{2-2g} = \mathcal{D}^{N_v/2} M_g, \tag{4.29}$$

where $\mathcal{P} \subseteq \mathcal{F}$ is the set of *pure fluxons*, for which $n_{C,1} = d_C$ (we will discuss pure fluxons in detail in Chap. 5) and we have introduced the notation $M_g = \sum_{C \in \mathcal{P}} n_{C,1}^{2-2g}$.

4.5 Special cases

In the previous sections, all results were given in terms of data from the Drinfeld center and the tube algebra. Yet, for some special cases, we can also write Eq. (4.24) completely or partially in terms of data from the input category. We will discuss these cases here, namely when the input category is a UMTC and when the input category is commutative.

4.5.1 Modular categories

When the input category of the string-net model is modular, it is possible to compute the degeneracies of the excited levels by using only the fusion properties of the input category. This approach is presented in Ref. [110], where the partition function is computed from a microscopic point of view for string-net models built from an input category \mathcal{C} which is a UMTC. We aim here at making the link between the results of the previous sections and the ones of Ref. [110].

In the case where the input category \mathcal{C} is a UMTC, the Drinfeld center is the product of two copies of \mathcal{C} of opposite chiralities [51] (see also Sec. 2.5.2):

$$\mathcal{Z}(\mathcal{C}) = \mathcal{C} \times \bar{\mathcal{C}}. \quad (4.30)$$

In this case, any object A of the center can be represented by a couple (i, j) of objects $i \in \mathcal{C}$ and $j \in \bar{\mathcal{C}}$. The S -matrix of the Drinfeld center $\mathcal{Z}(\mathcal{C})$ has a simple expression in terms of the S -matrix of the input category \mathcal{C} (for clarity, we will denote them respectively S and s):

$$S_{A,B} = S_{(i,j),(p,q)} = s_{i,p} s_{j,q}^*. \quad (4.31)$$

A particle $A = (i, j)$ of $\mathcal{Z}(\mathcal{C})$ is a fluxon if and only if $j = \bar{i}$ (where \bar{i} is the mirror object of i) and $n_{A,1} = 1$, so that $S_{1,A} = s_{1,i} s_{1,\bar{i}}^* = s_{1,i}^2$. In all other cases, $n_{A,1} = 0$. Thus, when $b = 0$, we can rewrite (4.21) as

$$\begin{aligned} D_{\mathcal{C}}(g, 0, q) &= \sum_{i,j \in \mathcal{C}} (s_{1,i} s_{1,j})^X \left(\frac{\delta_{i,j}}{s_{1,i} s_{1,j}} - 1 \right)^q, \\ &= (-1)^q \left\{ \sum_{i \in \mathcal{C}} s_{1,i}^{2X} [(1 - s_{1,i}^{-2})^q - 1] + D_{\mathcal{C}}(g, 0, 0) \right\}, \end{aligned} \quad (4.32)$$

where $D_{\mathcal{C}}(g, 0, 0) = \left(\sum_{i \in \mathcal{C}} s_{1,i}^X \right)^2$ is the ground-state degeneracy. Up to a binomial factor accounting for the number of possibilities to place q fluxons among N_p plaquettes, Eq. (4.32) is exactly Eq. (10) in Ref. [110]. In the same way, from the equation for the Hilbert space dimension Eq. (4.28), we obtain

$$\dim \mathcal{H} = \sum_{j \in \mathcal{C}} \left(\frac{\mathcal{D}_{\mathcal{C}}}{d_j} \right)^{N_V}, \quad (4.33)$$

where $\mathcal{D}_{\mathcal{C}}$ is the total quantum dimension of the input category \mathcal{C} [and $\mathcal{D} = \mathcal{D}_{\mathcal{C}}^2$ is the total quantum dimension of $\mathcal{Z}(\mathcal{C})$], which coincides with the expression given in Refs. [76, 110].

4.5.2 Commutative categories

The above equations do not hold in the case where the input category is commutative but not modular, since we cannot define a modular S -matrix. However, for any commutative input category, we can always find a unitary matrix \tilde{s} , called the mock S -matrix, that simultaneously diagonalizes its fusion matrices N_i . Unlike the S -matrix, this matrix is not symmetric in general. Naturally, one would label the matrix elements as $\tilde{s}_{i,j}$ with i and $j \in \mathcal{C}$. However, \tilde{s} can also be

understood as a unitary transformation between input objects and fluxons [see Eq. (B.2)]. In fact, the mock- S -matrix also diagonalizes the tube algebra in the 11 sector, and therefore its column vectors give the components of the fluxons A in terms of the tubes in the 11 sector, which are uniauey indexed by an object $s \in \mathcal{C}$. As such, it makes physically more sense to write a matrix element of \tilde{s} as $\tilde{s}_{i,A}$ with rows indexed by input labels $i = 1, \dots, N_{\mathcal{C}}$ and columns by fluxons $A \in \mathcal{F}$, and $N_{\mathcal{F}} = N_{\mathcal{C}}$ (see Sec. 2.5.3). The matrix \tilde{s} can be chosen such that its first row only contains strictly positive elements. In this case, $\tilde{s}_{1,A} = \sqrt{d_A/\mathcal{D}} = \sqrt{S_{1,A}}$. The mock S -matrix is not yet unique as its columns can always be permuted. By convention, we choose that the first column corresponds to the vacuum $A = 1$ of the output category so that $\tilde{s}_{i,1} = d_i/\sqrt{\mathcal{D}}$. Examples of mock S -matrices are given in Secs. 4.6.1, 4.6.2 and 4.6.4. For this mock- S matrix, we can write a Verlinde-like equation

$$N_{ij}^k = \sum_{A \in \mathcal{F}} \frac{\tilde{s}_{i,A} \tilde{s}_{j,A} \tilde{s}_{k,A}^*}{\tilde{s}_{1,A}}. \quad (4.34)$$

Also, for any commutative UFC, the multiplicities $n_{A,1}$ only take values 0 or 1, and the number of fluxons is equal to the number of simple objects in the input category. With these insights at hand, we can rewrite Eq. (4.24) as

$$D_{\mathcal{C}}(g, 0, q) = (-1)^q \left\{ \sum_{A \in \mathcal{F}} \tilde{s}_{1,A}^{2\chi} [(1 - \tilde{s}_{1,A}^{-2})^q - 1] + D_{\mathcal{C}}(g, 0, 0) \right\}, \quad (4.35)$$

which is very similar to Eq. (4.32) with $s_{1,i}$ replaced by $\tilde{s}_{1,A}$ and fluxons labeled by $A \in \mathcal{F}$ instead of $i \in \mathcal{C}$. However, in the present case, there is no general formula for the ground-state degeneracy $D_{\mathcal{C}}(g, 0, 0)$ in terms of \tilde{s} . One could think of using Eq. (4.23) to compute the ground-state degeneracy with $S_{1,A} = \tilde{s}_{1,A}^2$, but this relation only holds for fluxons and not for all $A \in \mathcal{Z}(\mathcal{C})$.

Generally speaking, it is not possible to compute the ground-state degeneracy $D_{\mathcal{C}}(g, 0, 0)$ simply from the knowledge of the fusion rules of the input category. In fact, two input categories that have the same fusion rules but different F -symbols generally lead to two different Drinfeld centers. In particular, the number of simple objects of the Drinfeld centers need not be the same. And even if the numbers match, the corresponding quantum dimensions d_A need not be equal and therefore the level degeneracies can differ. However, there still is a way to write $D_{\mathcal{C}}(g, 0, 0)$ only in terms of the input data. This way, which is a bit cumbersome, requires the use of the F -symbols of the category (see Ref. [103]).

4.6 Examples

This section is devoted to non-trivial examples that illustrate the formulas obtained in the previous sections. Before discussing some specific examples, let us give some general results that are valid for any input category \mathcal{C} . In Table 4.1, we give the degeneracies $D_{\mathcal{C}}(g, b, q)$ [see Eq. (4.24)] of the first three energy levels for various simple surface topologies.

To obtain these results, we used Eq. (4.17) which leads to

$$\sum_{A \in \mathcal{Z}(\mathcal{C})} S_{1,A} n_{A,1} = n_{1,1} = 1, \quad (4.36)$$

$D_{\mathcal{C}}$	$(g, b) = (0, 0)$	$(0, 1)$	$(0, 2)$	$(1, 0)$
$q = 0$	1	1	$N_{\mathcal{C}}$	$N_{\mathcal{Z}}$
1	0	$N_{\mathcal{C}} - 1$		
2	$N_{\mathcal{C}} - 1$			

Table 4.1: Degeneracies $D_{\mathcal{C}}(g, b, q)$ of the q -th excited level (row index: $q = 0, 1, 2$) for various surface topologies characterized by their genus g and their b boundaries [column index (g, b)]. The four columns correspond respectively to the case of a sphere, a disk, a cylinder and a torus. The number of simple objects in the input category \mathcal{C} and in its Drinfeld center $\mathcal{Z}(\mathcal{C})$ are denoted by $N_{\mathcal{C}}$ and $N_{\mathcal{Z}}$, respectively. Empty entries depend on the input category details.

and Eq. (2.56).

Whenever possible, i.e., if the Hilbert space is not too large, we checked these degeneracies by exact diagonalization of the Hamiltonian (3.8) on trivalent graphs with the corresponding topology. For instance, starting from a cube ($g = b = 0$, and $N_v = 8$), we can build a “disk” ($g = 0$, $b = 1$) by removing one plaquette operator in the Hamiltonian or a “cylinder” ($g = 0$, $b = 2$) by removing two opposite plaquette operators.

4.6.1 $\text{Rep}(S_3)$ and $\text{Vec}(S_3)$ categories

We present here two string-net models built from two Morita-equivalent categories: $\text{Rep}(S_3)$ and $\text{Vec}(S_3)$, where S_3 is the symmetric group of a set of 3 elements (symmetry group of the equilateral triangle). They correspond respectively to the category of irreducible representations of S_3 and the category of the elements of the group S_3 .

The category $\mathcal{C} = \text{Rep}(S_3)$ (see also Sec. 2.3) contains $N_{\mathcal{C}} = 3$ simple objects $\{1, 2, 3\}$ with quantum dimensions $\{1, 1, 2\}$, which correspond to the irreducible representations of S_3 . The fusion rules of this category are commutative, but the category is non-Abelian, braided, and nonmodular. The category $\mathcal{C} = \text{Vec}(S_3)$ contains $N_{\mathcal{C}} = 6$ simple objects $\{e, y, y^2, x, xy, xy^2\}$, which are the elements of the group S_3 , (e is the identity element, y is a $2\pi/3$ rotation and x is a mirror). The fusion rules are simply the multiplication rules of the group. All elements have quantum dimension $d_s = 1$. The fusion rules are noncommutative, but the category is Abelian. The two categories are Morita-equivalent and lead to the same Drinfeld center $\mathcal{Z}(S_3)$. The latter contains $N_{\mathcal{Z}} = 8$ simple objects, denoted by $\{A, B, C, D, E, F, G, H\}$ with A being the vacuum, see Ref. [121]. The quantum dimensions are $\{1, 1, 2, 3, 3, 2, 2, 2\}$, and the total quantum dimension is $\mathcal{D} = 6$. On table 4.2, we show the fusion rules of these objects.

While the two categories share the same center $\mathcal{Z}(S_3)$, the tube algebras are different. In particular, the internal multiplicities of the quasiparticles, $n_{A,s}$ differ. We give them as rectangular matrices

\otimes	A	B	C	D	E	F	G	H
A	A	B	C	D	E	F	G	H
B	B	A	C	E	D	F	G	H
C	C	C	$A \oplus B \oplus C$	$D \oplus E$	$D \oplus E$	$G \oplus H$	$F \oplus H$	$F \oplus G$
D	D	E	$D \oplus E$	$A \oplus C \oplus F \oplus G \oplus H$	$B \oplus C \oplus F \oplus G \oplus H$	$D \oplus E$	$D \oplus E$	$D \oplus E$
E	E	D	$D \oplus E$	$B \oplus C \oplus F \oplus G \oplus H$	$A \oplus C \oplus F \oplus G \oplus H$	$D \oplus E$	$D \oplus E$	$D \oplus E$
F	F	F	$G \oplus H$	$D \oplus E$	$D \oplus E$	$A \oplus B \oplus F$	$H \oplus C$	$G \oplus C$
G	G	G	$F \oplus H$	$D \oplus E$	$D \oplus E$	$H \oplus C$	$A \oplus B \oplus G$	$F \oplus C$
H	H	H	$F \oplus G$	$D \oplus E$	$D \oplus E$	$G \oplus C$	$F \oplus C$	$A \oplus B \oplus H$

 Table 4.2: Fusion rules for $\mathcal{Z}(S_3)$, taken from Ref. [121].

n_C with N_C columns and N_Z rows:

$$n_{\text{Rep}(S_3)} = \begin{pmatrix} 1 & 0 & 0 \\ 0 & 1 & 0 \\ 0 & 0 & 1 \\ 1 & 0 & 1 \\ 0 & 1 & 1 \\ 1 & 1 & 0 \\ 0 & 0 & 1 \\ 0 & 0 & 1 \end{pmatrix}, \quad n_{\text{Vec}(S_3)} = \begin{pmatrix} 1 & 0 & 0 & 0 & 0 & 0 \\ 1 & 0 & 0 & 0 & 0 & 0 \\ 2 & 0 & 0 & 0 & 0 & 0 \\ 0 & 0 & 0 & 1 & 1 & 1 \\ 0 & 0 & 0 & 1 & 1 & 1 \\ 0 & 1 & 1 & 0 & 0 & 0 \\ 0 & 1 & 1 & 0 & 0 & 0 \\ 0 & 1 & 1 & 0 & 0 & 0 \end{pmatrix}. \quad (4.37)$$

The first column corresponds to \mathbf{n}_1 of respectively $\text{Rep}(S_3)$ and $\text{Vec}(S_3)$. Quantum dimensions of the quasiparticles in the Drinfeld center and the multiplicities are the only quantities we need to compute the degeneracies of any energy level with Eq. (4.24). In both cases there are three types of fluxons (quasiparticles A with $n_{A,1} > 0$) but they correspond to two different subsets of the simple objects of $\mathcal{Z}(S_3)$: A, D, F for $\text{Rep}(S_3)$, and A, B, C for $\text{Vec}(S_3)$ (note that $n_{C,1} = 2$). Let us mention also that the pure fluxons are A for $\text{Rep}(S_3)$ and A, B, C for $\text{Vec}(S_3)$. Also note that by fusion of fluxons, $\{A, B, C\}$ form a closed subset, while $\{A, D, F\}$ generate all of $\mathcal{Z}(S_3)$.

To give a concrete example of how the formula for degeneracies works, we perform below an explicit counting for the two first energy levels of a torus for both $\text{Rep}(S_3)$ and $\text{Vec}(S_3)$ (to avoid confusion, here we denote generic excitations $\in \mathcal{Z}(S_3)$ by greek letters). For the ground state, the fusion diagram is simply

$$\begin{array}{c} \circlearrowleft \\ \alpha \end{array} \quad \text{with } \alpha \in \mathcal{Z}(S_3), \quad (4.38)$$

so we find $D_{\text{Rep}(S_3)}(1, 0, 0) = D_{\text{Vec}(S_3)}(1, 0, 0) = 8$. For the first excited state, the fusion diagram is

$$\begin{array}{c} \alpha \\ \circlearrowleft \\ \beta \end{array} \quad \text{with } \alpha \in \mathcal{Z}(S_3), \beta \in \mathcal{F}^*. \quad (4.39)$$

Comparing with Table 4.2, we see that for $\text{Rep}(S_3)$ the following pairs (α, β) are possible: (D, F) , (E, F) , (F, F) . A single excitation of type D cannot exist at the surface of the torus because there is no object $\alpha \in \mathcal{Z}(S_3)$ that yields D when fused with a copy of itself. Therefore, for $\text{Rep}(S_3)$ we have

$D_{\text{Rep}(S_3)}(1, 0, 1) = 3$. On the other hand, for $\text{Vec}(S_3)$ the possible pairs are $(C, B), (F, B), (G, B), (H, B), (D, C), (E, C)$ and (C, C) . Additionally, the pairs $(C, C), (D, C), (E, C)$ can appear in two different flavors as $n_{C,1} = 2$. Hence, the degeneracy is $D_{\text{Vec}(S_3)}(1, 0, 1) = 4 + 3 \times 2 = 10$. Clearly, the spectral degeneracies of the two models are different. More values for degeneracies are provided on Tables 4.3 and 4.4.

$D_{\text{Rep}(S_3)}$	$(g, b) = (0, 0)$	$(0, 1)$	$(0, 2)$	$(1, 0)$
$q = 0$	1	1	3	8
1	0	2	8	3
2	2	6	30	35
3	4	24	134	129
4	20	110	642	647

Table 4.3: Degeneracies of the q^{th} excited state of a string net built from $\text{Rep}(S_3)$ for various surface topologies up to $q = 4$. Here g is the genus and b is the number of boundaries.

$D_{\text{Vec}(S_3)}$	$(g, b) = (0, 0)$	$(0, 1)$	$(0, 2)$	$(1, 0)$
$q = 0$	1	1	6	8
1	0	5	30	10
2	5	25	150	80
3	20	125	750	370
4	105	625	3750	1880

Table 4.4: Degeneracies of the q^{th} excited state of a string net built from $\text{Vec}(S_3)$ for various surface topologies up to $q = 4$. Here g is the genus and b is the number of boundaries.

The dimension of the Hilbert space [see Eq. (4.27)] is

$$\dim \mathcal{H} = \left(1 + 3^{-N_v/2} + 2^{-N_v/2}\right) \sqrt{6}^{N_v}, \quad (4.40)$$

for $\text{Rep}(S_3)$ and

$$\dim \mathcal{H} = (1 + 1 + 2^{2-2g}) \sqrt{6}^{N_v}, \quad (4.41)$$

for $\text{Vec}(S_3)$. We provide a few values of $\dim \mathcal{H}$ in Table 4.5 for some simple trivalent graphs.

The fusion matrices of the commutative category $\text{Rep}(S_3)$ are simultaneously diagonalized by the following mock S -matrix:

$$\tilde{s} = \frac{1}{\sqrt{6}} \begin{pmatrix} 1 & \sqrt{3} & \sqrt{2} \\ 1 & -\sqrt{3} & \sqrt{2} \\ 2 & 0 & -\sqrt{2} \end{pmatrix}. \quad (4.42)$$

This matrix contains the transformation $\tilde{s}_{i,J}$ between the simple objects $i \in \{1, 2, 3\} = \mathcal{C}$ of the input category and the fluxons $J \in \{A, D, F\} = \mathcal{F}$ of the output category $\mathcal{Z}(\mathcal{C})$. Here, it was chosen such that the first row only contains strictly positive elements, in which case, one has $\tilde{s}_{1,J} = \sqrt{d_J/\mathcal{D}}$ and $\tilde{s}_{i,1} = d_i/\sqrt{\mathcal{D}}$ (see Sec. 4.5).

In conclusion, $\text{Rep}(S_3)$ and $\text{Vec}(S_3)$ are two Morita-equivalent UFCs that correspond to the same Drinfeld center but lead to different Hilbert spaces and spectral degeneracies.

$\dim \mathcal{H}$	$(g, N_v) = (0, 2)$	(1,2)	(0,4)	(1,4)	(0,6)	(1,6)
$\text{Rep}(S_3)$	11	11	49	49	251	251
$\text{Vec}(S_3)$	36	18	216	108	1296	648
TY_3	18	18	90	90	486	486
\mathcal{H}_3	63	45	1431	1323	46494	45846

Table 4.5: Hilbert-space dimension $\dim \mathcal{H}$ for some simple closed surfaces ($b = 0$) and for some input categories. Each row corresponds to a given category and each column is indexed by (g, N_v) with g the genus and N_v the number of vertices.

the original string-net model [48]. Its halfbraidings and multiplicities are provided in [78]. It is commutative (but non-Abelian and non-braided), so that $n_{A,1} = 1$ for all fluxons. It has $N_c = 4$ simple objects $\{1, 2, 3, \sigma\}$, with quantum dimensions $\{1, 1, 1, \sqrt{3}\}$. There are two different solutions to the pentagonal equations indexed by $p = \pm 1$ (see [78] for more details on the F -symbols). The Drinfeld center $\mathcal{Z}(\text{TY}_3)$ contains $N_{\mathcal{Z}} = 15$ elements $\{1, \dots, 15\}$ with dimensions $\{1, 1, 1, 1, 1, 1, 2, 2, 2, \sqrt{3}, \sqrt{3}, \sqrt{3}, \sqrt{3}, \sqrt{3}, \sqrt{3}\}$ and the total quantum dimension is $\mathcal{D} = 6$. For the $p = 1$ model, the internal multiplicities are:

$$n_{\text{TY}_3} = \begin{pmatrix} 1 & 0 & 0 & 0 \\ 1 & 0 & 0 & 0 \\ 0 & 1 & 0 & 0 \\ 0 & 1 & 0 & 0 \\ 0 & 0 & 1 & 0 \\ 0 & 0 & 1 & 0 \\ 1 & 1 & 0 & 0 \\ 1 & 0 & 1 & 0 \\ 0 & 1 & 1 & 0 \\ 0 & 0 & 0 & 1 \\ 0 & 0 & 0 & 1 \\ 0 & 0 & 0 & 1 \\ 0 & 0 & 0 & 1 \\ 0 & 0 & 0 & 1 \\ 0 & 0 & 0 & 1 \\ 0 & 0 & 0 & 1 \end{pmatrix}. \quad (4.45)$$

The fluxons are therefore 1, 2, 7 and 8 and pure fluxons are 1, 2. Using Eq. (4.24), we can easily compute the degeneracies. Some examples are given in Table 4.6.

The Hilbert-space dimension [see Eq. (4.27)] is

$$\dim \mathcal{H} = 2 \left(1 + 2^{-N_v/2} \right) \sqrt{6}^{N_v}, \quad (4.46)$$

and a few examples are given in Table 4.5. Interestingly, this topological order breaks time-reversal symmetry (TRS) [78] but still has a vanishing topological central charge ($c \bmod 8 = 0$). The fact that $\mathcal{Z}(\text{TY}_3)$ breaks TRS can be seen from the twist of its objects. For example, for the $p = 1$ model,

D_{TY_3}	$(g, b) = (0, 0)$	$(0, 1)$	$(0, 2)$	$(1, 0)$
$q = 0$	1	1	4	15
1	0	3	14	3
2	3	11	58	69
3	8	47	266	255
4	39	219	1282	1293

Table 4.6: Degeneracies of the q^{th} excited state of a string net built from TY_3 for various surface topologies up to $q = 4$. Here g is the genus and b is the number of boundaries.

the twists are [78]

$$\begin{aligned} & \{e^{i\theta_1}, \dots, e^{i\theta_{15}}\} \\ & = \{1, 1, e^{-\frac{i2\pi}{3}}, e^{-\frac{i2\pi}{3}}, e^{-\frac{i2\pi}{3}}, e^{-\frac{i2\pi}{3}}, 1, 1, e^{\frac{i2\pi}{3}}, e^{\frac{i3\pi}{4}}, e^{-\frac{i\pi}{4}}, e^{-\frac{i11\pi}{12}}, e^{\frac{i\pi}{12}}, e^{-\frac{i11\pi}{12}}, e^{\frac{i\pi}{12}}\}. \end{aligned} \quad (4.47)$$

Under time reversal, the twist of an anyon a transforms as $\theta_a \rightarrow \theta_{T(a)}^{-1}$, where $T(a)$ is the image of a under time-reversal. Thus, if there is no anyon b in the center with $\theta_b = \theta_a^{-1}$, the topological phase must break time reversal symmetry [124]. As can be seen from Eq. (4.47), several objects in $\mathcal{Z}(\text{TY}_3)$ are without time-reversal partner. The same is also true for the $p = -1$ model (see [78]). The fusion matrices of TY_3 are simultaneously diagonalized by the following mock S -matrix:

$$\tilde{s} = \frac{1}{\sqrt{6}} \begin{pmatrix} 1 & 1 & \sqrt{2} & \sqrt{2} \\ 1 & 1 & \sqrt{2}e^{i2\pi/3} & \sqrt{2}e^{-i2\pi/3} \\ 1 & 1 & \sqrt{2}e^{-i2\pi/3} & \sqrt{2}e^{i2\pi/3} \\ \sqrt{3} & -\sqrt{3} & 0 & 0 \end{pmatrix}. \quad (4.48)$$

It contains the transformation $\tilde{s}_{i,A}$ between the simple objects $i \in \{1, 2, 3, \sigma\} = \mathcal{C}$ of the input category and the fluxons $A \in \{1, 2, 7, 8\} = \mathcal{F}$ of the output category $\mathcal{Z}(\mathcal{C})$.

4.6.3 Haagerup category \mathcal{H}_3

The Haagerup category \mathcal{H}_3 is a good example of the universality of our formula: it is neither commutative, nor braided, nor Abelian, nor does it respect tetrahedral symmetry, see e.g. [125]. It has $N_{\mathcal{C}} = 6$ simple objects $\{1, \alpha, \alpha^*, \rho, \alpha\rho, \alpha^*\rho\}$ with quantum dimensions $\{1, 1, 1, d_\rho, d_\rho, d_\rho\}$ where $d_\rho = \frac{3+\sqrt{13}}{2}$. The Drinfeld center \mathcal{H}_3 contains $N_{\mathcal{Z}} = 12$ simple objects $\{1, \mu^1, \mu^2, \mu^3, \mu^4, \mu^5, \mu^6, \pi_1, \pi_2, \sigma^1, \sigma^2, \sigma^3\}$ with quantum dimensions $\{1, 3d_\rho, 3d_\rho, 3d_\rho, 3d_\rho, 3d_\rho, 3d_\rho + 1, 3d_\rho + 2, 3d_\rho + 2, 3d_\rho + 2, 3d_\rho + 2, 3d_\rho + 2\}$ so that the total quantum dimension is $\mathcal{D} = 3(1 + d_\rho^2)$ [125]. The internal

multiplicities are given by [126]

$$n_{\mathcal{H}_3} = \begin{pmatrix} 1 & 0 & 0 & 0 & 0 & 0 \\ 0 & 0 & 0 & 1 & 1 & 1 \\ 0 & 0 & 0 & 1 & 1 & 1 \\ 0 & 0 & 0 & 1 & 1 & 1 \\ 0 & 0 & 0 & 1 & 1 & 1 \\ 0 & 0 & 0 & 1 & 1 & 1 \\ 0 & 0 & 0 & 1 & 1 & 1 \\ 1 & 0 & 0 & 1 & 1 & 1 \\ 2 & 0 & 0 & 1 & 1 & 1 \\ 0 & 1 & 1 & 1 & 1 & 1 \\ 0 & 1 & 1 & 1 & 1 & 1 \\ 0 & 1 & 1 & 1 & 1 & 1 \end{pmatrix}, \quad (4.49)$$

so that the three fluxons are $\mathbf{1}$, π_1 , and π_2 (the only pure fluxon is the vacuum). Some degeneracies computed from Eq. (4.24) are given in Table 4.7.

$D_{\mathcal{H}_3}$	$(g, b) = (0, 0)$	$(0, 1)$	$(0, 2)$	$(1, 0)$
$q = 0$	1	1	6	12
1	0	5	57	33
2	5	52	1311	1245
3	47	1259	42384	42000
4	1212	41125	1456539	1454673

Table 4.7: Degeneracies of the q^{th} excited state of a string net built from \mathcal{H}_3 for various surface topologies up to $q = 4$. Here g is the genus and b is the number of boundaries.

The Hilbert-space dimension [see Eq. (4.27)] is given by

$$\dim \mathcal{H} = \left[1 + \frac{1}{(3d_\rho + 1)^{\frac{N_V}{2}}} + \frac{2^{2-2g+\frac{N_V}{2}}}{(3d_\rho + 2)^{\frac{N_V}{2}}} \right] \mathcal{D}^{\frac{N_V}{2}}, \quad (4.50)$$

(see also Table 4.5).

4.6.4 Hagge-Hong category \mathcal{E}

This is a simple example of an input category $\mathcal{C} = \mathcal{E}$ with fusion multiplicities [125]. It contains $N_{\mathcal{C}} = 3$ simple objects $\{1, x, y\}$ with quantum dimensions $\{1, d_x, 1\}$, where $d_x = \sqrt{3} + 1$ (see Ref. [125] for more details), and the fusion rules are: $x \times x = 1 + 2x + y$, $x \times y = y \times x = x$ and $y \times y = 1$. It is commutative, not braided and it breaks the tetrahedral symmetry. The Drinfeld center $\mathcal{Z}(\mathcal{E})$ contains $N_{\mathcal{Z}} = 10$ simple objects $\{1, Y, X_1, X_2, X_3, X_4, X_5, U, V, W\}$ with quantum dimensions $\{1, 1, d_x, d_x, d_x, d_x, d_x, d_x + 1, d_x + 1, d_x + 2\}$ so that $\mathcal{D} = 2d_x + 4$. Internal multiplicities

are given by [125]

$$n_{\mathcal{E}} = \begin{pmatrix} 1 & 0 & 0 \\ 0 & 0 & 1 \\ 0 & 1 & 0 \\ 0 & 1 & 0 \\ 0 & 1 & 0 \\ 0 & 1 & 0 \\ 0 & 1 & 0 \\ 1 & 1 & 0 \\ 0 & 1 & 1 \\ 1 & 1 & 1 \end{pmatrix}, \quad (4.51)$$

so that the three fluxons are $\mathbf{1}$, U , and W . This allows us to compute the degeneracies for a few systems (see Table 4.8). The Hilbert-space dimension [see Eq. 4.27] is therefore

$D_{\mathcal{E}}$	$(g, b) = (0, 0)$	$(0, 1)$	$(0, 2)$	$(1, 0)$
$q = 0$	1	1	3	10
1	0	2	11	4
2	2	9	75	82
3	7	66	611	604
4	59	545	5139	5146

Table 4.8: Degeneracies of the q^{th} excited state of a string net built from \mathcal{E} for various surface topologies up to $q = 4$. Here g is the genus and b is the number of boundaries.

$$\dim \mathcal{H} = \left[1 + (\sqrt{3} + 2)^{\frac{-N_V}{2}} + (\sqrt{3} + 3)^{\frac{-N_V}{2}} \right] \mathcal{D}^{\frac{N_V}{2}}, \quad (4.52)$$

(see Table 4.5).

The mock S -matrix is

$$\tilde{s} = \frac{1}{\sqrt{2d_x + 4}} \begin{pmatrix} 1 & \sqrt{d_x + 1} & \sqrt{d_x + 2} \\ d_x & -\sqrt{2} & 0 \\ 1 & \sqrt{d_x + 1} & -\sqrt{d_x + 2} \end{pmatrix}, \quad (4.53)$$

where $\tilde{s}_{i,A}$ with $i \in \{1, x, y\}$ and $A \in \{\mathbf{1}, U, W\} = \mathcal{F}$.

4.7 Refined string-net model

The original string-net Hamiltonian assigns the same energy penalty +1 to each fluxon which is not the vacuum. However, we can assign different energy penalties to each fluxon type, and more precisely to each fluxon subtype indexed by (A, a) with $A \in \mathcal{F}^*$ and a ranging from 1 to $n_{A,1}$. Furthermore, we can also assign plaquette-dependent energy penalties. Following up on the discussion of Sec. 4.4.1, we can construct the projector on a fluxon subtype (A, a) by acting with the correspondent simple idempotent from the tube algebra $p_A^{11,aa}$ on plaquette p . This corresponds to inserting closed loops B_p^s (or equivalently tubes Q_{11s}^s) with a certain weight inside

the plaquette p and fusing them into the edges of the plaquette. Generically, we can write such a projector as

$$B_p^{A,a} = p_A^{11,aa} = \sum_{s \in \mathcal{C}} [M_{A,11s}^s]_{a,a}^{-1} B_p^s, \quad (4.54)$$

which is simply a reformulation of Eq. (2.47). In particular, when $A = \mathbf{1}$, then $B_p^{\mathbf{1},1} = B_p$, the standard plaquette operator of the string-net model. Using these projectors one can write a refined version of the string-net Hamiltonian

$$H = \sum_{p=1}^{N_p} \sum_{A \in \mathcal{F}} \sum_{a=1}^{n_{A,1}} \mathcal{J}_p^{A,a} B_p^{A,a}, \quad (4.55)$$

where $\mathcal{J}_p^{A,a}$ are a set of coefficients which can take different values for each plaquette and each fluxon subtype. The original string-net model is recovered for $\mathcal{J}_p^{A,a} = \delta_{A,\mathbf{1}} \forall p$. As long as $\mathcal{J}_p^{\mathbf{1},1}$ is smaller than any $\mathcal{J}_p^{A,a}$ for all $A \neq \mathbf{1}$ and $a = 1, \dots, n_{A,1}$, the ground-state is still the state where all plaquettes are in the vacuum state. However, other choices may now lead to ground states with non-trivial fluxons.

The calculation of excited states degeneracies can in principle be done analytically also for this Hamiltonian. One still starts with the Moore-Seiberg-Banks formula, and sums over all possible fluxon labelings of each plaquette. The remaining degeneracy is purely topological in the sense that it cannot be split further by local operators acting at the level of a plaquette, and depends only on the fusion rules of $\mathcal{Z}(\mathcal{C})$. However, one still needs the knowledge of \mathcal{C} in order to determine the set of fluxons \mathcal{F} .

4.8 Conclusion

In this chapter, we have studied the spectral degeneracies of the generalized string-net model with arbitrary input category and restricted to the charge-free sector (all vertex constraints are satisfied). In this model, only certain objects of the Drinfeld center known as fluxons $A \in \mathcal{F}$ are present as excitations at the single-plaquette level. We show that these fluxons can be determined from the tube algebra thanks to the multiplicities $n_{A,1}$. These multiplicities depend on the input UFC \mathcal{C} . The main results are analytical expressions for the level degeneracies, both for closed manifolds and manifolds with smooth boundaries. The degeneracy arising from the fusion of fluxons and the topology of the manifold can be determined in terms of the modular S -matrix of the Drinfeld center using the Moore-Seiberg-Banks formula, Eq. (4.24). This degeneracy is topological in the sense that it only depends on the fusion rules of the Drinfeld center, and cannot be lifted by local operators acting at the level of single plaquettes. In addition to this topological degeneracy, we have shown that there can be a degeneracy associated with multiplicities $n_{A,1} > 1$ when the input UFC has noncommutative fusion rules. This degeneracy is nontopological in the sense that it can be split by local disorder at the level of a single plaquette. This motivates the introduction of a refined Hamiltonian in which this non-topological degeneracy is completely lifted. Once the degeneracies are known, calculating the partition function of the generalized string-net model is straightforward. This allows for analyzing finite temperature properties of the string-net model,

and will be the subject of the next chapter (Chap. 5). Finally, we wish to use a similar approach to extend the computation of level degeneracies to models that have all elementary excitations of the Drinfeld center and not only fluxons. We will do this for the case of the Kitaev quantum double model [47] in Chap.6. The study of more general models hosting the full excitation spectrum, such as the extended string-nets [93], have been the subject of a subsequent recent work [94].

Finite-temperature properties

5.1 Introduction

While topological order is robust to local perturbations at zero temperature [56], it is known that it may be fragile with respect to thermal fluctuations [38, 39]. In particular, an exact result derived by Hastings [67] states that topological order in two dimensions does not survive at finite temperature in the thermodynamic limit, for Hamiltonians built from local commuting terms. Nevertheless, results on the toric code and Kitaev quantum double model reveal that topological order can persist below a size-dependent temperature [68, 69, 70]. A precise understanding of the behaviour of topologically ordered systems under the influence of temperature is of particular importance in view of experimental realizations [62, 60, 61, 59, 112, 66], and the use of these systems to realize self-correcting memories [127, 71, 73, 57].

The study of topological order at finite temperature has been approached through different angles. Thermalization dynamics of the toric code and the quantum double model have been studied, e.g., in [71, 72]. By a duality mapping, it has been shown that the toric code model is in the same universality class as the 1D Ising model, and therefore does not exhibit a finite temperature phase transition [39, 75]. The absence of a finite temperature phase transition has also been derived for string-net models based on a UMTC in [110]. Finally, the topological entanglement entropy, and related topological mutual information, have been studied for the toric code and the Kitaev quantum double model in [68, 69, 70].

In this chapter, we study the finite temperature properties of string-net models. More specifically, we consider the refined string-net model, corresponding to the refined Hamiltonian introduced in Eq. (4.55), in which all fluxons can have a different energy, and which encompasses the original string-net model as a special case. As previously, we restrict to the Hilbert space in which all vertex constraints are satisfied and only plaquette excitations can exist. We analyze the finite temperature behavior of these models from three main perspectives.

First, we derive the partition function of the refined string-net, using the results of the energy-level degeneracies obtained in Chap. 4. We derive the specific heat, and show that there is no phase transition at finite temperature in the thermodynamic limit in the string-net model, for any choice of coupling.

Second, we analyze the behavior of Wegner-Wilson loops (WWL) [41, 43] at finite temperature. These loops can be used as a non-local probe for the confinement or deconfinement of anyons [128, 129]. In a deconfined phase, contractible WWLs decay slowly, i.e., with the perimeter of the contour along which they are defined. In a confined phase, WWLs decay rapidly, with the area enclosed in the contour. In a topologically trivial phase, we expect anyons to be confined.

Finally, we consider entanglement properties through the topological mutual information. The latter was proposed in [69, 70] as the finite-temperature alternative to topological entanglement entropy. In particular, we use a conjecture [69, 70] for the topological mutual information to analyze the interplay between system size and temperature.

Importantly, both the WWL and the topological mutual information can be expressed in terms of the thermal average of projectors onto quasiparticles, which we derive along different contours on the lattice (handles, throats and contractible loops).

This chapter is organized as follows. Using the results obtained in Chap. 4, we start with computing the partition function for generalized string-net models and analyze the resulting equilibrium thermodynamics. We then discuss pure fluxons, a subset of excitations that plays a particular role at finite temperature, in Sec. 5.4. Next, we turn to the thermal average of projectors onto given quasiparticle sectors in a given region in 5.5. From there, it is easy to compute the thermal average of Wegner-Wilson loops and to discuss the confinement of quasiparticles (Sec. 5.6). Finally, we study entanglement properties and especially the topological mutual information at finite temperature in Sec. 5.7.4. We conclude in Section 5.8. The results presented in this chapter have been published in [130].

5.2 Partition function for the RSN model

In this first section, we will consider a *refined string-net model* (RSN), corresponding to the refined Hamiltonian introduced in Chap. 4 and in which all non-topological degeneracies are split. As presented in Eq. (4.55), this refined Hamiltonian is

$$H = - \sum_{p=1}^{N_p} \sum_{A \in \mathcal{F}} \sum_{a=1}^{n_{A,1}} \mathcal{J}_p^{A,a} B_p^{A,a}, \quad (5.1)$$

where \mathcal{F} denotes the set of fluxons, and a 's are positive integers that index the subtype of a given fluxon A and range from 1 to $n_{A,1}$ ($n_{A,1} > 1$ if \mathcal{C} is noncommutative). The plaquette operators $B_p^{A,a}$ project on the fluxon subtype (A, a) , and their general form is discussed in Sec. 4.4.1. This Hamiltonian attributes an energy $\mathcal{J}_p^{A,a}$ to every fluxon subtype on every plaquette p . The original string-net model (SN) Hamiltonian [c.f. Eq. (3.8)] is recovered by setting $\mathcal{J}_p^{A,a} = \delta_{1,A} \forall p$. The projector on the vacuum in Eq. (5.1) $B_p^{1,1} = B_p$, the plaquette operator of the SN Hamiltonian.

The energy of a state with fluxon types (including the vacuum) (A_p, a_p) on every plaquette $p \in \{1, \dots, N_p\}$ is

$$E = - \sum_{p=1}^{N_p} \mathcal{J}_p^{A_p, a_p}. \quad (5.2)$$

In Chap. 4, we showed that the corresponding degeneracy on a surface of genus g [see Eq. (5.3)]:

$$\dim(g; A_1, \dots, A_{N_p}) = \sum_{C \in \mathcal{Z}(C)} \left[\prod_{p=1}^{N_p} S_{A_p, C} \right] S_{1, C}^{2-2g-N_p}. \quad (5.3)$$

Once the degeneracies of the energy levels are determined, it is quite simple to compute the finite-temperature partition function of the RSN model (5.1). For a genus- g surface with N_p plaquettes, this partition function is given by

$$\begin{aligned} Z(g, N_p) &= \text{Tr}(e^{-\beta H}) \\ &= \sum_{A_1, \dots, A_{N_p} \in \mathcal{F}} \sum_{a_1=1}^{n_{A_1,1}} \sum_{a_2=1}^{n_{A_2,1}} \dots \sum_{a_{N_p}=1}^{n_{A_{N_p},1}} \dim(g; A_1, \dots, A_{N_p}) e^{\beta \sum_{p=1}^{N_p} \mathcal{J}_p^{A_p, a_p}}, \end{aligned} \quad (5.4)$$

where $\beta = 1/T$ is the inverse temperature (we set $k_B = 1$), and where the energy associated with a fixed fluxon configuration of $\{A_1, A_2, \dots, A_{N_p}\}$ with multiplicity indices $\{a_1, a_2, \dots, a_{N_p}\}$ is given by Eq. (5.2) (note also that the degeneracy is the same for any choice of $\{a_1, a_2, \dots, a_{N_p}\}$). Using Eq. (5.3), one obtains:

$$\begin{aligned} Z(g, N_p) &= \sum_{A_1, \dots, A_{N_p} \in \mathcal{F}} \sum_{a_1=1}^{n_{A_1,1}} \sum_{a_2=1}^{n_{A_2,1}} \dots \sum_{a_{N_p}=1}^{n_{A_{N_p},1}} \sum_{C \in \mathcal{Z}(C)} S_{1, C}^{2-2g-N_p} \left[\prod_{p=1}^{N_p} S_{A_p, C} \right] e^{\beta \sum_{p=1}^{N_p} \mathcal{J}_p^{A_p, a_p}}, \\ &= \sum_{C \in \mathcal{Z}(C)} S_{1, C}^{2-2g-N_p} \prod_{p=1}^{N_p} \left[\sum_{A_p \in \mathcal{F}} \sum_{a_p=1}^{n_{A_p,1}} S_{A_p, C} e^{\beta \mathcal{J}_p^{A_p, a_p}} \right], \\ &= \sum_{C \in \mathcal{Z}(C)} S_{1, C}^{2-2g} \prod_{p=1}^{N_p} z_{p, C}, \end{aligned} \quad (5.5)$$

where to go from the first to the second line we have simply rearranged terms and in the last line we introduced

$$z_{p, C} = \sum_{A_p \in \mathcal{F}} \sum_{a_p=1}^{n_{A_p,1}} \frac{S_{A_p, C}}{S_{1, C}} e^{\beta \mathcal{J}_p^{A_p, a_p}}. \quad (5.6)$$

It is interesting to analyze the global structure of Eq. (5.5). Indeed, the RSN or SN Hamiltonians are simply sums of mutually commuting projectors, each of them acting on a different plaquette. For such a simple Hamiltonian, one might expect a partition function which also simply factorizes as terms acting on each plaquette [such as the $z_{p, C}$ in Eq. (5.6)]. The fact that the partition function does not fully factorizes, and contains a term which depends on the genus, reflects the presence of nonlocal constraints that make the partition function sensitive to the manifold topology. We will further comment on the form of the partition function in Sec. 5.3.2.

5.2.1 Thermodynamic limit

In the thermodynamic limit, the sum in Eq. (5.6) is dominated by a special set of objects C which maximizes the ratio $S_{A, C}/S_{1, C}$. For $A \in \mathcal{F}$, this quantity is maximized if C belongs to the *pure fluxon* set $\mathcal{P} \subseteq \mathcal{F}$. A pure fluxon C is a fluxon which obeys

$$d_C = n_{C,1}. \quad (5.7)$$

On the one hand, using Eq. (2.22), one shows that (for $A \in \mathcal{F}$)¹

$$|S_{A,C}| \leq \frac{1}{\mathcal{D}} \sum_{X \in \mathcal{Z}(C)} N_{A,\bar{C}}^X \left| \frac{\theta_X}{\theta_C} \right| d_X, \quad (5.8)$$

$$\leq \frac{1}{\mathcal{D}} \sum_{X \in \mathcal{Z}(C)} N_{A,\bar{C}}^X d_X = \frac{d_A d_C}{\mathcal{D}}. \quad (5.9)$$

In the last step, we used the property that the quantum dimensions follow the fusion rules [see Eq. (2.4)]. On the other hand, if $A \in \mathcal{F}$ and $C \in \mathcal{P}$, the inequality (5.9) becomes an equality

$$S_{A,C} = \frac{d_A d_C}{\mathcal{D}}. \quad (5.10)$$

In other words, pure fluxons C braid trivially with all fluxons. We will discuss pure fluxons in detail in Sec. 5.4.

Hence, when C is a pure fluxon, one has

$$z_{p,C} = \sum_{A \in \mathcal{F}} \sum_{a=1}^{n_{A,1}} d_A e^{\beta \mathcal{J}_p^{A,a}} = z_p, \quad (5.11)$$

which is actually independent of C . For any $T > 0$, we therefore get

$$\begin{aligned} Z(g, N_p) &\underset{N_p \rightarrow \infty}{\simeq} \sum_{C \in \mathcal{P}} S_{1,C}^{2-2g} \prod_{p=1}^{N_p} z_p, \\ &= M_g \mathcal{D}^{2g-2} \prod_{p=1}^{N_p} z_p, \end{aligned} \quad (5.12)$$

where in the second line we used $S_{1,C} = \frac{d_C}{\mathcal{D}}$ and

$$M_g = \sum_{C \in \mathcal{P}} d_C^{2-2g} = \sum_{C \in \mathcal{P}} n_{C,1}^{2-2g}. \quad (5.13)$$

was already defined in Eq. (4.29). For a commutative input category, all internal multiplicities of fluxons are equal to 1, so M_g is simply the number of pure fluxons $M_g = |\mathcal{P}|$, for any genus. It also corresponds to the number of Abelian fluxons ($A \in \mathcal{F}$ with $d_A = 1$).

5.2.2 Infinite-temperature limit and Hilbert-space dimension

The Hilbert space dimension can be computed by taking the infinite-temperature limit of the partition function Eq. (5.5). In this limit, using the fluxon identity [see also Eq. (4.17)]

$$S \mathbf{n}_1 = \mathbf{n}_1, \quad (5.14)$$

where \mathbf{n}_1 is the vector with components $n_{C,1}$ ($n_{C,1} = 0$, if $C \notin \mathcal{F}$), one gets

$$\lim_{T \rightarrow \infty} z_{p,C} = \sum_{A \in \mathcal{F}} \frac{S_{A,C}}{S_{1,C}} n_{A,1} = \frac{n_{C,1}}{S_{1,C}}. \quad (5.15)$$

¹This can also be shown by using the monodromy matrix $M_{A,C}$. In general, the S -matrix element $S_{A,C}$ in Eq. (5.6) can be expressed as $S_{A,C} = \frac{d_A d_C}{\mathcal{D}} M_{A,C}$, where $|M_{A,C}| \leq 1$ [82]. It follows directly that $|S_{A,C}| \leq 1$. When $M_{A,C} = 1$, it means that A and C have a trivial braiding.

Then, one straightforwardly obtains:

$$\begin{aligned}
 \dim \mathcal{H} &= \lim_{T \rightarrow \infty} Z(g, N_p), \\
 &= \sum_{C \in \mathcal{Z}(C)} S_{1,C}^{2-2g} \left(\frac{n_{C,1}}{S_{1,C}} \right)^{N_p}, \\
 &= \sum_{C \in \mathcal{F}} S_{1,C}^{-N_v/2} n_{C,1}^{N_p}.
 \end{aligned} \tag{5.16}$$

To go to the last line, we used the fact that, for a trivalent graph, the Euler-Poincaré characteristic gives

$$2 - 2g - N_p = -N_v/2, \tag{5.17}$$

where N_v is the number of vertices. This result coincides as expected with the one given in Eq. (4.27).

In the limit of large N_p , the sum over fluxons C is dominated by the pure fluxons $C \in \mathcal{P}$, which maximize the inequality

$$\frac{n_{C,1}}{S_{1,C}} = \mathcal{D} \frac{n_{C,1}}{d_C} \leq \mathcal{D}. \tag{5.18}$$

We can therefore write in the thermodynamic limit:

$$\dim \mathcal{H} \underset{N_p \rightarrow \infty}{\simeq} M_g \mathcal{D}^{N_v/2}. \tag{5.19}$$

which is in agreement with Eq. (4.29).

5.3 Partition function for the SN model

The simple form of the general partition function given in Eq. (5.5) allows one to study several thermodynamic quantities. Here, we shall discuss them for the SN model, for which $\mathcal{J}_p^{A,a} = \delta_{A,1}$ for all p 's. We then obtain from Eq. (5.6)

$$\begin{aligned}
 z_{p,C} &= e^\beta + \sum_{A \in \mathcal{F}^*} \frac{S_{A,C} n_{A,1}}{S_{1,C}}, \\
 &= e^\beta + \frac{n_{C,1}}{S_{1,C}} - 1.
 \end{aligned} \tag{5.20}$$

Here, \mathcal{F}^* denotes the set of fluxons without the vacuum, and we have used that $d_1 = n_{1,1} = 1$ and also the fluxon identity Eq. (5.14). The result of Eq. (5.20) is independent of p and is particularly simple as it depends only on the internal multiplicities $n_{C,1}$ and on $S_{1,C} = d_C/\mathcal{D}$.

As explained in Sec. 5.2, in the large N_p limit, the sum in Eq. (5.5) is dominated by pure fluxons ($n_{C,1} = d_C$) so that, for the SN model, one has:

$$Z(g, N_p) \underset{N_p \rightarrow \infty}{\simeq} (\mathcal{D} - 1 + e^\beta)^{N_p} \sum_{C \in \mathcal{P}} S_{1,C}^{2-2g}. \tag{5.21}$$

This result agrees with the results given in [109] for the case of the Fibonacci input category and in [110] for input UMTCs. Eq. (5.21) is valid for any input UFC.

By taking the zero- T limit of the partition function $Z(g, N_p)$, one recovers the ground-state degeneracy of the SN Hamiltonian. This topology-dependent degeneracy is given by:

$$\lim_{T \rightarrow 0} Z(g, N_p) e^{\beta E_0} = \sum_{C \in \mathcal{Z}(C)} S_{1,C}^{2-2g}, \quad (5.22)$$

where $E_0 = -N_p$ is the ground-state energy. This result coincides exactly with the result given in Eq. (4.9) and [27, 111].

5.3.1 Energy, specific heat, and entropy

Using Eq. (5.20), it is straightforward to compute several thermodynamical quantities for the SN model. Here, we discuss some of them by considering directly the thermodynamic limit (5.21) for which expressions becomes especially simple. In the large N_p limit, the free energy per plaquette is given by

$$f = \lim_{N_p \rightarrow \infty} -\frac{1}{N_p} \frac{\ln Z}{\beta} = -\frac{1}{\beta} \ln(\mathcal{D} - 1 + e^\beta). \quad (5.23)$$

Similarly, the energy per plaquette is given by

$$e = \lim_{N_p \rightarrow \infty} -\frac{1}{N_p} \frac{\partial \ln Z}{\partial \beta} = -\frac{e^\beta}{\mathcal{D} - 1 + e^\beta}, \quad (5.24)$$

and the specific heat per plaquette is given by

$$c = \lim_{N_p \rightarrow \infty} \frac{\beta^2}{N_p} \frac{\partial^2 \ln Z}{\partial \beta^2} = \frac{e^\beta \beta^2 (\mathcal{D} - 1)}{(\mathcal{D} - 1 + e^\beta)^2}. \quad (5.25)$$

These expressions, which hold for any UFC, are exactly the same as the ones derived in Ref. [110] where only modular input UFCs were considered. It is interesting to observe that in the thermodynamic limit, the behaviour is no longer dependent on the genus, nor on the choice of couplings, and depends only on the total quantum dimension. Thus, one expects models with the same total quantum dimension to behave in a similar way in the thermodynamic limit. The specific heat c is shown on Fig. 5.1 for different string-net models on Fig. 5.1. For any total quantum dimension \mathcal{D} , c is always a smooth function of the temperature, indicating the *absence of finite-temperature phase transition in this model*. This latter result also holds for the RSN model, and is in agreement with the general result derived by Hastings [67] that there is no topological order at $T > 0$ for two-dimensional Hamiltonians which are a sum of commuting local terms. In other words, in the thermodynamical limit, we expect a phase transition at $T_c = 0^+$.

Finally, we can compute the entropy from

$$S = -\beta \frac{\partial \ln Z}{\partial \beta} + \ln Z. \quad (5.26)$$

Using Eq. (5.21), one gets in the thermodynamic limit at $T > 0$

$$S \underset{N_p \rightarrow \infty}{\simeq} N_p \left[\ln(\mathcal{D} - 1 + e^\beta) - \frac{\beta e^\beta}{\mathcal{D} - 1 + e^\beta} \right] + \ln \frac{M_g}{\mathcal{D}^{2-2g}}, \quad (5.27)$$

where M_g is given in Eq. (5.13). This entropy consists of an extensive term proportional to the volume (number of plaquettes N_p) of the system, and of a constant term. In the infinite-temperature limit, this expression simply becomes

$$\lim_{\beta \rightarrow 0} S = \ln(\dim \mathcal{H}) \underset{N_p \rightarrow \infty}{\simeq} \frac{N_v}{2} \ln \mathcal{D} + \ln M_g. \quad (5.28)$$

Note that, as we will discuss later on in Sec. 5.7.4, the constant term, $\ln M_g$, is not related to quantum entanglement but to the fact that the Hilbert space is constrained by the fusion rules (vertex defects are forbidden).

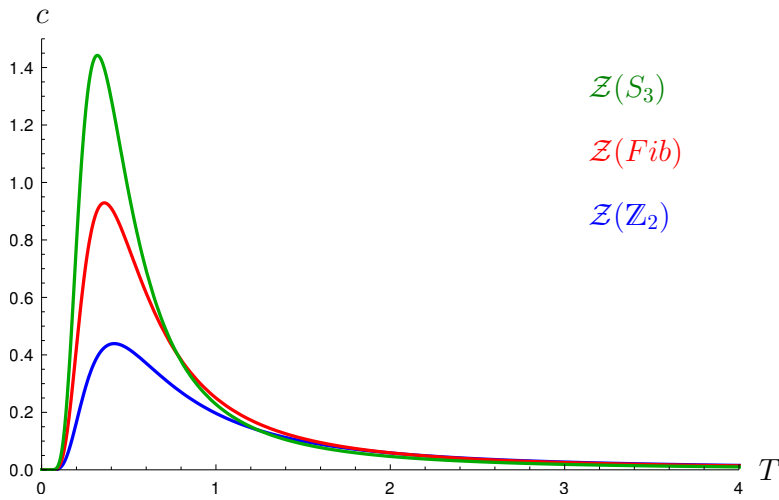


Figure 5.1: The specific heat c as a function of temperature T for different string-net models. The total quantum dimensions are respectively: 2 for $\mathcal{Z}(\mathbb{Z}_2)$, $1 + \phi^2$ with $\phi = (1 + \sqrt{5})/2$ for $\mathcal{Z}(Fib)$, and 6 for $\mathcal{Z}(S_3)$.

5.3.2 Comparison with classical models

A model with topological order whose partition function has been extensively studied [39, 70, 74, 131] is the toric code model [47]. This model is closely related to the \mathbb{Z}_2 string-net model (see Sec. 2.3), but is usually studied with both vertex and plaquettes operators. In [38, 39], the authors point out that the toric code model can be mapped onto a product of two decoupled 1D Ising chains, where one chain corresponds to the vertices and one to the plaquettes. Here, we consider the possible mapping of general string-net models onto classical models.

A generalization of the Ising model is the Potts model (see e.g. [132]), in which the classical spin variables can take q different discrete values. When $q = 2$, then the Potts model is exactly the Ising model. On a 1D chain with n sites and periodic boundary conditions, the Hamiltonian of the Potts model reads

$$H_{\text{Potts}} = - \sum_{i=1}^n \delta_{s_i, s_{i+1}}, \quad s_{n+1} = s_1. \quad (5.29)$$

The partition function of the Potts model can be easily computed (e.g. by the transfer matrix approach) and is

$$Z_{\text{Potts}}(\beta, n) = \left(e^\beta + q - 1\right)^n + (q - 1) \left(e^\beta - 1\right)^n. \quad (5.30)$$

In the thermodynamic limit ($n \rightarrow \infty$), the first term in the sum dominates over the second, and one obtains, e.g., for the free energy per site

$$f_{\text{Potts}} = -\frac{1}{\beta} \ln(q - 1 + e^\beta). \quad (5.31)$$

It is interesting to compare expression (5.30) with the partition function Eq. (5.5) for the SN model when the input category $\mathcal{C} = \mathbb{Z}_N$. In this case, as the fusion rules are commutative, all $n_{A,1} \leq 1$. Moreover, the number of fluxons is N and the number of objects in the Drinfeld center is N^2 . Finally, the quantum dimensions of all objects are $d_A = 1$ and the total quantum dimension $\mathcal{D} = N$ [82]. Using Eq. (5.5) and Eq. (5.20) one then obtains:

$$\begin{aligned} Z_{\mathcal{Z}(\mathbb{Z}_N)}(\beta, N_p) &= N^{2g-2} \left(\sum_{\mathcal{C} \in \mathcal{F}} (e^\beta + N - 1)^{N_p} + \sum_{\mathcal{C} \notin \mathcal{F}} (e^\beta - 1)^{N_p} \right), \\ &= N^{2g-2} \left(N(e^\beta + N - 1)^{N_p} + (N^2 - N)(e^\beta - 1)^{N_p} \right), \\ &= N^{2g-1} \left((e^\beta + N - 1)^{N_p} + (N - 1)(e^\beta - 1)^{N_p} \right), \end{aligned} \quad (5.32)$$

where we have used that $n_{A,1} = 1$ if $A \in \mathcal{F}$ and 0 otherwise. The final expression is, up to a global factor of N^{2g-1} , exactly the partition function of a 1d Potts model with $n = N_p$ sites and $q = N$ colours. We interpret this global factor as arising from topological constraints, as well as from the additional constraint on the Hilbert space which forbids vertex defects.

In the thermodynamic limit, this analogy can even be pushed further. In fact, as can be seen from Eq. (5.31), the free energy per site is exactly the same for a Potts model with N colours and the \mathbb{Z}_N string-net model. Furthermore, the general form of the free energy of Eq. (5.23) is also analog to the free energy of the Potts model, only with a potentially non-integer number of colours \mathcal{D} . A way to understand this form of the free energy in the general case is the following. Let us consider the projector B_p as a classical \mathbb{Z}_2 variable that takes the value 1 if the plaquette p is in the vacuum state and 0 if there is a non-trivial fluxon, and let us assign a weight to each fluxon A given by an "effective dimension" $n_{A,1}d_A$. Then, in the calculation of the partition function $\text{Tr}(e^{-\beta H})$, for each plaquette the trivial fluxon gives a contribution $e^{\beta \times 1}$ with a weight 1 ($n_{1,1} = 1$ and $d_1 = 1$) and each non-trivial fluxon $A \neq 1$ gives $e^{\beta \times 0} = 1$ with a weight $n_{A,1}d_A$. Since $\sum_{A \neq 1} n_{A,1}d_A = \mathcal{D} - 1^2$, one obtains the overall contribution $\mathcal{D} - 1 + e^\beta$. However, although B_p has eigenvalues 0 and 1, these operators are not completely independent. This leads to the additional term depending on the topology in the expression of the partition function (5.5).

5.4 Fluxons, pure fluxons and fusion product of fluxons

As discussed in the previous sections of this chapter, the set of pure fluxons $\mathcal{P} \subseteq \mathcal{F}$ dominates the behaviour of the string-net model at finite temperature in the thermodynamic limit. This section

²To show this, one starts from Eq. (4.17) from which follows $\sum_A S_{1,A}n_{A,1} = 1$ or equivalently $\sum_A d_{An_{A,1}} = \mathcal{D}$.

summarizes and demonstrates a few properties of these pure fluxons.

In Chap. 4, we have seen that fluxons are defined as the subset of simple objects of $\mathcal{F} \subset \mathcal{Z}(\mathcal{C})$ which verify

$$A \in \mathcal{F} \Leftrightarrow n_{A,1} > 0. \quad (5.33)$$

One can relate the quantum dimensions of the anyons $A \in \mathcal{Z}(\mathcal{C})$ with those of the simple objects of \mathcal{C} via [see also Eq. (2.34)]

$$d_A = \sum_{s \in \mathcal{C}} n_{A,s} d_s = n_{A,1} + \sum_{s \neq 1} n_{A,s} d_s. \quad (5.34)$$

Since both $n_{A,s}$ and d_s are nonnegative, it follows for fluxons that

$$n_{A,1} \leq d_A. \quad (5.35)$$

Among fluxons, we then distinguish pure fluxons [93] as those fluxons that saturate the inequality [see also Eq. (5.7)]:

$$A \in \mathcal{P} \Leftrightarrow n_{A,1} = d_A. \quad (5.36)$$

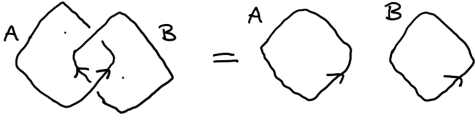


Figure 5.2: When the braiding between A and B is trivial, the worldlines of two anyons A and B can simply be unknot.

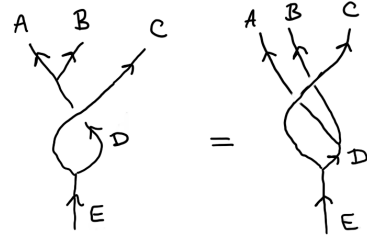


Figure 5.3: The braiding of C with a group of anyons (here, A and B) should be the same as braiding with their fusion product (D).

It also follows from Eq. (5.34) that a pure fluxon contains only the trivial input object, i.e., with the definition of Eq. (2.33),

$$A \in \mathcal{P} \Leftrightarrow A = (n_{A,1}1, \Omega_A). \quad (5.37)$$

As mentioned below Eq. (5.10), another property of pure fluxons is

$$A \in \mathcal{P} \Leftrightarrow S_{A,B} = \frac{d_A d_B}{D}, \quad \forall B \in \mathcal{F}, \quad (5.38)$$

i.e., a pure fluxon braids trivially with all fluxons (but not necessarily with non-fluxons) (see Fig. 5.2). A corollary of Eq. (5.38), stemming from the hexagon equation (see Eq. (2.11)) is that Eq. (5.38) also holds if A is a pure fluxon and B is any fusion product of fluxons ($B \in \mathcal{F}^{\otimes}$). In fact, any fusion product of fluxons can be split into its composing fluxons, and the hexagon equations imply that braiding with an object is the same as braiding with its products from splitting (see Fig. 5.3).

The vacuum 1 is a pure fluxon, since $n_{1,1} = d_1 = 1$. It also braids trivially with fluxons and product of fluxons, and even with all other particles of $\mathcal{Z}(\mathcal{C})$. In fact, the vacuum is the only

transparent particle of $\mathcal{Z}(\mathcal{C})$. It is also worth mentioning that when \mathcal{C} is modular, the number of fluxons corresponds to the number of Abelian objects in \mathcal{C} . In fact, when \mathcal{C} is modular, any fluxon $d_A \in \mathcal{Z}(\mathcal{C})$ can be written as a pair (s, \bar{s}) where $s \in \mathcal{C}$ and $\bar{s} \in \bar{\mathcal{C}}$. The quantum dimension of a fluxon is then $d_A = d_s^2$. Since $n_{A,1} \leq 1$, pure fluxons correspond to all pairs (s, \bar{s}) where $d_s = 1$. Besides, if \mathcal{C} is commutative (even if not modular), $n_{A,1}$ takes only two values 1 (if $A \in \mathcal{F}$) or 0 (if $A \notin \mathcal{F}$). Then, Eq. (5.36) implies that pure fluxons are exactly Abelian fluxons (i.e. fluxons which have Abelian fusion rules), since for them $d_A = 1$.

In the following, we wish to prove that the two definitions (5.36) and (5.38) are equivalent. In order to prove that the right-hand side (r.h.s.) of Eq. (5.38) implies the r.h.s. of Eq. (5.36), we start from the fluxon identity (5.14)

$$n_{A,1} = \sum_{B \in \mathcal{Z}(\mathcal{C})} S_{A,B} n_{B,1} = \sum_{B \in \mathcal{F}} S_{A,B} n_{B,1}, \quad (5.39)$$

and note that, on the r.h.s., only fluxons contribute non-zero terms. Therefore, if A is a pure fluxon, we can use Eq. (5.38) in the r.h.s. to get

$$n_{A,1} = \sum_{B \in \mathcal{F}} \frac{d_A d_B}{\mathcal{D}} n_{B,1} = d_A \frac{1}{\mathcal{D}} \sum_{B \in \mathcal{F}} d_B n_{B,1}. \quad (5.40)$$

Then, we can use Eq. (5.39) again for the special case $A = \mathbf{1}$ ($n_{\mathbf{1},1} = 1$), to prove that:

$$\frac{1}{\mathcal{D}} \sum_{B \in \mathcal{F}} d_B n_{B,1} = 1, \quad (5.41)$$

and we obtain Eq. (5.36).

In order to prove that the r.h.s. of Eq. (5.36) implies the r.h.s. of Eq. (5.38), we start again from the expression in terms of twist factors of the S -matrix [c.f. Eq. (2.22)]

$$S_{A,B} = \frac{1}{\mathcal{D}} \sum_{C \in \mathcal{Z}(\mathcal{C})} N_{A,\bar{B}}^C \frac{\theta_C}{\theta_A \theta_B} d_C, \quad (5.42)$$

which we apply to the case where $A \in \mathcal{P}$ and $B \in \mathcal{F}$. As fluxons, A and B have trivial twists ($\theta_A = \theta_B = 1$) (see Eq. 4.16 and comment below). Thus, Eq. (5.42) gives

$$S_{A,B} = \frac{1}{\mathcal{D}} \sum_{C \in \mathcal{Z}(\mathcal{C})} N_{A,\bar{B}}^C \theta_C d_C. \quad (5.43)$$

We prove in Appendix C that the fusion product of a pure fluxon A with a fluxon B is always a fluxon. Using this fact, one further gets

$$S_{A,B} = \frac{1}{\mathcal{D}} \sum_{C \in \mathcal{Z}(\mathcal{C})} N_{A,\bar{B}}^C d_C = \frac{d_A d_B}{\mathcal{D}}, \quad (5.44)$$

which completes the proof.

5.5 Projectors on topological quasiparticles

So far, we have considered the general thermodynamical properties of the RSN and the SN model. In this and the following sections, we turn to consider different non-local probes of topological order at finite temperature. In particular, in the present section we compute the thermal average of projectors onto quasiparticles $A \in \mathcal{Z}(\mathcal{C})$. These projectors will play a central role in deriving the expressions of Wegner-Wilson loop operators in Sec. 5.6 and of the topological mutual information in Sec. 5.7.4.

5.5.1 Degeneracies from gluing surfaces

In Chap. 4, we have seen that the degeneracy for a surface of genus g with m punctures labeled A_1, \dots, A_m was given by the quantity $\dim_{\mathcal{Z}(\mathcal{C})}(g, A_1, A_2, \dots, A_m)$ which could be calculated by using the Moore-Seiberg-Banks formula [111] [see Eq. (4.11)]. In the context of string-nets, these labels take values in the subset of fluxons \mathcal{F} . In this section, we will need to calculate the degeneracy of a surface in which not only the labels of punctures are fixed, but also a label (or topological quantum number, or flux) running through a handle or a throat of the surface. Contrary to the punctures corresponding to plaquette excitations and thus fluxons, these "internal" labels can take any value in $\mathcal{Z}(\mathcal{C})$. Using the gluing property of surfaces with punctures (see Sec. 4.2), it is actually possible to still use the Moore-Seiberg-Banks formula in this case.

Consider a surface of genus g with N_p plaquettes which carry some fluxons $A_1, A_2, \dots, A_{N_p} \in \mathcal{F}$, and two additional punctures X and \bar{X} , where $X \in \mathcal{Z}(\mathcal{C})$ (see Fig. 5.4). The degeneracy of this surface is given by $\dim_{\mathcal{Z}(\mathcal{C})}(g, A_1, A_2, \dots, A_{N_p}, X, \bar{X})$. The two punctures X and \bar{X} can be glued together (see Sec. 4.2), creating thus a surface of genus $g + 1$, N_p fluxons A_1, A_2, \dots, A_{N_p} , and a flux X through the newly created handle, see Fig. 5.4. This gluing does not change the degeneracy of the surface³, which is still given by $\dim_{\mathcal{Z}(\mathcal{C})}(g, A_1, A_2, \dots, A_{N_p}, X, \bar{X})$.

Similarly, one may take two surfaces, one of genus g_1 and with a puncture labeled X , and one of genus g_2 and with a puncture labeled \bar{X} , and sew them together so as to create a surface of genus $g = g_1 + g_2$, see Fig. 5.5. The newly created surface then has a fixed flux X running through the throat across which the two old surfaces have been connected. If the surface of genus g_1 carries fluxons $A_1, A_2, \dots, A_{N_p^1}$ in addition to the puncture X , the corresponding degeneracy is given by $\dim_{\mathcal{Z}(\mathcal{C})}(g_1, A_1, A_2, \dots, A_{N_p^1}, X)$. Similarly, the degeneracy of the surface of genus g_2 , if it carries some excitations $B_1, B_2, \dots, B_{N_p^2}$ besides the puncture labeled \bar{X} , will have a degeneracy given by $\dim_{\mathcal{Z}(\mathcal{C})}(g_2, B_1, B_2, \dots, B_{N_p^2}, \bar{X})$. The degeneracy of the surface created by gluing these two surfaces together at their punctures is then simply the product of the degeneracies, $\dim_{\mathcal{Z}(\mathcal{C})}(g_1, A_1, A_2, \dots, A_{N_p^1}, X) \times \dim_{\mathcal{Z}(\mathcal{C})}(g_2, B_1, B_2, \dots, B_{N_p^2}, \bar{X})$.

³In fact, the Moore-Seiberg-Banks formula can be derived by counting all possible fusion channels of the N_p fluxons and the two fluxes X and \bar{X} in the punctures, see Eqs. (4.6) and (4.10). There is just one possibility for X to fuse to the vacuum with \bar{X} ($N_{X, \bar{X}}^1 = 1$) so the degeneracy does not change when the two punctures are glued together.

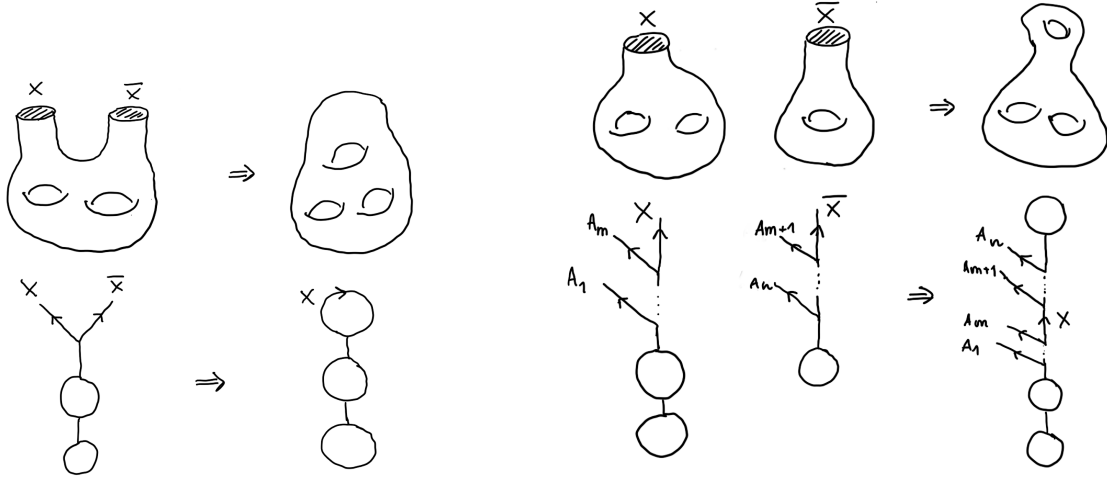


Figure 5.4: A surface of genus g (here, $g = 2$) with two punctures labeled X and \bar{X} can be sewed in order to create a surface of genus $g + 1$ without punctures. The number of ways of obtaining a surface of genus 2 and two punctures X and \bar{X} corresponds to counting all possible labelings for the non-labeled edges on the left fusion diagram. This dimension is the same as for the right fusion diagram, where X and \bar{X} have fused together.

Figure 5.5: Two punctured surfaces of genus $g = 2$ and $g = 1$, carrying some excitations A_1, A_2, \dots, A_m and $A_{m+1}, A_{m+2}, \dots, A_n$ can be sewed together to form a surface of genus 3 with n excitations and a fixed flux X through a throat. This corresponds to pasting together the fusion diagrams corresponding to the two surfaces.

5.5.2 General definition of projectors

We now turn to calculate the thermal expectations of topological projection operators $P_X(L)$, for $X \in \mathcal{Z}(\mathcal{C})$ and L a closed path on our surface. As a complete set of orthogonal projection operators, these satisfy

$$P_X(L)P_Y(L) = \delta_{X,Y}P_X(L) \quad \text{and} \quad \sum_{X \in \mathcal{Z}(\mathcal{C})} P_X(L) = 1, \quad (5.45)$$

where the sum is over all objects of the Drinfeld center $\mathcal{Z}(\mathcal{C})$.

Physically, the action of such a projector is to project to a configuration where the flux through the loop L is given by the particle type $X \in \mathcal{Z}(\mathcal{C})$. This projection is shown graphically in Fig. 5.6. For definiteness, when the region of interest is contractible, we define the direction of the loop L such that it travels counterclockwise around the region. The expectation value of the projector $P_X(L)$ informs on the probability to observe a certain quantum number (or flux) inside the closed path L . At zero temperature, this quantum number is fixed by the fusion rules of the Drinfeld center $\mathcal{Z}(\mathcal{C})$, as well as the nature of the ground-state (which, depending on the couplings $\mathcal{J}_p^{A,a}$ may or may not have nontrivial fluxons through plaquettes).

At any finite temperature, however, there is a nonzero probability for each plaquette to be excited. Plaquette excitations carry topological quantum numbers, and we should expect that, for a sufficiently large system, the topological properties of the system will be scrambled. For example, a contractible loop encircling a large enough region will surround a completely unknown

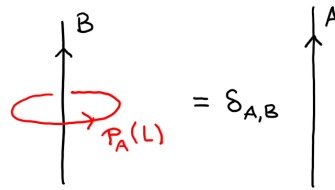


Figure 5.6: Schematic representation of a projector $P_A(L)$ acting on a particle B . The loop L goes counterclockwise around the region being projected.

topological quantum number. However, not all topological information will be erased at finite temperature at long distances. Since we have enforced the vertex constraint at the level of the Hilbert space, we have forbidden certain types of defects, and topological information associated to them can remain at any temperature.

In the following, we will consider three different types of closed paths L : non-contractible loops around handles and throats, as well as contractible loops (see Fig. 5.7). Remarkably, the obtained expressions for projectors are exact for any temperature, any system size, any choice of coupling, and any input UFC.

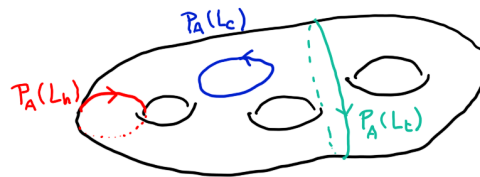


Figure 5.7: Three different contours for a projector on a genus g two-dimensional manifold: around a handle (in red), around a throat (in green) and on a contractible loop (in blue).

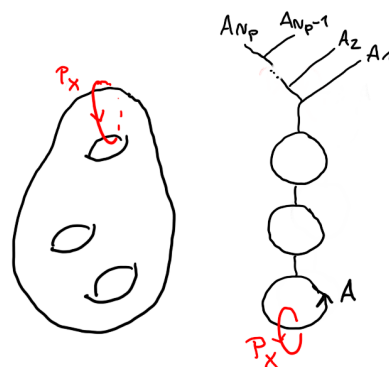


Figure 5.8: On the left, a surface with $g = 3$ and a projector P_X around a handle. On the right, a fusion diagram representing this surface, with N_p plaquettes carrying fluxons A_1, \dots, A_{N_p} . P_X projects on states with label $A = X$ in one handle.

5.5.3 Loops around handles

We begin by considering a projector $P_X(L_h)$ defined along a loop L_h around a handle of a surface of genus $g \geq 1$. For simplicity, we first compute the expectation value of this projector in the ground-state of the SN model, that is, when a ground state corresponds to a state with vacuum in every plaquette. As discussed in Chap. 4.2, a ground-state of a surface of genus g may be represented by a fusion diagram with g loops (see Fig. 5.8). A projector P_X acting on this state will return 1 if the quantum number inside the handle it is encircling is X , and 0 otherwise. Therefore, computing the average of P_X on the ground-state space amounts to counting all possible ways to label a fusion diagram as the one in Fig. 5.8, so that there is a label X in the handle around which P_X acts. As discussed in Sec. 5.5.1, this can be done using the Moore-Seiberg-Banks formula (4.11) for a surface of genus $g - 1$ carrying two labeled punctures X and \bar{X} . We thus obtain for the expectation value of $P_X(L_h)$ on the ground state:

$$\begin{aligned} \langle P_X(L_h) \rangle_{\text{GS}} &= \frac{\dim_{\mathcal{Z}(C)}(g-1, X, \bar{X})}{\dim_{\mathcal{Z}(C)}(g)}, \\ &= \frac{\sum_{C \in \mathcal{Z}(C)} S_{X,C} S_{\bar{X},C} S_{1,C}^{2-2g}}{\sum_{C \in \mathcal{Z}(C)} S_{1,C}^{2-2g}}. \end{aligned} \quad (5.46)$$

where $\dim_{\mathcal{Z}(C)}(g)$ is the ground-state degeneracy of a surface of genus g [see Eq. (4.9)]. Using the unitarity of the S -matrix (2.18), it is clear that the expression of Eq. (5.46) verifies Eq. (5.45).

Now, let us move on to finite temperature. The thermal average of a projector P_X acting on a contour on a genus- g surface with N_p plaquettes is given by

$$\langle P_X \rangle = \frac{\text{Tr}(e^{-\beta H} P_X)}{Z(g, N_p)}. \quad (5.47)$$

In other terms,

$$\langle P_X(L_h) \rangle = \frac{1}{Z(g, N_p)} \sum_{\text{all labelings with } X \text{ through } L_h} e^{-\beta E(\text{labeling})}, \quad (5.48)$$

where, by labeling, we mean the labeling of the edges of a fusion diagram representing the surface, as shown in Fig. 5.8. In particular, in addition to the g loops for the genus of the surface, this fusion diagram also takes into account that there might be non-trivial fluxons on the N_p plaquettes of the surface. The energy corresponding to a possible labeling of the fusion diagram is completely fixed by the labels of the fluxons $(A_1, a_1), (A_2, a_2), \dots, (A_{N_p}, a_{N_p})$, where $A \in \mathcal{F}$ and a is an interger denoting the fluxon subtype and running from 1 to $n_{A,1}$. As given in Eq. (5.2),

$$E = - \sum_{p=1}^{N_p} \mathcal{J}_p^{A_p, a_p}. \quad (5.49)$$

For a given fluxon configuration $(A_1, a_1), (A_2, a_2), \dots, (A_{N_p}, a_{N_p})$, there will be a topological degeneracy, sensitive to the genus, and depending on the fusion rules. This degeneracy can again be determined using the Moore-Seiberg-Banks formula, for a surface of genus $g - 1$, two punctures

X and $\bar{X} \in \mathcal{Z}(\mathcal{C})$, and N_p punctures labeled $A_1, \dots, A_{N_p} \in \mathcal{F}$. Summing over all fluxon types and fluxon subtypes $a \in \{1, \dots, n_{A,1}\}$, we thus obtain

$$\langle P_X(L_h) \rangle = \frac{1}{Z(g, N_p)} \sum_{A_1, \dots, A_{N_p} \in \mathcal{F}} \sum_{a_1=1}^{n_{A_1,1}} \cdots \sum_{a_{N_p}=1}^{n_{A_{N_p},1}} \dim_{\mathcal{Z}(\mathcal{C})}(g-1, X, \bar{X}, A_1, \dots, A_{N_p}) e^{\beta \sum_{j=1}^{N_p} \mathcal{J}_j^{A_j, a_j}}. \quad (5.50)$$

The expression for the partition function $Z(g, N_p)$ is given for arbitrary couplings in Eq. (5.5). For convenience, we may also introduce the notation

$$\begin{aligned} Z_{X, \bar{X}}(g, N_p) &= \sum_{A_1, \dots, A_{N_p} \in \mathcal{F}} \sum_{a_1=1}^{n_{A_1,1}} \cdots \sum_{a_{N_p}=1}^{n_{A_{N_p},1}} \dim_{\mathcal{Z}(\mathcal{C})}(g, X, \bar{X}, A_1, \dots, A_{N_p}) e^{\beta \sum_{j=1}^{N_p} \mathcal{J}_j^{A_j, a_j}}, \\ &= \sum_{A_1, \dots, A_{N_p} \in \mathcal{F}} \sum_{a_1=1}^{n_{A_1,1}} \cdots \sum_{a_{N_p}=1}^{n_{A_{N_p},1}} \sum_{C \in \mathcal{Z}(\mathcal{C})} \left(\prod_{j=1}^{N_p} S_{A_j, C} \right) S_{X, C} S_{\bar{X}, C} S_{1, C}^{-2g - N_p} e^{\beta \sum_{j=1}^{N_p} \mathcal{J}_j^{A_j, a_j}}, \\ &= \sum_{C \in \mathcal{Z}(\mathcal{C})} S_{X, C} S_{\bar{X}, C} S_{1, C}^{-2g} \prod_{p=1}^{N_p} z_{p, C}, \end{aligned} \quad (5.51)$$

where $z_{p, C}$ was defined in Eq. (5.6). Then, we can simply write

$$\langle P_X(L_h) \rangle = \frac{Z_{X, \bar{X}}(g-1, N_p)}{Z(g, N_p)}. \quad (5.52)$$

$Z_{X, \bar{X}}(g, N_p)$ is the effective ⁴ partition function for a surface of genus g , N_p plaquettes and two additional punctures labeled with X and $\bar{X} \in \mathcal{Z}(\mathcal{C})$ (as represented in Fig. 5.4 for $g = 2$). Using the unitarity of the S -matrix and Eq. (5.5), one has

$$\sum_{X \in \mathcal{Z}(\mathcal{C})} Z_{X, \bar{X}}(g-1, N_p) = \sum_{C \in \mathcal{Z}(\mathcal{C})} S_{1, C}^{2-2g} \prod_{p=1}^{N_p} z_{p, C} = Z(g, N_p), \quad (5.53)$$

from which it directly follows that $\langle P_X(L_h) \rangle$ satisfies the identity (5.45).

The expression Eq. (5.50) is valid for all choices of couplings of the refined Hamiltonian. In order to study the behavior of $\langle P_X(L_h) \rangle$, we now specify to one choice of couplings, namely the one of the standard string-net model: $\mathcal{J}_p^{A_p, a_p} = \delta_{A,1} \forall p$. Then, replacing $z_{p, C}$ with Eq. (5.20), we find that

$$\langle P_X(L_h) \rangle = \frac{\sum_{C \in \mathcal{Z}(\mathcal{C})} S_{X, C} S_{\bar{X}, C} S_{1, C}^{2-2g} \left(\frac{n_{C,1}}{S_{1, C}} - 1 + e^\beta \right)^{N_p}}{\sum_{C \in \mathcal{Z}(\mathcal{C})} S_{1, C}^{2-2g} \left(\frac{n_{C,1}}{S_{1, C}} - 1 + e^\beta \right)^{N_p}}. \quad (5.54)$$

First of all, we remark that when $T \rightarrow 0$, one recovers the formula (5.46), for all N_p . Next, let us consider the large N_p limit at *any* nonzero temperature. In this limit, as explained in Sec. 5.2, the sums over all objects of the Drinfeld center appearing in Eq. (5.54) are dominated by the pure

⁴We say effective because this partition function does not correspond to a realization of the string-net model, as X can take all values in the Drinfeld center, instead of being a fluxon. Moreover, we do not associate an energy with the punctures X and \bar{X} as we intend to sew them.

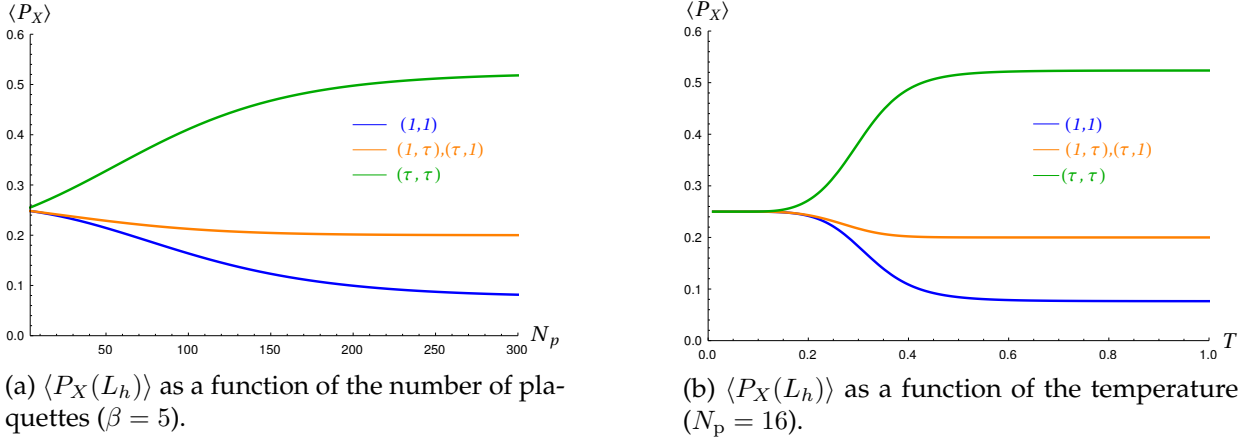


Figure 5.9: The thermal average for the simple objects of $\mathcal{Z}(Fib)$, around the handle of a torus ($g = 1$), as a function of the number of plaquettes N_p ($\beta = 4$). For small system size, the thermal average is $1/4$ for all four objects of the Drinfeld center, as expected for the torus. At large system size, or large temperature, the expectation values tend towards the quantity d_X^2/\mathcal{D}^2 , i.e., $1/\mathcal{D}^2$ for $(1, 1)$, ϕ^2/\mathcal{D}^2 for $(1, \tau)$ and $(\tau, 1)$ and ϕ^4/\mathcal{D}^2 for (τ, τ) .

fluxons, and $z_{p,C}$ becomes independent of C [see Eq. (5.11)]. Hence, one simply obtains:

$$\lim_{N_p \rightarrow \infty} \langle P_X(L_h) \rangle = \frac{\sum_{C \in \mathcal{P}} S_{X,C} S_{\bar{X},C} S_{1,C}^{2-2g}}{\sum_{C \in \mathcal{P}} S_{1,C}^{2-2g}}. \quad (5.55)$$

The result of Eq. (5.55) is independent of the couplings and of the temperature, as long as $T > 0$. It differs from the zero- T expectation value in that the sum over X is now only over pure fluxons, instead of all simple objects of the Drinfeld center. One can also easily get the behavior of $\langle P_X(L_h) \rangle$ in the infinite-temperature limit. In this limit, using Eq. (5.15), Eq. (5.54) becomes

$$\lim_{T \rightarrow \infty} \langle P_X(L_h) \rangle = \frac{\sum_{C \in \mathcal{Z}(C)} S_{X,C} S_{\bar{X},C} S_{1,C}^{2-2g-N_p} n_{C,1}^{N_p}}{\sum_{C \in \mathcal{Z}(C)} S_{1,C}^{2-2g-N_p} n_{C,1}^{N_p}}. \quad (5.56)$$

From this expression, we recover the expression of Eq. (5.55) by taking $N_p \rightarrow \infty$.

As an example, the behavior of $\langle P_X(L_h) \rangle$ is displayed on Fig. 5.9 for the Fibonacci double $\mathcal{Z}(Fib)$ on a torus ($g = 1$). There are four quasiparticles: $(1, 1)$, $(\tau, 1)$, $(1, \tau)$ and (τ, τ) . $(1, 1)$ (the vacuum) and (τ, τ) are fluxons. The only pure fluxon in this case is the vacuum. On the torus, the number of ground states is equivalent to the number of quasiparticles (4 in this case), and every ground-state corresponds to another flux of quasiparticle through the handle of the torus. The ground-state expectation value of $1/4$ of $\langle P_X(L_h) \rangle$, at low temperature and small system size, reflects the presence of four different ground-states. For a large number of plaquettes or a large temperature, $\langle P_X(L_h) \rangle$ tends towards d_X^2/\mathcal{D} , where the quantum dimensions of the quasiparticles are $d_{(1,1)} = 1$, $d_{(1,\tau)} = d_{(\tau,1)} = \phi$, $d_{(\tau,\tau)} = \phi^2$ and the total quantum dimension is $\mathcal{D} = 1 + \phi^2$. $\phi = (1 + \sqrt{5})/2$. This result is recovered from Eqs. (5.55) and (5.56) by setting $C = \mathbf{1} = (1, 1)$ and using the unitarity of the S -matrix.

5.5.4 Loops around throats



Figure 5.10: A projector $P_A(L_t)$ acting around the throat of a genus 3 surface.

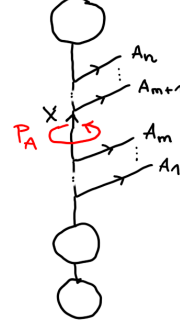


Figure 5.11: Fusion tree for a surface of genus $g = 3$ and a flux X through a throat separating a region with fluxons A_1, \dots, A_m and genus 1 from a region with fluxons A_{m+1}, \dots, A_n and genus 2. The projector on the throat acts as $\delta_{A,X}$.

In a similar way as for closed paths around handles, one can also compute the thermal average of a projector along a closed path which goes around the throat of a surface, see Fig. 5.10. Such a loop divides the lattice in two regions, which we will call \mathcal{R} and $\overline{\mathcal{R}}$, where the first one has genus $g_{\mathcal{R}}$ and $N_{\text{p}}^{\mathcal{R}}$ plaquettes, and the second genus $g_{\overline{\mathcal{R}}}$ and $N_{\text{p}}^{\overline{\mathcal{R}}}$ plaquettes, so that the total number of plaquettes is $N_{\text{p}} = N_{\text{p}}^{\mathcal{R}} + N_{\text{p}}^{\overline{\mathcal{R}}}$ and the total genus $g = g_{\mathcal{R}} + g_{\overline{\mathcal{R}}}$. We start again by considering the ground-state of the SN model. In this case, computing the expectation value of P_X corresponds to counting all fusion diagrams which allow for X in the throat -i.e., X labeling the edge linking $g_{\mathcal{R}}$ and $g_{\overline{\mathcal{R}}}$ loops in the fusion diagram (see Fig. 5.11). As discussed in Sec. 5.5.1, this counting can be performed by using a product of two Moore-Seiberg-Banks formulas (4.11): one for a surface of genus $g_{\mathcal{R}}$ and a puncture labeled with X , and one for a surface of genus $g_{\overline{\mathcal{R}}}$ and a puncture labeled with \bar{X} , so that

$$\begin{aligned} \langle P_X(L_t) \rangle_{\text{GS}} &= \frac{\dim_{\mathcal{Z}(\mathcal{C})}(g_{\mathcal{R}}, X) \dim_{\mathcal{Z}(\mathcal{C})}(g_{\overline{\mathcal{R}}}, \bar{X})}{\dim_{\mathcal{Z}(\mathcal{C})}(g)}, \\ &= \frac{\sum_{C \in \mathcal{Z}(\mathcal{C})} S_{X,C} S_{1,C}^{1-2g_{\mathcal{R}}} \sum_{D \in \mathcal{Z}(\mathcal{C})} S_{\bar{X},D} S_{1,D}^{1-2g_{\overline{\mathcal{R}}}}}{\sum_{C \in \mathcal{Z}(\mathcal{C})} S_{1,C}^{2-2g}}. \end{aligned} \quad (5.57)$$

Note that by summing this expression over X , the unitarity of the S -matrix leads to $\delta_{C,D}$, so that the expression of (5.57) is in agreement with Eq. (5.45).

To compute the thermal average $\langle P_X(L_t) \rangle$, we follow the same strategy as previously, now writing

$$\langle P_X(L_t) \rangle = \frac{1}{Z(g, N_{\text{p}})} \sum_{\text{all labelings with } X \text{ through } L_t} e^{-\beta E(\text{labelings})}, \quad (5.58)$$

where the labelings are those of a fusion diagram as shown in Fig. 5.11. With a similar reasoning

as for Eq. (5.50), the thermal average for the projector around a throat can then be written as

$$\begin{aligned} \langle P_X(L_t) \rangle = & \frac{1}{Z(g, N_p)} \sum_{A_1, \dots, A_{N_p} \in \mathcal{F}} \sum_{a_1=1}^{n_{A_1,1}} \dots \sum_{a_{N_p}=1}^{n_{A_{N_p},1}} \dim_{\mathcal{Z}(\mathcal{C})}(g_{\mathcal{R}}, X, A_1, \dots, A_{N_p}^{\mathcal{R}}), \\ & \times \dim_{\mathcal{Z}(\mathcal{C})}(g_{\overline{\mathcal{R}}}, \bar{X}, A_{N_p}^{\overline{\mathcal{R}}+1}, \dots, A_{N_p}) e^{\beta \sum_{j=1}^{N_p} J_j^{A_j, a_j}}. \end{aligned} \quad (5.59)$$

This expression can also be written in terms of an effective partition function. We define the effective partition function of a surface of genus g with N_p plaquettes and a puncture labeled with X (see Fig. 5.5) as:

$$\begin{aligned} Z_X(g, N_p) &= \sum_{A_1, \dots, A_{N_p} \in \mathcal{F}} \dim(g, A_1, \dots, A_{N_p}, \bar{X}) \sum_{a_1=1}^{n_{A_1,1}} \dots \sum_{a_{N_p}=1}^{n_{A_{N_p},1}} e^{\beta \sum_{p=1}^{N_p} J_p^{A_p, a_p}}, \\ &= \sum_{C \in \mathcal{Z}(\mathcal{C})} S_{\bar{X}, C} S_{1, C}^{1-2g} \prod_{p=1}^{N_p} z_{p, C}. \end{aligned} \quad (5.60)$$

where $z_{p, C}$ is given in Eq. (5.6). Then, the thermal average of the projector can be written in the concise form

$$\langle P_X(L_t) \rangle = \frac{Z_X(g_{\mathcal{R}}, N_p^{\mathcal{R}}) Z_{\bar{X}}(g_{\overline{\mathcal{R}}}, N_p^{\overline{\mathcal{R}}})}{Z(g, N_p)}. \quad (5.61)$$

Note, finally, that

$$\sum_{X \in \mathcal{Z}(\mathcal{C})} Z_X(g_{\mathcal{R}}, N_p^{\mathcal{R}}) Z_{\bar{X}}(g_{\overline{\mathcal{R}}}, N_p^{\overline{\mathcal{R}}}) = Z(g_{\mathcal{R}} + g_{\overline{\mathcal{R}}}, N_p^{\mathcal{R}} + N_p^{\overline{\mathcal{R}}}), \quad (5.62)$$

which follows by unitarity of the S -matrix. As for $\langle P_X(L_h) \rangle$, it is straightforward to extract various limiting cases (such as large $N_p^{\mathcal{R}}$, large $N_p^{\overline{\mathcal{R}}}$, or infinite-temperature limits) using Eqs. (5.11) and (5.15). We will discuss these limits for the special case of contractible loops.

5.5.5 Contractible loops

Contractible loops are a special case of loops around throats, where the genus on one side of the throat (let's say $g_{\overline{\mathcal{R}}}$) is 0. From the fusion diagram represented on Fig. 5.12, it is clear that a flux going through such a loop must necessarily arise as the product of fusion of the fluxons contained in the $N_p^{\overline{\mathcal{R}}}$ plaquettes on the genus 0 side of the loop. Thus, $\langle P_X(L_c) \rangle$ must vanish if $X \notin \mathcal{F}^{\otimes}$, the subset of simple objects of $\mathcal{Z}(\mathcal{C})$ that can be obtained by fusion of fluxons. In particular, one has:

$$\mathcal{F} \subseteq \mathcal{F}^{\otimes} \subseteq \mathcal{Z}(\mathcal{C}). \quad (5.63)$$

If L_c is the contour of a single plaquette, the expectation value of the projector is non-zero only if $X \in \mathcal{F}$.

The thermal average of $P_X(L_c)$ can be easily obtained by setting $g_{\overline{\mathcal{R}}} = 0$ in Eq. (5.61):

$$\langle P_X(L_c) \rangle = \frac{Z_X(g_{\mathcal{R}}, N_p^{\mathcal{R}}) Z_{\bar{X}}(0, N_p^{\overline{\mathcal{R}}})}{Z(g, N_p)}. \quad (5.64)$$

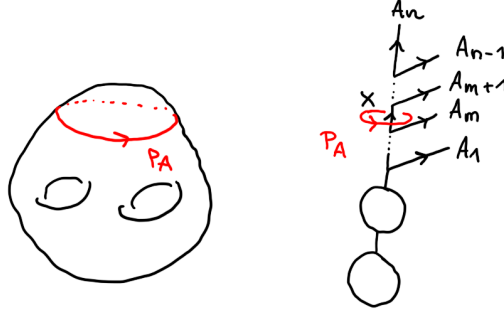


Figure 5.12: Left: a projector $P_A(L_c)$ along a contractible loop surrounding a region on a surface of genus 2. Right: A fusion tree representing the projector $P_A(L_c)$ acting on a surface of genus g and separating a region of genus g , with excitations A_1, \dots, A_m , from a region with genus $g = 0$ and excitations A_{m+1}, \dots, A_n . The projector measures the flux X , which is the fusion product of the fluxons A_{m+1}, \dots, A_n .

For the special case of the SN model, Eq. (5.64) becomes very simple. The explicit expression is then [using Eq. (5.60) and (5.20)]

$$\langle P_X(L_c) \rangle = \frac{1}{Z(g, N_p)} \sum_{C \in \mathcal{Z}(C)} S_{\bar{X}, C} S_{1, C}^{1-2g} \left(\frac{n_{C,1}}{S_{1,C}} - 1 + e^\beta \right)^{N_p^{\mathcal{R}}} \sum_{D \in \mathcal{Z}(C)} S_{X, D} S_{1, D} \left(\frac{n_{D,1}}{S_{1,D}} - 1 + e^\beta \right)^{N_p^{\mathcal{R}}}. \quad (5.65)$$

In the zero- T limit, by using Eq. (5.22) and the unitarity of the S -matrix, one can check that

$$\lim_{T \rightarrow 0} \langle P_X(L_c) \rangle = \delta_{X,1}, \quad (5.66)$$

which simply indicates that, as expected, for all ground states of the SN model, there can only be the trivial fluxon in any contractible loop [note the difference with the result for handles, which may contain nontrivial fluxes, see Eq. (5.46)]. In the limit where the side with genus $g_{\mathcal{R}}$ is large ($N_p^{\mathcal{R}} \gg 1$) using Eqs. (5.20), (5.21), and the fact that in the thermodynamic limit, the sum over C is dominated by fluxons, one gets:

$$\begin{aligned} \lim_{N_p^{\mathcal{R}} \rightarrow \infty} \langle P_X(L_c) \rangle &= \frac{\sum_{C \in \mathcal{P}} S_{\bar{X}, C} S_{1, C}^{1-2g}}{\sum_{C \in \mathcal{P}} S_{1, C}^{2-2g}} \sum_{D \in \mathcal{Z}(C)} S_{X, D} S_{1, D} \left(\frac{\frac{n_{D,1}}{S_{1,D}} - 1 + e^\beta}{\mathcal{D} - 1 + e^\beta} \right)^{N_p^{\mathcal{R}}}, \\ &= d_X \sum_{D \in \mathcal{Z}(C)} S_{X, D} S_{1, D} \times \left(\frac{\frac{n_{D,1}}{S_{1,D}} - 1 + e^\beta}{\mathcal{D} - 1 + e^\beta} \right)^{N_p^{\mathcal{R}}}, \end{aligned} \quad (5.67)$$

if $X \in \mathcal{F}^\otimes$, and 0 otherwise. To go from the first to the second line, we used the fact that a pure fluxon $C \in \mathcal{P}$ braids trivially with $X \in \mathcal{F}^\otimes$, see Eq. (5.38).

Let us consider what happens if the region inside the loop also gets large, i.e., $N_p^{\mathcal{R}} \rightarrow \infty$. Then, as discussed in previous cases, the objects D dominating the sum are pure fluxons, $D \in \mathcal{P}$. Since for these fluxons, $S_{X, D} = \frac{d_X d_D}{\mathcal{D}}$, we obtain

$$\lim_{N_p^{\mathcal{R}}, N_p^{\bar{\mathcal{R}}} \rightarrow \infty} \langle P_X(L_c) \rangle = \frac{d_X^2}{\mathcal{D}^2} \sum_{D \in \mathcal{P}} d_D^2 = \frac{d_X^2}{\mathcal{D}^2} M_0, \quad (5.68)$$

where M_0 is defined in Eq. (5.13).

As stated in the beginning of this section, as we expect topological order to vanish in the thermodynamic limit, we should expect that the topological quantum numbers are completely scrambled. In a model where all excitations of $\mathcal{Z}(\mathcal{C})$ are possible, one would expect to observe $\langle P_X(L_c) \rangle = \frac{d_X^2}{\mathcal{D}^2}$. However, in the restricted Hilbert space in which we are working, all excitations are not allowed ($\langle P_X(L_c) \rangle = 0$ if $X \notin \mathcal{F}^\otimes$). As a consequence, some "topological information" associated to the vertex constraint remains even in the thermodynamic limit at finite temperature. The consequence is the result of Eq. (5.68).

Another interesting case to consider is the special case where $N_p^{\overline{\mathcal{R}}} = 1$ (i.e., L_c is the loop encircling only one plaquette) and $X = 1$. Then, the projection operator $P_1(L_c)$ is exactly the plaquette operator B_p of the standard string-net model. In this case, using the fact that S is unitary and symmetric as well as Eq. (5.14), one finds from Eq. (5.67):

$$\lim_{N_p^{\overline{\mathcal{R}}} \rightarrow \infty} \langle B_p \rangle = \lim_{N_p^{\overline{\mathcal{R}}} \rightarrow \infty} -\frac{\langle H \rangle}{N_p} = \frac{e^\beta}{\mathcal{D} - 1 + e^\beta} = -e, \quad (5.69)$$

where e is the energy per plaquette in the thermodynamic limit, as given in Eq. (5.24) (see also Ref. [110] for a similar result), and

$$\lim_{N_p^{\overline{\mathcal{R}}} \rightarrow \infty} \langle P_X(L_c) \rangle = \frac{d_X n_{X,1}}{\mathcal{D} - 1 + e^\beta}, \quad (5.70)$$

when $X \in \mathcal{F}^*$, i.e., is a non-trivial fluxon. This thermal average of a non-trivial fluxon projector has been computed for the Fibonacci string-net model in [109]⁵, and can be understood as a generalized Pauli exclusion principle for fluxons.

5.6 Wegner-Wilson loops

5.6.1 Wegner-Wilson loops at zero temperature

The concept of Wegner-Wilson loops (WWL) stems from lattice gauge theories, where they were introduced independently by Wegner [41] and Wilson [43] as gauge-invariant non-local operators, defined along a closed contour. For a pure gauge theory⁶, the scaling of the WWL (either with the perimeter, or with the area of the contour) allows to diagnose a confinement-deconfinement phase transition even in the absence of spontaneous symmetry breaking [41, 43, 133, 131, 42].

The action of a WWL can be understood as a generalization of the Aharonov-Bohm effect [7]. A WWL defined along a closed path on the lattice will measure the flux through this contour, or, in other words, the total quantum number contained inside the loop. While in the Aharonov-Bohm effect, the loop would correspond to an electric charge being moved around a magnetic flux, in a string-net model with topological order $\mathcal{Z}(\mathcal{C})$, there are as many WWL as simple objects in $\mathcal{Z}(\mathcal{C})$

⁵In fact, the only non-trivial fluxon of $\mathcal{Z}(Fib)$ is (τ, τ) which has $d_{(\tau, \tau)} = \phi^2$ and $n_{(\tau, \tau), 1} = 1$. The total quantum dimension is $\mathcal{D} = 1 + \phi^2$. From Eq. (5.70), one then obtains $\lim_{N_p^{\overline{\mathcal{R}}} \rightarrow \infty} \langle P_X(L_c) \rangle = \frac{1}{1 + e^\beta \phi^{-2}}$ which is exactly Eq. (21) of [109]. This has the same form as a Fermi-Dirac occupation factor with fugacity $e^{\beta\mu} = \phi^2$.

⁶In the presence of matter, due to a phenomenon known as "string breaking", WWL scale with the perimeter of the contour in both phases and lose their significance as diagnostic of a confinement-deconfinement phase transition [131].

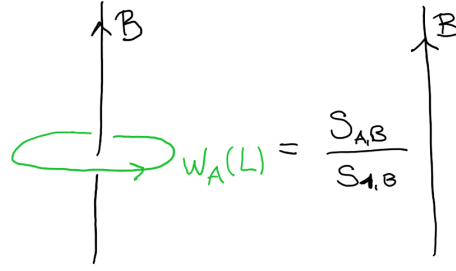


Figure 5.13: A Wegner-Wilson loop operator W_A acting on a string B . This is also known as the “unlinking” relation. It can be inferred from the definition of the S -matrix, Fig. 2.13.

[48]. The WWL W_A , associated to $A \in \mathcal{Z}(C)$, corresponds to a quasiparticle operator creating a pair of anyons A and \bar{A} , moving A around some region on the lattice and reannihilating it with \bar{A} . In this way, it measures the total anyonic charge contained inside the region. Graphically, the action of a WWL W_A can be represented as in Fig. 5.13, where the ratio of S -matrix elements plays the role of a generalized Aharonov-Bohm phase.

The string-net models are closely related to lattice gauge theories [48]. In particular, the model in the restricted Hilbert space corresponds to the pure-gauge sector of a lattice gauge theory (electric charges, i.e. matter, would be located at the vertices of a lattice gauge theory). The WWL may then be used to diagnose the presence of topological order at $T = 0$, corresponding to the deconfinement of quasiparticles or anyons. For a deconfined quasiparticle A , the decay of the WWL $W_A(L_c)$, defined on a contractible contour, is slow. The WWL then follows a *perimeter law*, i.e., it decays exponentially with the perimeter $|L_c|$ of the loop L_c

$$\langle W_A(L_c) \rangle \sim e^{-c_1 |L_c|}, \quad (5.71)$$

when L_c grows and where $c_1 > 0$. This slow decay corresponds to a weak effective potential between a pair of anyons sitting at the two open ends of a string operator. Thus, strings can be very long (and WWL very large), and anyons are deconfined [134, 135]. WWL operators, or in other words, closed quasiparticle operators, commute with the SN Hamiltonian [48, 47] and are thus conserved quantities. In the SN ground state, WWL do not decay, no matter how large they are. This corresponds to $c_1 = 0$ in Eq. (5.71). Such a perimeter law is known as the *zero law* [136].

On the other hand, a confined quasiparticle A corresponds to a fast decay of the WWL or to an *area law*, i.e., the WWL decays exponentially with the area \mathcal{A} of the region delimited by L_c :

$$\langle W_A(L_c) \rangle \sim e^{-c_2 \mathcal{A}}, \quad (5.72)$$

when L_c grows and where $c_2 > 0$. In terms of open string operators, it means there is a strong effective potential between the two anyons at the extremities of the string (typically proportional to the length of the string). Hence, anyons are confined.

It is known that string-net models can undergo a confinement-deconfinement transition of anyons at zero temperature when an additional term is added to the Hamiltonian [48, 129, 128]. This term takes the form of a string-tension, which acts on the links of the lattice and destroys long-range entanglement in the ground-state wave function. In this context, WWL have been

computed perturbatively for the toric code [129] and for string-net models with input UMTC [128].

In Ref. [128], we found that, for a weak string tension, topological order is conserved, and all WWL follow either a zero law or a perimeter law. For a sufficiently strong string tension, topological order is destroyed. The trivial phase is identified by WWL following an area law - with one exception: we observed that WWL associated with Abelian fluxons always follow a zero law $\langle W_A \rangle = 1$, i.e., these anyons remain always deconfined. These Abelian anyons are also pure fluxons.

In the rest of the section, we compute the thermal average of Wegner-Wilson loops in the generalized string-net model, both on contractible and non-contractible contours. At finite temperature, it is of use, in the context of quantum chromodynamics [43, 134] to consider rather Polyakov loops instead of WWL in order to diagnose confinement or deconfinement. Polyakov loops are string operators along non-contractible loops, which wind in the direction of imaginary time. In the string-net models which we consider, anyons have no dynamics, so Polyakov loops correspond simply to an anyon staying still (see App. C of [130]). However, in the restricted Hilbert space (i.e., pure gauge-sector) we expect the WWL to still be meaningful even at finite temperature.

5.6.2 From projectors to WWL

WWL are closely related to the projection operators $P_A(L)$ discussed in the previous section. In fact, for any given closed loop L on our surface, the unlinking relation (see, e.g., Refs. [32, 28]) shown in Fig. 5.13 directly gives:

$$W_A(L) = \sum_{B \in \mathcal{Z}(C)} \frac{S_{A,B}}{S_{1,B}} P_B(L). \quad (5.73)$$

Using the unitarity of S , one also gets the inverse transformation

$$P_A(L) = S_{1,A} \sum_{B \in \mathcal{Z}(C)} S_{A,B}^* W_B(L). \quad (5.74)$$

A remarkable case of this relation is obtained for the projector onto the vacuum $A = 1$ (the Kirby strand) for which

$$P_1(L) = \sum_{B \in \mathcal{Z}(C)} \frac{d_B}{\mathcal{D}^2} W_B(L). \quad (5.75)$$

In particular, as discussed close to Eq. (2.57) and Eq. (4.13), if L is the contour of a single plaquette this projector is also nothing else than the plaquette operator B_p :

$$P_1(p) = \sum_{s \in \mathcal{C}} \frac{d_s}{\mathcal{D}^2} B_p^s = \sum_{B \in \mathcal{Z}(C)} \frac{d_B}{\mathcal{D}} W_B(p). \quad (5.76)$$

Using Eqs. (5.45) and (5.73), it is furthermore possible to show that W_1 is the identity operator $\mathbb{1}$. This is in agreement with what one would expect physically, as adding a loop of vacuum should not modify the state of the system.

The closed string operators W_A satisfy the fusion algebra [48]

$$W_A(L)W_B(L) = \sum_{C \in \mathcal{Z}(C)} N_{A,B}^C W_C(L), \quad (5.77)$$

where $N_{A,B}^C$ are the fusion multiplicity coefficients of $\mathcal{Z}(C)$. This formula can be proven by using Eq. (5.73) along with Eq. (5.45), (5.74) and the Verlinde formula Eq. (4.9).

5.6.3 WWL at finite temperature

WWL around handles

Using the results obtained in Sec. 5.5 for the projectors and (5.73), it is straightforward to obtain expressions for the thermal average of WWL operators. For instance, for a large genus- g surface, at any nonzero temperature and for arbitrary couplings, one gets from Eq. (5.55)

$$\begin{aligned} \lim_{N_p \rightarrow \infty} \langle W_A(L_h) \rangle &= \sum_{B \in \mathcal{Z}(C)} \sum_{C \in \mathcal{P}} \frac{S_{A,B} S_{B,C} S_{\bar{B},C} d_C^{2-2g}}{S_{1,B} M_g} \\ &= \frac{\sum_{C \in \mathcal{P}} N_{C\bar{C}}^{\bar{A}} d_C^{2-2g}}{M_g}, \end{aligned} \quad (5.78)$$

where M_g is given in Eq. (5.13). To go from the first to the second line, we have used the property of the S -matrix $S_{A,\bar{B}} = S_{A,B}^*$ [85] and the Verlinde formula (2.20). Such a loop around a handle is similar to the generalized symmetry operators studied in Ref. [39]. Their behavior at finite temperature is different from the one at zero temperature:

$$\lim_{T \rightarrow 0} \langle W_A(L_h) \rangle = \frac{\sum_{C \in \mathcal{Z}(C)} N_{AC}^C S_{1,C}^{2-2g}}{\sum_{C \in \mathcal{Z}(C)} S_{1,C}^{2-2g}}, \quad (5.79)$$

where we used Eqs. (5.46) and (5.73). Note how the Drinfeld center replaces the set of pure fluxons in the above sums when contrasting the $T = 0$ and $T > 0$ behaviors, similarly to what we observed for the projectors.

Contractible loops

In the simple case of the SN model, at zero temperature, for any $A \in \mathcal{Z}(C)$, and for any contractible loop L_c ,

$$\lim_{T \rightarrow 0} \langle W_A(L_c) \rangle = d_A. \quad (5.80)$$

Indeed, for any ground state of the SN model, one has only the vacuum in each plaquette. Thus, this result can be directly obtained from the unlinking relation (see Fig. 5.13 for $B = 1$). This result is in agreement with the zero law that one expects in the SN ground state. It means that all quasiparticles are deconfined in the ground state, which is a fingerprint of a topologically ordered phase.

One can also obtain a simple expression of the WWL operators in the SN model at finite temperature. Using Eq. (5.67) and (5.73) one gets:

$$\lim_{N_p^{\bar{R}} \rightarrow \infty} \langle W_A(L_c) \rangle = d_A \left(\frac{\mathcal{D} \frac{n_{A,1}}{d_A} - 1 + e^\beta}{\mathcal{D} - 1 + e^\beta} \right)^{N_p^{\bar{R}}}, \quad (5.81)$$

where the loop separates a region with $N_p^{\overline{\mathcal{R}}}$ and genus $g = 0$ from a region of genus g with $N_p^{\mathcal{R}}$ plaquettes. In the limit where also $N_p^{\overline{\mathcal{R}}} \rightarrow \infty$, one observes that $\langle W_A(L_c) \rangle$ decreases to zero, unless A is a pure fluxon. Indeed, for pure fluxons, as $n_{A,1} = d_A$, one always has

$$\langle W_A(L_c) \rangle = d_A, \quad (5.82)$$

At any finite temperature, Eq. (5.81) can be exponentiated into:

$$\lim_{N_p^{\overline{\mathcal{R}}} \rightarrow \infty} \langle W_A(L_c) \rangle = d_A e^{N_p^{\overline{\mathcal{R}}} \ln \left(\frac{\mathcal{D} \frac{n_{A,1}}{d_A} - 1 + e^\beta}{\mathcal{D} - 1 + e^\beta} \right)}. \quad (5.83)$$

This result indicates a confinement for all particles of the Drinfeld center, except for pure fluxons. For the latter, Eq. (5.82) indicates a deconfinement of these particles at any temperature. This is in agreement with the results of [128], where it was observed for input UMTCs that Abelian fluxons are always deconfined. In fact, when \mathcal{C} is commutative, Abelian fluxons are exactly the pure fluxons. Equation (5.82) suggests that pure fluxons are insensitive to the presence of other fluxons in the system, i.e., that they braid trivially with all fluxons. This trivial braiding property translates into the fact that for $A \in \mathcal{P}$ and $B \in \mathcal{F}^\otimes$, $S_{A,B} = \frac{d_A d_B}{\mathcal{D}}$, as discussed in Sec. 5.4. For all other particles $A \notin \mathcal{P}$, one has $n_{A,1} < d_A$, and Eq. (5.83) describes an area law. More generally, one may write

$$\langle W_A(L_c) \rangle = d_A e^{-N_p^{\overline{\mathcal{R}}}/N_A^*}, \quad (5.84)$$

where we introduced the temperature-dependent characteristic area

$$N_A^* = \left[\ln \left(\frac{\mathcal{D} - 1 + e^\beta}{\mathcal{D} \frac{n_{A,1}}{d_A} - 1 + e^\beta} \right) \right]^{-1}, \quad (5.85)$$

which diverges for $A \in \mathcal{P}$ ($n_{A,1} = d_A$) and is minimum for $A \notin \mathcal{F}$ ($n_{A,1} = 0$). In other words, particles that are not fluxons are strongly confined.

5.6.4 Numerical implementation of WWL

In this section, we present how to express the Wegner-Wilson loop operators in the link basis, in order to get numerical results for expectation values of WWL. Using the relation of Eq. (5.74), this allows also for a numerical test of the thermal expectation values of the projectors $\langle P_X \rangle$. A prescription for computing closed quasiparticle operators is given in Ref. [48], and is valid for UFCs with tetrahedral reflection symmetry. A more general expression could be obtained by using the quasiparticle operators without tetrahedral symmetry presented in [78] and the F -moves defined in Chap. 2.

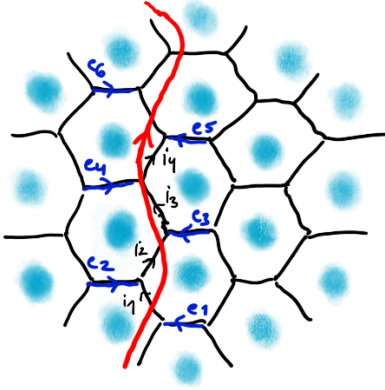


Figure 5.14: A quasiparticle operator (in red) inserted on the lattice in the fat lattice picture.

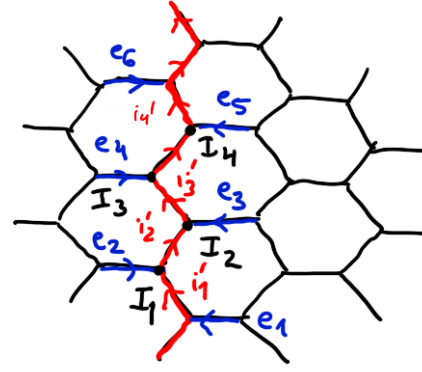


Figure 5.15: The quasiparticle operator represented in Fig. 5.14 modifies the labels on the edges drawn in red. These edges define the path P of the quasiparticle operator in the lattice.

In order to compute the matrix elements of a Wegner-Wilson loop operator W_A associated to $A \in \mathcal{Z}(\mathcal{C})$, one inserts a string of type A into the lattice. In the fat lattice picture, this looks as represented in Fig. 5.14. The exact position of this string inside the fat lattice is not important as it is allowed to move over vertices [48]:

$$\begin{array}{c} i \\ \swarrow \\ j \end{array} \begin{array}{c} \uparrow A \\ \downarrow \\ k \end{array} = \begin{array}{c} \swarrow \\ i \\ \downarrow \\ j \end{array} \begin{array}{c} \uparrow A \\ \downarrow \\ k \end{array} \quad (5.86)$$

One can then use the halfbraiding Ω_A , defined in Eq. (2.36), in order to fuse the string corresponding to the quasiparticle $A \in \mathcal{Z}(\mathcal{C})$ into the (fat) lattice. Every crossing of A with an edge of the lattice labeled i is described by a half-braiding $[\Omega_{A,sti}^j]_{\alpha,\beta}$ (or $[\bar{\Omega}_{A,sti}^j]_{\alpha,\beta}$), with $i, j, s, t \in \mathcal{C}$ and $\alpha \in \{1, \dots, n_{A,s}\}, \beta \in \{1, \dots, n_{A,t}\}$. Over regions where A does not cross an edge of the lattice, the indices s and t must stay the same, and the matrix indices α, β get contracted. For example, a quasiparticle operator A crossing two edges labeled i_1 and i_2 leads to [78]:

$$\begin{array}{c} i_2 \\ \swarrow \\ i_1 \end{array} \begin{array}{c} \uparrow A \\ \downarrow \\ k \end{array} = \sum_{\substack{s_1, s_2 \\ t_1, j_1, j_2 \\ \alpha_1, \alpha_2, \beta_1}} [\Omega_{A, s_1 t_1 j_1}^{i_1}]_{\alpha_1 \beta_1} [\Omega_{A, s_2 s_1 j_2}^{i_2}]_{\alpha_2 \beta_1} \begin{array}{c} i_2 \\ \swarrow \\ j_2 \\ \downarrow \\ s_2 \\ \swarrow \\ i_1 \\ \downarrow \\ t_1 \end{array} \quad (5.87)$$

Finally, in a similar way as for the plaquette operator B_p (Sec. 3.3), one can use F -moves in order to come back to the original lattice (see Fig. 5.15). The general formula for a closed string operator W_A along a path P is given in Eq. 19 and 20 of Ref. [48] (the labels of edges $\{e_k\}$, $\{i_k\}$ and vertices $\{I_k\}$ refer to the notations of Figs. 5.14, 5.15):

$$W_{A, i_1, i_2, \dots, i_N}^{i'_1, i'_2, \dots, i'_N}(e_1, e_2, \dots, e_N) = \sum_{\{s_k\}} \left(\prod_{k=1}^N F_k^{s_k} \right) \text{Tr} \left(\prod_{k=1}^N \Omega_{A, k}^{s_k} \right), \quad (5.88)$$

where

$$F_k^s = \begin{cases} [F_s^{i_k \bar{e}_k \bar{i}'_{k-1}}]_{i_{k-1} \bar{i}'_k} & \text{if } P \text{ turns left at } I_k \\ [F_s^{i_{k-1} \bar{e}_k \bar{i}'_k}]_{i_k \bar{i}'_{k-1}} & \text{if } P \text{ turns right at } I_k \end{cases}, \quad (5.89)$$

and

$$\Omega_{A,k}^{s_k} = \begin{cases} \sqrt{\frac{d_{i_k} d_{s_k}}{d_{i'_k}}} \Omega_{A,s_k s_{k+1} i_k}^{i'_k} & \text{if } P \text{ turns right, left at } I_k, I_{k+1} \\ \sqrt{\frac{d_{i_k} d_{s_k}}{d_{i'_k}}} \bar{\Omega}_{A,s_k s_{k+1} i_k}^{i'_k} & \text{if } P \text{ turns left, right at } I_k, I_{k+1} \\ \delta_{s_k s_{k+1}} & \text{otherwise.} \end{cases} \quad (5.90)$$

Here, the $\Omega_{A,s_k s_{k+1} i_k}^{i'_k}$ are rectangular matrices of dimension $n_{A,s_k} \times n_{A,s_{k+1}}$, with elements $[\Omega_{A,sti}^j]_{\alpha,\beta}$. For a commutative UFC, they are just complex numbers.

In summary, similarly to the plaquette operators, the WWL operators modify only the labels on the N edges $\{i_k\}$ along the path P , but depend also on the outer edges $\{e_k\}$. In fact, by setting $N = 6$ and $A = 1$, one recovers the expression for the matrix elements of B_p for a honeycomb lattice given in [48]. If the path P (drawn in red in Fig. 5.15) defines a contractible contour, or goes around the throat of a surface of genus $g \geq 1$, it separates a region with $N_p^{\mathcal{R}}$ plaquettes from a region with $\bar{N}_p^{\mathcal{R}}$ plaquettes, so that the total number of plaquettes is $N_p = N_p^{\mathcal{R}} + \bar{N}_p^{\mathcal{R}}$. This is the information we have used in the rest of this chapter to compute the expectation values of the WWL W_A and projectors P_A .

5.7 Topological mutual information

In the last section of this chapter, we study the topological mutual information of string-net models at finite temperature.

One way to characterize topological order at zero temperature is to compute the topological entanglement entropy introduced in Refs. [29, 30] (see also Ref. [31, 137]). However, at finite temperature, this quantity, defined as the constant term of the von Neumann entanglement entropy, suffers from several problems which have led Iblisdir *et al.* to rather consider the topological mutual information I_{topo} [69, 70]. The main issue is that the finite-temperature entanglement entropy no longer follows an "area" law but also features an extensive "volume" term. It is therefore no longer symmetric between the inner and outer region of the contour, and cannot be thought of as measuring only the entanglement between these regions.

In the first part of this section, we introduce the concept of topological entanglement entropy at zero temperature, and briefly explain how to compute the entanglement entropy for string-nets following [30]. We also recall a result on the entanglement entropy of classical string-nets (i.e., at infinite temperature) [76]. Then, we conjecture a result at finite temperature for the topological mutual information, based on the results by Refs. [69, 70] and our expectation values of projectors computed in Sec. 5.5, and discuss a scaling law between temperature and system size. Finally, we discuss numerical results, both on the ground-state entanglement entropy and on the topological mutual information.

5.7.1 Entanglement entropy and topological order at $T = 0$

For a bipartite system, where the Hilbert space \mathcal{H} can be written as $\mathcal{H} = \mathcal{H}_A \otimes \mathcal{H}_B$, a pure state $|\psi\rangle$ is entangled if it cannot be written as a product state $|\psi\rangle = |\psi_A\rangle \otimes |\psi_B\rangle$. For example, if one considers a two spin system, where each spin can point either up ($|\uparrow\rangle$) or down ($|\downarrow\rangle$), an example of a product state would be the state $|\uparrow\uparrow\rangle = |\uparrow\rangle \otimes |\uparrow\rangle$, while the state $\frac{1}{\sqrt{2}}(|\uparrow\downarrow\rangle - |\downarrow\uparrow\rangle)$ cannot be factorized and is hence entangled (see e.g. [138] for a general introduction to entanglement in quantum systems).

For many-body systems, one can instead consider a bipartition by separating the system into two regions A and B (see Fig. 5.16). The entanglement between the two regions for a pure state $|\psi\rangle$ can be quantified by using the Von Neumann entropy [31], defined as

$$S_A = -\text{Tr}_A(\rho_A \ln(\rho_A)), \quad (5.91)$$

where ρ_A is the reduced density matrix of the region A , obtained by tracing the full density matrix $\rho = |\psi\rangle\langle\psi|$ over the degrees of freedom in B :

$$\rho_A = \text{Tr}_B \rho. \quad (5.92)$$

If ρ_A is the density matrix of a pure state, then $S_A = 0$ and there is no entanglement between regions A and B . If ρ_A is mixed, then $S_A > 0$ and there is some entanglement between A and B . In general, the larger S_A (or S_B), the more regions A and B are entangled. The same result is obtained if one computes instead S_B , i.e., the entropy is symmetric between regions A and B .

Generally, one might expect the entanglement entropy S_A to grow proportionally to the number of degrees of freedom contained inside region A . However, for ground-states of gapped, locally interacting Hamiltonians, the entanglement entropy generally grows instead just like the linear size $|\partial A|$ of the boundary. This is usually called an *area law*, in reference to 3D systems with a 2D boundary, although the result applies also to 2D systems with a 1D boundary [31, 138]. This is due to the fact that correlations are short-ranged, and therefore the relevant region for entanglement between regions A and B is just the width corresponding to the correlation-length. As shown in [31], in the case of a degenerate ground state, the entanglement entropy is the same for all ground-state wave functions. In the presence of topological order, this area law is completed by a constant, size-independent term, called the *topological entanglement entropy* γ . The entanglement entropy then takes the form [30, 29]

$$S_A = S_B = \alpha |\partial A| - \gamma + \dots \quad (5.93)$$

where $\gamma > 0$ and the ellipse means terms which vanish in the large system size limit, α is a non-universal constant, and the boundary between A and B is smooth. The constant term γ reflects long-range entanglement, and is a signature of topological order. It is universal, in the sense that it does not depend on microscopic properties of the system, but only on the type of topological order.

This topological entanglement entropy was computed analytically by Kitaev and Preskill [29] and Levin and Wen [30]. They found that the topological entanglement entropy of a topological

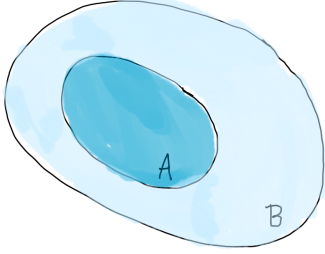


Figure 5.16: Illustration of the bipartition of a system into regions A and B .

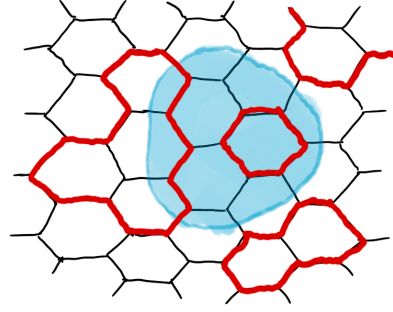


Figure 5.17: Example of a lattice configuration of \mathbb{Z}_2 on a honeycomb lattice. Links in red are in the state s and black links in the vacuum state 1 . As one can see, due to the closed loop configuration, only an even number of red links can cross the boundary.

order corresponding to a UMTC \mathcal{U} in the ground-state is given by the logarithm of the total quantum dimension of \mathcal{U} , i.e.

$$\gamma = \ln(\mathcal{D}). \quad (5.94)$$

The easiest example to consider to understand how this constant contribution arises is to look at the ground-state of the toric code (see e.g.[28]). The toric code string-net is built from the elements of the group \mathbb{Z}_2 (see also Sec. 2.3), i.e., the links can only be in two states, 1 and s , where 1 is the vacuum. Fusion rules are commutative and non-Abelian, and the only non-trivial fusion rule is $s \times s = 1$. Due to these fusion rules, all vertices in the ground state must have an even number of incident s strings. The string-net wave function is therefore a superposition of lattice configurations where s strings form closed loops (this is sometimes called a loop gas). If we consider a region A with a boundary crossing m links (see Fig. 5.17), one might expect that the freedom of the configurations of these links is 2^m , since every link can be in two possible states. However, due to the constraint of closed loops, only an even number of strings s can cross the boundary in a given configuration. Hence, the state of the m -th link is fully determined by the state of the other $m - 1$ links on the boundary. The long-range constraint thus provides one with more information on the state of the system so that, counter-intuitively, the long-range entanglement leads to lowering the entanglement entropy by γ . Note, finally, that the Von Neumann entropy is not the only way to quantify entanglement. For instance, the Rényi entropy of string-net models has been studied in [139], and the entanglement spectrum in [140, 122].

5.7.2 Area law for string-net models

An analytic result for the area-law contribution for the string-net ground-state wave function has been obtained by Levin and Wen [30]. For a string-net build from a UFC⁷ \mathcal{C} with $N_{\mathcal{C}}$ simple

⁷The proof of Ref. [48] has been performed only for the original string-net construction, i.e., for UFCs with tetrahedral symmetry.

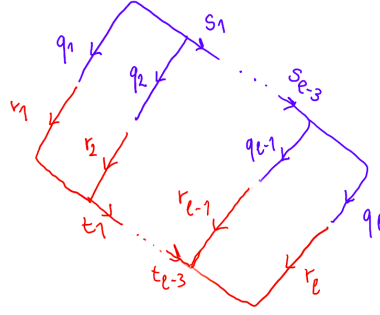


Figure 5.18: A boundary configuration for a string-net model. In violet, links in region A , in red, links in region B .

objects, the entanglement entropy of a region A is

$$S_A = -l \sum_{s=1}^{N_C} \frac{d_s^2}{\mathcal{D}} \log \left(\frac{d_s}{\mathcal{D}} \right) - \ln(\mathcal{D}), \quad (5.95)$$

where l is the number of links crossed around the contour of region A , and the contour is chosen to pass through the links, as shown in Fig. 5.17. This result can also be extended to the case of region A having several disconnected boundaries [30]. In the case where $\mathcal{C} = \text{Vec}(G)$, the entanglement entropy takes the simple form

$$S_A = (l - 1) \ln(|G|), \quad (5.96)$$

where $|G| = \mathcal{D}$ is the total number of elements in the group (see also [31, 70]). In the following, we give a brief account on how to obtain the result of Eq. (5.95), following the descriptions given in [30, 141] (similar descriptions can also be found in [142], [143] and [28]). In Sec. 5.7.5, we will compare this analytic approach with our numerical approach.

The lattice is separated into two regions A and B by defining a contour cutting through l links. The Hilbert space is enlarged so as to double the degrees of freedom of these boundary links and make the regions A and B symmetric with respect to the boundary. This enlarged Hilbert space can be partitioned into two pieces, $\mathcal{H} = \mathcal{H}_A \otimes \mathcal{H}_B$, by attributing every degree of freedom to one of the two regions. One can then search for the Schmidt decomposition of the ground-state wave-function $|\psi\rangle$:

$$|\psi\rangle = \sum_{k=1}^r \alpha_k |\psi_k^A\rangle |\psi_k^B\rangle, \quad (5.97)$$

where r is the Schmidt rank, $|\psi_k^A\rangle$ are orthonormal wavefunctions in \mathcal{H}_A and $|\psi_k^B\rangle$ are orthonormal wavefunctions in \mathcal{H}_B . The Schmidt coefficients α_k are non-negative real numbers that verify

$$\sum_k \alpha_k^2 = 1. \quad (5.98)$$

In the ground-state wave-function of string-nets, different lattice configurations can be related to each other using local diagrammatic moves (see Chap. 3). This property can be applied both to states in \mathcal{H}_A and in \mathcal{H}_B , as long as the configuration at the interface between A and B is not

changed. A state $|\psi_k^A\rangle$ ($|\psi_k^B\rangle$) can therefore be represented by a reference diagram as shown in Fig. 5.18, only parametrized by the set of strings $\{q\}$ ($\{r\}$) on the boundary and the set of strings $\{s\}$ ($\{t\}$) linking them together. Every such diagram actually represents a superposition of all diagrams that can be obtained from it by local moves restricted to A (B).

The Schmidt weights of these configurations can be derived by using diagrammatic rules to reduce the boundary configuration of Fig. 5.18 to the vacuum, as described in [30] (an alternative way using probabilities of fusion trees is described e.g. in [142]). One finds

$$\alpha_{k \equiv \{q,r,s,t\}} = \frac{1}{\sqrt{\mathcal{N}}} \delta_{\{q\},\{r\}} \delta_{\{s\},\{t\}} \prod_{i=1}^l \sqrt{d_{q_i}} \quad (5.99)$$

where d_{q_i} is the quantum dimension of the string q_i . \mathcal{N} is a normalization constant which can be determined using (5.98), from where one gets $\mathcal{N} = \mathcal{D}^{l-1}$.

Finally, the entanglement entropy can be computed as

$$S_A = - \sum_k \alpha_k^2 \ln \alpha_k^2, \quad (5.100)$$

which can be simplified to Eq. (5.95).

5.7.3 Entanglement entropy at infinite temperature

Analytical results for the opposite limit of infinite temperature also exist in the literature. String-net models at infinite temperature have been studied under the name of "classical string-nets" in Refs. [74] (for the toric code) and [76] ($SU(N)_k$ string-nets and string-nets based on finite groups). These papers compute a classical equivalent to the entanglement entropy by considering the Shannon entropy of a bipartition. Ref. [76] derives a formula for the entanglement entropy of a region A in the thermodynamic limit:

$$\begin{aligned} S_A &= \frac{N_v^A}{2} \ln \mathcal{D} + l \ln \left(\mathcal{D} \prod_{j=1}^{N_C} (d_s)^{-d_s^2/\mathcal{D}} \right) - (n_B - 1) \ln M, \\ &= \frac{N_v^A}{2} \ln \mathcal{D} - l \sum_{s=1}^{N_C} \frac{d_s^2}{\mathcal{D}} \ln \left(\frac{d_s}{\mathcal{D}} \right) - (n_B - 1) \ln M. \end{aligned} \quad (5.101)$$

where d_s are the quantum dimensions of the simple object of \mathcal{C} , N_v^A is the number of vertices inside the region A (i.e., that do not share links with the complementary region B), l is the number of links crossing the boundary of the region, and n_B is the number of disconnected regions in B . M , finally, is the number of Abelian objects in \mathcal{C} . In particular, for string-nets based on groups, the formula is

$$S_A = N_v^A \ln \sqrt{|G|} + l \ln |G| - (n_B - 1) \ln |G|. \quad (5.102)$$

Note that the area term (proportional to l) in Eq. (5.101) is exactly the same as in Eq. (5.95).

5.7.4 Topological mutual information at finite temperature

At finite temperature, the density matrix of the system,

$$\rho = \frac{1}{Z} e^{-\beta H}, \quad (5.103)$$

describes a mixed state. One can still compute the Von Neumann entropy of a region \mathcal{R} for a bipartition of the system into two regions \mathcal{R} and $\overline{\mathcal{R}}$, but this entropy will now have a volume contribution (i.e., some term that scales proportionally to the area of \mathcal{R}) and the entropy will no longer be symmetric between \mathcal{R} and $\overline{\mathcal{R}}$. Instead, as proposed by Ref. [68, 69, 70], one can use the mutual information, which remains symmetric between both regions at finite temperature. The mutual information is defined as:

$$I_{\mathcal{R}} = S_{\mathcal{R}} + S_{\overline{\mathcal{R}}} - S_{\mathcal{R} \cup \overline{\mathcal{R}}} = I_{\overline{\mathcal{R}}}, \quad (5.104)$$

where $S_{\mathcal{R}} = -\text{Tr}_{\mathcal{R}} \rho_{\mathcal{R}} \ln \rho_{\mathcal{R}}$ is the von Neumann entropy, and $\rho_{\mathcal{R}} = \text{Tr}_{\overline{\mathcal{R}}} (e^{-\beta H})/Z$. In the limit where the length $|L_c|$ of the boundary L_c between the two regions goes to infinity, one expects the mutual information to behave as [69, 70]

$$I_{\mathcal{R}} = \alpha' |L_c| - \gamma'. \quad (5.105)$$

That is, contrary to the entropy, the mutual information still follows an area law at finite temperature. The topological mutual information is then defined as $I_{\text{topo}} = -\gamma'$. Under some simple assumptions, Iblisdir *et al.* conjectured a general form of I_{topo} at finite temperature for the Kitaev quantum double model [47] based on the Kullback-Leibler divergence [69, 70]. This divergence between two probability distributions $\{p^1\}$ and $\{p^2\}$ is defined as

$$D_{\text{KL}}(\{p^1\} || \{p^2\}) = - \sum_i p_i^1 \ln \left(\frac{p_i^1}{p_i^2} \right). \quad (5.106)$$

By substituting p_i^1 by the thermal probability distribution $\langle P_A(L_c) \rangle$ associated with having a total quantum number $A \in \mathcal{Z}(\mathcal{C})$ inside region \mathcal{R} and p_i^2 with the probability given by the quantum dimensions, $\frac{d_A^2}{\mathcal{D}^2}$, to observe a quantum number A , Iblisdir *et al.* conjectured that

$$I_{\text{topo}}(T) = - \sum_{A \in \mathcal{Z}(\mathcal{C})} \langle P_A(L_c) \rangle \ln \left[\langle P_A(L_c) \rangle \frac{\mathcal{D}^2}{d_A^2} \right], \quad (5.107)$$

for a surface with $g = 0$, and in the limit where $|L_c| \rightarrow \infty$. While this formula was conjectured for the Kitaev quantum double model, the close connections between this model (which we will discuss in further detail in Chap. 6) and the string-net model allow us to assume that it also holds for the string-net model, where the projector $P_A(L_c)$ is the projector whose thermal average is given in Eq. (5.64). As we shall see, this conjecture reproduces the exact results in the zero- T and infinite- T limits presented in the two previous sections. Proving the conjecture is still work in progress. A few more details on this point are provided in Chap. 7.

Infinite-temperature limit

Generically, one would expect the topological mutual information to be zero at infinite temperature due to a loss of quantum correlations. However, for the SN model, some nontrivial residual information remains in the system even at infinite temperature because we are working in a restricted Hilbert space with the vertex constraint being strictly imposed.

The general expression of $\langle P_A(L_c) \rangle$ is given in Eq. (5.64). Here, for simplicity, we consider the thermodynamic limit where both $N_p^{\mathcal{R}}$ and $N_p^{\overline{\mathcal{R}}}$ go to infinity which, using Eq. (5.67), yields

$$\lim_{N_p^{\mathcal{R}}, N_p^{\overline{\mathcal{R}}} \rightarrow \infty} \langle P_A(L_c) \rangle = d_A \sum_{C \in \mathcal{P}} S_{A,C} S_{1,C} = \frac{d_A^2}{\mathcal{D}^2} M_0, \quad (5.108)$$

for $A \in \mathcal{F}^{\otimes}$, and 0 otherwise. We recall the expression of

$$M_0 = \sum_{C \in \mathcal{P}} d_C^2, \quad (5.109)$$

which is defined in Eq. (5.13) by setting $g = 0$. Expression (5.108) is valid at any finite temperature. Plugging this expression into Eq. (5.107) and using Eq. (5.45), one then obtains

$$I_{\text{topo}}(T = \infty) = -\ln M_0. \quad (5.110)$$

On the other hand, using the result for the entropy in the infinite temperature limit of [76] [Eq. (5.101)] and the total entropy computed in Eq. (5.28), one obtains

$$I(T = \infty) = -l \ln \mathcal{D} - \ln M. \quad (5.111)$$

The result (5.110) is compatible with the one of Eq. (5.111). Indeed, the result of Eq. (5.111) holds for input categories that are either Abelian or modular. In both cases, it is easy to prove that $M_0 = M$ (see Sec. 5.4). However, in general, M_0 and M may be different. For instance, if $\mathcal{C} = \text{Rep}(S_3)$, one has $M = 2$ (since the group S_3 has two one-dimensional irreducible representations), but $M_0 = 1$ (since the only pure fluxon in $\mathcal{Z}[\text{Rep}(S_3)]$ is the vacuum).

As mentioned above, this non-vanishing contribution only stems from the fact that, for the model at hand, we work in a restricted Hilbert space. It has no quantum origin, and it does not reflect any long-range entanglement feature of the system. However, it does reflect some topological property, as only vertex configurations resulting from the fusion rules are allowed.

Zero-temperature limit

In the zero-temperature limit, every plaquette is in the vacuum ($A = 1$) state. Thus, $\langle P_A(L_c) \rangle$ is given by Eq. (5.66) and one readily gets from Eq. (5.107):

$$I_{\text{topo}}(T = 0) = -2 \ln \mathcal{D}, \quad (5.112)$$

which is the well-known zero-temperature result for a topological phase with total quantum dimension \mathcal{D} [29, 30, 70]. Again, this is compatible with previous results in the literature. At zero temperature, $S_{\mathcal{R} \cup \overline{\mathcal{R}}} = 0$ and using Eqs. (5.104) and (5.95), one obtains

$$I_{\mathcal{R}} = S_{\mathcal{R}} + S_{\overline{\mathcal{R}}} - 0 = 2S_{\mathcal{R}}, \quad (5.113)$$

with $S_{\mathcal{R}, \text{topo}} = -\gamma = -\ln \mathcal{D}$.

Finite temperature and scaling behavior

Away from the two extreme cases discussed above, the situation is more subtle. As can already be inferred from Eq. (5.67), using the same arguments as in the previous section, one always gets

$$\lim_{N_p^{\mathcal{R}}, N_p^{\overline{\mathcal{R}}} \rightarrow \infty} I_{\text{topo}}(T > 0) = -\ln M_0, \quad (5.114)$$

which is also the infinite-temperature limit [see Eq. (5.110)]. This indicates that topological quantum order is destroyed in the thermodynamic limit for any $T > 0$ as anticipated by Hastings [67]. This phenomenon is similar to the one observed in the toric code [47] (see Refs. [68, 38, 69, 70]).

For a given contour L_c , one observes a crossover between a low- T region where $I_{\text{topo}} \simeq -2 \ln \mathcal{D}$, and a high- T region where $I_{\text{topo}} \simeq -\ln M_0$ (see Fig. 5.20). When increasing the system size while keeping L_c fixed, I_{topo} converges towards a unique curve, see Fig. 5.19. The crossover temperature can be estimated from Eq. (5.67) as follows.

The dominant behavior of $\langle P_X(L_c) \rangle$ in the thermodynamic limit comes from pure fluxons and is given in Eq. (5.108). The first finite-size correction comes from the non-pure fluxon (call it C) with largest ratio $n_{C,1}/d_C < 1$:

$$\langle P_X(L_c) \rangle - \frac{d_X^2}{\mathcal{D}^2} M_0 \simeq \frac{d_X d_C}{\mathcal{D}} S_{\overline{X}, C} e^{-N_p^{\overline{\mathcal{R}}}/N_p^*}, \quad (5.115)$$

with the characteristic area

$$N_p^* = \max_{A \notin P} N_A^* = \left[\ln \left(\frac{\mathcal{D} - 1 + e^\beta}{\mathcal{D} \frac{n_{C,1}}{d_C} - 1 + e^\beta} \right) \right]^{-1}, \quad (5.116)$$

where N_A^* is given in Eq. (5.85). The quantity N_p^* reaches a constant $1/\ln \frac{d_C}{n_{C,1}}$ in the high- T limit and diverges as

$$N_p^* \simeq \frac{e^\beta}{\mathcal{D}(1 - \frac{n_{C,1}}{d_C})} \quad (5.117)$$

in the low- T limit. The crossover temperature is reached when $N_p^* \simeq N_p^{\overline{\mathcal{R}}}$ and is roughly given by

$$T_c \simeq \frac{1}{\ln[N_p^{\overline{\mathcal{R}}}\mathcal{D}(1 - n_{C,1}/d_C)]} \simeq \frac{1}{\ln N_p^{\overline{\mathcal{R}}}} \quad (5.118)$$

when $N_p^{\overline{\mathcal{R}}}$ is large. Such a behavior is analogous to that of the 1D classical Ising model, which has a vanishing critical temperature. That the toric code model is in the same universality class as the 1D classical Ising model is well-known, see e.g. [75]. Here, we suspect that this is also the case of the string-net model for any input category.

A close inspection shows a nontrivial interplay between the temperature T and the total system size $N_p = N_p^{\mathcal{R}} + N_p^{\overline{\mathcal{R}}}$, similar to the one found in Refs. [68, 69, 70] for the toric code. More precisely, if one sets $N_p^{\overline{\mathcal{R}}} = \nu N_p$, with a fixed ratio, $0 < \nu < 1$, one can show that, in the large- N_p limit, I_{topo} depends on ν and on the scaling variable N_p/N_p^* , where N_p^* is defined in Eq. (5.116).

Such a scaling law indicates that topological quantum order can persist at finite temperature provided the system size is small enough. We display in Fig. 5.20 the topological mutual information I_{topo} as a function of the inverse temperature for various system sizes at ratio $\nu = 1/4$.

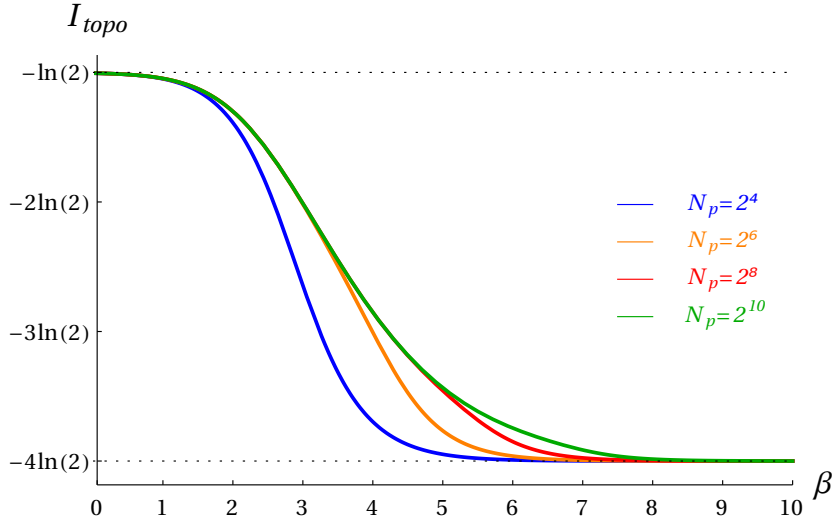


Figure 5.19: Topological mutual information of the SN model for the Ising category ($\mathcal{D} = 4$, $M_0 = 2$) as a function of $\beta = 1/T$ at fixed $N_p^{\overline{\mathcal{R}}} = 2^3$. $I_{\text{topo}}(T = 0) = -2 \ln \mathcal{D}$ and $I_{\text{topo}}(T = \infty) = -\ln M_0$ are indicated by dashed lines.

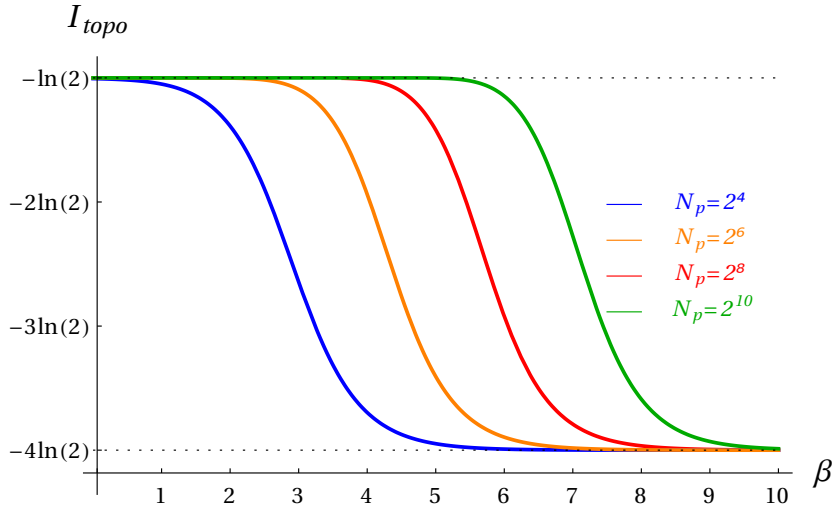


Figure 5.20: Topological mutual information of the SN model for the Ising category ($\mathcal{D} = 4$, $M_0 = 2$) as a function of $\beta = 1/T$ at fixed $\nu = 1/4$. $I_{\text{topo}}(T = 0) = -2 \ln \mathcal{D}$ and $I_{\text{topo}}(T = \infty) = -\ln M_0$ are indicated by dashed lines.

One clearly observes that when the system size N_p increases, the topological order characterized by $I_{\text{topo}} = -4 \ln 2$ is destroyed at a temperature which decreases and vanishes in the thermodynamic limit. However, when plotted as a function of the scaling variable N_p/N_p^* (see Fig. 5.21), I_{topo} converges towards a “universal” function which interpolates between $-4 \ln 2$ at $T = 0$ [see Eq. (5.112)] and $-\ln 2$ at $T = \infty$ [see Eq. (5.110)]. In summary, the crossover line $N_p = N_p^*$ separates two domains in the $(T, N_p^{\overline{\mathcal{R}}})$ plane: a low- T and small- $N_p^{\overline{\mathcal{R}}}$ domain with $I_{\text{topo}} \simeq -2 \ln \mathcal{D}$ (indicative of topological order), and a high- T and large- $N_p^{\overline{\mathcal{R}}}$ domain with $I_{\text{topo}} \simeq -\ln M_0$ (absence of topological order, but deconfined pure fluxons) (see also Fig. 5.22).

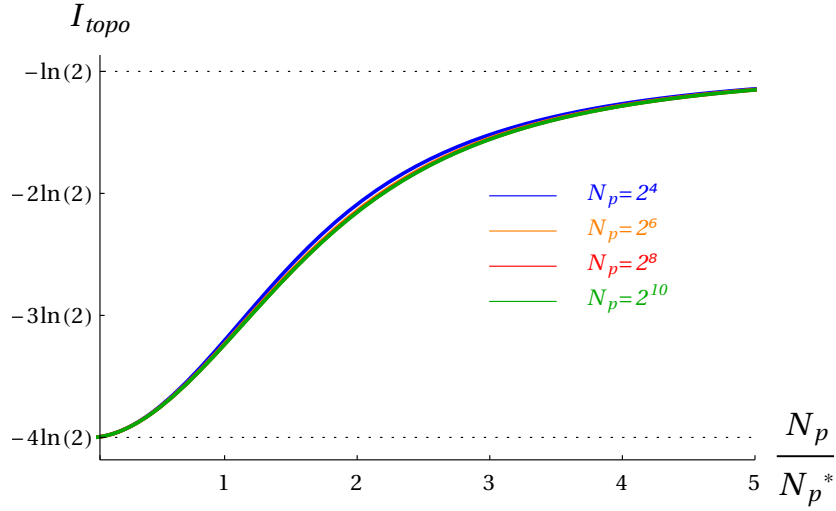


Figure 5.21: Topological mutual information of the Ising string-net model as a function of the scaling variable N_p/N_p^* at fixed $\nu = 1/4$, where N_p^* is defined in Eq. (5.116).

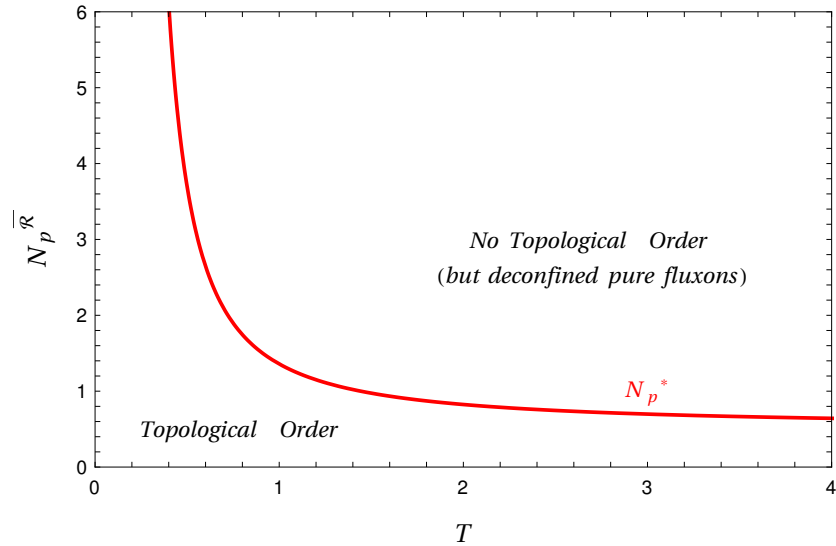


Figure 5.22: Phase diagram for topological order in string-net models. the crossover line $N_p^* = N_p^{\overline{\mathcal{R}}}$ separates two domains in the $(T, N_p^{\overline{\mathcal{R}}})$ plane: a low- T and small- $N_p^{\overline{\mathcal{R}}}$ domain with $I_{\text{topo}} \simeq -2 \ln \mathcal{D}$ (indicative of topological order), and a high- T and large- $N_p^{\overline{\mathcal{R}}}$ domain with $I_{\text{topo}} \simeq -\ln M_0$ (absence of topological order, but deconfined pure fluxons).

5.7.5 Numerical results on entanglement entropy

Ground-state entanglement entropy

While Ref. [30] does not give limitations on the size of the system for the validity of the ground-state entanglement entropy Eq. (5.95), we observe that this result is not easily reproducible numerically on small graphs [we performed numerical calculations on small trivalent graphs on a sphere, with up to 18 vertices, for the categories Fibonacci, Ising, \mathbb{Z}_2 and $\text{Vec}(S_3)$]. In fact, in a numerical approach of the entropy calculation, one would like to attribute each link of the lattice to either region \mathcal{R} or $\overline{\mathcal{R}}$. This means that the boundary is chosen rather to pass through the

vertices, than through the links of the lattice, as in the analytical approaches of Refs. [30, 76]. As a result, there are two different possible choices for the boundary of a simply connected region \mathcal{R} with the rest of the system: either smooth or rough (see Fig. 5.23). In general, these two choices lead to different results for the entanglement entropy $S_{\mathcal{R}}$. As an exception, the entanglement entropy of a string-net model built from an Abelian UFC [e.g., $\text{Vec}(G)$] is not sensitive to the type of boundary chosen. The reason for this is that, for a rough boundary, the labels of the external links of region \mathcal{R} are entirely determined by the labels of the links in region $\overline{\mathcal{R}}$. Thus, a rough boundary leads to the same result as a smooth boundary, where these links are inside of region $\overline{\mathcal{R}}$. The analytic approach of Levin and Wen [30] discussed above works in an enlarged Hilbert space (for a boundary of length l , there are l additional degrees of freedom), so that both \mathcal{R} and $\overline{\mathcal{R}}$ have a rough boundary (see Fig. 5.18). The trace is taken in the enlarged Hilbert space, and subsequently the boundary degrees of freedom of \mathcal{R} and $\overline{\mathcal{R}}$ are matched in order to come back to the original Hilbert space. We find that, for an Abelian string-net model, the analytic result for the entanglement entropy (5.95) coincides with the numerical results both for a smooth and for a rough boundary. However, for non-Abelian string-nets, we observe that the analytic method provides a result which is different both from the numerical result for a rough boundary and from the numerical result for a smooth boundary, at least when region \mathcal{R} is small. Some of our results are reproduced on Table 5.1. For very small regions (e.g., only one or two plaquettes), numerical results do not coincide with the formula of Eq. (5.95) for non-Abelian UMTCs such as Fibonacci or Ising. The numerical result gets closer to the one predicted in Eq. (5.95) when the number of links increases in region \mathcal{R} . In particular, in all studied cases, the numerical result coincides with Eq. (5.95) if all boundary edges are separated by at least one vertex. We therefore suppose that for non-Abelian categories, the area law contribution in Eq. (5.95) is valid only above a certain size of region \mathcal{R} . The exact conditions of validity remain to be determined.

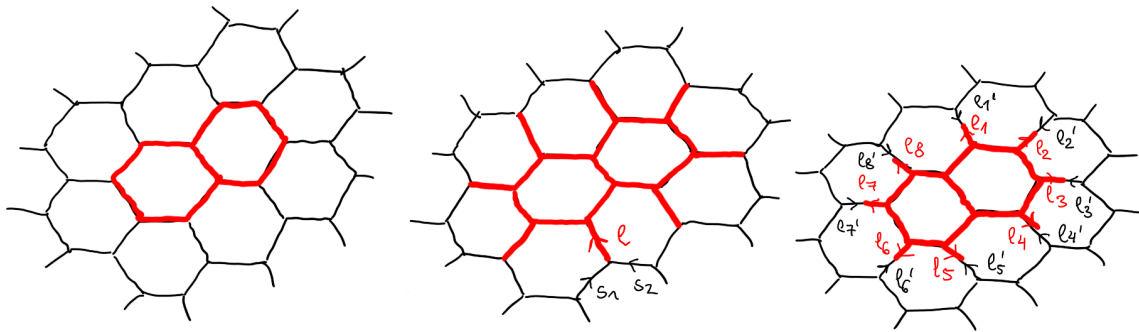


Figure 5.23: Three different choices of region \mathcal{R} (links in red) containing two plaquettes on a honeycomb lattice. Black links belong to the complementary region $\overline{\mathcal{R}}$. On the left, a smooth boundary for \mathcal{R} (and rough boundary for $\overline{\mathcal{R}}$). In the center, a rough boundary for \mathcal{R} (and a smooth boundary for $\overline{\mathcal{R}}$). If the string-net is Abelian, then the label on the boundary link l is completely determined by the labels of the links s_1 and s_2 in $\overline{\mathcal{R}}$, as there is only one fusion outcome $s_1 \times s_2 = l$. On the right, the choice of regions for [30]. The boundary goes through the links, and on each link, the degrees of freedom are doubled, with $l_i \in \mathcal{R}$ and $l'_i \in \overline{\mathcal{R}}$. By setting $l_i = l'_i$ for all link configurations, one recovers the original Hilbert space.

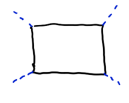
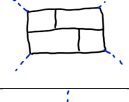



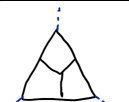
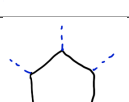
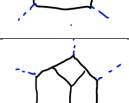
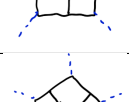
\mathcal{R}	\mathcal{C}	numerical $S_{\mathcal{R}}$	$S_{\mathcal{R}}$ with Eq. (5.95)	l
	<i>Fib</i>	2.03613	2.46496	4
	<i>Fib</i>	2.46496	2.46496	4
	<i>Fib</i>	1.30676	1.52724	3
	<i>Fib</i>	1.52724	1.52724	3
	<i>Ising</i>	2.17475	2.25273	3
	<i>Ising</i>	2.25273	2.25273	3
	<i>Fib</i>	2.73826	3.40268	5
	<i>Fib</i>	3.3204	3.40268	5
	<i>Fib</i>	3.40268	3.40268	5

Table 5.1: Comparison between numerical results for the ground-state entanglement entropy and results obtained with Eq. (5.95). All results are obtained for a sphere. The left picture shows the configuration of the region \mathcal{R} , which is always chosen to have a smooth boundary (black links are in \mathcal{R} , the l dotted blue links are the boundary links, in $\overline{\mathcal{R}}$).

Topological mutual information

As suggested in [70, 69], the topological part of the mutual information, I_{topo} , can be extracted by considering a linear combination of the mutual informations of different regions \mathcal{R} , so that the area-law contributions cancel out mutually. Ref. [70, 69] show that such a linear combination can be found by dividing the system into four regions A, B, C, D (see Fig. 5.24). Then, the topological mutual information can be computed as

$$I_{\text{topo}} = I_A + I_B + I_C - I_{AB} - I_{AC} - I_{BC} + I_{ABC}. \quad (5.119)$$

Numerically, the mutual information of a region \mathcal{R} can be obtained by computing the entanglement entropies $S_{\mathcal{R}}$, $S_{\overline{\mathcal{R}}}$ and $S_{\mathcal{R} \cup \overline{\mathcal{R}}}$ and using the definition of Eq. (5.104).

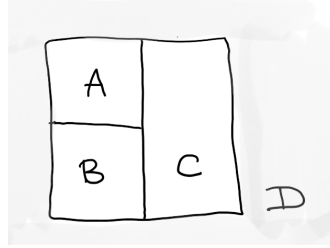


Figure 5.24: Division of a lattice system into four regions.

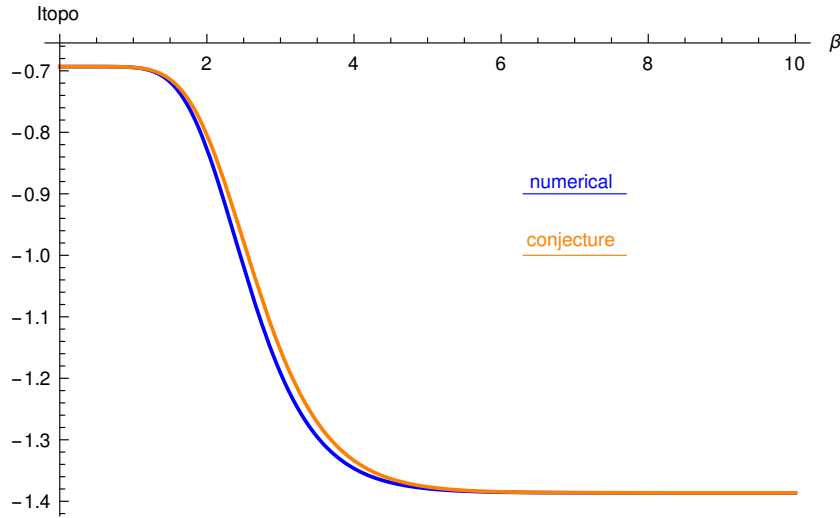


Figure 5.25: I_{topo} for \mathbb{Z}_2 string-nets as a function of inverse temperature β on a sphere of 11 plaquettes. Here the region $\mathcal{R} = ABC$ contains 7 plaquettes. In blue, I_{topo} as obtained numerically from $I_A + I_B + I_C - I_{AB} - I_{AC} - I_{BC} + I_{ABC}$. In orange, I_{topo} as defined in Eq. (5.107).

On Fig. 5.25 we plot I_{topo} extracted numerically [using Eq. (5.119)] on a sphere with 11 plaquettes for \mathbb{Z}_2 and a region ABC of 7 plaquettes, and $I_{\text{topo}}(\mathcal{R})$ as obtained from the conjecture for the same system and $\mathcal{R} = ABC$. We observe that the conjecture and the numerical result coincide in the limits of $T \rightarrow 0$ and $T \rightarrow \infty$. The agreement is less good at intermediate temperature scales. However, this may be a finite-size effect, as the conjecture supposes a long boundary length for region \mathcal{R} [see Eq. (5.107)].

5.8 Conclusion

In this chapter, we explored the finite-temperature properties of the refined string-net model, an extension of the original string-net model. Using the exact expression of the degeneracies obtained in Chap. 4, we provided an exact expression of the partition function [see Eq. (5.5)] valid for any UFC, any trivalent graph, and any compact orientable surface. This partition function allowed us to analyze the finite-temperature behavior of several quantities. In particular, using simple surgery arguments, we computed the thermal average of the projector onto a given particle sector for three different types of closed loop: non-contractible loops around a handle and around a throat of a surface of genus $g \geq 1$, and contractible loops [see Eqs. (5.52), (5.61), and (5.64), respectively].

These projectors are directly related to WWL operators [see Eq. (5.73)] which provide information about the confinement of the excitations. Interestingly, they are also the key ingredients to compute the topological mutual information according to a conjecture [see Eq. (5.107)] proposed by Iblisdir *et al.* [69, 70].

We found that, as seen from different probes such as the specific heat, confinement of anyons, or entanglement, topological order does not survive at $T > 0$ in the thermodynamic limit. This is in line with previous results [67]. Nevertheless, the phase is never completely trivial due to the vertex constraint that we imposed at the level of the Hilbert space. This also is in agreement with previous results on the toric code [68]. In the "trivial" phase, certain objects of the Drinfeld center, the pure fluxons \mathcal{P} which braid trivially with all fluxons and fusion products of fluxons, remain always deconfined. This is also reflected in the topological mutual information, which depends on the number of pure fluxons and is not necessarily zero. The pure fluxons also drive the behavior of the model in the thermodynamic limit.

Below the thermodynamic limit, we find that there is a scaling behavior between the temperature and the system size, generalizing what was found by Iblisdir *et al.* [68, 38, 69, 70]. This scaling is essentially the same as that of the 1D classical Ising model. It shows that topological order can survive at low temperature below a size-dependent critical temperature. This is summarized in the phase diagram Fig. 5.22.

In the next chapter, we will do a step towards studying models featuring all types of excitations in the Drinfeld center and not only fluxons, by studying the Kitaev Quantum Double model [47]. Such a study will allow us to analyze the interplay between the various excitations of topologically ordered phases.

Part III

Kitaev quantum double models

Introduction to Kitaev quantum double models

In this chapter, we provide a brief introduction to the quantum model developed by Kitaev [47], following mainly the discussions of Refs. [144, 145, 146]. The Kitaev quantum double model is a Hamiltonian realization of a lattice gauge theory [41, 43, 133]. Taking as an input a discrete gauge group G , it realizes a topological phase (or topological quantum field theory) that corresponds to the quantum double $D(G)$ of G . The simplest KQD model is the toric code, built from the group \mathbb{Z}_2 . Several connections exist between the KQD and the string-net models. In particular, the TQFT described by $D(G)$ is equivalent to the TQFT described by the Drinfeld centers $\mathcal{Z}(\text{Vec}G)$ and $\mathcal{Z}(\text{Rep}G)$.

6.1 Hamiltonian

As the string-net model, the KQD model is defined on a lattice embedded in a two-dimensional oriented manifold. It attributes to every oriented edge of this lattice a value out of the objects of a discrete finite group G . In the simplest case of the toric code, where $G = \mathbb{Z}_2$, these objects can be interpreted as spin degrees of freedom (up and down). The full Hilbert space is spanned by all possible lattice labelings. That is, there are $|G|$ possible choices for every edge (with $|G|$ the number of elements in the group), and thus the full Hilbert space dimension is:

$$\dim \mathcal{H}_{\text{KQD}} = |G|^{N_l}, \quad (6.1)$$

where N_l is the number of links on the lattice. For notational convenience, we index the vertices of the lattice with roman letters a, b, c, \dots , so that any edge label can be written $g_{ab} \in G$, with the subscript ab indicating that the edge is pointing from vertex a towards vertex b . Reversing the orientation of an edge changes the label from g_{ab} to $g_{ba} = g_{ab}^{-1}$. Fig. 6.1 shows a possible lattice configuration for a quantum double model. In the following discussion, we restrict to a triangular lattice.

The Hamiltonian of the KQD model is composed of a sum of operators acting either on the

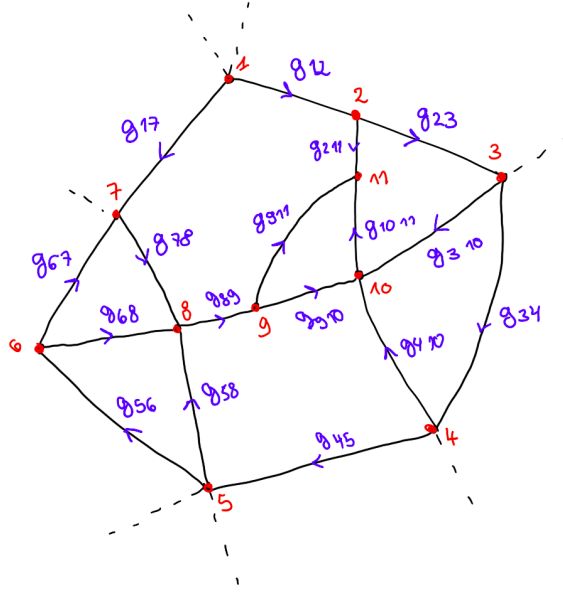


Figure 6.1: Example of a lattice configuration of the Kitaev quantum double model. Here vertices are drawn as red dots and numbered $a \in \{1, 2, 3, \dots\}$. Labels are $g_{ab} \in G$ meaning that the corresponding link is oriented from vertex a to vertex b .

vertices v or on the plaquettes p of the lattice:

$$\mathcal{H}_{\text{KQD}} = -J_v \sum_v A_v - J_p \sum_p B_p, \quad (6.2)$$

with J_v and J_p the coupling constants for vertex and plaquette terms respectively.

At every vertex v , one can define a group of local operators A_v^h , with $h \in G$. These operators preserve the group operation

$$A_v^h A_v^{h'} = A_v^{hh'}, \quad (6.3)$$

and thus form a representation of G [145, 146]. The action of such an operator A_v^h is to premultiply all (outwards oriented) edges g_{av} around vertex v by the group element h :

$$A_v^h \begin{array}{c} g_{av} \uparrow \\ \swarrow \downarrow \\ g_{bv} \rightarrow \quad v \quad \leftarrow g_{cv} \\ \downarrow \downarrow \\ g_{dv} \end{array} = \begin{array}{c} g_{av} h^{-1} \uparrow \\ \swarrow \downarrow \\ g_{bv} h^{-1} \rightarrow \quad v \quad \leftarrow h g_{cv} \\ \downarrow \downarrow \\ h g_{dv} \end{array} \quad (6.4)$$

These operators implement local gauge transformations on the lattice. In fact, if two operators $A_{v_1}^h$ and $A_{v_2}^h$ act on two vertices connected by an edge labeled $g_{v_2 v_1}$, this edge label transforms to $h g_{v_2 v_1} h^{-1}$.

The vertex operator A_v is defined as

$$A_v = \frac{1}{|G|} \sum_{h \in G} A_v^h. \quad (6.5)$$

Using Eq. 6.3 one can show that A_v is invariant under the action of all A_v^h , and that $A_v^2 = A_v$. Therefore, A_v projects on gauge invariant states at the vertex v . This means that it is the projector on the trivial representation of G at v [146].

For the plaquettes, one can define projectors B_p^h which ensure that the product of all labels around a plaquette gives the group element h . By convention, the product is always taken counterclockwise around a plaquette with all labels oriented in the same direction. In particular, the plaquette operator $B_p \equiv B_p^e$ appearing in the KQD Hamiltonian projects on states where the product of labels around a plaquette is equal to the identity e of the group G :

$$B_p^e \begin{array}{c} \text{1} \\ \swarrow \quad \searrow \\ g_{12} \quad g_{31} \\ \downarrow \quad \uparrow \\ \text{2} \quad \text{3} \\ \leftarrow \quad \rightarrow \\ g_{23} \end{array} = \delta_{g_{12}g_{23}g_{31},e} \begin{array}{c} \text{1} \\ \swarrow \quad \searrow \\ g_{12} \quad g_{31} \\ \downarrow \quad \uparrow \\ \text{2} \quad \text{3} \\ \leftarrow \quad \rightarrow \\ g_{23} \end{array} \quad (6.6)$$

This corresponds to a trivial flux in the plaquette.

All plaquette and vertex operators commute with each other. This is clear when operators act on far-away plaquettes or vertices, but is less obvious when A_v and B_p act on a vertex and a neighboring plaquette. It can be seen, for example, by taking a square plaquette on which the edge labels give $g_{12}g_{23}g_{34}g_{41} = e$. Acting with a A_2^h on vertex $v = 2$ transforms label $g_{12} \rightarrow g_{12}h^{-1}$ and label $g_{23} \rightarrow hg_{23}$, so that the product of labels around the plaquette still yields e .

A ground state of the KQD Hamiltonian is invariant under the action of A_v and B_p , i.e. it corresponds to a state $|\psi\rangle$ where $A_v|\psi\rangle = B_p|\psi\rangle = |\psi\rangle \quad \forall p, v$. A vertex excitation corresponds to $A_v = 0$ at a given v , and a plaquette excitation to $B_p = 0$ at a given plaquette p .

The ground-state energy is thus $E_0 = -J_v N_v - J_p N_p$ and the excited energy levels are easily obtained: a state with c excited vertices and f excited plaquettes has energy

$$E_{c,f} = E_0 + J_v c + J_p f, \quad (6.7)$$

and a state with all vertices and all plaquettes excited has energy $E_{N_v, N_p} = 0$.

Example: the toric code model

As an illustration of the above presentation, let us discuss the most prominent KQD model, the toric code. We consider a square lattice placed on a torus (see Fig. 6.2). The edges of this lattice can take two possible values, which correspond to the group elements of \mathbb{Z}_2 , and which we will

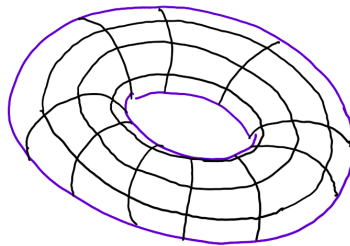


Figure 6.2: Illustration of a square lattice on a torus.

denote 1 (the identity) and s (the non-trivial element of \mathbb{Z}_2). The dimension of the Hilbert space for a lattice with N_l links is thus 2^{N_l} .

The multiplication rules of \mathbb{Z}_2 are $1 \times 1 = 1$, $1 \times s = s \times 1 = s$ and $s \times s = 1$. Below, we show examples of the vertex and plaquettes operators acting on some states. Here, we have adopted the convention of drawing labels carrying the label 1 in black and edges with label s in red. We do not draw arrows as both group elements are their own inverse. The plaquette and vertex operators of the toric code model are frequently expressed in terms of Pauli matrices. The Hamiltonian Eq. (6.2) can then be written

$$H_{\text{TC}} = -\frac{J_v}{2} \sum_v (\mathbb{1} + \prod_{i \in v} \sigma_i^x) - \frac{J_p}{2} \sum_p (\mathbb{1} + \prod_{i \in p} \sigma_i^z), \quad (6.8)$$

where $i \in v$ means all the links i joining at the vertex i , and $i \in p$ means all the links i that define the contour of a plaquette p . $\sigma^x = \begin{pmatrix} 0 & 1 \\ 1 & 0 \end{pmatrix}$ and $\sigma^z = \begin{pmatrix} 1 & 0 \\ 0 & -1 \end{pmatrix}$ are Pauli matrices, and we have chosen a basis $|1\rangle = \begin{pmatrix} 1 \\ 0 \end{pmatrix}$ and $|s\rangle = \begin{pmatrix} 0 \\ 1 \end{pmatrix}$.

$$\begin{aligned}
 A_v \left| \begin{array}{c} s \\ \hline 1 \\ \hline 1 \end{array} \right\rangle &= \frac{1}{2} \left[\left| \begin{array}{c} s \\ \hline s \\ \hline 1 \end{array} \right\rangle + \left| \begin{array}{c} 1 \\ \hline 1 \\ \hline s \end{array} \right\rangle \right] \\
 B_p \left| \begin{array}{c} s \\ \square \\ s \end{array} \right\rangle &= \left| \begin{array}{c} s \\ \square \\ s \end{array} \right\rangle ; \quad B_p \left| \begin{array}{c} s \\ \square \\ s \end{array} \right\rangle = 0
 \end{aligned}$$

The toric code model provides a simple way to illustrate one of the topological properties of the KQD model. As A_v and B_p are projectors, they only have two eigenvalues (0 and 1). Therefore, one might want to compute the Hilbert space dimension by writing $2^{N_v} 2^{N_p}$, with N_v the number of vertices and N_p the number of plaquettes. However, all plaquettes and vertex operators are not independent. In fact, one has

$$\prod_{v=1}^{N_v} (2A_v - \mathbb{1}) = \mathbb{1} \quad \text{and} \quad \prod_{p=1}^{N_p} (2B_p - \mathbb{1}) = \mathbb{1}. \quad (6.9)$$

These constraints arise because each link of the lattice appears in two vertex and two plaquettes operators, so that each Pauli operator σ_i^x or σ_i^z appears in pairs in the product and yields $\mathbb{1}$. Therefore, the degrees of freedom of the system are fully fixed once the values of $N_v - 1$ vertex operators ($N_p - 1$ plaquette operators) are known. However, this is still not enough to correctly count the Hilbert space dimension. By comparing with the Hilbert space dimension obtained from counting the edge degrees of freedom 2^{N_l} and using the Euler characteristic for the torus $N_l = N_v + N_p$, one finds that the dimension of the Hilbert space is actually given by

$$\dim \mathcal{H}_{\text{TC}} = 2^{N_l} = 2^{N_p - 1} 2^{N_v - 1} \times 4. \quad (6.10)$$

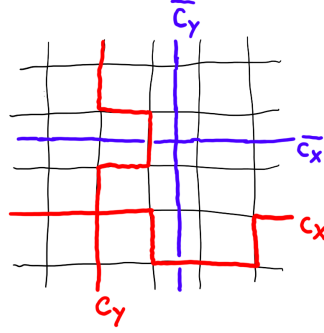


Figure 6.3: Square lattice with periodic boundary conditions in both x and y direction. The red paths correspond to the operators $W_{x,y}$ defined on the direct lattice. The blue paths correspond to the operators $V_{x,y}$ defined on the dual lattice.

The factor 4 appearing in this counting reflects the presence of some hidden degrees of freedom that have no corresponding term in the Hamiltonian. In fact, there are four additional operators that commute with the Hamiltonian. These operators are defined along closed paths winding around one of the two cycles of the torus, either on the lattice or on the dual lattice (see Fig. 6.3). In terms of Pauli matrices, they are defined as [42]:

$$W_x = \prod_{i \in C_x} \sigma_i^z, \quad W_y = \prod_{i \in C_y} \sigma_i^z, \quad [W_x, H_{\text{TC}}] = [W_y, H_{\text{TC}}] = 0, \quad (6.11)$$

and

$$V_x = \prod_{i \in \bar{C}_x} \sigma_i^x, \quad V_y = \prod_{i \in \bar{C}_y} \sigma_i^x, \quad [V_x, H_{\text{TC}}] = [V_y, H_{\text{TC}}] = 0. \quad (6.12)$$

Each of these operators has two eigenvalues ± 1 . However, the four operators are not completely independent of each other as some of them anticommute:

$$V_x W_y = -W_y V_x, \quad V_y W_x = -W_x V_y. \quad (6.13)$$

A complete set of commuting observables is therefore given by $N_p - 1$ plaquette operators B_p , $N_v - 1$ vertex operators A_v , and, for example, W_y and V_y . There are thus four groundstates, corresponding to the eigenvalue pairs $(w_x, v_x) = (1, 1)$, $(w_x, v_x) = (-1, 1)$, $(w_x, v_x) = (1, -1)$ and $(w_x, v_x) = (-1, -1)$. Note that this argument can be extended to higher genus surfaces, and that the ground-state degeneracy of a genus g surface is 2^{2g} . The operator W_y defined on the direct lattice, can be interpreted as a closed quasiparticle operator for a vertex excitation, also called *chargeon* (if this operator had two open ends, they would be located on vertices). The operator V_y , on the other hand, corresponds to a closed quasiparticle operator for a plaquette excitation, also called *fluxon* (open ends would be situated in plaquettes). These operators are associated to 1-form generalized symmetries [39]. In fact, V_y and W_y are symmetries of the Hamiltonian, but their support is a non-contractible loop.

6.2 Topological phase

Despite its simple-looking Hamiltonian and energy spectrum, the KQD model actually realizes a non-trivial topologically-ordered phase described by the Drinfeld center $\mathcal{Z}(G)$ of the input group

G . While the simple objects of $\mathcal{Z}(G)$ behave as anyons just as described in Chap.2, and one might very well construct the center using the tube algebra described in Sec. 2.5.3, we introduce here an alternative way to classify excitations of $\mathcal{Z}(G)$ based on group theory.

As the vertex operator of the KQD Hamiltonian projects onto the trivial representation of G , vertex excitations should correspond to non-trivial representations, i.e., vertex excitations (also called *chargeons*) are indexed by the irreducible representations of G . Similarly, while the plaquette operator projects on states which correspond to a trivial flux in the plaquette, one could expect that plaquette excitations (or *fluxons*) are indexed by the non-trivial group elements of G .

However, this labeling is not gauge invariant. Imagine taking a charge labeled by some irreducible representation Γ of G and taking it around a flux labeled g . If the group is non-Abelian, the representation might be of dimension larger than 1. The process of taking the charge around the flux will then lead to a sort of Aharonov-Bohm effect [7, 145]. In fact, let's choose some basis for the d_Γ dimensional representation Γ : $|\Gamma, i\rangle$ with $i = 1, 2, \dots, d_\Gamma$. By circling around the flux g , this basis gets rotated:

$$|\Gamma, j\rangle \rightarrow \sum_{i=1}^{d_\Gamma} |\Gamma, i\rangle \langle \Gamma, i| D^\Gamma(g) |\Gamma, j\rangle, \quad (6.14)$$

where $D^\Gamma(g)$ is a matrix that represents g . However, one could also choose a different basis for Γ (e.g., a basis already rotated by going around a flux h):

$$|\Gamma, i\rangle' = \sum_{k=1}^{d_\Gamma} |\Gamma, k\rangle \langle \Gamma, k| D^\Gamma(h) |\Gamma, i\rangle. \quad (6.15)$$

In this basis, the non-Abelian Aharonov-Bohm effect would then take the form

$$|\Gamma, j\rangle' \rightarrow \sum_{i=1}^{d_\Gamma} |\Gamma, i\rangle' \langle \Gamma, i| D^\Gamma(h^{-1}gh) |\Gamma, j\rangle. \quad (6.16)$$

An observer who would like to measure the flux by using the Aharonov-Bohm effect (as can be done in principle using interferometry [82, 145]) could only determine the flux g up to conjugation with any other group element h . Therefore, the actual gauge-invariant way to label fluxons is by conjugacy classes of G

$$C_g = \{hgh^{-1} | h \in G\}. \quad (6.17)$$

The number of elements inside the conjugacy class, $|C_g|$, corresponds to internal, non-topological, degrees of freedom. A different presentation of the same phenomenon, also called *flux metamorphosis*, can be found e.g. in [44, 147, 148].

In the most general case, one could have a quasiparticle that carries simultaneously some charge and some flux. Such a composite quasiparticle is then called a *dyon*, and it corresponds to the excitation of a *site*, i.e. of a vertex and an adjacent plaquette. In principle, one would then like to label a dyon by a conjugacy class and an irreducible representation of G . Here again, however, subtleties arise when one thinks about how one would measure such a dyon. One could imagine performing an experiment in which a charge is hidden behind a screen with two slits, shoot some fluxons $g \in G$ at it, and determine the label of the charge by studying the interference pattern

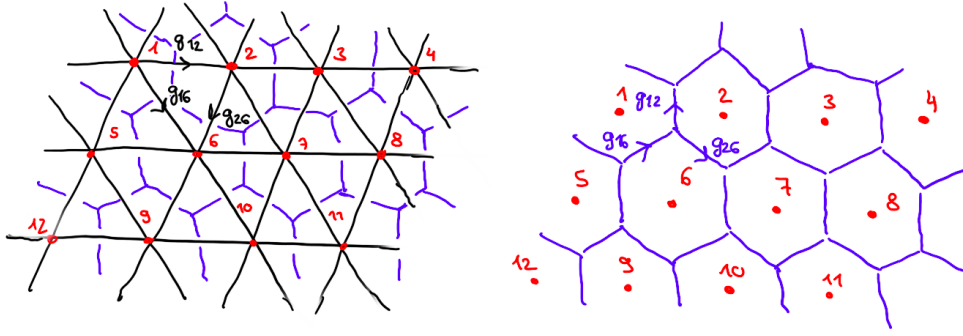


Figure 6.4: Labeling of a triangular lattice (black) and its dual honeycomb lattice (blue). In the triangular lattice, vertices (shown in red) are numbered with integer numbers. A label $g_{ab} \in G$ corresponds to a link oriented from vertex a to vertex b . On the dual lattice, vertices become plaquettes. A link g_{ab} means that the plaquette a is on the left and plaquette b is on the right.

of the fluxons [145]. However, if the charge also carries some flux h , this will affect the labels of the fluxons (carrying one fluxon g around a fluxon h changes its label to ghg^{-1}) and destroy the interference, unless g and h commute. The correct label for a charge carrying a flux g is therefore not given by an irreducible representation of the full group, but of the normalizer of g , which is defined as:

$$\mathcal{N}_g = \{h \in G | hg = gh\}. \quad (6.18)$$

The normalizers of elements within a conjugacy class C_g are isomorphic to each other, so we can associate normalizers with conjugacy classes rather than group elements.

Finally, an anyon type J can most generally be written as:

$$J \equiv (C_g, \Gamma_g), \quad (6.19)$$

where Γ is an irreducible representation of the normalizer of C_g .

A few special cases can be distinguished here. First, there always is an anyon which corresponds to the conjugacy class of the identity $C_1 = \{1\}$, and to the trivial representation Γ_1^G . This particle is the vacuum, i.e., the absence of both plaquette and vertex excitations.

Second, fluxons are those particles which have a trivial irreducible representation Γ_1 . Chargeons are all in the conjugacy class of the identity.

Finally, the quantum dimensions of the anyons can be easily determined from the formalism of Eq. (6.19):

$$d_J = d_{\Gamma_g} |C_g|. \quad (6.20)$$

For chargeons, $d_J = d_{\Gamma_g}$ and for fluxons, $d_J = |C_g|$. The total quantum dimension of the quantum double is always $\mathcal{D} = |G|$. This can be shown easily by considering that the quantum dimensions of the elements of G are all 1 and $\mathcal{D} = \mathcal{D}_G^2 = \sum_{s=1}^{|G|} d_s^2$.

6.3 Relation to string-net models

As shown in Refs. [49, 101], in the limit where $J_v \rightarrow \infty$ (i.e., only plaquette excitations) the KQD model G on the honeycomb lattice maps via a generalized Fourier transform to the string-net model built from $\text{Rep}(G)$ (and with constrained Hilbert space) on the same lattice. This means, in particular, that one expects for both models not only the same ground state degeneracy, but also the same excitation spectrum. Plaquette excitations in the string-net model then correspond to the fluxons of the KQD model on the same lattice.

There is a second way in which the KQD model and the string-net model are related. In fact, the KQD model built from G is, in the absence of plaquette excitations, equivalent to the string-net model $\text{Vec}(G)$ on the dual lattice [28]. Consider for example a KQD model (of G) on the triangular lattice. The dual lattice is the honeycomb lattice, as shown in Fig. 6.4. A plaquette operator on the triangular lattice of the KQD model (c.f. Eq. (6.6)) is equivalent to a vertex operator on the dual lattice in the string-net model:

$$A_v^{\text{SN}} \begin{array}{c} g_{12} \\ \swarrow \quad \searrow \\ \cdot 1 \\ \downarrow \quad \uparrow \\ \cdot 2 \quad \cdot 3 \\ \swarrow \quad \searrow \\ g_{23} \quad g_{31} \end{array} = \delta_{g_{12}g_{23}g_{31},e} \begin{array}{c} g_{12} \\ \swarrow \quad \searrow \\ \cdot 1 \\ \downarrow \quad \uparrow \\ \cdot 2 \quad \cdot 3 \\ \swarrow \quad \searrow \\ g_{23} \quad g_{31} \end{array} \quad (6.21)$$

On the direct lattice, a label $g_{ab} \in G$ corresponds to a link oriented from vertex a to vertex b . By convention, we have chosen the dual lattice so that a link is labeled g_{ab} when the plaquette a is on its left and plaquette b is on its right.

In the constrained Hilbert space in which we considered the string-net model, vertex constraints are strictly imposed. For the KQD model on the direct lattice, this translates into imposing the absence of plaquette excitations, i.e. taking $J_p \rightarrow \infty$ and considering only low-energy physics. The vertex operator of the KQD model translates into a plaquette operator on the dual lattice. On the honeycomb lattice, this plaquette operator acts on the six links on the contour of the plaquettes. In principle, a string-net plaquette operator on the honeycomb plaquette takes twelve links as an input: the links on the contour of the plaquette and the six outer links. The action of the plaquette operator does not modify the value of the outer edges, but depends on them in general. In particular, it yields zero if a vertex around the plaquette does not respect the fusion rules. In the constrained Hilbert space where fusion rules are imposed, this latter difference between the KQD vertex operator (c.f. Eq. (6.4)) on the dual lattice and the string-net plaquette operator does not arise. Moreover, as fusion rules are Abelian, the matrix elements of the string-net plaquette operator do not depend in practice on the labels of the outer edges

$$B_p^{\text{SN}} \begin{array}{c} g_{vb} \\ \swarrow \quad \searrow \\ \cdot v \\ \downarrow \quad \uparrow \\ g_{va} \quad g_{vd} \\ \swarrow \quad \searrow \\ g_{vc} \quad g_{ve} \end{array} = \frac{1}{|G|} \sum_h \begin{array}{c} g_{vb} \\ \swarrow \quad \searrow \\ \cdot h \\ \downarrow \quad \uparrow \\ g_{va} \quad g_{vd} \\ \swarrow \quad \searrow \\ g_{vc} \quad g_{ve} \end{array} = \frac{1}{|G|} \sum_h \begin{array}{c} hg_{va} \\ \swarrow \quad \searrow \\ \cdot v \\ \downarrow \quad \uparrow \\ g_{vb}h^{-1} \quad g_{vd}h^{-1} \\ \swarrow \quad \searrow \\ hg_{vc} \quad hg_{ve} \end{array} \quad (6.22)$$

It follows from this relation between the KQD model and the string-net model is that the meaning of fluxons and chargeons is interchanged between the two models. Fluxons, i.e., plaquette

excitations in the string-net model $\text{Vec}(G)$ correspond to chargeons, i.e., vertex excitations, in the KQD model G .

As an important consequence of the relationship between KQD and string-net models, in the ground state, all three models [KQD built from G , string-net model built from $\text{Rep}(G)$, string-net model built from $\text{Vec}(G)$], realize the same topological quantum field theory associated to the quantum double $\mathcal{D}(G)$. Therefore, topological properties of the ground state such as the ground-state degeneracy and the topological entanglement entropy are the same for all three models. This is also an example of Morita equivalence [49, 93].

6.4 Examples

6.4.1 Toric code

We already mentioned the toric code [47] Hamiltonian in Sec. 6.1. Here, we discuss the topological phase resulting from this Hamiltonian. The group underlying the toric code construction is \mathbb{Z}_2 (see also Sec. 2.3). It has two elements 1 and s , with 1 the trivial object, and $s \times s = 1$. As an Abelian group, every element is its own conjugacy class, and all irreducible representations (irreps) are one-dimensional. Thus there are two conjugacy classes $C_1 = \{1\}$ and $C_s = \{s\}$. The corresponding normalizers are $\mathcal{N}_1 = \mathcal{N}_s = \mathbb{Z}_2$. The two irreducible representations of \mathbb{Z}_2 are the trivial representation Γ_1 and the sign representation Γ_{-1} . By pairing up conjugacy classes and irreps, it is straightforward to see that the toric code has four topological sectors, which are listed in Table 6.1: the vacuum $\mathbb{1}$, a chargeon e (where the e stands for "electric charge", in analogy with lattice gauge theory), a fluxon m (where the m stands for "magnetic charge"), and a dyon f , which is the combination of an e and an m . All quantum dimensions are equal to 1, and the total quantum dimension is $\mathcal{D} = 2$.

J	(C, Γ)	$ C $	$ \Gamma $	d_J	type	$n_{J,1}^{\text{rep}}$	$n_{J,1}^{\text{vec}}$
$\mathbb{1}$	(C_1, Γ_1)	1	1	1	vacuum	1	1
e	(C_1, Γ_{-1})	1	1	1	chargeon	0	1
m	(C_s, Γ_1)	1	1	1	fluxon	1	0
f	(C_s, Γ_{-1})	1	1	1	dyon	0	0

Table 6.1: Here, $J \equiv (C, \Gamma)$ are the elements of $\mathcal{D}(\mathbb{Z}_2)$, C are the conjugacy classes, and Γ the irreducible representations of the normalizers, and d_J the quantum dimensions. The vacuum is both a chargeon and a fluxon. In the last two columns, we recall the multiplicities in the $\mathbb{1}$ sector stemming from the tube algebra of both $\text{Vec}(\mathbb{Z}_2)$ and $\text{Rep}(\mathbb{Z}_2)$.

6.4.2 S_3 quantum double

In order to obtain non-Abelian anyons (i.e., anyons with quantum dimension larger than 1) through the KQD construction, one needs to start with a non-Abelian group. Here, we consider again the example of the group S_3 [149, 121], which we already discussed in the context of the

J	(C, Γ)	$ C $	$ \Gamma $	d_J	type	$n_{J,1}^{\text{rep}}$	$n_{J,1}^{\text{vec}}$
A	$(C_e, \Gamma_1^{S_3})$	1	1	1	vacuum	1	1
B	$(C_e, \Gamma_{-1}^{S_3})$	1	1	1	chargeon	0	1
C	$(C_e, \Gamma_2^{S_3})$	1	2	2	chargeon	0	2
D	$(C_x, \Gamma_1^{\mathbb{Z}_2})$	3	1	3	fluxon	1	0
E	$(C_x, \Gamma_{-1}^{\mathbb{Z}_2})$	3	1	3	dyon	0	0
F	$(C_y, \Gamma_1^{\mathbb{Z}_3})$	2	1	2	fluxon	1	0
G	$(C_y, \Gamma_\omega^{\mathbb{Z}_3})$	2	1	2	dyon	0	0
H	$(C_y, \Gamma_{\bar{\omega}}^{\mathbb{Z}_3})$	2	1	2	dyon	0	0

Table 6.2: Here, $J \equiv (C, \Gamma)$ are the elements of $D(S_3)$, C are the conjugacy classes, and Γ the irreducible representations of the normalizers, and d_J the quantum dimensions. The vacuum is both a chargeon and a fluxon. Chargeons are labeled by the irreps of S_3 and fluxons by conjugacy classes of S_3 . Dyons are labeled by conjugacy classes of S_3 and by the irreps of the normalizer of S_3 with respect to the conjugacy class. In the last two columns, we recall the multiplicities in the 11 sector stemming from the tube algebra of both $\text{Vec}(S_3)$ and $\text{Rep}(S_3)$ (see Sec. 4.6).

string-net model in Sec. 4.6. It is a well-known example, as it is the simplest non-Abelian group. Remember from the previous discussion that S_3 is the group of symmetries of the equilateral triangle, comprising the identity e , two rotations of angle $2\pi/3$ y and y^2 and three reflections along the symmetry axes x, xy and xy^2 . The multiplication rules of the group are non-commutative (see Sec. 4.6), in fact one has $xy^2 = yx$. Other relevant relations are $y^3 = e$ and $x^2 = e$. The total number of elements of the group is $|G|=6$, and as a consequence $\mathcal{D}_G = \sqrt{6}$.

The elements of S_3 form three conjugacy classes:

$$\begin{aligned}
 C_e &= \{e\} \\
 C_x &= \{x, xy, xy^2\} \\
 C_y &= \{y, y^2\}.
 \end{aligned} \tag{6.23}$$

The normalizers of each element are easily found from the definition Eq. (6.18):

$$\begin{aligned}
 \mathcal{N}_e &= S_3 \\
 \mathcal{N}_y &= \mathcal{N}_{y^2} = \{e, y, y^2\} \simeq \mathbb{Z}_3 \\
 \mathcal{N}_x &= \{e, x\} \simeq \mathcal{N}_{xy} \simeq \mathcal{N}_{xy^2} \simeq \mathbb{Z}_2.
 \end{aligned} \tag{6.24}$$

Note that the normalizer of the elements of C_x are not strictly the same, but isomorphic to each other. S_3 has three irreducible representations, which we will denote $\Gamma_1^{S_3}$ (the trivial representation, of dimension 1), $\Gamma_{-1}^{S_3}$ (the alternating representation, of dimension 1), and a two-dimensional representation $\Gamma_2^{S_3}$. We do not give the explicit expressions of these irreducible representations here, but they can be found, e.g., in [149] and [146]. The sum of the squares of the dimensions of the irreps is equal to the number of elements in G :

$$\sum_{\Gamma} |\Gamma|^2 = 1^2 + 1^2 + 2^2 = 6 = |G|, \tag{6.25}$$

with $|\Gamma|$ denoting the dimension of the irreducible representation Γ .

Furthermore, \mathbb{Z}_2 has two 1-dimensional representations $\Gamma_1^{\mathbb{Z}_2}$ and $\Gamma_{-1}^{\mathbb{Z}_2}$. \mathbb{Z}_3 finally has three 1-dimensional representations denoted $\Gamma_1^{\mathbb{Z}_3}$, $\Gamma_\omega^{\mathbb{Z}_3}$ and $\Gamma_{\bar{\omega}}^{\mathbb{Z}_3}$. The possible quasiparticles that arise from pairing up conjugacy classes and irreducible representations, and their quantum dimensions, are listed in Table 6.2. The nomenclature in terms of letters in the very first column follows the one of Ref. [121]. In the last two columns, we recall the multiplicities in the 11 sector stemming from the tube algebra of both $\text{Vec}(S_3)$ and $\text{Rep}(S_3)$ (see Sec. 4.6). This relates to the discussion of the connections between string-nets and KQD model. In fact, in the pure-gauge sector, the only excitations of the KQD model are the fluxons A , D and F : these are the same as for the string-net model built from $\text{Rep}(S_3)$. In the no-flux sector of the KQD model, the only excitations are the chargeons A , B and C : these correspond to the excitations of the string-net model built from $\text{Vec}(S_3)$ on the dual lattice, where vertex excitations (chargeons) become plaquette excitations (fluxons).

Degeneracies and finite temperature properties

7.1 Introduction

In the previous chapter, we introduced the Kitaev quantum double model (KQD) [47] as an exactly solvable toy-model, defined on a 2D lattice and realizing a topological order corresponding to a quantum double $D(G)$. The quantum double $D(G)$ describes the same topological phase as the Drinfeld center $\mathcal{Z}(\text{Vec}(G))$. It has been shown that string-net models and KQD models are connected in multiple ways [49, 50, 28]. In particular, the topological quantum field theories realized by the KQD in the ground state are also encompassed by those realized by the string-net models. In this sense, string-net models are usually considered a generalization of the KQD model.

However, there is a difference in the lattice implementations of the two models. In the string-net model, it is impossible to excite vertices without also exciting plaquettes, which is why it is typically studied only in the low energy sector with the vertex term $J_v \rightarrow \infty$, i.e., in the restricted Hilbert space where the branching rules are imposed at every vertex. In contrast, the KQD model allows for independent excitation of vertices and plaquettes. This makes it possible to study the full excitation spectrum on the lattice, rather than a truncated spectrum limited to fluxons and fusion products of fluxons, as we did in Chapters 4 and 5.

In this chapter, we want to extend the study which we performed on string-net models in Chapters 4 and 5 to the KQD model. This allows us to highlight the similarities between the string-net and Kitaev quantum double (KQD) constructions. Specifically, we demonstrate that spectral degeneracies can be computed in a very similar manner in both models. We also comment on the relations between group structure and the tube algebra construction. The KQD model is also the simplest model which allows to study the full excitation spectrum (vertex and plaquette excitations). Understanding how to characterize the full spectrum in this model is a first step towards understanding the spectrum of more intricate string-net model constructions such as the extended string-net model [93, 94]. Finally, this study is the first step towards proving a conjecture on the topological mutual information, which we used in Chap. 5 to derive a scaling law between

system size and temperature for the string-net models. Elements of the proof of this conjecture are provided in Appendix D.

This chapter presents the intermediate results of ongoing work.

7.2 Spectral degeneracies

In the ground-state, the KQD model based on a group G and the string-net models $\text{Rep}(G)$ and $\text{Vec}(G)$ realize the same topological phase corresponding to the quantum double $D(G) \simeq \mathcal{Z}(\text{Vec}(G)) \simeq \mathcal{Z}(\text{Rep}(G))$ [49, 50]. Therefore, the ground-state degeneracy of the KQD model on a surface of genus g can be computed in the same way as the ground-state degeneracy for string-net models presented in Sec. 4.2.

Building on this observation, we compute in this section the degeneracies of the excited states of the KQD Hamiltonian of Eq. (6.2) following very similar ideas as for the degeneracies of the SN model in Chap.4.

7.2.1 Plaquette and vertex excitations

As with the string-net model, we aim to apply the Moore-Seiberg-Banks formula [Eq. (4.11)] to a state featuring some excitations. The question is then how to identify correctly the excitations and their internal (non-topological) degeneracies.

The string-net Hamiltonian of Eq. (3.8) contains only plaquette terms, and only plaquettes can be excited. We identified these plaquette excitations as simple objects A of the Drinfeld center that have $n_{A,1} > 0$, where $n_{A,1}$ are non-negative integer quantities derived from the tube algebra. These objects were called fluxons and their set denoted \mathcal{F} . In particular, we noticed that only the subtype of $A \in \mathcal{F}$ corresponding to the 11 sector of the tube algebra corresponds to a plaquette excitation, but A can have other subtypes as well ($n_{A,s} \neq 0$ for $s \neq 1$). While only fluxons are plaquette excitations, the fusion of several fluxons can generate some $A \notin \mathcal{F}$. This set of fusion products of fluxons was denoted \mathcal{F}^\otimes , with $\mathcal{F} \subseteq \mathcal{F}^\otimes \subseteq \mathcal{Z}(\mathcal{C})$.

The KQD Hamiltonian of Eq. (6.2) has both vertex and plaquette excitations. As seen in Chap. 6, fluxons¹ $A \in \text{Fl}$ are labeled by conjugacy classes of G (and trivial irrep) while chargeons $A \in \text{Ch}$ are indexed by an irreducible representation of G (and the conjugacy class of the identity). The number of subtypes for fluxons is given by the cardinal of the conjugacy class $|C|$, and the number of subtypes of chargeons by the dimension of the associated irrep $|\Gamma|$ [47]. However, are all subtypes of fluxons and chargeons elementary plaquette or vertex excitations? Based on the connections between string-net models and KQD models discussed in Chap. 6, we argue that the set of chargeons Ch of a KQD model built from a group G is equivalent to the set of fluxons \mathcal{F}^{vec} for the $\text{Vec}(G)$ string-net model. Similarly, the set of fluxons Fl is equivalent to the set of

¹We have chosen a different notation for the set of fluxons of the SN model, \mathcal{F} , and the set of fluxons of the KQD model, Fl , as these sets may be different from each other even when the topological order in question is described by $D(G)$ in both cases.

fluxons for the $\text{Rep}(G)$ string-net model, \mathcal{F}^{rep} ². Therefore, the chargeon subtypes $A \in \text{Ch}$ that excite only vertices (and no adjacent plaquette) are identified by $n_{A,1}^{\text{vec}} > 0$, where the latter are the multiplicities obtained from the tube algebra $\mathcal{TA}^{\text{vec}}$ built from $\text{Vec}(G)$. The fluxon subtypes that excite only plaquettes are identified by $n_{A,1}^{\text{rep}} > 0$, the multiplicities obtained from the tube algebra $\mathcal{TA}^{\text{rep}}$ built from $\text{Rep}(G)$.

For the vacuum particle $\mathbf{1}$, the labelings of both tube algebras agree (i.e., in $\mathcal{TA}^{\text{vec}}$ as well as in $\mathcal{TA}^{\text{rep}}$, the vacuum lives in the $\mathbf{1}\mathbf{1}$ sector of the tube algebra and its multiplicity is $n_{\mathbf{1},\mathbf{1}} = 1$), so the vacuum is both $\in \text{Ch}$ and $\in \text{Fl}$, as expected.

Besides fluxons and chargeons, the quantum double $D(G)$ also contains dyons, i.e., excitations that are identified by a conjugacy class C which is not the one of the identity, and by the irreducible representation of the normalizer of this conjugacy class, Γ . These excitations arise as a fusion product of a vertex and plaquette excitations, and they always excite both a plaquette and a vertex. The number of subtypes of a dyon J corresponds to its quantum dimension $d_J = |\Gamma||C|$.

We should expect that the fusion of elementary plaquette and vertex excitations can generate the full excitation spectrum of the quantum double $D(G)$. In fact, one can show that the quantum dimension of any anyon $J \in D(G)$ (i.e., the number of all subtypes of J) can be generated by the fusion of plaquette and vertex excitations, together with their multiplicities:

$$d_J = \sum_{A \in \text{Ch}, B \in \text{Fl}} N_{AB}^J n_{B,1}^{\text{rep}} n_{A,1}^{\text{vec}}. \quad (7.1)$$

Note that in the KQD model, in contrast to the SN model, the quantum dimensions are always integers. The proof of this relation follows from using the Verlinde equation (2.20) to write the fusion coefficient N_{AB}^J in terms of the S matrices of $D(G)$, and then using the S -matrix relations [see also Eq. (4.17)]

$$\begin{aligned} S_{\mathbf{1}} \vec{n}_1^{\text{vec}} &= \vec{n}_1^{\text{vec}} \\ S_{\mathbf{1}} \vec{n}_1^{\text{rep}} &= \vec{n}_1^{\text{rep}}, \end{aligned} \quad (7.2)$$

to get:

$$\begin{aligned} \sum_{A \in \text{Ch}, B \in \text{Fl}} N_{AB}^J n_{A,1}^{\text{vec}} n_{B,1}^{\text{rep}} &= \sum_{A \in \text{Ch}, B \in \text{Fl}, X \in D(G)} \frac{S_{A,X} S_{B,X} S_{X,J}^*}{S_{\mathbf{1},X}} n_{A,1}^{\text{vec}} n_{B,1}^{\text{rep}} \\ &= \sum_{X \in D(G)} \frac{S_{X,J}^*}{S_{\mathbf{1},X}} n_{X,1}^{\text{rep}} n_{X,1}^{\text{vec}} = \frac{S_{\mathbf{1},J}^*}{S_{\mathbf{1},\mathbf{1}}} = d_J. \end{aligned} \quad (7.3)$$

In the last step, we have used that the only anyon in $D(G)$ which is both $\in \text{Ch} = \mathcal{F}^{\text{vec}}$ and $\in \text{Fl} = \mathcal{F}^{\text{rep}}$ is the vacuum $\mathbf{1}$:

$$n_{A,1}^{\text{vec}} n_{A,1}^{\text{rep}} = \delta_{A,\mathbf{1}}, \quad (7.4)$$

and $S_{\mathbf{1},J} = \frac{d_J}{\mathcal{D}}$.

²Note that while $A \in \mathcal{F}^{\text{rep}} \iff A \in \text{Fl}$, the number of fluxon subtypes is not defined in the same way in both cases and may differ. Indeed, for the SN model, the number of fluxon subtypes in a sector s of the tube algebra is given by $n_{A,s}^{\text{rep}}$, while it is rather given by $n_{A,s}^{\text{rep}} d_s$ (where d_s is the dimension of an irrep of G) for a fluxon of the KQD model, so that the total number of subtypes of a fluxon $A \in \text{Fl}$ is indeed $\sum_s n_{A,s}^{\text{rep}} d_s = d_A$.

It is possible to show that the multiplicities $n_{A,1}^{\text{rep}}$ and $n_{A,1}^{\text{vec}}$ verify the following relations with the quantum dimension d_A :

$$n_{A,1}^{\text{rep}} \leq d_A \text{ if } A \in \text{Fl and } 0 \text{ otherwise,} \quad (7.5)$$

$$n_{A,1}^{\text{vec}} = d_A \text{ if } A \in \text{Ch and } 0 \text{ otherwise.} \quad (7.6)$$

The first relation [Eq. (7.5)] follows because the category $\text{Rep}(G)$ always has commutative fusion rules. Therefore, for all $A \in D(G)$, $n_{A,1}^{\text{rep}} = 1$, if $A \in \text{Fl}$, or 0 , if $A \notin \text{Fl}$ (see Sec. 2.5.3 for more details). This is smaller than d_A if A is a non-Abelian anyon. In order to prove the second relation [Eq. (7.6)], one can use a special case of Eq. (7.2):

$$\sum_{B \in D(G)} S_{1,B} n_{B,1}^{\text{vec}} = \sum_{B \in D(G)} \frac{d_B}{\mathcal{D}} n_{B,1}^{\text{vec}} = 1. \quad (7.7)$$

Combining this with Eq. (2.34), one finds

$$\sum_{B \in D(G)} \sum_{s \in G} n_{B,1}^{\text{vec}} n_{B,s}^{\text{vec}} d_s = \sum_{B \in \text{Ch}} (n_{B,1}^{\text{vec}})^2 + \sum_{B \in D(G)} \sum_{s \in G, s \neq 1} n_{B,1}^{\text{vec}} n_{B,s}^{\text{vec}} = \mathcal{D}, \quad (7.8)$$

where $d_s = 1 \forall s \in G$. Finally, we use

$$\sum_{B \in \text{Ch}} (n_{B,1}^{\text{vec}})^2 = \mathcal{D}, \quad (7.9)$$

to prove that for $B \in \text{Ch}$, $n_{B,s}^{\text{vec}} = 0$ if $s \neq 1$, so that $d_B = n_{B,1}^{\text{vec}} d_1 = n_{B,1}^{\text{vec}}$.

Let us discuss the implications of Eqs. (7.5) and (7.6) by specifying to the example of $G = S_3$, which we presented in Sec. 6.2. In this case, the chargeons are A, B, C (where $A \equiv 1$ is the vacuum), with respective quantum dimensions $d_A = 1, d_B = 1, d_C = 2$. In agreement with Eq. (7.6), the quantum dimensions are equivalent to the multiplicities stemming from $\mathcal{TA}^{\text{vec}}$ (c.f. Table 6.2). The chargeon C exists in two different subtypes, which we call C_1 and C_2 [146]. On the other hand, for the nontrivial fluxons D, F with respective quantum dimensions $d_D = 3, d_F = 2$, we observe that $n_{D,1}^{\text{rep}} = 1 < d_D$ and $n_{F,1}^{\text{rep}} = 1 < d_F$. This means that some subtypes of the fluxons D and F are not elementary plaquette excitations, but arise as a combination of a vertex and a plaquette excitation (similarly to what one expects for dyons). This is in line with the observation made in Ref. [146] that "anyons are not energy eigenspaces". In fact, let us call F_1 and F_2 the two subtypes of F . While F_1 is an elementary plaquette excitation, F_2 corresponds to the fusion product of $F_1 \times B$ (this is in agreement with the fusion rules of $D(S_3)$, see Table 4.2, and Fig. 6 of [146]). So, F_2 actually arises, similar to a dyon, from the fusion of a plaquette excitation (F_1) with a vertex excitation (B). Similarly, out of the three subtypes of D , D_1 is an elementary plaquette excitation, while D_2 and D_3 arise as fusion products of C with D_1 [this is also in agreement with Eq. (7.1)]. Therefore, while the fluxon subtypes D_1 and F_1 will correspond to an energy penalty of $+J_p$, the other fluxon subtypes of D and F will correspond to energy penalties $+J_p + J_v$.

Finally, the dyons E, G and H can also be generated by the fusion of a vertex and a plaquette excitation. For example, one has $C \times F_1 = G + H$, so that the two dyons G and H (with $d_G = d_H = 2$) are generated by the fusion of the two subtypes of C (vertex excitations) with F_1 (plaquette excitation).

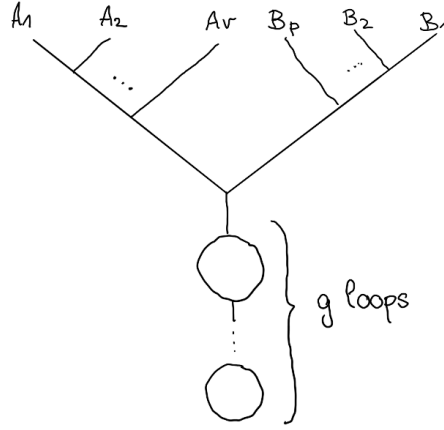


Figure 7.1: Fusion tree for degeneracies of the KQD model on a surface of genus g , v vertex excitations $A_1, A_2, \dots, A_v \in \text{Ch}^*$ and p plaquette excitations $B_1, B_2, \dots, B_p \in \text{Fl}^*$. Each vertex excitation A can exist in $n_{A,1}^{\text{vec}} = d_A$ subtypes.

7.2.2 Formula for degeneracies

Let us consider a two-dimensional closed manifold of genus g with v vertex excitations (A, a) with $A \in \text{Ch}$ and $a \in \{1, \dots, n_{A,1}^{\text{vec}} = d_A\}$, and p plaquette excitations $(B, 1)$ with $B \in \text{Fl}$ (and $n_{B,1}^{\text{rep}} = 1$). As discussed for the string-net model in Chap. 4, there will be a topological degeneracy for this configuration, depending on the fusion rules of $D(S_3)$, and on the genus g of the manifold. This degeneracy can be computed with the Moore-Seiberg-Banks formula Eq. (4.11) [111]:

$$\dim(g; A_1, \dots, A_v, B_1, \dots, B_p) = \sum_{C \in D(G)} \left[\prod_{j=1}^v S_{A_j, C} \prod_{k=1}^p S_{B_k, C} \right] S_{1, C}^{2-2g-(p+v)}. \quad (7.10)$$

This formula gives the number of ways to label a fusion diagram as represented in Fig. 7.1. Note that this fusion diagram can be restructured (see Chap. 2) as long as the number of fusion vertices is conserved. On Fig. 7.1, we have therefore for convenience represented all vertex excitations on one side and all plaquette excitations on the other side, even if this does not reflect the positions of these excitations on the lattice.

The KQD Hamiltonian Eq. (6.2) does not distinguish between different types of vertex excitations and their subtypes. Therefore, in order to obtain the full degeneracy for a state with v excited vertices and p excited plaquettes, one needs to take into account the internal degeneracy $n_{A,1}^{\text{vec}} = d_A$ of the chargeons. Up to combinatorial factors $\binom{N_v}{v}$ and $\binom{N_p}{p}$, that account for the choice for placing the vertex and plaquette excitations on the lattice, the full degeneracy is thus given by

$$\begin{aligned} D_G(g, p, v) &= \sum_{A_1, \dots, A_v \in \text{Ch}^*} \sum_{B_1, \dots, B_p \in \text{Fl}^*} \dim(g; A_1, \dots, A_v, B_1, \dots, B_p) \prod_{j=1}^v n_{A_j, 1}^{\text{vec}} \prod_{k=1}^p n_{B_k, 1}^{\text{rep}} \\ &= \sum_{A \in D(G)} S_{1, A}^{2-2g-(p+v)} \prod_{j=1}^v \left(\sum_{A_j \in \text{Ch}^*} S_{A, A_j} n_{A_j, 1}^{\text{vec}} \right) \times \prod_{k=1}^p \left(\sum_{B_k \in \text{Fl}^*} S_{A, B_k} n_{B_k, 1}^{\text{rep}} \right). \end{aligned} \quad (7.11)$$

Here, Ch^* (Fl^*) means chargeons (fluxons) without the trivial chargeon (fluxon) $\mathbf{1}$. The factors $n_{B,\mathbf{1}}^{\text{rep}}$ are simply 1 if $B \in \text{Fl}$ and 0 otherwise. They are made explicit in view of simplifying the expression using Eq. (7.2).

In fact, using Eq. (7.2) one has

$$\sum_{A_j \in \text{Ch}^*} S_{A,A_j} n_{A_j,\mathbf{1}}^{\text{vec}} = \sum_{A_j \in \text{Ch}} S_{A,A_j} n_{A_j,\mathbf{1}}^{\text{vec}} - S_{A,\mathbf{1}} = n_{A,\mathbf{1}} - S_{A,\mathbf{1}}, \quad (7.12)$$

and similarly for the fluxons. Therefore, we obtain the final expression

$$D_G(g, v, p) = \sum_{A \in D(G)} S_{\mathbf{1},A}^{2-2g} \left(\frac{n_{A,\mathbf{1}}^{\text{rep}}}{S_{\mathbf{1},A}} - 1 \right)^p \times \left(\frac{n_{A,\mathbf{1}}^{\text{vec}}}{S_{\mathbf{1},A}} - 1 \right)^v, \quad (7.13)$$

which is the main result of this section. We verified this formula numerically on small trivalent graphs on the sphere and on the torus, for the smallest Abelian and non-Abelian groups, \mathbb{Z}_2 and S_3 .

Note that if $v = 0$ (i.e., there are only plaquette excitations) one recovers the degeneracy for the $\text{Rep}(G)$ string-net model with p plaquettes and fluxons \mathcal{F}^{rep} [c.f. Eq. (4.21)]. On the other hand, if $p = 0$ (i.e., there are only vertex excitations), one recovers the degeneracy for the $\text{Vec}(G)$ string-net model on a dual lattice, with v plaquettes and fluxons \mathcal{F}^{vec} . This is in agreement with the connections between string-net and quantum double models [49, 50] discussed in Chap. 6.

7.2.3 Hilbert space dimension

We now want to show that our formula for the degeneracies Eq. (7.13) correctly gives the total quantum dimension of the system. To do so, we sum over all possible numbers of plaquette or vertex excitations:

$$\begin{aligned} \dim \mathcal{H} &= \sum_{v=0}^{N_v} \sum_{p=0}^{N_p} \binom{N_p}{p} \binom{N_v}{v} D_G(g, v, p) \\ &= \sum_{A \in D(G)} S_{\mathbf{1},A}^{2-2g} \left(\frac{n_{A,\mathbf{1}}^{\text{rep}}}{S_{\mathbf{1},A}} \right)^{N_p} \left(\frac{n_{A,\mathbf{1}}^{\text{vec}}}{S_{\mathbf{1},A}} \right)^{N_v} \\ &= S_{\mathbf{1},\mathbf{1}}^{2-2g-N_p-N_v} \\ &= \mathcal{D}^{N_l}, \end{aligned} \quad (7.14)$$

where \mathcal{D} is the total quantum dimension of $\mathcal{Z}(G)$ and the number of links $N_l = N_v + N_p + 2g - 2$ through the Euler characteristic. To go from the second to the third line, we have used that $n_{A,\mathbf{1}}^{\text{rep}}$ and $n_{A,\mathbf{1}}^{\text{vec}}$ are only simultaneously non-zero when $A = \mathbf{1}$. Finally, we also used $S_{\mathbf{1},\mathbf{1}} = \frac{1}{\mathcal{D}}$. Since $\mathcal{D} = |G|$ the number of elements in the group G , Eq. (7.14) agrees with the expression of the Hilbert space dimension computed from link degrees of freedom on the lattice Eq. (6.1), see Fig. 7.1.

Although vertex and plaquettes excitations can be treated mostly independently, Eq. (7.14) shows that the Hilbert space does not factorize into a plaquette and a vertex part (even if $g = 0$ or 1). The reason for this is the global constraint that all plaquette and vertex excitations fuse to the vacuum together with the flux coming from the handles.

7.3 Partition Function

From the degeneracies, it is simple to derive the partition function for the KQD model:

$$\begin{aligned}
Z(g, N_p, N_v) &= \text{Tr} e^{-\beta H_{\text{KQD}}}, \\
&= \sum_{v=0}^{N_v} \sum_{p=0}^{N_p} \binom{N_p}{p} \binom{N_v}{v} D_G(g, v, p) e^{\beta J_v(N_v-v) + \beta J_p(N_p-p)}, \\
&= \sum_{A \in D(G)} S_{1,A}^{2-2g} \left(\frac{n_{A,1}^{\text{vec}}}{S_{1,A}} - 1 + e^{\beta J_v} \right)^{N_v} \left(\frac{n_{A,1}^{\text{rep}}}{S_{1,A}} - 1 + e^{\beta J_p} \right)^{N_p}. \tag{7.15}
\end{aligned}$$

Just as the Hilbert space, the partition function does not in general factorize fully between vertex and plaquette excitations.

Let us take $J_v \rightarrow \infty$ in the model (i.e., we allow only for plaquette excitations). We then obtain

$$\lim_{J_v \rightarrow \infty} Z(g, N_p, N_v) e^{-\beta J_v N_v} = \sum_{A \in D(C)} S_{1,A}^{2-2g} \left(\frac{n_{A,1}^{\text{rep}}}{S_{1,A}} - 1 + e^{\beta J_p} \right)^{N_p}. \tag{7.16}$$

By comparing this expression with Eqs. (5.20) and (5.5), one recognizes that this is the partition function for a string-net model with $\mathcal{C} = \text{Rep}(G)$ and N_p plaquettes, up to a global shift in energy $e^{\beta J_v N_v}$. On the other hand, taking $J_p \rightarrow \infty$ (allowing only vertex excitations) we obtain:

$$\lim_{J_p \rightarrow \infty} Z(g, N_p, N_v) e^{-\beta J_p N_p} = \sum_{A \in D(C)} S_{1,A}^{2-2g} \left(\frac{n_{A,1}^{\text{vec}}}{S_{1,A}} - 1 + e^{\beta J_v} \right)^{N_v}, \tag{7.17}$$

which is, up to a general shift in energy given by the exponential factor, the partition function of a string-net model with $\mathcal{C} = \text{Vec}(G)$ with N_v plaquettes (note here that one has to go on the dual lattice so that the vertices of the KQD model become the plaquettes of the SN model). Again, these limits are in agreement with the relations between string-net and KQD models discussed in Sec. 6.3.

In the thermodynamic limit, the vacuum term is dominant in the sum of Eq. (7.15) because it maximizes both $n_{A,1}^{\text{vec}}/S_{1,A}$ and $n_{A,1}^{\text{rep}}/S_{1,A}$, so the partition function is

$$\lim_{N_p, N_v \rightarrow \infty} Z(g, N_p, N_v) \simeq \frac{1}{\mathcal{D}^{2-2g}} \left(\mathcal{D} - 1 + e^{J_p \beta} \right)^{N_p} \left(\mathcal{D} - 1 + e^{J_v \beta} \right)^{N_v}. \tag{7.18}$$

Contrary to the general expression of Eq. (7.15), in the thermodynamic limit the partition function fully factorizes into a term for plaquettes, a term for excitations, and a term for the genus of the surface.

Partition function for the toric code

The partition function for the toric code model has been derived by various authors, e.g. [39, 68, 70, 131]. From Eq. (7.15), for $g = 1$, $G = \mathbb{Z}_2$, $A \in D(\mathbb{Z}_2) = \{\mathbf{1}, m, e, \varepsilon\}$, $d_A = 1 \forall A$, $\mathcal{D} = 2$,

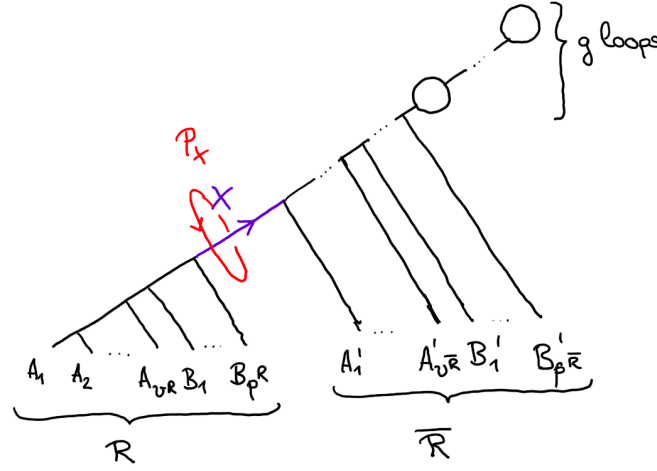


Figure 7.2: Fusion tree corresponding to a particular configuration of excitations on which the projector is acting. The projector measures the fusion product resulting from the fusion of all plaquette and vertex excitations inside region \mathcal{R} .

$n_{A,1}^{\text{rep}} = \{1, 1, 0, 0\}$ and $n_{A,1}^{\text{vec}} = \{1, 0, 1, 0\}$ (see also Sec. 6.4), one obtains

$$\begin{aligned} Z(1, N_p, N_v) &= \left(1 + e^{\beta J_v}\right)^{N_v} \left(1 + e^{\beta J_p}\right)^{N_p} + \left(1 - e^{\beta J_v}\right)^{N_v} \left(1 + e^{\beta J_p}\right)^{N_p} \\ &+ \left(1 + e^{\beta J_v}\right)^{N_v} \left(1 - e^{\beta J_p}\right)^{N_p} + \left(1 - e^{\beta J_v}\right)^{N_v} \left(1 - e^{\beta J_p}\right)^{N_p}. \end{aligned} \quad (7.19)$$

By rearranging terms, one arrives at the more standard form of the toric code partition function:

$$\begin{aligned} Z(1, N_p, N_v) &= e^{\beta J_v N_v} \left[\left(e^{\beta J_v} + e^{-\beta J_v} \right)^{N_v} + \left(e^{\beta J_v} - e^{-\beta J_v} \right)^{N_v} \right] \\ &\times e^{\beta J_p N_p} \left[\left(e^{\beta J_p} + e^{-\beta J_p} \right)^{N_p} + \left(e^{\beta J_p} - e^{-\beta J_p} \right)^{N_p} \right], \\ &= e^{\beta J_v N_v} \left[(2 \cosh \beta J_v)^{N_v} + (2 \sinh \beta J_v)^{N_v} \right] \\ &\times e^{\beta J_p N_p} \left[(2 \cosh \beta J_p)^{N_p} + (2 \sinh \beta J_p)^{N_p} \right]. \end{aligned} \quad (7.20)$$

Note that here we work with the Hamiltonian of Eq. (6.8), where the plaquette and vertex operators are projectors. Frequently, the toric code Hamiltonian is instead defined with operators that are involutions (i.e., have eigenvalues ± 1), which results in a shift of the ground-state energy (no exponential factors in the partition function) and coupling constants divided by two $J_{v,p} \rightarrow \frac{J_{v,p}}{2}$.

7.4 Projectors and mutual information

In a similar way as for the string-net models in Sec. 5.5, one can calculate projectors P_X on quasiparticles $X \in D(G)$ for the KQD model (see Fig. C.2 for a graphical representation of the action of such a projector). Although the calculatory approach is essentially the same here as in Sec. 5.5, we expect to observe different behaviors as for the string-net model. This allows,

by comparison with the string-net model, to better identify the role of the vertex constraints in the latter ones. Moreover, these projectors appear in the conjecture on the topological mutual information [69, 70] which we already discussed in the context of SN models. Elements of a proof for this conjecture in the context of the KQD model are provided in Appendix D.

Based on arguments of cutting and gluing surfaces (see Sec. 4.2), in Sec. 5.5 we have derived a general form for the thermal average of a projector $\langle P_X(L_c) \rangle$ on a contractible region \mathcal{R} of boundary L_c (see Fig. 7.2 for a graphical representation of $\langle P_X(L_c) \rangle$):

$$\langle P_X(L_c) \rangle = \frac{Z_X(0, N_p^{\mathcal{R}}, N_v^{\mathcal{R}}) Z_{\bar{X}}(g, N_p^{\bar{\mathcal{R}}}, N_v^{\bar{\mathcal{R}}})}{Z(g, N_p, N_v)}, \quad (7.21)$$

where the surface is of genus g , region \mathcal{R} contains $N_p^{\mathcal{R}}$ plaquettes and $N_v^{\mathcal{R}}$ vertices, $\bar{\mathcal{R}}$ contains $N_p^{\bar{\mathcal{R}}}$ plaquettes and $N_v^{\bar{\mathcal{R}}}$ vertices, and the total number of plaquettes (vertices) N_p (N_v) is the sum of the plaquettes (vertices) in \mathcal{R} and $\bar{\mathcal{R}}$. $Z_X(0, N_p^{\mathcal{R}}, N_v^{\mathcal{R}})$ is the effective partition function for a surface of genus 0, $N_p^{\mathcal{R}}$ plaquettes, $N_v^{\mathcal{R}}$ vertices and a puncture labeled with $X \in D(G)$. No energy is associated to the flux X , and X results from the fusion of all plaquette and vertex excitations. Similarly, $Z_{\bar{X}}(g, N_p^{\bar{\mathcal{R}}}, N_v^{\bar{\mathcal{R}}})$ is an effective partition function for a surface of genus g , with a puncture labeled \bar{X} . The explicit form of these effective partition functions is obtained by using Eq. (7.10) for the degeneracies of the KQD model with an additional "excitation" X :

$$\begin{aligned} Z_X(g, N_p, N_v) &= \sum_{A_1, \dots, A_{N_v} \in \text{Ch}} \sum_{B_1, \dots, B_{N_p} \in \text{Fl}} \dim(g, A_1, \dots, A_{N_v}, B_1, \dots, B_{N_p}, X) \\ &\times \prod_{j=1}^{N_v} n_{A_j, 1}^{\text{vec}} \prod_{k=1}^{N_p} n_{B_k, 1}^{\text{rep}} e^{-\beta(\sum_{j=1}^{N_v} E_{A_j} + \sum_{k=1}^{N_p} E_{B_k})}. \end{aligned} \quad (7.22)$$

The energies are $E_{A_j} = -J_v \delta_{A_j, 1}$ and $E_{B_k} = -J_p \delta_{B_k, 1}$. Using Eq. (7.10) and the S -matrix identities Eq. (7.12), this can be further simplified into

$$Z_X(g, N_p, N_v) = \sum_{B \in D(G)} S_{1, B}^{1-2g} S_{B, X} \left(\frac{n_{B, 1}^{\text{rep}}}{S_{B, 1}} - 1 + e^{J_p \beta} \right)^{N_p} \left(\frac{n_{B, 1}^{\text{vec}}}{S_{B, 1}} - 1 + e^{J_v \beta} \right)^{N_v}. \quad (7.23)$$

In particular, for $X = 1$, one recovers Eq. (7.15).

Let us now consider the different limits of Eq. (7.21). At zero temperature, using Eq. (7.23) and Eq. (7.15), one finds

$$\begin{aligned} \lim_{T \rightarrow 0} \langle P_X(L_c) \rangle &= \frac{1}{Z(g, N_p, N_v)} \sum_{B, C \in D(G)} S_{1, B} S_{B, X} S_{1, C}^{1-2g} S_{C, \bar{X}} e^{J_p N_p \beta} e^{J_v N_v \beta} \\ &= \frac{1}{\sum_{A \in D(G)} S_{1, A}^{2-2g}} \sum_{B, C \in D(G)} S_{1, B} S_{B, X} S_{1, C}^{1-2g} S_{C, \bar{X}} \\ &= \delta_{X, 1}. \end{aligned} \quad (7.24)$$

The last line follows from the unitarity of the S -matrix. At zero temperature, the only topological charge which we can measure with a contractible loop is thus the vacuum. This agrees with what

one would expect physically, as there are no excitations in the ground state. The same result was also observed for string-net models.

In the opposite limit of infinite temperature, one finds

$$\begin{aligned} \lim_{T \rightarrow \infty} \langle P_X(L_c) \rangle &= \frac{1}{Z(g, N_p, N_v)} \sum_{B \in D(G)} S_{1,B} S_{B,X} \left(\frac{n_B^{\text{rep}}}{S_{B,1}} \right)^{N_p^{\mathcal{R}}} \left(\frac{n_B^{\text{vec}}}{S_{B,1}} \right)^{N_v^{\mathcal{R}}} \\ &\times \sum_{C \in D(G)} S_{1,C}^{1-2g} S_{C,\bar{X}} \left(\frac{n_C^{\text{rep}}}{S_{C,1}} \right)^{N_p^{\bar{\mathcal{R}}}} \left(\frac{n_C^{\text{vec}}}{S_{C,1}} \right)^{N_v^{\bar{\mathcal{R}}}}. \end{aligned} \quad (7.25)$$

This is zero unless $B = C = \mathbf{1}$ (see Eq. (7.4)), so we finally obtain

$$\lim_{T \rightarrow \infty} \langle P_X(L_c) \rangle = \frac{d_X^2}{\mathcal{D}^2}. \quad (7.26)$$

The same result is obtained when taking the thermodynamic limit of Eq. (7.21) at any finite temperature:

$$\begin{aligned} \lim_{N_v, N_p \rightarrow \infty} \langle P_X(L_c) \rangle &= \frac{1}{Z(g, N_p, N_v)} \sum_{B, C \in D(G)} S_{1,B} S_{B,X} S_{1,C}^{1-2g} S_{C,\bar{X}} \left(\mathcal{D} - 1 + e^{J_p \beta} \right)^{N_p} \left(\mathcal{D} - 1 + e^{J_v \beta} \right)^{N_v} \\ &= \frac{d_X^2}{\mathcal{D}^2}. \end{aligned} \quad (7.27)$$

The quantity $\frac{d_X^2}{\mathcal{D}^2}$ is the "uniform" probability distribution to observe a quasiparticle $X \in D(G)$ given by the quantum dimensions. It is interesting to compare this value with the result obtained for the string-net model [c.f. Eq. (5.68)]. There, in the thermodynamic limit, the thermal average of a projector on X is given by $\frac{d_X^2}{\mathcal{D}^2} M_0$ if X is in the fusion product of fluxons, and zero otherwise. The additional factor M_0 for string-net models was defined in (5.13), and comes from the fact that the Hilbert space is constrained to those states that respect the fusion rules at all vertices. In the KQD model, this constraint does not exist, and so topological information is completely lost in the infinite temperature limit. On Fig. 7.3 below, we show an example of the behaviour of $\langle P_X(L_c) \rangle$ with the temperature for the toric code.

As discussed in Sec. 5.7.4, at zero temperature, the topological entanglement entropy - a constant contribution to the Von Neumann entropy of a bipartition - is believed to be a typical characteristic of the presence of topological order. This topological entanglement entropy is given by the logarithm of the total quantum dimension of the topological order considered [30, 29]. For the KQD model, the topological entanglement entropy is therefore $\gamma = \ln \mathcal{D} = \ln |G|$. Additionally, the Von Neumann entropy for a bipartition of the system is supposed to grow with the length of boundary between the two regions, a behavior usually called *area law*. This area law term was computed in [31, 70] for KQD models, so that the complete form of the entanglement entropy in the ground-state reads

$$S_{\mathcal{R}}^{\text{GS}} = |\partial \mathcal{R}| \ln |G| - \gamma. \quad (7.28)$$

The length of the boundary, $|\partial \mathcal{R}|$, is defined in [70] as the number of vertices shared between regions \mathcal{R} and $\bar{\mathcal{R}}$. On a trivalent lattice, this is the same as the number of links crossed by the

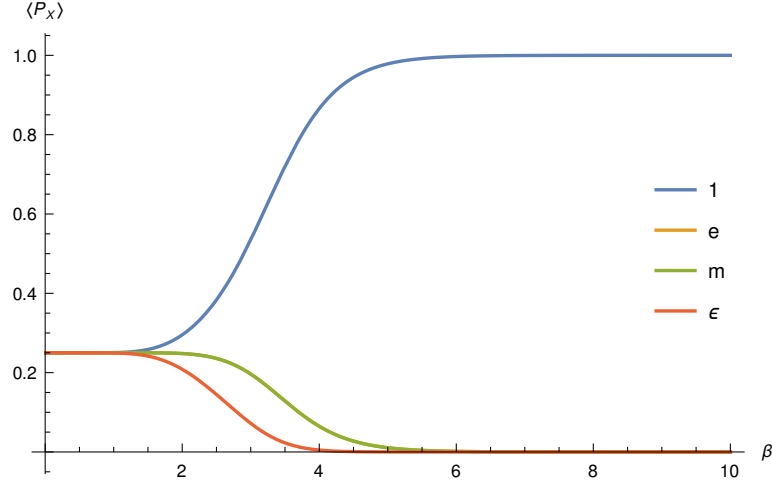


Figure 7.3: Evolution of the thermal average of the projectors on the quasiparticles of the toric code as a function of the inverse temperature $\beta = \frac{1}{T}$. Here, we consider the case of a projector inside a region with 9 plaquettes and 9 vertices, in a system of overall size $N_p = 36$ and $N_v = 36$. At low temperature, the vacuum is predominant, as expected for the ground state. Then, the expectation values of the other quasiparticles start to increase until reaching the uniform value $1/4$ as predicted by Eq. (7.26). The curves of e and m are overlaid on top of each other. The thermal average of the projector P_ϵ increases slower because ϵ arises only as a fusion product of e and m .

boundary and Eq. (7.28) is the same expression as the ground-state entropy for a $\text{Vec}(G)$ string-net model [30] [see Eq. (5.95), with $l = |\partial\mathcal{R}|$].

At finite temperature, the entanglement entropy of the KQD model has been studied in [68, 69, 70]. In particular, Refs. [69, 70] suggest that at finite temperature, it is more relevant to consider the mutual information, defined as

$$I_{\mathcal{R}} = S_{\mathcal{R}} + S_{\tilde{\mathcal{R}}} - S_{\mathcal{R} \cup \tilde{\mathcal{R}}}, \quad (7.29)$$

instead of the entanglement entropy. Here, $\tilde{\mathcal{R}}$ denotes the complementary region to \mathcal{R} in terms of links ($N_l^{\mathcal{R}} + N_l^{\tilde{\mathcal{R}}} = N_l$), which may be different from $\bar{\mathcal{R}}$, the complementary region in terms of plaquettes and vertices (for more details, see Appendix D).

In fact, at finite temperature, the entanglement entropy is expected to also have a volume contribution, which makes it non-symmetric between \mathcal{R} and $\tilde{\mathcal{R}}$. Instead, the mutual information is expected to follow an area law at finite temperature. In the ground state, the topological mutual information I_{topo} is twice the topological entanglement entropy:

$$I_{\text{topo}}(T = 0) = -2\gamma = -2 \ln|G|. \quad (7.30)$$

At finite temperature, Refs. [69, 70] show that the topological mutual information for the toric code model can be expressed, for a sufficiently large system, as the Kullback-Leibler divergence between the thermal probability distribution of anyons X $\langle P_X(L_c) \rangle$, and the probability distribution given by the quantum dimensions:

$$I_{\text{topo}}(T) = - \sum_{X \in D(G)} \langle P_X(L_c) \rangle \ln \left[\langle P_X(L_c) \rangle \frac{\mathcal{D}^2}{d_X^2} \right]. \quad (7.31)$$

The authors of Refs. [70, 69] also conjecture that this formula should hold for other quantum double models, in particular also non-Abelian ones. From the expression for the projector Eq. (7.27), one sees that $I_{\text{topo}}(T) = 0$ in the thermodynamic limit at finite temperature. This stands in contrast with the string-net model, where we found that $I_{\text{topo}}(T) = -\ln M_0$ using the same conjecture. In particular, we observe that, when considering temperature scales $J_v \ll T \ll J_p$, one recovers from Eq. (7.31) the $T \rightarrow \infty$ limit for the $\text{Vec}(G)$ string-net model. On the other hand, for $J_p \ll T \ll J_v$, one recovers the $T \rightarrow \infty$ limit for the $\text{Rep}(G)$ string-net model. This is illustrated on Fig. 7.4 for $G = S_3$. A similar behavior was noticed for the entanglement entropy of the toric code model in [68].

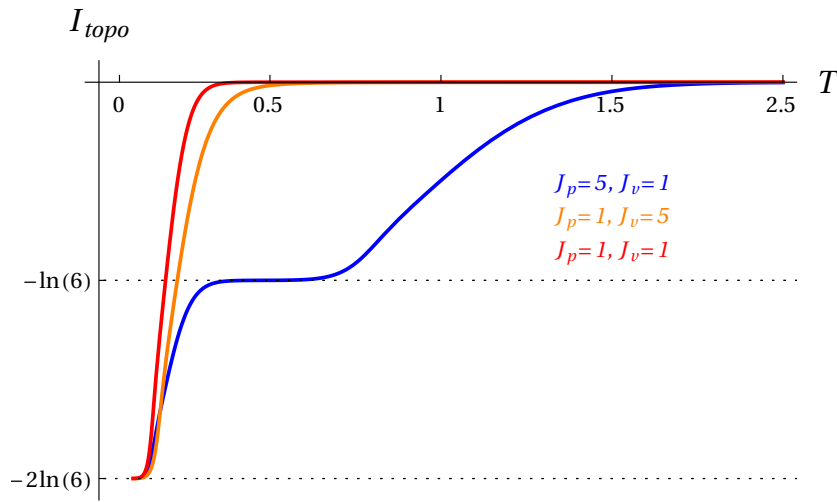


Figure 7.4: I_{topo} as a function of temperature for $D(S_3)$ on a sphere, where \mathcal{R} contains 2^3 plaquettes and 2^3 vertices, while the total number of plaquettes is 2^8 and the total number of vertices as well. At temperatures were $J_v \ll T \ll J_p$, we observe a plateau corresponding to the topological mutual information of the $\text{Vec}(S_3)$ string-net model, with $M_0 = 6$. For the $\text{Rep}(S_3)$ string-net model, $M_0 = 1$.

7.5 Outlook and conclusion

In this chapter, applying similar tools as for the string-net models, we have obtained the degeneracies of the full spectrum of the Kitaev quantum model. In particular, we have shown that these degeneracies can be obtained by considering fusion trees featuring only fluxons or chargeons, i.e., without explicit appearance of dyons. We have identified the subtypes of vertex or plaquette excitations with our knowledge from the tube algebra. For fluxons, only one subtype corresponds to a plaquette excitation, while other subtypes also excite the plaquettes.

From the degeneracies, we have derived a general form for the partition function of the KQD model, as well as the thermal average of projectors on quasiparticles. In the limits $J_p \rightarrow \infty$ ($J_v \rightarrow \infty$), we recover the expressions for the string-net models $\text{Vec}(S_3)$ ($\text{Rep}(S_3)$).

Our next step is to prove the conjecture on the topological mutual information of [69, 70], both for the Kitaev quantum double model, and for string-net models. A general expression for the entropy $S_{\mathcal{R}}$ at finite temperature for the KQD model is given in [70] and could serve as a starting point. We find that the $J_p \rightarrow \infty$ limit of this formula corresponds to numerical results obtained for the entanglement entropy of the $\text{Vec}(S_3)$ string-net model on small trivalent graphs. However, the opposite limit $J_v \rightarrow \infty$ does not coincide with numerical results for $\text{Rep}(S_3)$. Understanding these differences between the two string-net models is another point that needs to be clarified.

Conclusion

General conclusion

In this thesis, we have studied the energy spectrum and finite temperature properties of two exactly solvable models for topological order: the string-net model and the quantum double model.

The main focus of this work has been on the string-net model. We have considered the generalized version of this model, allowing for any input unitary fusion category, and realizing all topological orders described by a Drinfeld center. As is usually done in the literature, we have considered the string-net model in a restricted Hilbert space, where fusion rules at the vertices of the lattice are imposed as hard constraints.

In this model, only fluxons (plaquette excitations) are present as real excitations at the single plaquette level. We have explained how to identify these fluxons through the structure of the tube algebra (which is a way to construct the Drinfeld center from the input category). Although the energy spectrum of this model is very simple (an equidistant ladder), it hides complicated degeneracies which are a signature of the topological order. An important result of this thesis are analytical expressions for the level degeneracies, both for closed manifolds and manifolds with boundaries. We have shown that topological degeneracies can be obtained using a result from topological quantum field theory, the Moore-Seiberg-Banks formula. Additionally, the string-net model may feature non-topological degeneracies (i.e., degeneracies that may be lifted by a local perturbation) in the case where the input category has non-commutative fusion rules. These non-topological degeneracies are given by the multiplicities stemming from the tube algebra. An important conclusion of this study is that, while the ground-state degeneracy can be fully expressed in terms of the content of the Drinfeld center, the degeneracies of excited states also depend on the lattice realization of this Drinfeld center, i.e., on the input category. As a consequence, two Morita-equivalent categories such as $\text{Rep}(S_3)$ and $\text{Vec}(S_3)$ have the same Drinfeld center $\mathcal{Z}(S_3)$ but the corresponding string-net models have different fluxons, different level degeneracies, and different Hilbert spaces. Finally, we introduced a refined Hamiltonian in which all non-topological degeneracies can be split.

These results have been verified numerically by exact diagonalisation on small systems for a few representative categories; we have provided a certain number of examples of unitary fusion categories, their Drinfeld center, and numerical results for their degeneracies.

In a second step, using the results on the spectral degeneracies, we have derived an exact analytical expression for the partition function of these models, valid on any surface, and for any energy coupling. This partition function allowed us to analyze the finite-temperature behavior of several quantities. In particular, the behaviour of the specific heat shows that there is no finite temperature phase transition, in agreement with a general result [67] stating that topological order does not survive at $T > 0$ in the thermodynamic limit. By studying the partition function, we also identified a special set of fluxons which drive the thermodynamic limit: pure fluxons. We analyzed in detail the properties of these pure fluxons, showing how to obtain them from the tube algebra, and proving that they braid trivially with all other fluxons and with all fusion products of fluxons.

Using simple surgery arguments, we then computed the thermal average of the projector onto a given quasiparticle sector for three different types of closed loops: handle, throat, and contractible. These projectors are directly related to Wegner-Wilson loop operators, which provide information about the confinement of the excitations. We found that, in the thermodynamic limit at finite temperature, the only particles that remain deconfined are pure fluxons, which braid trivially with all other particles. We also gave a prescription on how to implement these loop operators numerically.

The projectors on contractible loops are also the key ingredient to compute the topological mutual information according to a conjecture proposed by Iblisdir *et al.* [69, 70] in the context of the quantum double model. Extending this conjecture to the string-net models, we found that there is a scaling behavior between the temperature and the system size, generalizing what was found by Iblisdir *et al.* [68, 38, 69, 70]. In particular, we observed that the topological mutual information does not go to zero as temperature and system size increase, but to a constant determined by the pure fluxons. We interpret this as a consequence of the hard constraint imposed on the Hilbert space. This also generalizes a result found for the toric code model [68] and certain string-nets at infinite temperature [76]. As a side result, we discussed some issues when trying to recover numerically the analytical result for the ground-state entanglement entropy by Levin and Wen [30].

In the last part of this thesis, we turned to study the quantum double model, by carrying over to this model the tools we used for the string-net models. In contrast to string-net models, we considered the quantum double model with its full Hilbert space, allowing for all types of excitations to exist at the surface of the lattice, fluxons (plaquette excitations), chargeons (vertex excitations) and dyons as a simultaneous excitations of a vertex and a plaquette. We showed that the spectral degeneracies on closed surfaces for the quantum double model can also be obtained by using the Moore-Seiberg-Banks formula, upon correctly identifying the plaquette and vertex excitations. Our main insight is that these degeneracies can be obtained by considering fusion trees featuring only fluxons or chargeons, i.e., without explicit appearance of dyons. We identified the relevant vertex and plaquette excitations with our knowledge from the tube algebra. We then derived from these results exact expressions for the partition function and the thermal average of projectors on quasiparticles inside contractible loops, and commented on the connections between string-net and quantum double models.

A direct continuation of the work presented in this thesis is to search for a proof of the conjecture proposed in [70] on topological mutual information, which allows to derive a scaling law between temperature and system size in both the quantum double and the string-net models. Achieving this proof requires a deeper comprehension of the description of the entanglement at finite temperatures in these models. This, in turn, could offer new insights into the connections between string-net and quantum double models.

In this thesis, we restricted our study to the effect of thermal fluctuations on topological order. Previous works also studied string-net models at zero temperature in the presence of quantum fluctuations [128, 129]. Studying the interplay of thermal and quantum fluctuations in these models may reveal interesting behaviours. For example, introducing an interaction term between anyons may lead to a finite-temperature phase transition (see sec. IV in [57]).

In a broader perspective, we may extend our approach to study the finite-temperature properties of other models. For example, using the tube algebra decomposition to identify plaquette and vertex excitations, as well as the Moore-Seiberg-Banks formula, has been proven to be successful for deriving the degeneracies and the partition function [94] of the extended string-net model [93], which allows for all excitations of the Drinfeld center to be present at the level of plaquettes. In particular, it seems interesting to consider models of topological order in higher dimensions. In fact, in three or four dimensions, some topologically ordered systems display a finite-temperature phase transition, and admit finite-temperature topological order, while still being a sum of local commuting projectors [150, 151, 75].

Finally, one may venture beyond the family of achiral topological orders studied in this thesis and explore chiral topological orders at finite temperature (see, e.g., [152]). This is particularly relevant since the most well-known experimental realization of topological order is chiral topological order in the fractional quantum Hall effect. Studying chiral topological order at finite temperature could provide further insights into the range of validity and applicability of the results presented in this thesis.

Appendices

In the notations of Chap. 2, this gives:

$$Q_{cda}^a Q_{hgb}^e = \delta_{dh} \sum_{n,k} \sqrt{\frac{d_a d_f}{d_k}} [F_f^{abe}]_{dk} [F_a^{fgn}]_{ek} [F_a^{ekc}]_{bn} Q_{cgk}^n. \quad (\text{A.3})$$

Two particular cases can be distinguished. Firstly, when the two tubes are in the 11 sector, (i.e. they are simply made of a horizontal line labeled by some element $i \in \mathcal{C}$, Q_{11i}^i), their fusion rules reproduce the fusion rules of the input objects of \mathcal{C} . That is, one can write

$$Q_{11i}^i Q_{11j}^j = \sum_k N_{ij}^k Q_{11k}^k, \quad (\text{A.4})$$

where N_{ij}^k are the fusion matrices of \mathcal{C} . Secondly, tubes that are made of a vertical line (i.e., of the form Q_{rrr}^1) act as projectors on the sector rr of the tube algebra. In fact, one has

$$Q_{rrr}^1 Q_{rrr}^1 = Q_{rrr}^1, \quad (\text{A.5})$$

and these tubes act as the identity on tubes in the rr sector, but give zero if acting on a sector ss with $s \neq r$.

Fluxon identities

As discussed in Chap. 4, fluxons are those simple objects $A \in \mathcal{Z}(\mathcal{C})$ that have $n_{A,1} > 0$. One can define a vector \mathbf{n}_1 with components $n_{A,1}$ with $A = 1, \dots, N_{\mathcal{Z}}$ [where $N_{\mathcal{Z}}$ is the number of simple objects in $\mathcal{Z}(\mathcal{C})$] such that it has non-zero entries only when A is a fluxon. Equations (4.17, 4.16 and 4.19) are extra relations satisfied by the vector \mathbf{n}_1 that we call fluxon identities. Similar equations first appeared in the context of anyon condensation [116, 118] and gapped boundaries [104, 117]. In this Appendix, we provide a proof of the fluxon identities from the tube algebra, and comment on the relation with anyon condensation.

B.1 S and T identities from the tube algebra

In the 11 sector, each tube Q_{11i}^i corresponds to a horizontal closed string labeled by i , where i is one of the $\mathcal{N}_{\mathcal{C}}$ simple objects of the input category \mathcal{C} . Therefore, the tube algebra restricted to the 11 sector is just the fusion algebra of the input category and it decouples from the rest of the tube algebra [see Eq. (A.4)]. In particular, the vacuum tube Q_{111}^1 ,

$$Q_{111}^1 Q_{111}^1 = \sum_k N_{11}^k Q_{11k}^k = Q_{111}^1, \quad (\text{B.1})$$

is the projector onto the 11 sector (see Eq. A.5).

Commutative input category

In the commutative case, we can use the mock S -matrix \tilde{s} to diagonalize simultaneously all the fusion matrices of the input category \mathcal{C} . \tilde{s} is a unitary matrix but, unlike the S -matrix, it is not symmetric in general (a special case is when the input category is modular, in which case \tilde{s} is precisely the modular S -matrix). In particular, \tilde{s} diagonalizes the tube algebra in the 11 sector. As a consequence, the $\mathcal{N}_{\mathcal{C}}$ idempotents in the 11 sector (corresponding to $\mathcal{N}_{\mathcal{F}} = \mathcal{N}_{\mathcal{C}}$ fluxons) are obtained as the column vectors of \tilde{s} . Therefore, we write a matrix element of \tilde{s} as $\tilde{s}_{i,A}$ with rows indexed by input labels $i = 1, \dots, \mathcal{N}_{\mathcal{C}}$ and columns by fluxons $A \in \mathcal{F}$. The matrix \tilde{s} can be chosen such that its first row only contains strictly positive elements, in which case, $\tilde{s}_{1,A} = \sqrt{d_A/\mathcal{D}} = \sqrt{S_{1,A}}$. The mock S -matrix is not yet unique as its columns can always be

permuted. By convention, we choose that the first column corresponds to the vacuum $A = 1$ of the output category so that $\tilde{s}_{i,1} = d_i/\sqrt{\mathcal{D}}$. Therefore, one can read the (square root of the) quantum dimensions of the fluxons in the first row of \tilde{s} , and the quantum dimensions of the input objects in the first column. Examples of mock S -matrix are given in Secs. 4.6.1, 4.6.2 and 4.6.4.

Using \tilde{s} , the simple idempotents p_A^{11} are easily found as linear combinations¹ of the horizontal tubes Q_{11i}^i

$$p_A^{11} = \tilde{s}_{1,A} \sum_{i \in \mathcal{C}} \tilde{s}_{i,A}^* Q_{11i}^i, \quad (\text{B.2})$$

and vice-versa:

$$Q_{11i}^i = \sum_{A \in \mathcal{F}} \frac{\tilde{s}_{i,A}}{\tilde{s}_{1,A}} p_A^{11}. \quad (\text{B.3})$$

Using the Verlinde-like equation

$$N_{ij}^k = \sum_{A \in \mathcal{F}} \frac{\tilde{s}_{i,A} \tilde{s}_{j,A} \tilde{s}_{k,A}^*}{\tilde{s}_{1,A}}, \quad (\text{B.4})$$

and the unitarity of the mock S -matrix, one can check that indeed

$$p_A^{11} p_B^{11} = p_A^{11} \delta_{A,B}. \quad (\text{B.5})$$

We now introduce the projector Q_1 onto the fluxons in the 11 sector of the tube algebra. By definition

$$Q_1 = \sum_{A \in \mathcal{Z}(\mathcal{C})} p_A^{11} = \sum_{A \in \mathcal{F}} p_A^{11}, \quad (\text{B.6})$$

where p_A^{11} only exists if A is a fluxon, i.e., if $n_{A,1} = 1$. The above sum puts a weight 1 on fluxons and 0 on non-fluxons, so that

$$\text{Tr } Q_1 = \sum_{A \in \mathcal{F}} \text{Tr } p_A^{11} = \sum_{A \in \mathcal{F}} n_{A,1} = \mathcal{N}_{\mathcal{C}}, \quad (\text{B.7})$$

which shows that Q_1 is closely related to the vector \mathbf{n}_1 .

From (B.3) with $i = 1$, one gets

$$\sum_{A \in \mathcal{F}} p_A^{11} = Q_{111}^1, \quad (\text{B.8})$$

which is simply the empty tube. Therefore, the projector Q_1 onto the fluxons in the 11 sector is also the projector Q_{111}^1 onto the 11 sector.

The action of the modular matrices S and T on the tubes is well-known: they act trivially on the empty tube (see Sec. 28.3 in [28]). So that

$$SQ_1 = Q_1 \text{ and } TQ_1 = Q_1, \quad (\text{B.9})$$

which are the fluxon identities, Eqs. (4.17) and (4.16).

¹Note that the relations (B.2) and (B.3) are similar in structure to the relations linking a projector P_B to a Wegner-Wilson loop W_A , where $A, B \in \mathcal{Z}(\mathcal{C})$, see Eqs. (5.73) and (5.74).

Noncommutative input category

In the noncommutative case, there is no mock- S matrix which diagonalizes simultaneously the fusion matrices. A consequence is that the number of tubes \mathcal{N}_C in the 11 sector is strictly larger than the number of simple idempotents in this sector, which is strictly larger than the number of fluxons \mathcal{N}_F (see also Sec. 2.5.3).

From the N_C tubes Q_{11i}^i , we build idempotents and nilpotents $p_A^{11,ab}$ so that their total number is \mathcal{N}_C , corresponding to only \mathcal{N}_F (non-simple) idempotents $P_A^{11} = \sum_{a=1}^{n_{A,1}} p_A^{11,aa}$ in the 11 sector (the central idempotents are $P_A = \sum_{s \in C} P_A^{ss}$). Now $\text{Tr} P_A^{11} = n_{A,1}$ can be larger than 1. We can again define the projector Q_1 onto the fluxons in the 11 sector by:

$$Q_1 = \sum_{A \in \mathcal{F}} P_A^{11} = \sum_{A \in \mathcal{F}} \sum_{a=1}^{n_{A,1}} p_A^{11,aa}. \quad (\text{B.10})$$

From the transformation between tubes and idempotents [see Eq. (2.51)], one has

$$Q_{111}^1 = \sum_{A \in \mathcal{F}} \sum_{a=1}^{n_{A,1}} \sum_{b=1}^{n_{A,1}} (M_{A,111}^1)_{a,b} p_A^{11,ab} = \sum_{A,a} p_A^{11,aa}, \quad (\text{B.11})$$

as $(M_{A,111}^1)_{a,b} = (\Omega_{A,111}^1)_{a,b} = \delta_{a,b}$ (see above Eq. (40) in Ref. [78] or below Eq. (52) and Eq. (53) in Ref. [84]). Therefore, Q_1 is also the projector onto the 11 sector, i.e. the empty tube Q_{111}^1 , from which the fluxon identities (B.9) follow as in the previous subsection.

B.2 Stability inequality from anyon condensation

In order to prove the stability inequality Eq. (4.19) that \mathbf{n}_1 needs to satisfy, we make a detour into anyon condensation. Anyon condensation is a general mechanism that allows one to describe a phase transition from a topological order described by a UMTC \mathcal{A} to another described by a UMTC \mathcal{U} [118]. We therefore reverse the perspective and imagine that, instead of building the Drinfeld center from an input category, we condense some bosons of the Drinfeld center to recover the input category. We will use the general formalism of anyon condensation [118, 116] and apply it to the particular case in which we start from the Drinfeld center $\mathcal{Z}(\mathcal{C})$ and condense it towards a trivial order. This is known as anyon condensation to the vacuum, which is intimately related to finding how many types of gapped boundaries are possible for a given topological order [96, 117, 153].

Condensation to the vacuum relates the UMTC $\mathcal{A} = \mathcal{Z}(\mathcal{C})$ to the trivial UMTC \mathcal{U} (total quantum dimension $\mathcal{D}_{\mathcal{U}} = 1$), via a UFC $\mathcal{T} = \mathcal{C}$, where \mathcal{U} is included in \mathcal{T} . Generally speaking, anyon condensation

$$\mathcal{A} \rightarrow \mathcal{T} \rightarrow \mathcal{U}, \quad (\text{B.12})$$

is described by a rectangular matrix $n_{A,s}$, called restriction or lifting matrix, with $A \in \mathcal{A}$ and $s \in \mathcal{U}$. If \mathcal{U} is the trivial UMTC, $s = 1$ only. Then, the matrix $n_{A,s}$ is the vector \mathbf{n}_1 and the condensing bosons are the fluxons. The condensation equations (see, e.g., Eqs. (20a) and (20b) in Ref. [116]) relate the S - and T - matrices of the two UMTCs \mathcal{A} and \mathcal{U} as

$$T_{\mathcal{A}} \mathbf{n}_1 = \mathbf{n}_1 T_{\mathcal{U}} \text{ and } S_{\mathcal{A}} \mathbf{n}_1 = \mathbf{n}_1 S_{\mathcal{U}}. \quad (\text{B.13})$$

As $T_U = 1$ and $S_U = 1$ are trivial 1×1 matrices, and $T_A = T$ and $S_A = S$ are the T - and S -matrices of $\mathcal{Z}(\mathcal{C})$, we find Eq. (4.17-4.16). Anyon condensation should also hold in the case where the UFC \mathcal{T} has noncommutative fusion rules, as briefly discussed in Ref. [118].

In the context of anyon condensation, one requires the commutation of fusion and restriction [116, 118], i.e.,

$$\sum_{C \in \mathcal{A}} N_{AB}^C n_{C,t} = \sum_{r,s \in \mathcal{T}} n_{A,r} n_{B,s} \tilde{N}_{rs}^t. \quad (\text{B.14})$$

In this appendix, in order to avoid confusion, \tilde{N} denotes the fusion matrices for $\mathcal{T} = \mathcal{C}$, whereas N denotes the fusion matrices for $\mathcal{A} = \mathcal{Z}(\mathcal{C})$. The stability inequality (4.19) follows by taking $t = 1$ so that

$$\sum_{C \in \mathcal{A}} N_{AB}^C n_{C,1} = n_{A,1} n_{B,1} + \sum_{r \neq 1} n_{A,r} n_{B,\bar{r}} \geq n_{A,1} n_{B,1}, \quad (\text{B.15})$$

An advantage of this inequality is that it can serve as a test of the coefficients $n_{A,1}$ without the knowledge of the complete lifting/restriction matrix $n_{A,s}$ and the fusion matrix \tilde{N} .

An interesting question to ask is: given an achiral topological order characterized by a Drinfeld center $\mathcal{Z}(\mathcal{C})$ with modular matrices S and T , what are the possible gapped boundaries or condensations to the vacuum [116, 117, 153] ?

A partial answer to that question is known (see, e.g., Refs [117, 154, 153]): a necessary (but not sufficient) condition for a gapped boundary is to have a vector \mathbf{n}_1 that satisfies the fluxon identities Eqs. (4.17)-(4.16) and the stability condition (4.19), i.e., to have a stable fluxon set. This is equivalent to the notion of Lagrangian algebras in $\mathcal{Z}(\mathcal{C})$ [120]. For each such stable \mathbf{n}_1 , there is a corresponding boundary theory described by a UFC \mathcal{C}_b . Obviously, \mathcal{C} is one of the possible boundary theories \mathcal{C}_b . Also, all the boundary theories are Morita-equivalent, i.e. $\mathcal{Z}(\mathcal{C}_b) \simeq \mathcal{Z}(\mathcal{C})$. This is the bulk-boundary correspondence for achiral topologically-ordered phases.

For example, given $\mathcal{Z}(S_3)$ (see Sec. 4.6.1 for the notations), one finds five possible \mathbf{n}_1 's satisfying (4.17) and (4.16), one of which ($\mathbf{n}_1 = \{1, 1, 1, 0, 0, 1, 0, 0\}^T$ which for short we note $\mathbf{n}_1 = (A, B, C, F)$ according to its non-zero elements) does not satisfy the stability condition (4.19) [153]. Among the four stable solutions, two are related by symmetry and correspond to $\text{Vec}(S_3)$ [i.e. $\mathbf{n}_1 = (A, B, 2 \times C)$ and $\mathbf{n}_1 = (A, B, 2 \times F)$], and two are related by symmetry and correspond to $\text{Rep}(S_3)$ [i.e. $\mathbf{n}_1 = (A, D, F)$ and $\mathbf{n}_1 = (A, C, D)$], accounting for the symmetry between the C and F quasiparticles [121].

Another example is that of $\mathcal{Z}(\mathcal{H}_3)$ (see Sec. 4.6.3 for the notations). In this case, we find three stable solutions. Two solutions related by symmetry [i.e. $\mathbf{n}_1 = \{1, 0, 0, 0, 0, 0, 0, 1, 2, 0, 0, 0\}^T = (\mathbf{1}, \pi_1, 2 \times \pi_2)$ and $\mathbf{n}_1 = (\mathbf{1}, \pi_1, 2 \times \sigma_1)$], due to the symmetry between the π_2 and σ_1 quasiparticles, point to the fusion ring H_6 and one [i.e. $\mathbf{n}_1 = (\mathbf{1}, \pi_1, \pi_2, \sigma_1)$] to the fusion ring H_4 [155]. The fusion ring H_6 corresponds to the UFCs \mathcal{H}_3 and \mathcal{H}_2 , whereas H_4 refers to the UFC \mathcal{H}_1 . The two categories \mathcal{H}_3 and \mathcal{H}_2 have the same fusion rules but different F symbols.

Fusion of tubes

In this Appendix we compute the fusion outcome C of two anyons A and B using the tube algebra. We also show that if A is a pure fluxon and B is a fluxon, then necessarily C is also a fluxon.

C.1 Fusion rules from the tube algebra

One way to obtain the fusion rules from the tube algebra is to use the half-braidings to compute the S -matrix and to use the Verlinde formula to obtain the fusion matrices. This is the way followed, e.g., in Refs [48, 84, 81]. Here, we follow a different path and obtain the fusion coefficients for the Drinfeld center directly from the tube algebra, without using the half-braidings.

We follow the general strategy described in Sec. V in Ref. [122] (see also Sec. IV in Ref. [156]). For simplicity, we concentrate on commutative and self-dual input categories, but the method can easily be generalized to the non-self-dual and noncommutative case. The first one only requires to put arrows on all strings, where reversing an arrow means going from an object $i \in \mathcal{C}$ to its dual. The second one implies to label sectors of the tube algebra by two indices r, α instead of one r , and to consider particles with $n_{A,1} \geq 1$ (see Appendix A in Ref. [81] for more details). In the following, by convention, we will denote simple objects in \mathcal{C} by lowercase letters and simple objects in $\mathcal{Z}(\mathcal{C})$ by capital letters.

The (central) projector P_A on a particle A can be written as

$$P_A = \sum_{r \in \mathcal{C}} p_A^{rr}. \quad (\text{C.1})$$

The simple idempotents p_A^{rr} and nilpotents p_A^{rs} decompose in the tube basis as [see Eq. (2.51)]

$$p_A^{rs} = \sum_{i,j \in \mathcal{C}} (M_{A,rsj}^i)^{-1} Q_{rsj}^i, \quad (\text{C.2})$$

where the coefficients M_A^{-1} depend on $A \in \mathcal{Z}(\mathcal{C})$, $r, s \in \mathcal{C}$ label the sectors of the tube algebra, and where the Q 's are the tubes. The reverse version of this formula is

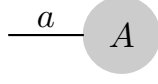


Figure C.1: A single quasiparticle basis state $|A, a\rangle$ corresponding to a simple idempotent $p_A^{aa} = |A, a\rangle\langle A, a|$, with $A \in \mathcal{Z}(\mathcal{C})$ and $a \in \mathcal{C}$.

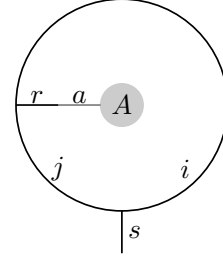


Figure C.2: Action of a tube on a one-quasiparticle state $|A, a\rangle$.

$$Q_{rsj}^i = \sum_{A \in \mathcal{Z}(\mathcal{C})} M_{A,rsj}^i p_A^{rs}. \quad (\text{C.3})$$

The M and M^{-1} together verify

$$\sum_{i,j \in \mathcal{C}} (M_{A,rsj}^i)^{-1} M_{B,rsj}^i = \delta_{A,B}. \quad (\text{C.4})$$

Following Ref. [84], we represent a one-quasiparticle basis state $|A, a\rangle$, with $A \in \mathcal{Z}(\mathcal{C})$ and $a \in \mathcal{C}$, as in Fig. C.1.

The dimension of the corresponding Hilbert space is:

$$\dim \mathcal{H}_{1\text{QP}} = \sum_{A,a} n_{A,a}. \quad (\text{C.5})$$

The action of a tube on this basis state, as represented on Fig. C.2, is

$$Q_{rsj}^i |A, a\rangle = \delta_{r,a} M_{A,rsj}^i |A, s\rangle. \quad (\text{C.6})$$

We now introduce a basis for a two-quasiparticle state. We write a state in this basis $|A, a, B, b, c\rangle$ and represent it graphically as in Fig. C.3. In other words, a two-quasiparticle state is entirely fixed if we specify the two quasiparticle types A and B , their tube-algebra sectors a and b , and the channel c in which a and b fuse. An alternative way to describe the two-quasiparticle Hilbert space is to take states $|A, B, C, c\rangle$ as a basis (see Fig. C.4). Here, we fix A, B and their fusion outcome C as well as the tube algebra sector c of C . These states are eigenvectors of the simple idempotents p_C^{cc} :

$$p_C^{cc} |A, B, C, c\rangle = \delta_{c,c'} \delta_{C,C'} |A, B, C, c\rangle. \quad (\text{C.7})$$

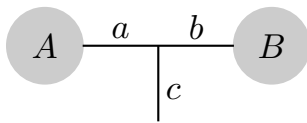


Figure C.3: A two-quasiparticle state $|A, a, B, b, c\rangle$.

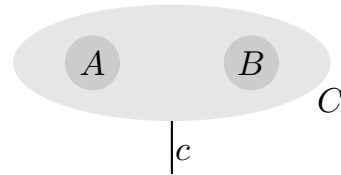


Figure C.4: A two-quasiparticle state $|A, B, C, c\rangle$.

The dimension of the two-quasiparticle Hilbert space is

$$\dim \mathcal{H}_{2\text{QP}} = \sum_{A,B,a,b,c} \tilde{N}_{a,b}^c n_{A,a} n_{B,b}, \quad (\text{C.8})$$

$$= \sum_{A,B,C,c} N_{A,B}^C n_{C,c}. \quad (\text{C.9})$$

The equality between these two lines follows from the commutation between fusion and restriction in anyon condensation, see Eq. (B.14). As in the previous appendix, we denote fusion matrices of \mathcal{C} by \tilde{N} and fusion matrices of $\mathcal{Z}(\mathcal{C})$ by N . Since

$$\sum_{A,B,a,b} n_{A,a} n_{B,b} \sum_c \tilde{N}_{a,b}^c \geq \sum_{A,B,a,b} n_{A,a} n_{B,b}, \quad (\text{C.10})$$

the dimension of the two-quasiparticle Hilbert space (C.8) is larger than the square of the dimension of the one-quasiparticle Hilbert space (C.5), which is a signature of entanglement.

The action of a tube Q_{ccj}^i on a state $|A, a, B, b, c\rangle$ can graphically be represented as in Fig. C.5. Applying a series of F -moves, this diagram can be modified into the diagram of Fig. C.6.

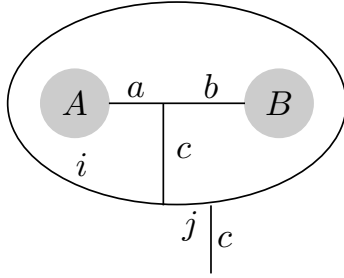


Figure C.5: Tube Q_{ccj}^i acting on $|A, a, B, b, c\rangle$.

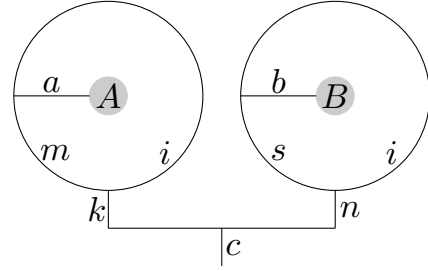


Figure C.6: Same situation as in Fig. C.5 after a series of F -moves. Now, there are two tubes Q_{akm}^i and Q_{bns}^i acting on single quasiparticle states $|A, a\rangle$ and $|B, b\rangle$.

In this figure, the diagram of the big tube around A and B has been reduced to two smaller tubes, one tube Q_{akm}^i around A and Q_{bns}^i around B . Using finally Eq. (C.6) we see that we can write

$$\begin{aligned} Q_{ccj}^i |A, a, B, b, c\rangle &= \sum_{\substack{i,j,s,r, \\ k,m,n}} [F_a^{iia}]_{0r} [F_b^{iib}]_{0s} [F_a^{isi}]_{br} [F_i^{rsj}]_{ck} [F_c^{ksi}]_{jn} [F_i^{aik}]_{rm} \\ &\times \sqrt{\frac{d_i d_a}{d_r}} M_{A,akm}^i M_{B,bns}^i |A, k, B, n, c\rangle. \end{aligned} \quad (\text{C.11})$$

The action of a simple idempotent p_C^{cc} on such a state is therefore

$$p_C^{cc} |A, a, B, b, c\rangle = \sum_{\substack{i,j,s,r, \\ k,m,n}} (M_{C,ccj}^i)^{-1} [F_a^{iia}]_{0r} [F_b^{iib}]_{0s} [F_a^{isi}]_{br} [F_i^{rsj}]_{ck} [F_c^{ksi}]_{jn} [F_i^{aik}]_{rm} \quad (\text{C.12})$$

$$\begin{aligned} &\times \sqrt{\frac{d_i d_a}{d_r}} M_{A,akm}^i M_{B,bns}^i |A, k, B, n, c\rangle \\ &= \sum_{k,n} \mathcal{M}_{kn,ab} |A, k, B, n, c\rangle, \end{aligned} \quad (\text{C.13})$$

where, in the last line, we have introduced the matrix-like notation:

$$\begin{aligned} \mathcal{M}_{kn,ab} &= \sum_{\substack{i,j,s \\ r,m}} [F_a^{iia}]_{0r} [F_b^{iib}]_{0s} [F_a^{isi}]_{br} [F_i^{rsj}]_{ck} [F_c^{kci}]_{jn} [F_i^{aik}]_{rm} \\ &\quad \times \sqrt{\frac{d_i d_a}{d_r}} (M_{C,iccj}^i)^{-1} M_{A,akm}^i M_{B,bns}^i. \end{aligned} \quad (\text{C.14})$$

An important property of Eq. (C.13) is that A , B and c are fixed and that only a and b are mixed into k and n .

The identity operator is obtained by summing Eq. (C.13) over all c and C :

$$\sum_{C,c} p_C^{cc} |A, a, B, b, c\rangle = |A, a, B, b, c\rangle. \quad (\text{C.15})$$

We can construct the eigenvectors of p_C^{cc} by solving the equation

$$\sum_{a,b} \mathcal{M}_{kn,ab} y_{ab} = y_{kn}, \quad (\text{C.16})$$

for all y_{kn} , where

$$|A, B, C, c\rangle = \sum_{a,b} y_{ab} |A, a, B, b, c\rangle. \quad (\text{C.17})$$

Since for every quasiparticle C there is a unique linear combination of the states $|A, a, B, b, c\rangle$, the trace of p_C^{cc} over a and b is always 1 (if C is a fusion outcome of A and B , i.e., the state $|A, B, C, c\rangle$ exists), and zero otherwise:

$$\begin{aligned} \sum_{a,b} \langle A, a, B, b, c | p_C^{cc} |A, a, B, b, c\rangle &= \sum_{a,b} \mathcal{M}_{ab,ab} \\ &= \begin{cases} 1, & \text{if } C \in A \times B \\ 0, & \text{otherwise.} \end{cases} \end{aligned} \quad (\text{C.18})$$

This is the key equation that allows one to obtain the fusion rules, i.e., $N_{A,B}^C$ of the Drinfeld center from the tube algebra.

We also have

$$\text{Tr}_{a,b}(P_C) = \sum_{a,b,c} \mathcal{M}_{ab,ab} = n_C. \quad (\text{C.19})$$

The dimension of the two-quasiparticle Hilbert space can be recovered by computing

$$\dim \mathcal{H}_{2\text{QP}} = \sum_{A,B,C,a,b,c} \mathcal{M}_{ab,ab}. \quad (\text{C.20})$$

C.2 Fusion of a pure fluxon with a fluxon

We now aim at showing that the product of a pure fluxon with another fluxon necessarily gives a fluxon. In the following, we will take A to be a pure fluxon. All its tubes are contained only in the sector 11, so that Eq. (C.18) simplifies to (using identities on the F -symbols):

$$\delta_{c,b} \sum_{i,j} (M_{C,ibbj}^i)^{-1} \frac{1}{d_i} M_{A,11i}^i M_{B,bbj}^i = \begin{cases} 1, & \text{if } C \in A \times B \\ 0, & \text{otherwise.} \end{cases} \quad (\text{C.21})$$

for any sector b of B . In particular, for $b = 1$, we have

$$\sum_i (M_{C,11i}^i)^{-1} \frac{1}{d_i} M_{A,11i}^i M_{B,11i}^i = 1 \quad (\text{C.22})$$

when $C \in A \times B$. If B is a fluxon, there is necessarily some i for which $M_{B,11i}^i$ is nonvanishing. In order to satisfy equation Eq. (C.22), we then see that C must have some nonvanishing $(M_{C,11i}^i)^{-1}$, which means it has weight on the 11 sector and is also a fluxon.

We can go further when the pure fluxon A is the vacuum. In this case, we have a simple expression for $M_{1,11i}^i = d_i$, so that Eq. (C.21) becomes

$$\sum_{i,j} (M_{C,bbj}^i)^{-1} M_{B,bbj}^i = 1. \quad (\text{C.23})$$

Using Eq. (C.4), we see that Eq. (C.23) is true only when $C = B$, as it is expected for the fusion with the vacuum.

C.3 Example: Fibonacci

As an example, let us consider the case where \mathcal{C} is the Fibonacci category. It is a non-Abelian UMTC which contains two objects, 1 and τ . As a UMTC, its Drinfeld center is built as the direct product $\mathcal{C} \times \bar{\mathcal{C}}$ where $\bar{\mathcal{C}}$ is the mirror image of \mathcal{C} (opposite chirality) (see Ref. [85] or Sec. 2.5 for more details).

There are five one-quasiparticle states $|A, a\rangle$: $|(1, 1), 1\rangle, |(1, \tau), \tau\rangle, |(\tau, 1), \tau\rangle, |(\tau, \tau), 1\rangle, |(\tau, \tau), \tau\rangle$, while there are 34 two-quasiparticle states. Let's look in particular at the case where $A = (\tau, \tau)$, $B = (\tau, \tau)$ and $c = 1$. In this subspace, we have two states written in the $|A, a, B, b, c\rangle$ basis as:

$$\begin{aligned} |a_1\rangle &= |(\tau, \tau), 1, (\tau, \tau), 1, 1\rangle, \\ |a_2\rangle &= |(\tau, \tau), \tau, (\tau, \tau), \tau, 1\rangle, \end{aligned} \quad (\text{C.24})$$

while in the basis $|A, B, C, c\rangle$ the two states are

$$\begin{aligned} |b_1\rangle &= |(\tau, \tau), (\tau, \tau), (1, 1), 1\rangle, \\ |b_2\rangle &= |(\tau, \tau), (\tau, \tau), (\tau, \tau), 1\rangle. \end{aligned} \quad (\text{C.25})$$

The relation between the two bases are:

$$|b_1\rangle = \frac{1}{\sqrt{2}}(|a_1\rangle - |a_2\rangle), \quad (\text{C.26})$$

$$|b_2\rangle = \sqrt{\frac{2}{5 + \sqrt{5}}} |a_1\rangle + \sqrt{\frac{5 + \sqrt{5}}{10}} |a_2\rangle. \quad (\text{C.27})$$

For other choices of A, B and c there might exist only one state in which case the two bases are equivalent. For example, when $A = (1, 1)$, $B = (1, 1)$ and $c = 1$, one has

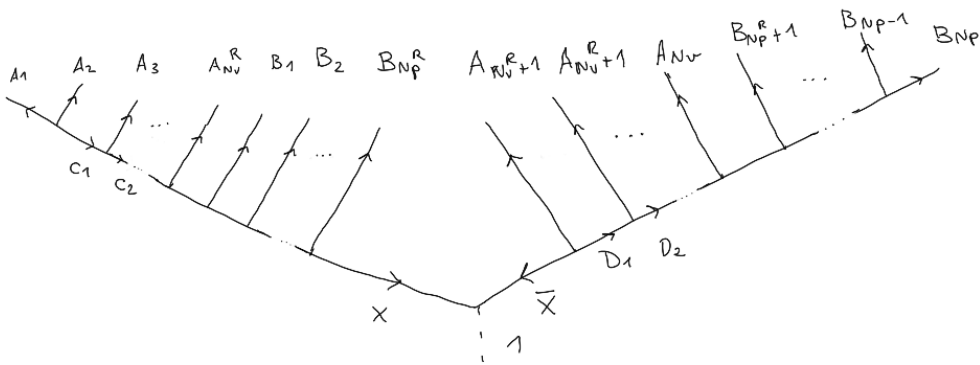
$$|(1, 1), 1, (1, 1), 1, 1\rangle = |(1, 1), (1, 1), (1, 1), 1\rangle. \quad (\text{C.28})$$

Elements of a proof for I_{topo}

This appendix contains the sketch of a proof for the conjecture of I_{topo} , the topological part of the mutual information at finite temperature [see Eqs. (5.107) and (7.31)]. This proof is not yet complete, and the unclear sections are highlighted in the text. In most of this appendix, we consider the KQD model. Additionally, we discuss how far the formulas can be applied to the string-net model.

D.1 Density matrix at finite temperature

For simplicity, we focus on a sphere (genus $g = 0$) in the following, with N_p plaquettes and N_v vertices. Let \mathcal{R} denote a contractible region within this sphere, and $\bar{\mathcal{R}}$ the complementary region, where the first one has $N_p^{\mathcal{R}}$ plaquettes and $N_v^{\mathcal{R}}$ vertices and the other region $N_p - N_p^{\mathcal{R}}$ plaquettes and $N_v - N_v^{\mathcal{R}}$ vertices. Note that this separation in \mathcal{R} and $\bar{\mathcal{R}}$ in terms of plaquettes and vertices (i.e., in terms of anyons) is not the same as a separation in terms of links (see below). Any state in the full Hilbert space of the system can be represented by the following fusion tree:



Here, $A_1, \dots, A_{N_v^{\mathcal{R}}} \in \text{Ch}$ are chargeons located at the vertices in \mathcal{R} , $a_1, \dots, a_{N_v^{\mathcal{R}}}$ index their internal multiplicities (a_i is a positive integer that ranges from 1 to $n_{A_i,1}^{\text{vec}} = d_{A_i}$), and $B_1, \dots, B_{N_p^{\mathcal{R}}} \in \text{Fl}$ are fluxons located at the plaquettes in \mathcal{R} . Similarly, $A_{N_v^{\mathcal{R}}+1}, \dots, A_{N_v}$ and $B_{N_p^{\mathcal{R}}+1}, \dots, B_{N_p}$ are chargeons and fluxons in $\bar{\mathcal{R}}$. All excitations in \mathcal{R} ($\bar{\mathcal{R}}$) can be fused together to give $X \in D(G)$ (\bar{X}). In order to specify a state in the Hilbert space, the labels of the excitations in \mathcal{R} and $\bar{\mathcal{R}}$ is not

enough. One also needs to specify all the fusion channels of these excitations that lead to X in \mathcal{R} and \bar{X} in $\bar{\mathcal{R}}$. These fusion channels correspond to the labels C_1, C_2, \dots and D_1, D_2, \dots in the above fusion tree. While we have only represented a few of these labels, all non-labeled links in the tree are intended to also carry such a label. This fusion tree is actually the same as in Fig. 7.2, where we used it to compute the thermal average of a projector P_X . The structure of this fusion tree shows that we can decompose the full Hilbert space as

$$\mathcal{H} = \bigoplus_{X \in D(G)} N_{X, \bar{X}}^1 \mathcal{H}_X^{\mathcal{R}} \otimes \mathcal{H}_{\bar{X}}^{\bar{\mathcal{R}}}, \quad (\text{D.1})$$

where a basis state in $\mathcal{H}_X^{\mathcal{R}}$ is given by

$$|\phi_X^{\mathcal{R}}\rangle \equiv |A_1, \dots, A_{N_v^{\mathcal{R}}}, a_1, \dots, a_{N_v^{\mathcal{R}}}, B_1, \dots, B_{N_p^{\mathcal{R}}}, C_1, C_2, \dots, X\rangle, \quad (\text{D.2})$$

and similarly for $\mathcal{H}_{\bar{X}}^{\bar{\mathcal{R}}}$. The energy associated with a state $|\phi_X^{\mathcal{R}}\rangle$ by the KQD Hamiltonian is determined by the labels of chargeons $A \in \text{Ch}$ and fluxons $B \in \text{Fl}$ in the region \mathcal{R} . It is

$$E(\phi_X^{\mathcal{R}}) = -J_v \sum_{i=1}^{N_v^{\mathcal{R}}} \delta_{A_i, 1} - J_p \sum_{i=1}^{N_p^{\mathcal{R}}} \delta_{B_i, 1}. \quad (\text{D.3})$$

Clearly, if one takes the sum of $E(\phi_X^{\mathcal{R}})$ and the similarly defined $E(\phi_{\bar{X}}^{\bar{\mathcal{R}}})$, one obtains the energy of a state of the entire system with N_p plaquettes and N_v vertices [see Eq. (6.7)]. With this information, the full density matrix of the system at a finite temperature $T = \frac{1}{\beta}$ can be written

$$\rho = \frac{1}{Z(0, N_p, N_v)} \sum_{X \in D(G)} \sum_{\{\phi_X^{\mathcal{R}}\}} \sum_{\{\phi_{\bar{X}}^{\bar{\mathcal{R}}}\}} e^{-\beta(E(\phi_X^{\mathcal{R}}) + E(\phi_{\bar{X}}^{\bar{\mathcal{R}}}))} |\phi_X^{\mathcal{R}}\rangle |\phi_{\bar{X}}^{\bar{\mathcal{R}}}\rangle \langle \phi_X^{\mathcal{R}}| \langle \phi_{\bar{X}}^{\bar{\mathcal{R}}}|. \quad (\text{D.4})$$

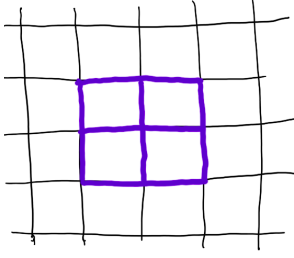
This expression is very similar to the expression of the density matrix for the KQD given in Eq. 50 of Ref. [70]. The main difference between the latter and our expression Eq. (D.4) is that we express the degeneracies in terms of plaquette and vertex excitations, rather than in terms of dyons. This allows us to consider the full Hilbert space instead of a truncated one as in [69, 70].

D.2 Entanglement entropy

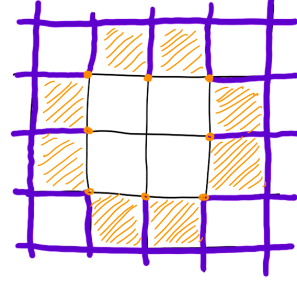
The Von Neumann entropy of a region \mathcal{R} is defined as [31]

$$S_{\mathcal{R}} = S(\rho_{\mathcal{R}}) = -\text{Tr}(\rho_{\mathcal{R}} \ln \rho_{\mathcal{R}}), \quad (\text{D.5})$$

where $\rho_{\mathcal{R}}$ is the reduced density matrix obtained by tracing ρ over the link degrees of freedom in the complementary region, which we will denote here by $\tilde{\mathcal{R}}$. This complementary region in terms of links is in general different from the complementary region $\bar{\mathcal{R}}$ defined above. For illustration, let us consider a region \mathcal{R} on a square lattice, such a shown on Fig. D.1a. This region contains $N_p^{\mathcal{R}}$ plaquettes and $N_v^{\mathcal{R}}$ and $N_l^{\mathcal{R}}$ links. The complementary region of \mathcal{R} in terms of plaquettes and vertices is the region $\bar{\mathcal{R}}$, which contains $N_p - N_p^{\mathcal{R}}$ plaquettes and $N_v - N_v^{\mathcal{R}}$ vertices. The complementary region of \mathcal{R} in terms of links is the region $\tilde{\mathcal{R}}$ which contains $N_l - N_l^{\mathcal{R}}$ links. $\bar{\mathcal{R}}$



(a) Example of a region \mathcal{R} containing four plaquettes and one vertex. The links attributed to this region are highlighted in blue. All other plaquettes and vertices belong to $\bar{\mathcal{R}}$.



(b) The complementary region $\tilde{\mathcal{R}}$ in terms of links contains the links highlighted in blue. Some plaquettes and vertices are neither in \mathcal{R} nor in $\tilde{\mathcal{R}}$. Those are shown in orange.

Figure D.1: Example of attributing links, plaquettes and vertices to two regions. The boundary length $|\partial\mathcal{R}|$ is $N_v - N_v^{\mathcal{R}} - N_v^{\tilde{\mathcal{R}}} = 8$.

and $\tilde{\mathcal{R}}$ do not coincide, as $|\partial\mathcal{R}|$ plaquettes and vertices on the boundary have some links in \mathcal{R} and some links in $\tilde{\mathcal{R}}$. In other words, $N_p = N_p^{\mathcal{R}} + N_p^{\tilde{\mathcal{R}}} = N_p^{\mathcal{R}} + N_p^{\tilde{\mathcal{R}}} + |\partial\mathcal{R}|$, where $N_p^{\tilde{\mathcal{R}}}$ are the plaquettes fully contained in $\tilde{\mathcal{R}}$ (a similar relation holds for the number of vertices). This is illustrated on Figs. D.1a and D.1b.

Reduced density matrix

One main point which remains unclear is how to take the partial trace on ρ defined in Eq. (D.4) over the complementary region $\tilde{\mathcal{R}}$. We approximate this trace by tracing over the degrees of freedom in $\bar{\mathcal{R}}$. For each state $\phi_X^{\mathcal{R}}$, the partial trace over $\bar{\mathcal{R}}$ leads to

$$\begin{aligned} \sum_{\{\phi_X^{\bar{\mathcal{R}}}\}} e^{-\beta E(\phi_X^{\bar{\mathcal{R}}})} &= \sum_{\substack{A_{N_v^{\bar{\mathcal{R}}+1}, \dots, A_{N_v}} \in \text{Ch} \\ B_{N_p^{\bar{\mathcal{R}}+1}, \dots, B_{N_p}} \in \text{Fl}}} \dim_G(0; A_{N_v^{\bar{\mathcal{R}}+1}, \dots, A_{N_v}}, B_{N_p^{\bar{\mathcal{R}}+1}, \dots, B_{N_p}}, \bar{X}) \prod_{k=N_v^{\bar{\mathcal{R}}+1}}^{N_v} n_{A_k, 1}^{\text{vec}} \\ &\times e^{\beta(J_v \sum_{i=N_v^{\bar{\mathcal{R}}+1}}^{N_v} \delta_{A_i, 1} + J_p \sum_{i=N_p^{\bar{\mathcal{R}}+1}}^{N_p} \delta_{B_i, 1})} \\ &= Z_{\bar{X}}(0, N_p - N_p^{\mathcal{R}}, N_v - N_v^{\mathcal{R}}) \equiv Z_{\bar{X}}^{\bar{\mathcal{R}}}, \end{aligned} \quad (\text{D.6})$$

where the effective partition function Z_X has been defined in Eq. (7.23) and in the last line we have introduced a simplified notation for this quantity. The term \dim_G arises from counting the degeneracy for vertex and plaquette excitations in $\bar{\mathcal{R}}$ to fuse into \bar{X} .

Thus, we can express the reduced density matrix as

$$\rho_{\mathcal{R}} = \frac{1}{Z} \sum_{X \in D(G)} \sum_{\{\phi_X^{\mathcal{R}}\}} e^{-\beta E(\phi_X^{\mathcal{R}})} Z_{\bar{X}}^{\bar{\mathcal{R}}} |\phi_X^{\mathcal{R}}\rangle \langle \phi_X^{\mathcal{R}}|, \quad (\text{D.7})$$

where $Z \equiv Z(0, N_p, N_v)$, and the quotation marks indicate that due to the difference between $\tilde{\mathcal{R}}$ and $\bar{\mathcal{R}}$, $|\phi_X^{\mathcal{R}}\rangle \langle \phi_X^{\mathcal{R}}|$ may not be a pure state and may still result in some entanglement entropy (in fact, this state is denoted $\text{Tr}_{\tilde{\mathcal{R}}} |\phi_X^{\mathcal{R}}; \bar{X}\rangle \langle \phi_X^{\mathcal{R}}; \bar{X}|$ in [70]). The matrix $\rho_{\mathcal{R}}$ has a block structure, and

can be rewritten as

$$\rho_{\mathcal{R}} = \bigoplus_X \lambda_X \rho_X^{\mathcal{R}}, \quad (\text{D.8})$$

where

$$\rho_X^{\mathcal{R}} = \sum_{\{\phi_X^{\mathcal{R}}\}} \frac{e^{-\beta E(\phi_X^{\mathcal{R}})}}{Z_X^{\mathcal{R}}} |\phi_X^{\mathcal{R}}\rangle \langle \phi_X^{\mathcal{R}}|, \quad (\text{D.9})$$

and

$$\lambda_X = \frac{Z_X^{\mathcal{R}} Z_X^{\bar{\mathcal{R}}}}{Z} = \langle P_X^{\mathcal{R}} \rangle. \quad (\text{D.10})$$

Entanglement entropy

Using the fact that $\rho_{\mathcal{R}}$ defined in Eq. (D.8) is block diagonal, the Von Neumann entropy can be written

$$S_{\mathcal{R}} = - \sum_X \lambda_X \ln \lambda_X - \sum_X \lambda_X \text{Tr}(\rho_{\mathcal{R}}^X \ln \rho_{\mathcal{R}}^X) = - \sum_X \lambda_X \ln \lambda_X + \sum_X \lambda_X S(\rho_{\mathcal{R}}^X). \quad (\text{D.11})$$

The first term on the right-hand-side of Eq. (D.11) yields an intensive term $-\sum_X \langle P_X^{\mathcal{R}} \rangle \ln \langle P_X^{\mathcal{R}} \rangle$. Understanding the second term is more intricate. Below, we discuss two naive approaches which give a partial answer but are too simple to grasp the entire topological contribution in this second term of Eq. (D.11). Then, we discuss the result for the entanglement entropy given in Ref. [70] and derive the conjecture for I_{topo} from there.

D.3 Topological entanglement entropy and I_{topo}

We will use in the following that the mutual information is obtained from

$$I_{\mathcal{R}} = S_{\mathcal{R}} + S_{\tilde{\mathcal{R}}} - S_{\mathcal{R} \cup \tilde{\mathcal{R}}}, \quad (\text{D.12})$$

where

$$S_{\mathcal{R} \cup \tilde{\mathcal{R}}} = - \frac{\beta}{Z} \frac{\partial Z}{\partial \beta} + \ln(Z). \quad (\text{D.13})$$

The conjecture of [69, 70] is that, for large enough \mathcal{R} and $\tilde{\mathcal{R}}$, the topological part of the mutual information can be written as the Kullback-Leibler divergence between two probability distributions, the thermal distribution $\langle P_X \rangle$ of anyon X and the probability distribution given by the quantum dimensions d_X^2/\mathcal{D}^2 :

$$I_{\text{topo}} = - \sum_{X \in D(G)} \langle P_X^{\mathcal{R}} \rangle \ln \left[\langle P_X^{\mathcal{R}} \rangle \frac{\mathcal{D}^2}{d_X^2} \right]. \quad (\text{D.14})$$

Two naive approaches

Let us in a first step assume that “ $|\phi_X^{\mathcal{R}}\rangle\langle\phi_X^{\mathcal{R}}|$ ” = $|\phi_X^{\mathcal{R}}\rangle\langle\phi_X^{\mathcal{R}}|$ is a pure state and does not contain any entanglement. Then starting from Eq. (D.9), we obtain after a little algebra

$$\begin{aligned}
S(\rho_{\mathcal{R}}^X) &= - \sum_{\{\phi_X^{\mathcal{R}}\}} \frac{e^{-\beta E(\phi_X^{\mathcal{R}})}}{Z_X^{\mathcal{R}}} \ln \frac{e^{-\beta E(\phi_X^{\mathcal{R}})}}{Z_X^{\mathcal{R}}} + S(|\phi_X^{\mathcal{R}}\rangle\langle\phi_X^{\mathcal{R}}|), \\
&= \beta \sum_{\{\phi_X^{\mathcal{R}}\}} E(\phi_X^{\mathcal{R}}) \frac{e^{-\beta E(\phi_X^{\mathcal{R}})}}{Z_X^{\mathcal{R}}} + \sum_{\{\phi_X^{\mathcal{R}}\}} \frac{e^{-\beta E(\phi_X^{\mathcal{R}})}}{Z_X^{\mathcal{R}}} \ln Z_X^{\mathcal{R}} + 0, \\
&= \beta \sum_{\{\phi_X^{\mathcal{R}}\}} E(\phi_X^{\mathcal{R}}) \frac{e^{-\beta E(\phi_X^{\mathcal{R}})}}{Z_X^{\mathcal{R}}} + \ln Z_X^{\mathcal{R}}.
\end{aligned} \tag{D.15}$$

To go to the last line, we have used the definition of the partial partition function $Z_X^{\mathcal{R}}$, see Eq. (7.22). The first term in the sum is proportional to the volume of \mathcal{R} through the energy $E(\phi_X^{\mathcal{R}})$. The second term contains both a volume and an intensive part. Thus we can write:

$$S_{\mathcal{R}}^{\text{topo}} \stackrel{?}{=} - \sum_X \langle P_X^{\mathcal{R}} \rangle \ln \langle P_X^{\mathcal{R}} \rangle + \sum_X \langle P_X^{\mathcal{R}} \rangle (\ln Z_X^{\mathcal{R}})_{\text{intensive}}. \tag{D.16}$$

Before proceeding further, let us analyze in more detail the form of the full entropy Eq. D.13. The first term of this equation is a volume contribution. In fact, a derivation with respect to β of the partition function (see Eq. (7.15)) generates terms that are proportional to N_p and N_v , i.e., the volume of the system. We assume that this contribution cancels with the volume contributions of $S_{\mathcal{R}}$ and $S_{\bar{\mathcal{R}}}$. The second term, $\ln Z$, contains both a volume part and an intensive part (this is straightforward to see from the thermodynamic limit expression of Z , Eq. (7.18) in which case the topological term is $-2 \ln \mathcal{D}$). Using the definition of the mutual information Eq. (D.12), we thus obtain

$$\begin{aligned}
I_{\text{topo}} &\stackrel{?}{=} - \sum_X \langle P_X^{\mathcal{R}} \rangle \ln \langle P_X^{\mathcal{R}} \rangle - \sum_X \langle P_X^{\bar{\mathcal{R}}} \rangle \ln \langle P_X^{\bar{\mathcal{R}}} \rangle + \sum_X \langle P_X^{\mathcal{R}} \rangle \ln \frac{Z_X^{\mathcal{R}} Z_X^{\bar{\mathcal{R}}}}{Z} \\
&= - \sum_X \langle P_X^{\mathcal{R}} \rangle \ln (\langle P_X^{\mathcal{R}} \rangle)^2 + \sum_X \langle P_X^{\mathcal{R}} \rangle \ln \frac{Z_X^{\mathcal{R}} Z_X^{\bar{\mathcal{R}}}}{Z} \\
&= - \sum_X \langle P_X^{\mathcal{R}} \rangle \ln \langle P_X^{\mathcal{R}} \rangle,
\end{aligned} \tag{D.17}$$

where to go from the first to the second line we have used that $\langle P_X^{\mathcal{R}} \rangle = \langle P_X^{\bar{\mathcal{R}}} \rangle$ and in the last line we have used that $\frac{Z_X^{\mathcal{R}} Z_X^{\bar{\mathcal{R}}}}{Z} = \langle P_X^{\mathcal{R}} \rangle$. Thus, this approach is too simple to capture all of the topological mutual information Eq. (D.27). This shows that “ $|\phi_X^{\mathcal{R}}\rangle\langle\phi_X^{\mathcal{R}}|$ ” cannot be a pure state but must still contain some entanglement.

In order to capture this entanglement, the simplest approach is to assume that the term $S(\rho_{\mathcal{R}}^X)$ takes the form

$$S(\rho_{\mathcal{R}}^X) = (\text{volume term}) + S_X^{\text{GS}} \tag{D.18}$$

where the volume contribution is unknown and

$$S_X^{\text{GS}} = \alpha |\partial \mathcal{R}| + \ln \frac{d_X}{\mathcal{D}}. \tag{D.19}$$

is the entropy of a system having a single excitation X in region \mathcal{R} and an excitation \bar{X} in region $\bar{\mathcal{R}}$, while being otherwise in the ground-state (GS) [29]. Here, $|\partial\mathcal{R}|$ is the perimeter of region \mathcal{R} . For a KQD model, $\alpha = \ln \mathcal{D}$.

Keeping only the topological terms in the expression of $S_{\mathcal{R}}$, we find

$$S_{\mathcal{R}}^{\text{topo}} \stackrel{?}{=} - \sum_X \langle P_X^{\mathcal{R}} \rangle \ln \langle P_X^{\mathcal{R}} \rangle + \sum_X \ln \langle P_X^{\mathcal{R}} \rangle \frac{d_X}{\mathcal{D}}. \quad (\text{D.20})$$

Using now Eq. (D.12) we find that the topological part of the mutual information should be written

$$\begin{aligned} I_{\text{topo}} & \quad (\text{D.21}) \\ & \stackrel{?}{=} - \sum_X \langle P_X^{\mathcal{R}} \rangle \ln \langle P_X^{\mathcal{R}} \rangle + \sum_X \langle P_X^{\mathcal{R}} \rangle \ln \frac{d_X}{\mathcal{D}} - \sum_X \langle P_{\bar{X}}^{\mathcal{R}} \rangle \ln \langle P_{\bar{X}}^{\mathcal{R}} \rangle + \sum_X \langle P_{\bar{X}}^{\mathcal{R}} \rangle \ln \frac{d_{\bar{X}}}{\mathcal{D}} - (\ln Z)_{\text{intensive}} \\ & = - \sum_X \langle P_X^{\mathcal{R}} \rangle \ln \frac{\langle P_X^{\mathcal{R}} \rangle \mathcal{D}^2}{d_X^2} - \sum_X \langle P_X^{\mathcal{R}} \rangle \ln \langle P_X^{\mathcal{R}} \rangle - (\ln Z)_{\text{intensive}}, \end{aligned}$$

where to go from the first to the second line we have again used that $\langle P_X^{\mathcal{R}} \rangle = \langle P_{\bar{X}}^{\mathcal{R}} \rangle$ and $d_X = d_{\bar{X}}$. While the first term of this expression corresponds to the conjecture Eq. (D.27), we should expect the two other terms to cancel each other, which is however not the case. This hints at the fact that with this approach, we are missing some terms in the expression of $S_{\mathcal{R}}^{\text{topo}}$ as defined in Eq. (D.20).

I_{topo} from the formula for $S_{\mathcal{R}}$ of Ref. [70]

Ref. [70] provides a formula (see Eq.(52) in the article) for the entanglement entropy at finite temperature of the KQD model. While this formula describes a situation where quasiparticles are pinned at sites (in [70] and [47], a *site* is defined as a combination of adjacent vertex and plaquette, on which lives a dyon) distant from each other, it can be quickly reformulated in terms of only vertex and plaquette excitations by using, amongst others, Eq. (7.1). This reformulation makes it obvious that the formula should hold also if excitations are close to each other, and that there is no need to have an equal number of vertices and plaquettes. This formula for the entropy is the following:

$$\begin{aligned} S_{\mathcal{R}} = & - \sum_{X \in D(G)} \sum_{\substack{A_1, \dots, A_{N_V^{\mathcal{R}}} \in \text{Ch} \\ B_1, \dots, B_{N_P^{\mathcal{R}}} \in \text{Fl}}} \prod_{i=1}^{N_V^{\mathcal{R}}} n_{A_i,1}^{\text{vec}} \prod_{i=1}^{N_P^{\mathcal{R}}} n_{B_i,1}^{\text{rep}} \dim_G(0; A_1, \dots, A_{N_V^{\mathcal{R}}}, B_1, \dots, B_{N_P^{\mathcal{R}}}, \bar{X}) \quad (\text{D.22}) \\ & \times e^{\beta(J_V \sum_{i=1}^{N_V^{\mathcal{R}}} \delta_{A_i,1} + J_P \sum_{i=1}^{N_P^{\mathcal{R}}} \delta_{B_i,1})} \frac{Z_{\bar{\mathcal{R}}}^{\bar{X}}}{Z} \left[\ln \left(e^{\beta(J_V \sum_{i=1}^{N_V^{\mathcal{R}}} \delta_{A_i,1} + J_P \sum_{i=1}^{N_P^{\mathcal{R}}} \delta_{B_i,1})} \frac{Z_{\bar{\mathcal{R}}}^{\bar{X}}}{Z} \right) - S_X^{\text{GS}} \right], \end{aligned}$$

where S_X^{GS} was defined in Eq. (D.19). We can separate this expression into different terms:

$$\begin{aligned}
S_{\mathcal{R}} &= -\beta \sum_{X \in D(G)} \sum_{\substack{A_1, \dots, A_{N_v^{\mathcal{R}}} \in \text{Ch} \\ B_1, \dots, B_{N_p^{\mathcal{R}}} \in \text{Fl}}} \prod_{i=1}^{N_v^{\mathcal{R}}} n_{A_i,1}^{\text{vec}} \prod_{i=1}^{N_p^{\mathcal{R}}} n_{B_i,1}^{\text{rep}} \dim_G(0; A_1, \dots, A_{N_v^{\mathcal{R}}}, B_1, \dots, B_{N_p^{\mathcal{R}}}, \bar{X}) \frac{Z_{\bar{\mathcal{R}}}^{\bar{X}}}{Z} \\
&\times (J_v \sum_{i=1}^{N_v^{\mathcal{R}}} \delta_{A_i,1} + J_p \sum_{i=1}^{N_p^{\mathcal{R}}} \delta_{B_i,1}) e^{-\beta(J_v \sum_{i=1}^{N_v^{\mathcal{R}}} \delta_{A_i,1} + J_p \sum_{i=1}^{N_p^{\mathcal{R}}} \delta_{B_i,1})} \\
&- \sum_X P_X^{\mathcal{R}} \ln \left[\frac{Z_{\bar{\mathcal{R}}}^{\bar{X}}}{Z} \right] + \sum_X P_X^{\mathcal{R}} \ln \left[\frac{d_X}{\mathcal{D}} \right] + |\partial \mathcal{R}| \ln \mathcal{D}. \tag{D.23}
\end{aligned}$$

With a few steps of algebra involving Eq. (7.10), (7.2) and (7.23), we arrive at

$$\begin{aligned}
S_{\mathcal{R}} &= -\frac{\beta J_p N_p^{\mathcal{R}}}{Z} e^{\beta J_p} \sum_A S_{1,A}^{2-2g} \left(\frac{n_{A,1}^{\text{rep}}}{S_{A,1}} - 1 + e^{\beta J_p} \right)^{N_p-1} \times \left(\frac{n_{A,1}^{\text{vec}}}{S_{A,1}} - 1 + e^{\beta J_v} \right)^{N_v} \\
&- \frac{\beta J_v N_v^{\mathcal{R}}}{Z} e^{\beta J_v} \sum_A S_{1,A}^{2-2g} \left(\frac{n_{A,1}^{\text{rep}}}{S_{A,1}} - 1 + e^{\beta J_p} \right)^{N_p} \left(\frac{n_{A,1}^{\text{vec}}}{S_{A,1}} - 1 + e^{\beta J_v} \right)^{N_v-1} \\
&- \sum_X \langle P_X^{\mathcal{R}} \rangle \ln \left[\frac{Z_{\bar{\mathcal{R}}}^{\bar{X}}}{Z} \right] + \sum_X \langle P_X^{\mathcal{R}} \rangle \ln \left[\frac{d_X}{\mathcal{D}} \right] + |\partial \mathcal{R}| \ln \mathcal{D}. \tag{D.24}
\end{aligned}$$

Here, only the last term depends on $|\partial \mathcal{R}|$ (i.e., is an area contribution). This term is temperature-independent. The two first terms are proportional to the volume of \mathcal{R} (through $N_p^{\mathcal{R}}$ and $N_v^{\mathcal{R}}$). The topological part of the entropy is thus contained in the two remaining terms, with the subtlety that $\sum_X P_X^{\mathcal{R}} \ln \left[\frac{Z_{\bar{\mathcal{R}}}^{\bar{X}}}{Z} \right]$ splits into a topological and a volume contribution. Using again $\frac{Z_X^{\mathcal{R}} Z_{\bar{X}}^{\mathcal{R}}}{Z} = \langle P_X^{\mathcal{R}} \rangle$, we obtain

$$S_{\mathcal{R}}^{\text{topo}} = \sum_X \langle P_X^{\mathcal{R}} \rangle \ln \frac{d_X}{\mathcal{D} \langle P_X^{\mathcal{R}} \rangle} + \sum_X \langle P_X^{\mathcal{R}} \rangle (\ln Z_X^{\mathcal{R}})_{\text{intensive}}. \tag{D.25}$$

It is interesting to note that this result appears to be a combination of our guesses of Eqs. D.16 and D.20.

What is the validity of Eq. (D.23)? We verified numerically on small lattice systems that this formula correctly gives the entanglement entropy of a region \mathcal{R} of the KQD model at any finite temperature. It also gives the correct results for $\text{Vec}(G)$ string-net models when taking $J_p \rightarrow \infty$. It is therefore reasonable to expect that in the limit $J_v \rightarrow \infty$, and replacing the area law term $|\partial \mathcal{R}| \ln \mathcal{D}$ with the area law term for string-net models of Eq. (5.95), one obtains the entanglement entropy for (at least $\text{Rep}(G)$) string-net models. In practice, Eq. (D.23) yields the correct results for a system at the thermodynamic limit at zero temperature and at infinite temperature. However, it does not give correct results for a string-net model on a small lattice system at intermediate temperatures.

Let us now use Eq. (D.23) to derive I_{topo} . For simplicity, we will assume in the following that the system is very large, and so is region \mathcal{R} , so that $N_v^{\mathcal{R}}$ and $N_p^{\mathcal{R}}$ are much larger than $|\partial \mathcal{R}|$. In this case, one has $\bar{\mathcal{R}} \simeq \tilde{\mathcal{R}}$.

Considering only the topological contributions in Eq. (D.12), we can then write, using Eq. (D.25):

$$I_{\text{topo}} = \sum_X P_X^{\mathcal{R}} \ln \frac{d_X}{\mathcal{D}P_X^{\mathcal{R}}} + \sum_X P_X^{\mathcal{R}} (\ln Z_X^{\mathcal{R}}) + \sum_X P_X^{\bar{\mathcal{R}}} \ln \frac{d_X}{\mathcal{D}P_X^{\bar{\mathcal{R}}}} + \sum_X P_X^{\bar{\mathcal{R}}} (\ln Z_X^{\bar{\mathcal{R}}}) - \ln Z. \quad (\text{D.26})$$

Using that $P_X^{\mathcal{R}} = P_X^{\bar{\mathcal{R}}}$ and $d_X = d_{\bar{X}}$, it is now easy to show that

$$I_{\text{topo}} = - \sum_{X \in \mathcal{Z}(G)} \langle P_X^{\mathcal{R}} \rangle \ln \left[\langle P_X^{\mathcal{R}} \rangle \frac{\mathcal{D}^2}{d_X^2} \right], \quad (\text{D.27})$$

which is exactly the conjecture of Ref. [70]. It is also possible to show that the volume terms of $S_{\mathcal{R}}$, $S_{\bar{\mathcal{R}}}$ and $S_{\mathcal{R} \cup \bar{\mathcal{R}}}$ cancel with each other, and that the area term of the mutual information for a large system is $2|\partial\mathcal{R}|$.

Bibliography

Bibliography

- [1] J. M. Leinaas and J. Myrheim. "On the theory of identical particles". In: *Nuovo Cim. B* 37 (1977), p. 1.
- [2] F. Wilczek. "Quantum mechanics of fractional-spin particles". In: *Phys. Rev. Lett.* 49 (1982), p. 957.
- [3] J. Froehlich and F. Gabbiani. "Braid statistics in local quantum theory". In: *Rev. Math. Phys.* 2 (1990), p. 251.
- [4] K. Fredenhagen, K. H. Rehren, and B. Schroer. "Superselection sectors with braid group statistics and exchange algebras". In: *Commun. Math. Phys.* 125 (1989), p. 201.
- [5] E. Witten. "Quantum field theory and the Jones polynomial". In: *Commun. Math. Phys.* 121 (1989), p. 351.
- [6] M. Schulz. "Topological phase transitions driven by non-Abelian anyons", Ph. D. Thesis, Universität Dortmund, (2013).
- [7] Y. Aharonov and D. Bohm. "Significance of electromagnetic potentials in the quantum theory". In: *Phys. Rev.* 115 (1959), p. 485.
- [8] D. C. Tsui, H. L. Stormer, and A. C. Gossard. "Two-dimensional magnetotransport in the extreme quantum limit". In: *Phys. Rev. Lett.* 48 (1982), p. 1559.
- [9] S. M. Girvin. "The quantum Hall effect: Novel excitations and broken symmetries", *arXiv:cond-mat/9907002*.
- [10] H. Bartolomei et al. "Fractional statistics in anyon collisions". In: *Science* 368 (2020), p. 173.
- [11] J. Nakamura et al. "Direct observation of anyonic braiding statistics". In: *Nat. Phys.* 16 (2020), p. 931.
- [12] R. L. Willett et al. "Magnetic-field-tuned Aharonov-Bohm oscillations and evidence for non-Abelian anyons at $\nu = 5/2$ ". In: *Phys. Rev. Lett.* 111 (2013), p. 186401.
- [13] X.-G. Wen. "Topological orders in rigid states". In: *Int. J. Mod. Phys. B* 04 (1990), p. 239.
- [14] X.-G. Wen. "Zoo of quantum-topological phases of matter". In: *Rev. Mod. Phys.* 89 (2017), p. 041004.

- [15] L. D. Landau. "The theory of phase transitions". In: *Nature* 138 (1936), p. 840.
- [16] R. B. Laughlin. "Anomalous quantum Hall effect: An incompressible quantum fluid with fractionally charged excitations". In: *Phys. Rev. Lett.* 50 (1983), p. 1395.
- [17] X.-G. Wen, F. Wilczek, and A. Zee. "Chiral spin states and superconductivity". In: *Phys. Rev. B* 39 (1989), p. 11413.
- [18] X.-G. Wen. "Vacuum degeneracy of chiral spin states in compactified space". In: *Phys. Rev. B* 40 (1989), p. 7387.
- [19] J. G. Bednorz and K. A. Müller. "Possible high T_c superconductivity in the Ba-La-Cu-O system". In: *Z. Phys. B* 64 (1986), p. 189.
- [20] X.-G. Wen and Q. Niu. "Ground-state degeneracy of the fractional quantum Hall states in the presence of a random potential and on high-genus Riemann surfaces". In: *Phys. Rev. B* 41 (1990), p. 9377.
- [21] J. Cayssol and J.-N. Fuchs. "Topological and geometrical aspects of band theory". In: *Journal of Physics: Materials* 4.3 (2021), p. 034007.
- [22] M. Oshikawa and T. Senthil. "Fractionalization, topological order, and quasiparticle statistics". In: *Phys. Rev. Lett.* 96.6 (2006).
- [23] T. H. Hansson, V. Oganesyan, and S. L. Sondhi. "Superconductors are topologically ordered". In: *Annals of Physics* 313.2 (2004), p. 497.
- [24] T. Lan, L. Kong, and X.-G. Wen. "Classification of $(3 + 1)$ D bosonic topological orders: The case when pointlike excitations are all bosons". In: *Phys. Rev. X* 8 (2018), p. 021074.
- [25] E. Keski-Vakkuri and X.-G. Wen. "The ground-state structure and modular transformations of fractional quantum Hall states on a torus". In: *Int. J. Mod. Phys. B* 07.25 (1993), p. 4227.
- [26] X.-G. Wen and A. Zee. "Topological degeneracy of quantum Hall fluids". In: *Phys. Rev. B* 58 (1998), p. 15717.
- [27] E. Verlinde. "Fusion rules and modular transformations in 2D conformal field theory". In: *Nucl. Phys. B* 300 (1988), p. 360.
- [28] S. H. Simon, "Topological Quantum", Oxford University Press (2023).
- [29] A. Kitaev and J. Preskill. "Topological entanglement entropy". In: *Phys. Rev. Lett.* 96 (2006), p. 110404.
- [30] M. A. Levin and X.-G. Wen. "Detecting topological order in a ground state wave function". In: *Phys. Rev. Lett.* 96 (2006), p. 110405.
- [31] A. Hamma, R. Ionicioiu, and P. Zanardi. "Ground state entanglement and geometric entropy in the Kitaev's model". In: *Phys. Lett. A* 337 (2005), p. 22.
- [32] A. Kitaev. "Anyons in an exactly solved model and beyond". In: *Ann. Phys. (NY)* 321 (2006), p. 2.
- [33] L. Kong and Z.-H. Zhang. "An invitation to topological orders and category theory", *arxiv:2205.05565*.

- [34] M. Mignard and P. Schauenburg. “Modular categories are not determined by their modular data”. In: *Lett. Math. Phys.* 111 (2021), p. 60.
- [35] Z.-C. Gu, Z. Wang, and X.-G. Wen. “Classification of two-dimensional fermionic and bosonic topological orders”. In: *Phys. Rev. B* 91.12 (2015), p. 125149.
- [36] X.-G. Wen. “A theory of 2+1D bosonic topological orders”. In: *National Science Review* 3.1 (2015), p. 68.
- [37] F. A. Bais and J. C. Romers. “The modular S-matrix as order parameter for topological phase transitions”. In: *New Journal of Physics* 14.3 (2012), p. 035024.
- [38] Z. Nussinov and G. Ortiz. “Autocorrelations and thermal fragility of anyonic loops in topologically quantum ordered systems”. In: *Phys. Rev. B* 77 (2008), p. 064302.
- [39] Z. Nussinov and G. Ortiz. “A symmetry principle for topological quantum order”. In: *Ann. Phys. (NY)* 324.5 (2009), p. 977.
- [40] Z. Nussinov and G. Ortiz. “Sufficient symmetry conditions for topological quantum order”. In: *Proc. Natl. Acad. Sci. U.S.A.* 106 (2009), p. 16944.
- [41] F. Wegner. “Duality in generalized Ising models and phase transitions without local order parameters”. In: *J. Math. Phys.* 12 (1971), p. 2259.
- [42] S. Sachdev. “Topological order, emergent gauge fields, and Fermi surface reconstruction”. In: *Rep. Prog. Phys.* 82 (2019), p. 014001.
- [43] K. G. Wilson. “Confinement of quarks”. In: *Phys. Rev. D* 10 (1974), p. 2445.
- [44] F. A. Bais. “Flux metamorphosis”. In: *Nucl. Phys. B* 170 (1980), p. 32.
- [45] F. A. Bais, P. van Driel, and M. de Wild Propitius. “Quantum symmetries in discrete gauge theories”. In: *Phys. Lett. B* 280.1–2 (1992), p. 63.
- [46] F. A. Bais, P. van Driel, and M. de Wild Propitius. “Anyons in discrete gauge theories with Chern-Simons terms”. In: *Nucl. Phys. B* 393.3 (1993), p. 547.
- [47] A. Kitaev. “Fault-tolerant quantum computation by anyons”. In: *Ann. Phys. (NY)* 303 (2003), p. 2.
- [48] M. A. Levin and X.-G. Wen. “String-net condensation: A physical mechanism for topological phases”. In: *Phys. Rev. B* 71 (2005), p. 045110.
- [49] O. Buerschaper and M. Aguado. “Mapping Kitaev’s quantum double lattice models to Levin and Wen’s string-net models”. In: *Phys. Rev. B* 80 (2009), p. 155136.
- [50] O. Buerschaper et al. “Electric–magnetic duality of lattice systems with topological order”. In: *Nucl. Phys. B* 876.2 (2013), p. 619.
- [51] M. Müger. “From subfactors to categories and topology II: The quantum double of tensor categories and subfactors”. In: *J. Pure Appl. Algebra* 180 (2003), p. 159.
- [52] A. Kapustin and L. Fidkowski. “Local commuting projector Hamiltonians and the quantum Hall effect”. In: *Commun. Math. Phys.* 373.2 (2019), p. 763.

- [53] C. Zhang, M. Levin, and S. Bachmann. "Vanishing Hall conductance for commuting Hamiltonians". In: *Phys. Rev. B* 105.8 (2022).
- [54] M. H. Freedman et al. "Topological quantum computation". In: *Bull. Amer. Math. Soc.* 40 (2003), p. 31.
- [55] C. Nayak et al. "Non-Abelian anyons and topological quantum computation". In: *Rev. Mod. Phys.* 80 (2008), p. 1083.
- [56] S. Bravyi, M. B. Hastings, and S. Michalakis. "Topological quantum order: Stability under local perturbations". In: *J. Math. Phys.* 51.9 (2010).
- [57] B. J. Brown et al. "Quantum memories at finite temperature". In: *Rev. Mod. Phys.* 88.4 (2016).
- [58] C. Song et al. "Demonstration of topological robustness of anyonic braiding statistics with a superconducting quantum circuit". In: *Phys. Rev. Lett.* 121 (2018), p. 030502.
- [59] C. K. Andersen et al. "Repeated quantum error detection in a surface code". In: *Nat. Phys.* 16 (2020), p. 875.
- [60] Google Quantum AI. "Exponential suppression of bit or phase errors with cyclic error correction". In: *Nature* 595 (2021), p. 383.
- [61] S. Xu et al. "Digital simulation of projective non-Abelian anyons with 68 superconducting qubits". In: *Chin. Phys. Lett.* 40 (2023), p. 060301.
- [62] K. J. Satzinger et al. "Realizing topologically ordered states on a quantum processor". In: *Science* 374.6572 (2021), p. 1237.
- [63] Z. Luo et al. "Experimentally probing topological order and its breakdown through modular matrices". In: *Nat. Phys.* 14.2 (2017), p. 160.
- [64] Z. K. Mineev et al. "Realizing string-net condensation: Fibonacci anyon braiding for universal gates and sampling chromatic polynomials", *arXiv.2406.12820*.
- [65] K. Li et al. "Experimental identification of non-Abelian topological orders on a quantum simulator". In: *Phys. Rev. Lett.* 118 (2017), p. 080502.
- [66] S. Xu et al. "Non-Abelian braiding of Fibonacci anyons with a superconducting processor". In: *Nat. Phys.* (2024).
- [67] M. Hastings. "Topological order at nonzero temperature". In: *Phys. Rev. Lett.* 107 (2011), p. 210501.
- [68] C. Castelnovo and C. Chamon. "Entanglement and topological entropy of the toric code at finite temperature". In: *Phys. Rev. B* 76 (2007), p. 184442.
- [69] S. Iblisdir et al. "Scaling law for topologically ordered systems at finite temperature". In: *Phys. Rev. B* 79 (2009), p. 134303.
- [70] S. Iblisdir et al. "Thermal states of anyonic systems". In: *Nucl. Phys. B* 829 (2010), p. 401.
- [71] R. Alicki, M. Fannes, and M. Horodecki. "On thermalization in Kitaev's 2D model". In: *J. Phys. A* 42.6 (2009), p. 065303.

- [72] A. Lucia, D. Pérez-García, and A. Pérez-Hernández. "Thermalization in Kitaev's quantum double models via tensor network techniques". In: *Forum of Mathematics, Sigma* 11 (2023).
- [73] O. Landon-Cardinal and D. Poulin. "Local topological order inhibits thermal stability in 2D". In: *Phys. Rev. Lett.* 110.9 (2013).
- [74] C. Castelnovo and C. Chamon. "Topological order and topological entropy in classical systems". In: *Phys. Rev. B* 76 (2007), p. 174416.
- [75] Z. Weinstein, G. Ortiz, and Z. Nussinov. "Universality classes of stabilizer code Hamiltonians". In: *Phys. Rev. Lett.* 123 (2019), p. 230503.
- [76] M. Hermanns and S. Trebst. "Renyi entropies for classical string-net models". In: *Phys. Rev. B* 89 (2014), p. 205107.
- [77] A. Hahn and R. Wolf. "Generalized string-net model for unitary fusion categories without tetrahedral symmetry". In: *Phys. Rev. B* 102 (2020), p. 115154.
- [78] C.-H. Lin, M. Levin, and F. J. Burnell. "Generalized string-net models: A thorough exposition". In: *Phys. Rev. B* 103 (2021), p. 195155.
- [79] K. Beer et al. "From categories to anyons: a travelogue", *arxiv:1811.06670*.
- [80] R. Wolf. "Microscopic models for fusion categories", Ph. D. thesis, Leibniz Universität Hannover, (2020).
- [81] A. Ritz-Zwilling et al. "Topological and nontopological degeneracies in generalized string-net models". In: *Phys. Rev. B* 109 (2024), p. 045130.
- [82] P. H. Bonderson. "Non-Abelian anyons and interferometry", Ph. D. thesis, Caltech, (2007).
- [83] Z. Wang, "Topological Quantum Computation", CBMS Regional Conference Series in Mathematics, No. 112 (American Mathematical Society, Providence, RI, 2010).
- [84] T. Lan and X.-G. Wen. "Topological quasiparticles and the holographic bulk-edge relation in $(2 + 1)$ -dimensional string-net models". In: *Phys. Rev. B* 90 (2014), p. 115119.
- [85] E. Rowell, R. Stong, and Z. Wang. "On classification of modular tensor categories". In: *Commun. Math. Phys.* 292 (2009), p. 343.
- [86] V. G. Turaev and O. Y. Viro. "State sum invariants of 3-manifolds and quantum 6j-symbols". In: *Topology* 31 (1992), p. 865.
- [87] V. Pasquier. "Operator content of the ADE lattice models". In: *J. Phys. A* 20 (1987), p. 5707.
- [88] C. L. Kane and M. P. A. Fisher. "Quantized thermal transport in the fractional quantum Hall effect". In: *Phys. Rev. B* 55 (1997), p. 15832.
- [89] J. Slingerland and G. Vercleyen. "AnyonWiki", www.thphys.nuim.ie/AnyonWiki/index.php.
- [90] A. Ocneanu. "Chirality for operator algebras, Subfactors" (World Scientific, Singapore, 1994), p. 39.
- [91] A. Ocneanu. "Operator algebras, topology and subgroups of quantum symmetry -construction of subgroups of quantum groups-". In: *Adv. Stud. Pure Math.* 31 (2001), p. 235.

- [92] L. Lootens, B. Vancraeynest-De Cuiper, N. Schuch and F. Verstraete. "Mapping between Morita-equivalent string-net states with a constant depth quantum circuit". In: *Phys. Rev. B* 105 (2022), p. 085130.
- [93] Y. Hu, N. Geer, and Y.-S. Wu. "Full dyon excitation spectrum in extended Levin-Wen models". In: *Phys. Rev. B* 97 (2018), p. 195154.
- [94] A. Soares. "Spectral degeneracies of extended string-net models", Master thesis, Université Paris-Saclay (2024).
- [95] C.-H. Lin and M. Levin. "Generalizations and limitations of string-net models". In: *Phys. Rev. B* 89 (2014), p. 195130.
- [96] A. Kitaev and L. Kong. "Models for gapped boundaries and domain walls ". In: *Commun. Math. Phys.* 313 (2012), p. 351.
- [97] L. Kong. "Anyon condensation and tensor categories". In: *Nucl. Phys. B* 886 (2014), p. 436.
- [98] M. Levin and X.-G. Wen. "Fermions, strings, and gauge fields in lattice spin models". In: *Phys. Rev. B* 67 (2003), p. 245316.
- [99] F. J. Burnell and S. H. Simon. "Space-time geometry of topological phases". In: *Ann. Phys. (NY)* 325 (2010), p. 2550.
- [100] F. J. Burnell and S. H. Simon. "A Wilson line picture of the Levin-Wen partition functions". In: *New J. Phys.* 13 (2011), p. 065001.
- [101] Z. Kádár, A. Marzuoli, and M. Rasetti. "Microscopic description of 2D topological phases, duality, and 3D state sums". In: *Adv. Math. Phys.* 2010 (2010), p. 671039.
- [102] A. Kirillov. *String-net model of Turaev-Viro invariants*. "String-net model of Turaev-Viro invariants", *arXiv:1106.6033*.
- [103] Y. Hu, S. D. Stirling, and Y.-S. Wu. "Ground-state degeneracy in the Levin-Wen model for topological phases". In: *Phys. Rev. B* 85 (2012), p. 075107.
- [104] M. A. Levin. "Protected edge modes without symmetry". In: *Phys. Rev. X* 3 (2013), p. 021009.
- [105] J. C. Wang, C. Juven, and X.-G. Wen. "Boundary degeneracy of topological order". In: *Phys. Rev. B* 91.12 (2015).
- [106] M. D. Schulz et al. "Topological phase transitions in the golden string-net model". In: *Phys. Rev. Lett.* 110 (2013), p. 147203.
- [107] M. D. Schulz et al. "Ising anyons with a string tension". In: *Phys. Rev. B* 89 (2014), 201103(R).
- [108] M. D. Schulz, S. Dusuel, and J. Vidal. "Russian doll spectrum in a non-Abelian string-net ladder". In: *Phys. Rev. B* 91 (2015), p. 155110.
- [109] Y. Hu, S. D. Stirling, and Y.-S. Wu. "Emergent exclusion statistics of quasiparticles in two-dimensional topological phases". In: *Phys. Rev. B* 89 (2014), p. 115133.
- [110] J. Vidal. "Partition function of the Levin-Wen model". In: *Phys. Rev. B* 105 (2022), p. L041110.
- [111] G. Moore and N. Seiberg. "Classical and quantum conformal field theory". In: *Commun. Math. Phys.* 123 (1989), p. 177.

- [112] M. Iqbal et al. "Non-Abelian topological order and anyons on a trapped-ion processor". In: *Nature* 626.7999 (2024), p. 505.
- [113] J. Jovanović, C. Wille, D. Timmers, S. H. Simon. "A proposal to demonstrate non-abelian anyons on a NISQ device", *arXiv:2306.13129*.
- [114] N. Reshetikhin and V. G. Turaev. "Invariants of 3-manifolds via link polynomials and quantum groups". In: *Invent. Math.* 103 (1991), p. 547.
- [115] Y. Zhao et al. "Characteristic properties of a composite system of topological phases separated by gapped domain walls via an exactly solvable Hamiltonian model". In: *SciPost Physics Core* 6.4 (2023).
- [116] T. Neupert et al. "Boson condensation in topologically ordered quantum liquids". In: *Phys. Rev. B* 93 (2016), p. 115103.
- [117] T. Lan, J. C. Wang, and X.-G. Wen. "Gapped domain walls, gapped boundaries, and topological degeneracy". In: *Phys. Rev. Lett.* 114 (2015), p. 076402.
- [118] F. A. Bais and J. K. Slingerland. "Condensate-induced transitions between topologically ordered phases". In: *Phys. Rev. B* 79 (2009), p. 045316.
- [119] F. J. Burnell. "Anyon Condensation and Its Applications". In: *Annual Review of Condensed Matter Physics* 9.1 (2018), p. 307.
- [120] I. Cong, M. Cheng, and Z. Wang. "Topological quantum computation with gapped boundaries", *arXiv:1609.02037*.
- [121] S. Beigi, P. W. Shor, and D. Whalen. "The quantum double model with boundary: Condensations and symmetries". In: *Commun. Math. Phys.* 306 (2011), p. 663.
- [122] N. Bultinck et al. "Anyons and matrix product operator algebras". In: *Ann. Phys. (NY)* 378 (2017), p. 183.
- [123] L. Lootens, C. Delcamp, and F. Verstraete. "Dualities in one-dimensional quantum lattice models: topological sectors", *arXiv:2211.03777*.
- [124] E. Lake and Y.-S. Wu. "Signatures of broken parity and time reversal symmetry in generalized string-net models". In: *Phys. Rev. B* 94.11 (2016), p. 115139.
- [125] S.-M. Hong, E. Rowell, and Z. Wang. "On exotic modular categories". In: *Commun. Contemp. Math.* 10 (2008), p. 1049.
- [126] R. Vanhove et al. "Critical lattice model for a Haagerup conformal field theory". In: *Phys. Rev. Lett.* 128 (2022), p. 231602.
- [127] E. Dennis et al. "Topological quantum memory". In: *J. Math. Phys.* 43.9 (2002), p. 4452.
- [128] A. Ritz-Zwilling, J.-N. Fuchs, and J. Vidal. "Wegner-Wilson loops in string nets". In: *Phys. Rev. B* 103 (2021), p. 075128.
- [129] G. B. Halász and A. Hamma. "Probing topological order with Rényi entropy". In: *Phys. Rev. A* 86 (2012), p. 062330.
- [130] A. Ritz-Zwilling et al. "Finite-temperature properties of string-net models", *arxiv:2406.19713*.

- [131] K. Gregor et al. "Diagnosing deconfinement and topological order". In: *New J. Phys.* 13 (2011), p. 025009.
- [132] F. Y. Wu. "The Potts model". In: *Rev. Mod. Phys.* 54 (1982), p. 235.
- [133] J. Kogut. "An introduction to lattice gauge theory and spin systems". In: *Rev. Mod. Phys.* 51 (1979), p. 659.
- [134] D. Tong. Lectures on theoretical physics, University of Cambridge, www.damp.cam.ac.uk/user/tong/teaching.html.
- [135] E. Fradkin and S. H. Shenker. "Phase diagrams of lattice gauge theories with Higgs fields". In: *Phys. Rev. D* 19 (1979), p. 3682.
- [136] M. B. Hastings and X.-G. Wen. "Quasiadiabatic continuation of quantum states: The stability of topological ground-state degeneracy and emergent gauge invariance". In: *Phys. Rev. B* 72 (2005), p. 045141.
- [137] S. Dong et al. "Topological entanglement entropy in Chern-Simons theories and quantum Hall fluids". In: *J. High Energ. Phys.* 2008.05 (2008), p. 016.
- [138] X. Chen. "Many-body entanglement in gapped quantum systems", Ph. D. thesis, MIT, (2012).
- [139] S. T. Flammia et al. "Topological entanglement Rényi entropy and reduced density matrix structure". In: *Phys. Rev. Lett.* 103.26 (2009).
- [140] H. Li and F. D. M. Haldane. "Entanglement spectrum as a generalization of entanglement entropy: Identification of topological order in non-Abelian fractional quantum Hall effect states". In: *Phys. Rev. Lett.* 101.1 (2008).
- [141] J. C. Bridgeman, B. J. Brown, and S. J. Elman. "Boundary topological entanglement entropy in two and three dimensions". In: *Commun. Math. Phys.* 389.2 (2021), p. 1241.
- [142] A. Bullivant and J. K. Pachos. "Entropic manifestations of topological order in three dimensions". In: *Phys. Rev. B* 93 (2016), p. 125111.
- [143] P. Bonderson, C. Knapp, and K. Patel. "Anyonic entanglement and topological entanglement entropy". In: *Annals of Physics* 385 (2017), p. 399.
- [144] H. Bombin and M. A. Martin-Delgado. "Family of non-Abelian Kitaev models on a lattice: Topological condensation and confinement". In: *Phys. Rev. B* 78.11 (2008).
- [145] J. Preskill, Lecture notes for a course on quantum computation, Caltech, www.theory.caltech.edu/preskill/ph219.
- [146] A. Kómár and O. Landon-Cardinal. "Anyons are not energy eigenspaces of quantum double Hamiltonians". In: *Phys. Rev. B* 96.19 (2017).
- [147] M. de Wild Propitius. "Topological interactions in broken gauge theories", Ph. D. thesis, University of Amsterdam, (1995).
- [148] A. Beekman. "Quantum double symmetries of the even dihedral groups and their breaking", Master thesis, University of Amsterdam, (2005).

- [149] V. Lahtinen. "Anyons, quantum double symmetry and topological quantum computation", unpublished, (2006).
- [150] C. Castelnovo and C. Chamon. "Topological order in a three-dimensional toric code at finite temperature". In: *Phys. Rev. B* 78.15 (2008).
- [151] R. Alicki et al. "On Thermal stability of topological qubit in Kitaev's 4D Model". In: *Open Systems & Information Dynamics* 17.01 (2010), p. 1.
- [152] J. Nasu and Y. Motome. "Thermodynamics of chiral spin liquids with Abelian and non-Abelian anyons". In: *Phys. Rev. Lett.* 115.8 (2015).
- [153] T. Lan et al. "Gapped domain walls between 2+1D topologically ordered states". In: *Phys. Rev. Research* 2 (2020), p. 023331.
- [154] Y. Kawahigashi. "A remark on gapped domain walls between topological phases". In: *Lett. Math. Phys.* 105 (2015), p. 893.
- [155] P. Grossman and N. Snyder. "Quantum subgroups of the Haagerup fusion categories". In: *Commun. Math. Phys.* 311 (2012), p. 617.
- [156] C. Delcamp, B. Dittrich, and A. Riello. "Fusion basis for lattice gauge theory and loop quantum gravity". In: *J. High Energ. Phys.* 2017 (2017), p. 61.